I. Source Analysis of Large Earthquakes in Mexico

II. Study of Intermediate-depth Earthquakes and
Interplate Seismic Coupling

Thesis by
Luciana Maria de los Angeles Astiz Delgado

In Partial Fulfillment of the Requirements
for the Degree of
Doctor of Philosophy

California Institute of Technology
Pasadena, California

1987

(submitted May 14, 1987)

Acknowledgments

I would like to thank the "Seismo-Lab." faculty for providing a liberal, secure, friendly, and unselfish atmosphere in which to study. I am most grateful to Hiroo Kanamori, my thesis advisor, not only for his guidance and objectivity but also for his gentleness, humor and infinite patience. I thank Don V. Helmberger and Clarence R. Allen for their support and advice, and also Bob P. Sharp for all the fun-filled field trips. Thanks also to Shri K. Singh and Jens Havskov, who introduced me to Seismology and encouraged me to come to Caltech.

Many people have contributed to my growth and well being, both personally and scientifically, during my stay at the Seismo Laboratory; I thank you all. Although, it is truly difficult to select names, I give special thanks to Florence and Don Helmberger who sheltered me during my first few weeks in a foreign country. Jana and Dave Harkrider and Marianne Walck introduced me to the all-American traditions of Thanksgiving dinner and softball, respectively. Steve Wesnousky, Holly Eisler, Thorne Lay, and Gladys Engen have been great coworkers. Jeff Given and Larry Ruff were especially encouraging in my first year at Caltech. Scott King has been a wonderful office mate and Lori Hwang a very understanding roommate for the last two years. I would also like to thank my earlier office mates: Steve C., Hsui-Lin, and Steve G. for all their good advice, and John L., Vicki, Heidi and Steve S. for their

friendship , as well as my classmates: Jaime, Caroline, Vicki, Janice, Mark, and especially Bob and Chris.

I would like to acknowledge that life in Pasadena was very pleasant thanks to my close friends whom I thank for their loving care and support, especially Ronan, Holly, Cindy, Chris S. and Jeanny, who have stood by me at difficult times and also thanks to Gladys, Steve and Erica W., Barbara, Francisco, Steve G. and Sally R.. I also thank Phyllis (for cookies, notes and volleyball), Ann and Dave (for great parties and for that last push), John (for folkdancing), Doug, Cheryl, John V., Heidi, Bob, Richard, Henri, Lourdes, Chris, C., Jai-Jun, Marius, Huw, Hitoshi, Mindy (for those early hikes), Marie-B., and Agnes. David, Carlos and Raul, my college friends, have kept in touch all this time.

Finally, I thank my family for their unrestricted love, encouragement and understanding. To my parents, Paquita and Angel, to my sister Mariblanca and to Ronan, I would like to dedicate this thesis.

P.S. When I arrived at Caltech I was nick-named "Lucky-Lucy"; looking back, I think no other name could have been more appropriate.

General Abstract

Along the coast of Mexico and Central America several seismic gaps were defined by the timing, location and extent of large earthquakes. Among these regions with high seismic potential, the Ometepec and Michoacan gaps have broken since 1980. The 1982 Ometepec doublet and the 1981-1986 Michoacan sequence are studied in detail in Part I.

The seismic moment of each of the Ometepec doublet events is 2.8×10^{26} dyne cm. The first event involved a deeper asperity (at 20 km) that caused an incremental stress change large enough to trigger the second event at shallower depth. The second event is best modeled by two sources at 15 and 10 km depth. The largest event of the Michoacan sequence occurred on September 19, 1985 (M_w=8.0) and caused extensive structural damage and death to over ten thousand people in Mexico City. The first event of the sequence was the 1981 Playa Azul event, which broke the central part of the gap. It is 27 km deep and has a seismic moment of 7.2×10^{27} dyne cm. The seismic moment of the September 19, 1985 earthquake was released in two distinct events with the rupture starting in the northern portion of the seismic gap and propagating 95 km to the southeast with low moment release through the area already broken by the 1981 Playa Azul earthquake. The rupture propagated 125 km further southeast with an M_w=7.5 event on September 21, 1985. Another aftershock occurred on April 30, 1986, 50 km to the northwest of the September 19 mainshock. The most recent Michoacan events are shallower, 17-22 km, than the Playa Azul earthquake, which has a higher stress drop suggesting a higher stress level at greater depths in the Michoacan gap. The slip vectors of these events are consistent with

the convergence direction of the Cocos and North American plates.

Part II investigates the relation of intermediate-depth earthquakes to the shallower seismicity, especially since these events may reflect the state of inter-plate coupling at subduction zones. A catalog of earthquake focal mechanisms was gathered, which includes all events listed by NOAA and ISC catalogs with $M > 6$ and depth between 40 to 200 km, that occurred between 1960 and 1984. The final catalog includes a total of 335 events; 47 were determined by this study. Focal mechanism solutions for intermediate-depth earthquakes with $M > 6.8$ can be grouped into four: 1) Normal-fault events (44%), and 2) reverse-fault events (33%), both with a strike nearly parallel to the trench axis. 3) Normal or reverse fault events with a strike significantly oblique to the trench axis (10%) and 4) tear faulting events (13%).

Simple models of plate coupling and geometry suggest that Type 1 events occur at strongly coupled plate boundaries where a down-dip extensional stress prevails in a gently dipping plate. Continental loading may be another important factor. In contrast, large normal fault earthquakes occur at shallow depths in subduction zones that are decoupled. Type 2 events with strike subparallel to the subduction zone, most of them with near vertical tension axis, occur mainly in regions that have partially coupled or uncoupled subduction zones and the observed continuous seismicity is deeper than 300 km. In terms of our simple model, the increased dip of the downgoing slab associated with weakly coupled subduction zones and the weight of the slab may induce near vertical tensional stress at intermediate depth and, consequently, the change in focal mechanism from Type 1 to Type 2 events. Events of Type 3 occur where the trench axis bends sharply, causing horizontal extensional or compressional intraplate stress. Type 4 are hinge faulting events.

We also investigate the temporal variation of the mechanism of large intraplate earthquakes at intermediate depths in relation to the occurrence of large underthrusting earthquakes in Chile. Focal mechanisms were determined for three large events (March 1, 1934: M=7.1, d=120 km, April 20, 1949: M=7.3, d=70 km and May 8, 1971: M_w=7.2, d=150 km), which occurred down-dip of the great 1960 Chilean earthquake (M_w=9.5) rupture zone. The 1971 event is down-dip compressional, whereas the 1949 and the 1934 earthquake focal mechanisms are consistent with a down-dip tensional mechanism. Published fault plane solutions of large intermediate-depth earthquakes (March 28, 1965 and November 7, 1981), which occurred down-dip of the Valparaiso earthquakes of 1971 (M_w=7.8) and 1985 (M_w=8.0) are also down-dip tensional. These results suggest that before a major thrust earthquake, the interplate boundary is strongly coupled and the subducted slab is under tension at intermediate depths; after the occurrence of an interplate thrust event, the displacement on the thrust boundary induces transient compressional stress at intermediate depth in the downgoing slab. This interpretation is consistent with the hypothesis that temporal variations of focal mechanisms of outer-rise events are due to changes of interplate coupling.

The variation of intermediate-depth earthquake focal mechanisms with M≥6 is examined region by region in relation to local variations of the strength of interplate coupling. In summary, regions that are mostly uncoupled present down-dip tensional stresses in a steeply-dipping slab probably induced by the negative buoyancy of the subducted lithosphere (e.g., North Scotia arc). Double seismic zones may be present in partially coupled regions in response to unbending of the downgoing slab (e.g., Northeast Japan). Lateral bending or tearing of the slab influences the stress

distribution within the subducted plate (e.g., New Ireland). Subduction of topographic highs may also change the interplate coupling locally (e.g., Louiville ridge in Tonga). Regions that are mostly coupled are generally shallow dipping and the observed continuous seismicity is at most 300 km deep. In these regions normal faulting events occur at the base of the coupled region (e. g. South America). In contrast, normal faulting events occur at the trench axis at uncoupled regions where the strains due to bending of the plate are largest. Temporal variations in the interplate coupling due to the occurrence of large thrust events at the plate boundary are suggested in several regions such as Middle America and Chile.

Table of Contents

Part II: Study of Intermediate-depth Earthquakes and Interplate Seismic Coupling

Abstract to Part I

The Middle-America trench delineates the boundary between the subducting Rivera and Cocos plates beneath the North-American and Caribbean plates. It parallels the southwest coast of Mexico and Central America for about 3000 km. Large subduction earthquakes have occurred at this interplate boundary at short and regular intervals compared to other subduction zones. The seismotectonics of Mexico and Central America are discussed in Chapter 1. The timing, location, and extent of large earthquakes prior to 1980 indicated the presence of several regions with high seismic potential or seismic gaps. Among them the Ometepec and Michoacan gaps have broken in large earthquake sequences since 1980. Regions offshore the states of Jalisco and Guerrero in Mexico and those off coastal Guatemala, El Salvador and Nicaragua still have a high seismic risk. Most of these regions have not experienced a great earthquake since the turn of the century. The source characteristics of the large events that occurred in the Ometepec and Michoacan regions from 1981 to 1986 are studied in Chapters 2, 3 and 4. Comparison of seismograms recorded at Pasadena from many large Mexican earthquakes shows that the 1985 Michoacan earthquake is basically the same size as the great 1932 Jalisco, Mexico earthquake, and is clearly larger and more complex than the other significant events in Mexico since 1932.

On June 7, 1982, an earthquake doublet occurred in the Ometepec gap in Guerrero, Mexico; the events occurred within five hours of each other. Chapter 2 is a detailed study of the teleseismic characteristics of the Ometepec doublet. The same seismic moment $(M_o = 2.8 \times 10^{26}$ dyne cm$)$, is obtained for each event in the doublet from the inversion of 256 s period surface wave data. Each event has similar fault

parameters of azimuth ($\theta \approx 278°$), dip ($\delta \approx 13°$), and rake ($\lambda \approx 68°$), which are consistent with subduction of the Cocos plate. Modeling of long-period P waves suggests that the first event has an average depth of 20 km and may be well modeled with a single trapezoidal source time function with an effective duration of 6 seconds. The second event is best modeled by two sources at depths of 15 and 10 km. The combined effective source duration time for the two sources is about 10 seconds. These results suggest that the first event that involved a deeper asperity caused an incremental stress change large enough to trigger the second event. A regional distribution of comparable-size asperities may be responsible for the relatively frequent occurrence of doublets in the Middle-America trench during the last 70 years.

Chapter 3 presents the analysis of long-period surface and body waves of the earthquakes that occurred in the Michoacan, Mexico, seismic gap during the period from 1981 to 1986. The rupture pattern of the Michoacan gap during this period can be characterized by the sequential failure of five distinct asperities. Before 1981, the Michoacan region had not experienced a large earthquake since the 1911 $M_S = 7.8$ earthquake. The recent sequence started in October 1981 with the Playa Azul event which broke the central part of the gap. Body-wave modeling indicates that the Playa Azul event, is 27 km deep with a seismic moment of 7.2×10^{27} dyne cm. It is slightly deeper than the recent Michoacan earthquakes and its stress drop is higher, suggesting a higher stress level at greater depths in the Michoacan gap.

Analysis of long-period P-waves of the September 19, 1985 earthquake indicates that this is a multiple event with a second source of identical moment, fault geometry, and depth occurring approximately 26 s after the first. The total source duration of at least 42 s may be an important contributing factor for the extensive

structural damage that occurred in Mexico City. The seismic moment of the September 19, 1985 (M_w=8.0) earthquake was released in two distinct events with the rupture starting in the northern portion of the seismic gap and propagating to the southeast with low moment release through the area already broken by the 1981 Playa Azul earthquake. Directivity in the body wave time function indicates that the second subevent occurred 95 km to the southeast of the first. The rupture propagated 125 km farther southeast with an M_w=7.5 event on September 21, 1985. The September 1985 earthquakes were interplate subduction events on a shallowly dipping fault plane that strikes parallel to the Middle-America trench consistent with the convergence direction of the Cocos and North America plates (δ=9° , ϕ=288°, λ=72°), with a point source depth of 17 km for the main shock and 22 km for the aftershock. Another aftershock occurred on April 30, 1986, 50 km to the northwest of the September 19 mainshock. Body-wave modeling indicates that this event has a simple source 10 s long at 21 km depth, and fault parameters consistent with subduction of the Cocos plate (θ=280°, δ=12°, λ=70°) and M_o=2.0–3.1×10^{26} dyne cm (M_w=6.9).

Although this distribution of asperities is considered characteristic of the Michoacan gap, whether the temporal sequence exhibited by the 1981-1986 sequence is also characteristic of this gap or not is unclear. It is probable that, depending on the state of stress for each asperity, the entire gap may fail in either a single large event with a complex time history or a sequence of moderate-to-large events spread over a few years.

The relation among seismic source parameters of large subduction earthquakes is investigated in Chapter 4. Stress drop values for Mexican subduction earthquakes are

estimated from M_o and fault area estimates, which indicate that most events have average stress drop values of the order of 10 bars. However, the 1981 Playa Azul earthquake, which occurred in the middle of the Michoacan seismic gap, has a relatively higher value of about 50 bars, which may be associated with the presence of the Orozco fracture zone. The relation between the average recurrence time, T, and the average seismic moment, $\overline{M}_o$, along the Mexican subduction zone is $\log T \approx \frac{1}{3} \log \overline{M}_o$. The convergence rate and the properties along the subducted plate are more uniform than other subduction zones. A simple asperity model predicts this relation. Using 1907 as the last date for an event in Guerrero, this relation predicts that the next episode would involve a release of seismic moment of 1.6×10^{28} dyne cm. This is equivalent to one earthquake with $M_w = 8.1$, or alternatively, three with $M_w = 7.8$. Either scenario would have serious implications for damage in Mexico City.

Chapter 1

Seismotectonics of the Middle-America Trench

1.1   Regional Tectonic Setting

The Middle-America trench is a continuous topographic feature that extends parallel to the southwest coast of Mexico and Central America for about 3000 km (Fisher, 1961). Along the trench, the Cocos plate is subducted beneath the North America and Caribbean plates (Molnar and Sykes, 1969; Dean and Drake, 1978). The Cocos plate dips gently ($10°-20°$) beneath the North America plate (Chael and Stewart, 1982) and more steeply below the Caribbean plate (Molnar and Sykes, 1969). The triple junction of these plates is not well established, but it is probably located in the Tehuantepec Gulf region. In this region, the projection of the Cayman Trough-Motagua transform fault system, which is the boundary of the Caribbean and North American plates, intersects the Middle-America trench (Plafker, 1976). Seaward from the trench, relative structural homogeneity of the seafloor is observed, interrupted only by the Rivera and Orozco fracture zones and the Tehuantepec and Cocos ridges (Figure 1.1). However, the continental margin shows a duality. Northwestward of the Tehuantepec ridge the continental margin is narrow, with numerous submarine canyons. Trench turbidites are currently being accreted. Southeast of the ridge, the continental margin is wide with a well-developed fore-arc basin and no observed accretion (Shipley et al., 1980; Aubouin et al., 1982). Gravity anomalies offshore of

southern Mexico and northwestern Guatemala support the above observations (Couch and Woodcock, 1981). The shaded area in Figure 1.1 shows the line of active volcanoes that, in the Central America region, form a prominent chain parallel to the trench, but 150 km to the east (Stoiber and Carr, 1973). In contrast, in the Mexico segment, the Mexican volcanic belt is oblique to the trench and is located 200-300 km away from it (Mooser, 1972; Demaint, 1978).

1.2   Large Subduction Earthquakes prior to 1980

The Middle-America trench has been the site of numerous large thrust earthquakes that rupture discrete segments 100-200 km long. An average recurrence interval for the plate boundary of 33 ± 8 years was found by McNally and Minster (1981), although different subsegments have somewhat different recurrence intervals (Kelleher et al., 1973; McNally and Minster, 1981; Singh et al., 1981; Astiz and Kanamori, 1984). However, in the Tehuantepec region no large shallow earthquake has occurred for the last 180 years. This gap is considered to be either aseismic, or seismic with anomalously large recurrence times (McCann et al., 1979; Singh et al., 1981).

Figure 1.2 is a time-distance plot of large earthquakes along the Middle-America trench from 1800 to 1981. Stars and squares are this and last century events, respectively, and symbol size is proportional to magnitude. Location accuracy varies with time; however, it is evident that large earthquakes have occurred along most of this plate boundary in the last hundred years. Hatched segments indicate seismic gaps.

The Middle-America region has been subdivided into 21 regions more or less arbitrarily, since it has been made only on the basis of the distribution of aftershock
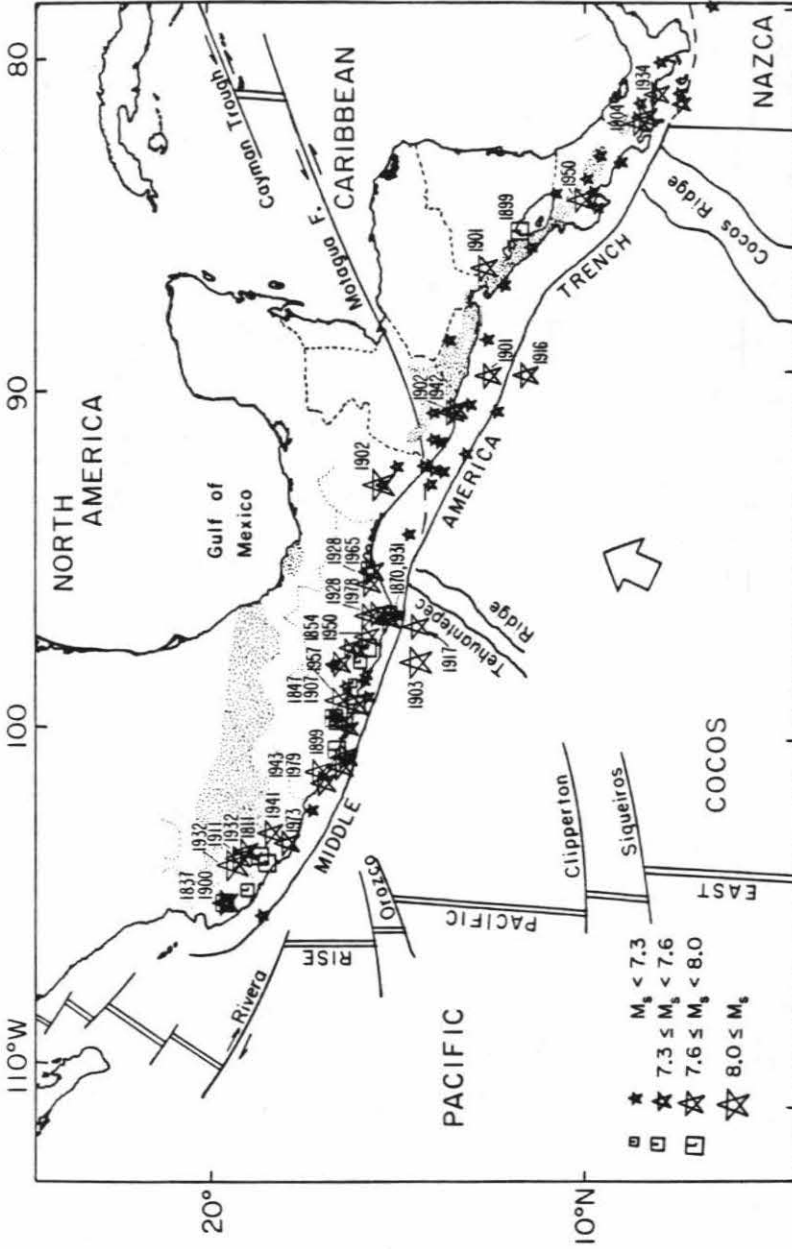
Figure 1.1: Main tectonic features of Middle America, simplified after Mammerickx et al. (1975). The arrow indicates the mean direction of convergence between the Cocos and North America and Caribbean plates. Shaded areas delineate the Quaternary volcano alignments in Mexico and Central America. Shallow large earthquakes that ($M_S \geq 7$) occurred along the Middle-America trench are shown. Squares correspond to last century events and stars to those that occurred during this century. The year of occurrence is indicated for events with $M_s > 7.5$.

- 8 -
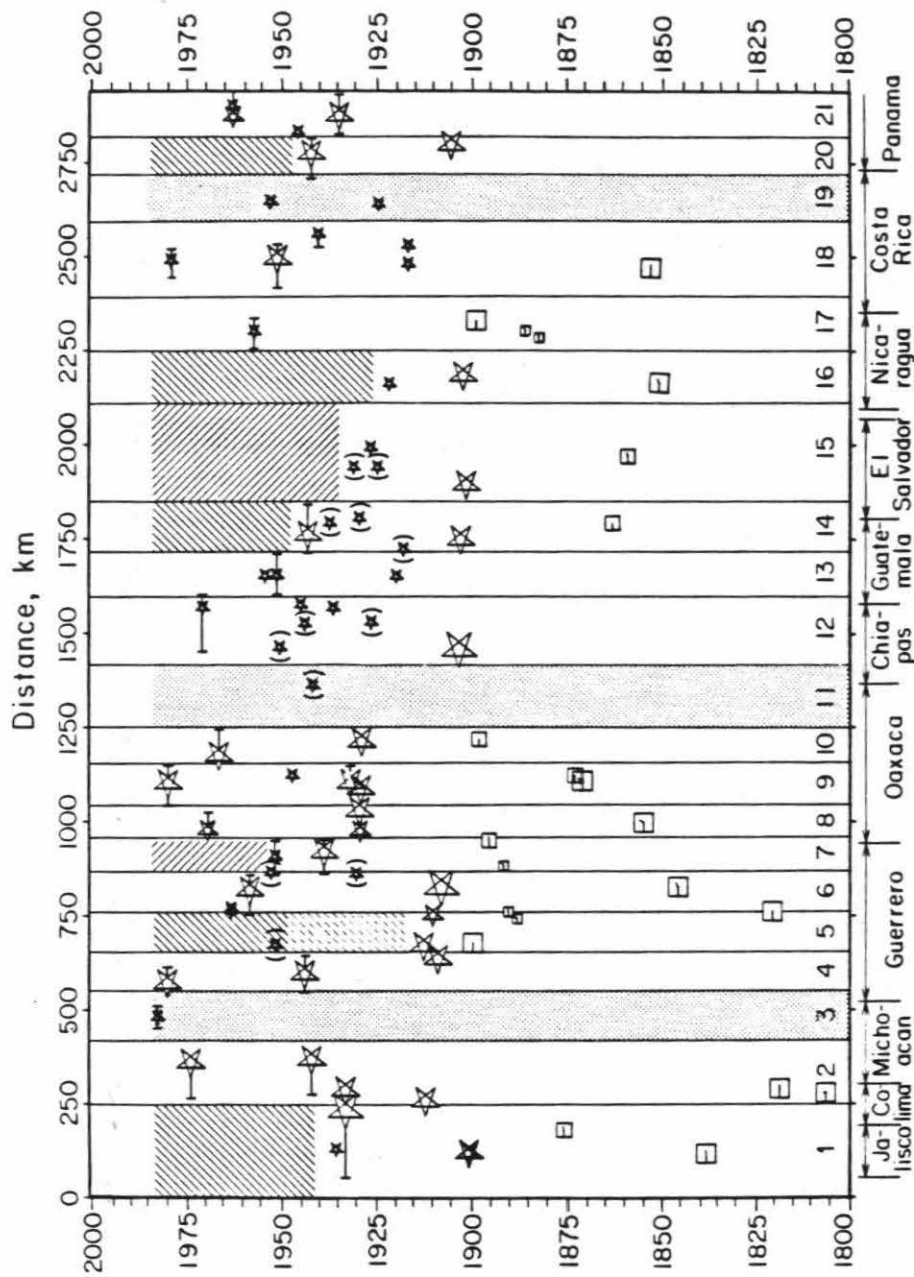
Figure 1.2: Time-distance plot along the Middle-American trench from 1800 to 1981. Symbols are the same as in Figure 1.1. Events listed by Miyamura (1976) as M =7 are in parentheses. Names at the bottom refer to Mexican coastal states and Central American countries. Numbers at the bottom indicate regions determined from recent aftershock area distributions. Dotted regions correspond to topographic features. The Orozco fracture zone (3) where the Michoacan seismic gap had been identified. The Tehuantepec (11) and Cocos (19) ridges are regions where seismicity has been lower in number and magnitude than other regions, at least during this century. Hatched sections indicate seismic gaps: Jalisco (1), Guerrero (5), Ometepec (7), Guatemala (14), El Salvador (15), Nicaragua (16) and West Panama(20).

areas of recent events. These subdivisions will be discussed further in Chapter 4. Note that most of the Central America coast has not experienced a major thrust earthquake during the last 30 years (regions 14,15,16,20). South of the Tehuantepec ridge (region 11), large earthquakes have occurred offshore Chiapas, Mexico, in 1970 (M_S=7.0), and offshore Costa Rica in 1978 (M_S=7.0) and 1983 (M_S=7.0). This last event occurred where the Cocos Ridge (region 19) is being subducted. In the Mexican subduction zone, north of Tehuantepec, major gaps are observed in Jalisco (region 1), Michoacan (region 3), Guerrero (region 5), and Ometepec (region 7). These seismic gaps were identified by Singh et al. (1981), based on aftershock areas and recurrence intervals of large earthquakes.

Recently, two of these gaps have been broken: on June 1982 an earthquake doublet occurred in the Ometepec region and the Michoacan gap broke in a series of events that occurred on October 1981 and later on September 1985. All of these events are discussed in detail in Chapters 2 and 3, respectively. A large event is expected to occur in the near future in the Guerrero gap, since no large earthquake has occurred in almost 80 years (Anderson et al., 1986; Eissler et al., 1986). On the other hand, the Jalisco gap is not expected to break soon since it is the boundary of the Rivera and the North American plates, which has a smaller convergence rate than the Cocos-North America interplate boundary (Eissler and McNally, 1982; Singh et al., 1985).

1.3   Comparison of Seismograms from Recent Large Events

Since the establishment of the World Wide Standardized Seismograph Network (WWSSN), numerous large earthquakes have occurred in the Middle-America trench. Figure 1.3 shows long-period body waves recorded at Eskdalemuir, Scotland (ESK), station for all large ($M_S \geq 7$) events that occurred in this region from 1965 to 1985. We can compare the waveforms since all earthquakes are at approximately the same distance and azimuth from ESK, 80° and 35°, respectively. Most events are relatively simple but the September 19 Michoacan earthquake is more complex and has the largest peak-to-peak amplitude (the P-wave was nearly offscale). Note that the ringing character of the September 19, 1985 trace between 3 and 5 min is due to the PP and PPP phases merging, due to the long source duration of this event.

Because of the high seismic activity and the relatively short (30 to 50 years) recurrence times of large events along the Middle-America trench, many detailed studies have been recently conducted on individual earthquakes (e.g., Singh et al., 1984; Havskov et al., 1983; Valdés et al., 1982; Tajima and McNally, 1983; Chael and Stewart, 1982; Wang et al., 1982; Stewart et al., 1981; Espindola et al., 1981; Reyes et at., 1979; Yamamoto, 1978; Ohtake et al., 1977) as well as on the regional seismicity (e.g., LeFevre and McNally, 1985; Singh et al., 1982b; McNally and Minster, 1981; Singh et al., 1981; Kelleher et al., 1973). The focal mechanisms of these events indicate thrusting consistent with the subduction of the Cocos plate to the northeast and with the gently dipping Benioff zone (Figure 1.4).

Detailed studies of the source parameters of the most recent large earthquakes along Middle America indicate that these events show remarkably simple fault
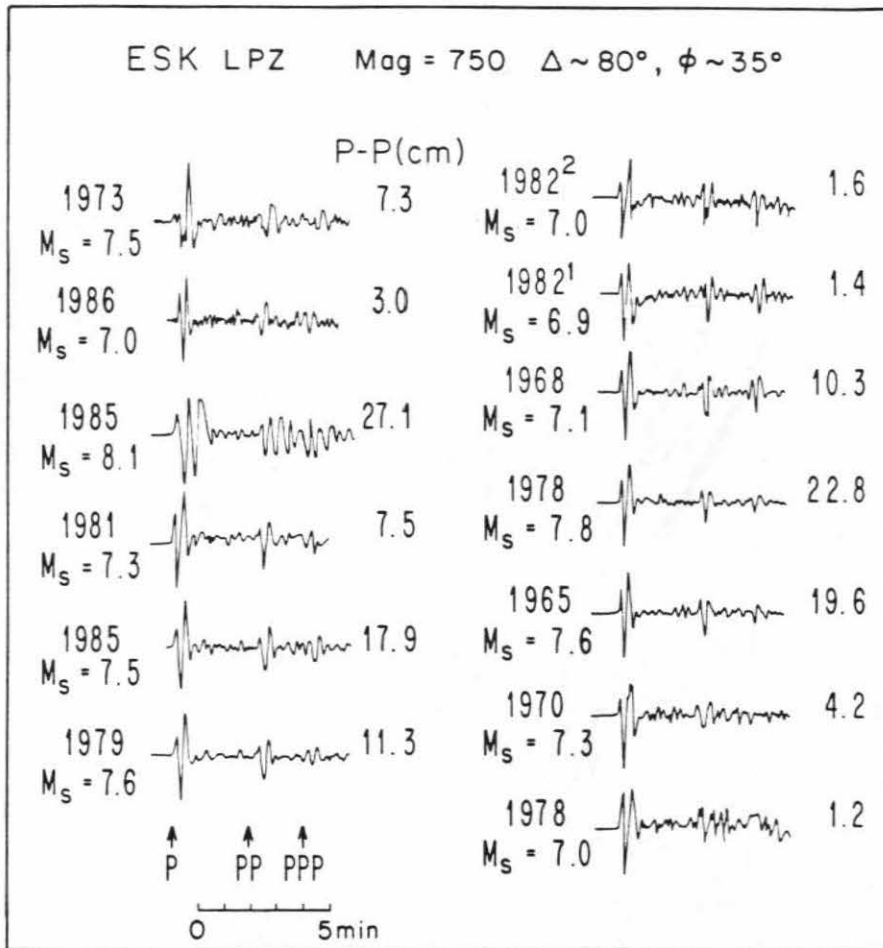
Figure 1.3: Vertical long-period WWSSN seismograms of P, PP and PPP waves recorded at Eskdalemuir, Scotland (ESK), are shown for large shallow ($M_S > 7$) subduction events that occurred along the Middle-America trench between 1965 and 1985. The events are shown from northwest (top left) to southeast (bottom right). Peak-to-peak amplitudes (P-P) in cm are indicated at the end of each trace. Note the relatively simple waveforms for most events; however, a more complex source is clearly seen for the 1985 Michoacan earthquake that also displays the largest peak-to-peak amplitude.
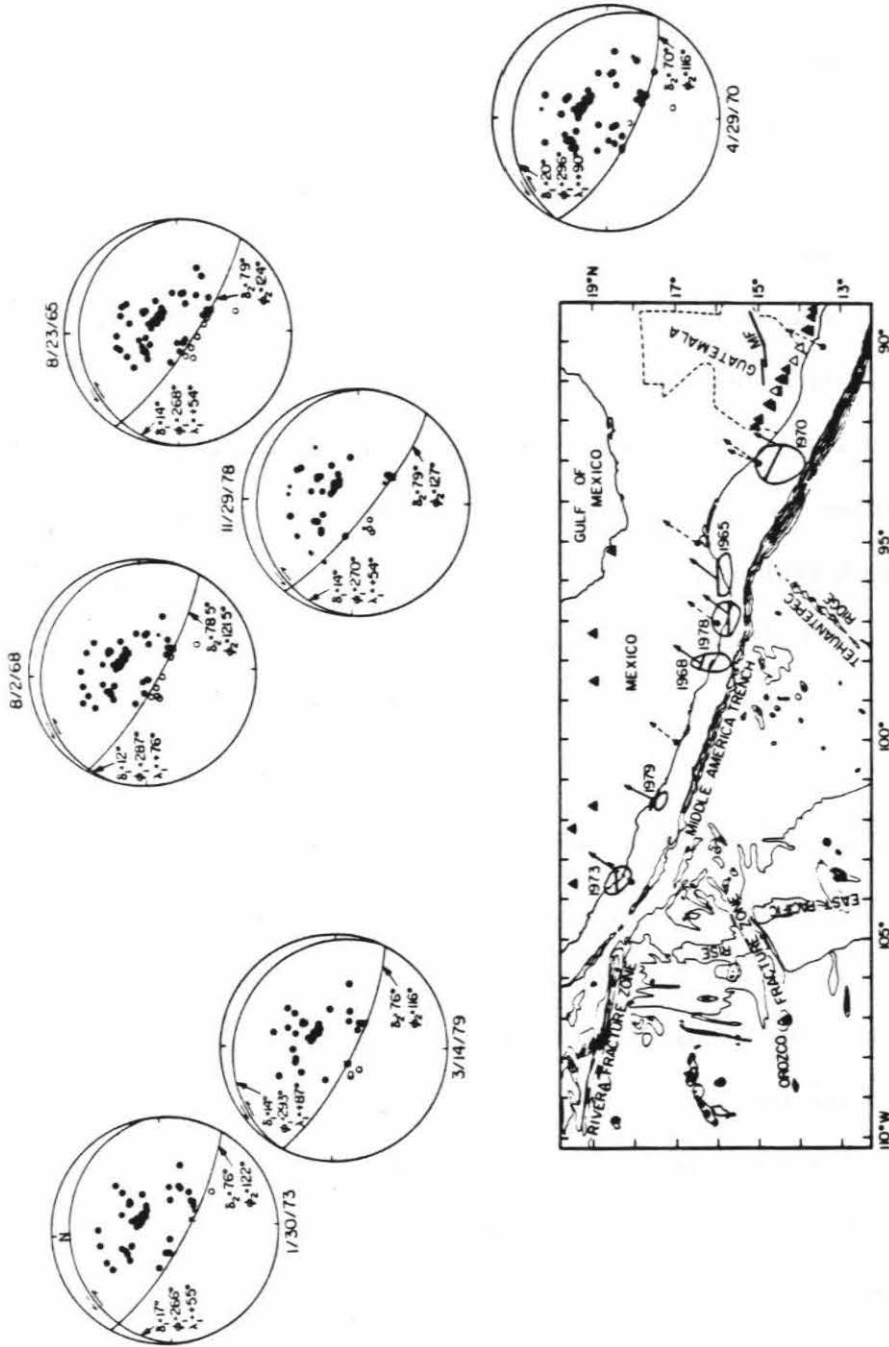
Figure 1.4: Focal mechanism for the large shallow earthquakes occurred from 1965 to 1980 in the Mexican subduction zone from studies of Chael and Stewart (1982) and Stewart et al. (1981). The location of the aftershock area and slip direction of these events are shown in the map below.

proces for long ($>$ 10s) periods (e.g. Reyes et al., 1979; Stewart et al., 1981; Chael and Stewart, 1982; Astiz and Kanamori, 1984), with stress drops from 1 to 10 bars and seismic moments from 1 to 3.2×10^{27} dyne cm. At short periods their sources are more complex (Tajima, 1984); however, when compared to similar size events that occur on other subduction zones the Mexican events have smoother source time functions even at short periods (Houston and Kanamori, 1986). These studies suggest that large earthquakes occur repeatedly at places with increased mechanical strength, which are often called asperities. European recordings of large Mexican earthquakes that occurred from 1907 to 1962 suggest that these events share the characteristics of the more recent well studied events: they are shallow thrust events (generally at about 16 km depth with a relatively simple source with the possible exception of multiple source earthquakes on June 7, 1911, in Michoacan, June 3 and 18, 1932, in Jalisco, and on February 22, 1943 near Petatlan (Singh et al., 1984; see also Figure 4 of UNAM Seismology Group, 1986).

Pasadena Seismograms from Large Mexico Earthquakes

Since about 1930 many seismic instruments at the Seismological Laboratory in Pasadena, CA, have been operating continuously. In this section we compare seismograms for the largest subduction events in Mexico since 1930 recorded on three instruments at Pasadena: the horizontal torsion Wood-Anderson instrument ($T_o = 10$ s); the long-period vertical Benioff ($T_p = 1$ s, $T_g = 90$ s, where T_p and T_g are the pendulum period and galvanometer period, respectively); and the short-period vertical Benioff ($T_p = 1$ s, $T_g = 0.2$ s). As mentioned above, these events have been found to have nearly identical focal mechanisms and source depths, so that the amplitudes and

waveforms can be compared directly for differences in magnitude and waveform. However, Pasadena lies within the upper-mantle triplication distance of these events (18–24°), and body-wave amplitudes may be affected by the complex variation with distance observed near this range.

Figure 1.5 shows about 12 minutes of the north-south component of the Wood-Anderson instrument for ten large subduction events in Mexico. We note that the surface-wave amplitudes show three characteristic sizes of events. The 1932 Jalisco earthquake is the largest and has offscale surface waves, and the Michoacan earthquake is nearly as large. The Colima 1973, Petatlán 1979, and Oaxaca 1978 earthquakes are comparably sized events smaller than the Jalisco and Michoacan earthquakes. The Colima 1941, Playa Azul 1981, Michoacan September 1985 aftershock, Petatlan 1943, and Acapulco 1957 earthquakes had surface waves with similar amplitudes which are smaller than the other two groups of events. The Acapulco earthquake is anomalous in that it has a large body-wave pulse compared to its surface waves. M_S values for the events determined from the Pasadena Wood-Anderson records are shown in the figure. The distance and azimuth from each of these events to Pasadena are also indicated.

Figure 1.6 shows records from the long-period vertical Benioff instrument. This instrument was not installed at the time of the 1932 earthquake, and the 1978 Oaxaca record was not available. The records show the P and S arrivals, approximately 4 minutes apart, and the beginning of the surface wave. The most remarkable feature is the similarity of the P and S waveforms between events, indicating similar focal mechanisms and source time functions. The notable exception is the September 19 Michoacan record, which is initially similar to the others, but then shows a later
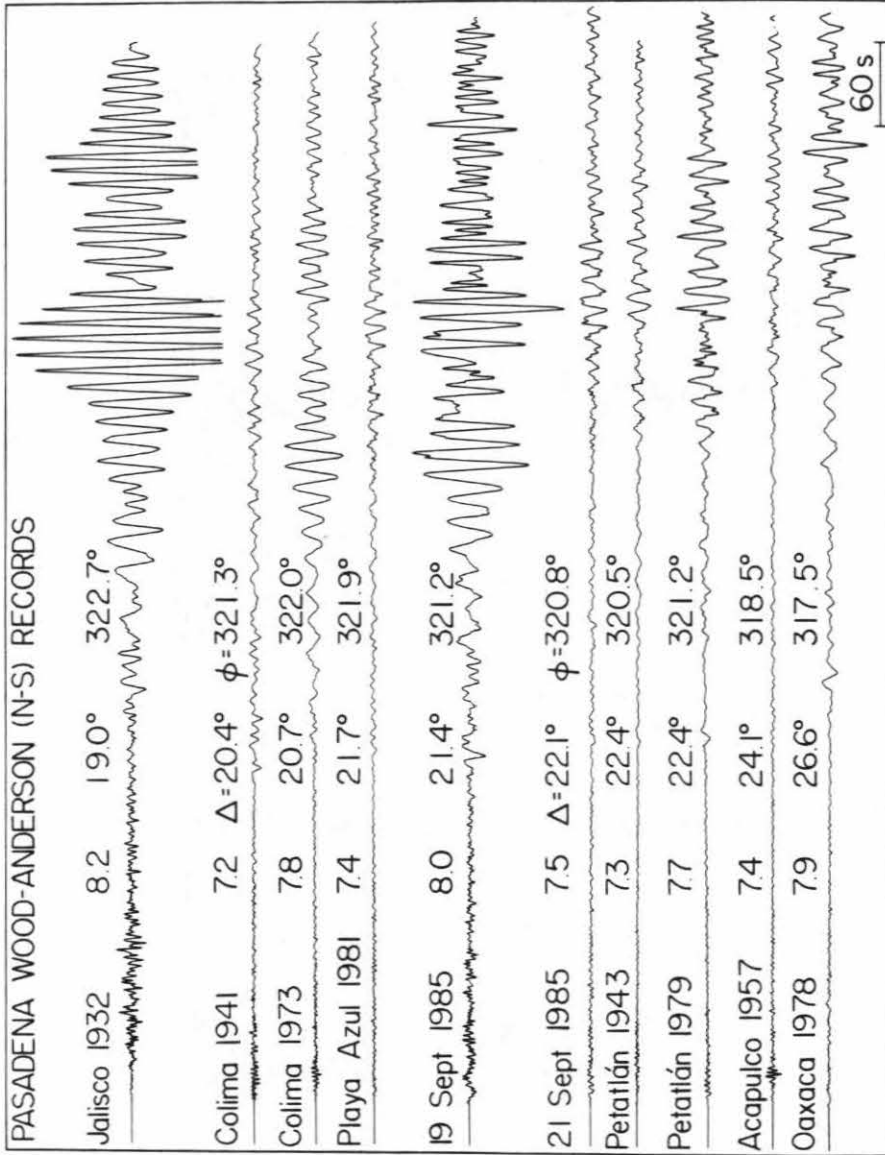
Figure 1.5: N-S components of Pasadena records of large interplate thrust events in Mexico from the horizontal Wood-Anderson instrument. Events are ordered geographically from northwest (top) to southeast (bottom). Surface wave amplitudes are indicative of magnitude because the events have similar depths and mechanisms. The September 19, 1985 Michoacan earthquake is larger than any other recent event excluding the 1932 Jalisco earthquake. M_S values determined from the surface wave amplitudes are shown over the traces.
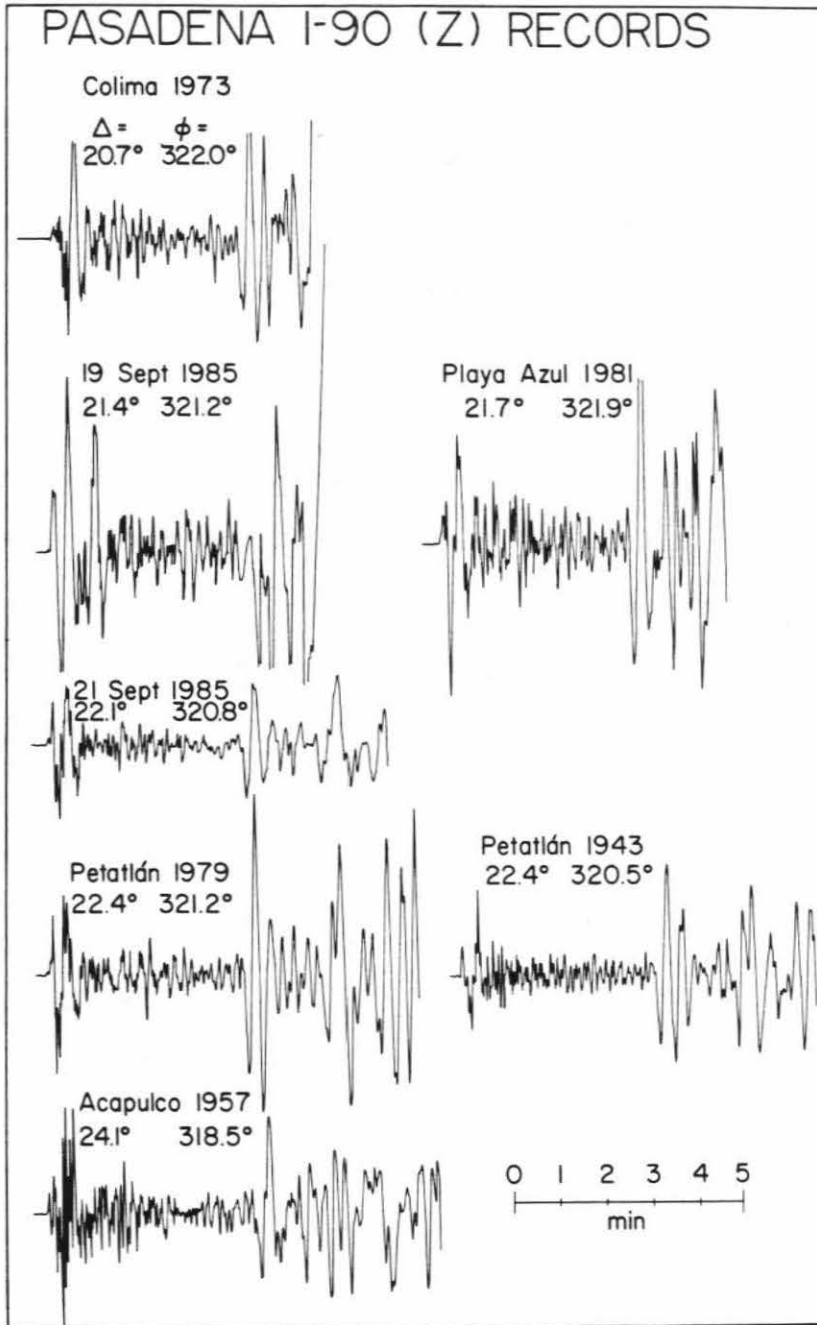
Figure 1.6: Pasadena seismograms of the same events on a vertical broad-band (T_o=1s, T_g=90s) Benioff instrument. The P and S waveforms are remarkably similar between events, except for the September 19, 1985 Michoacan record, which shows a second arrival within a minute of the P wave, indicative of source complexity.

large-amplitude arrival less than 1 min behind the characteristic P-waveform, indicative of a complex time function. The 1957 Acapulco record is anomalous in that the P wave has an unusual amount of high frequency, but the filtered waveform would have the same overall shape as those of other events.

Seismograms of the earthquakes from the short-period vertical Benioff instrument are shown in Figure 1.7, where the dark lines indicate the amplitude envelopes of the records. Most of the events have similar envelope shapes (e.g., 1973, 1979, 1957, 21 September 1985), but the September 19 Michoacan event clearly maintains larger amplitudes for a longer period of time and has a different envelope shape, indicating a longer source duration or multiple time function. The numbers in Figure 1.7 give a measure of coda duration; they are the time in minutes required for the amplitude to fall off to one-fourth its maximum, where the time is measured from the beginning of the signal. The September 19 Michoacan earthquake has the longest fall-off time at 4.5 min; the Colima 1941, Playa Azul 1981, and Oaxaca 1978 also have large fall-off times.
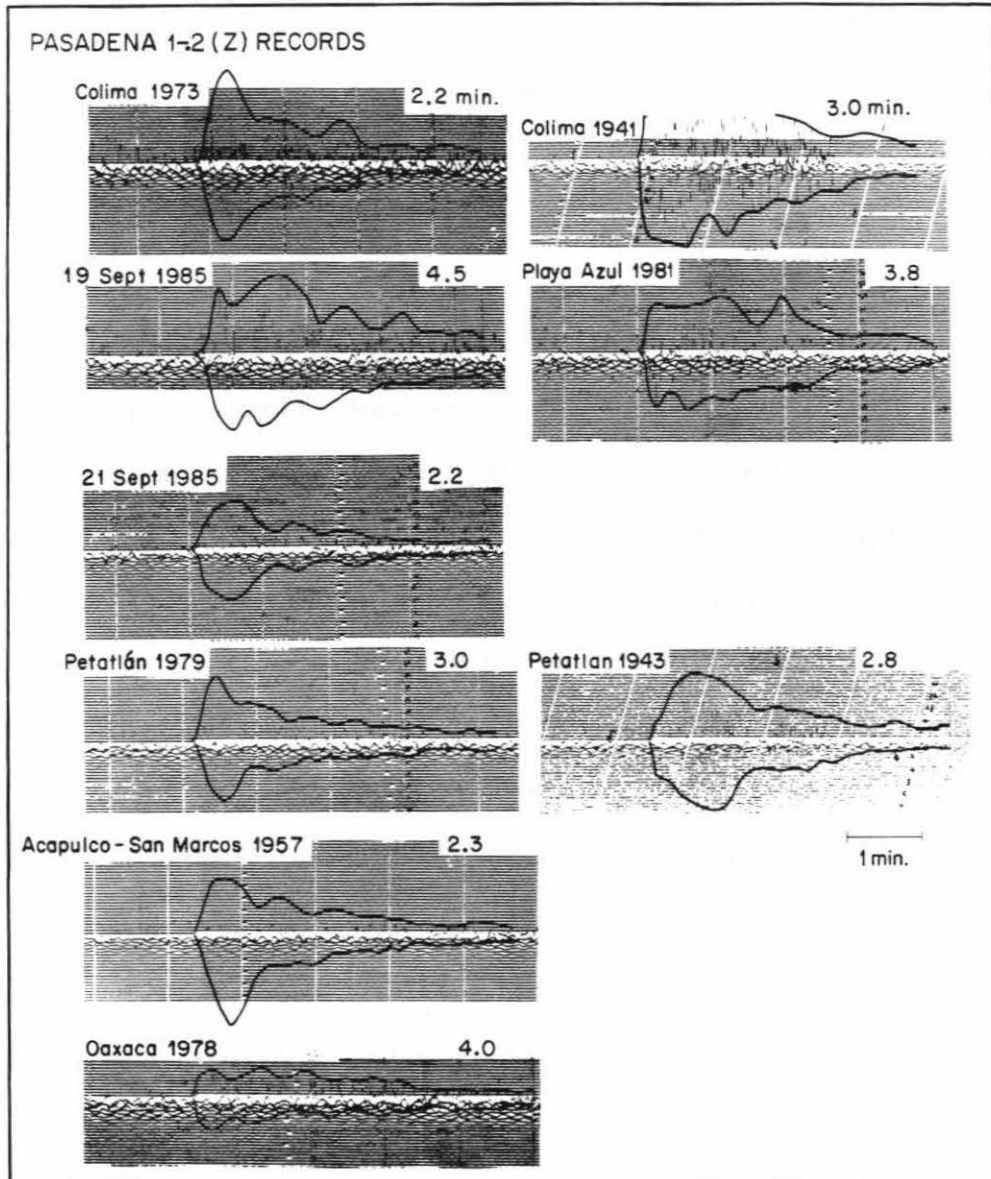
Figure 1.7: Vertical short-period Benioff ($T_o=1$s, $T_g=0.2$s) records at Pasadena for the same events in Figures 3 and 4. Continuous lines show the amplitude envelopes for each trace. Note that large amplitudes have a longer duration for the September 19, 1985 earthquake. Indicated values are coda length of P-waves in minutes.

Chapter 2

The 1982 Earthquake Doublet in Ometepec, Guerrero

2.1 Introduction

The Ometepec doublet events occurred on June 7, 1982, in a gap that had been given a high seismic potential (Singh et al., 1981). The U.S.G.S. location of the first event ($M_S = 6.9, m_b = 6.0$) is 16.607° N, 98.149° W, at 40.5 km depth, and the origin time is $06^h52^m37.37^s$; that of the second event ($M_S=7.0, m_b=6.3$) is 16.558° N, 98.358° W, at 33.8 km depth, and the origin time is $10^h59^m40.16^s$. The epicenters given by a local network are 16.348° N, 98.368° W , at 25 km depth (origin time $06^h52^m33.7^s$) for the first event, 16.399° N , 98.538° W , at 8 km depth (origin time $10^h59^m40.1^s$) for the second event. The locally determined epicenters are shallower than, and to the southwest of, the U.S.G.S. locations (Figure 2.1), as is typically found for events along the Mexican subduction zone (e.g., Havskov et al., 1983). Hereafter, these two events are referred to as 1982[1] and 1982[2] , respectively.

To try to understand the failure mechanism of seismic gaps, we determine the rupture process of the Ometepec doublet by detailed analysis of surface and body waves, and find that the Ometepec doublet has many features in common with similar doublets observed in other regions such as the Solomon subduction zone. The Ometepec doublet events are somewhat smaller than the large earthquakes characteristic of the Middle America subduction zone, and the average repeat time in the
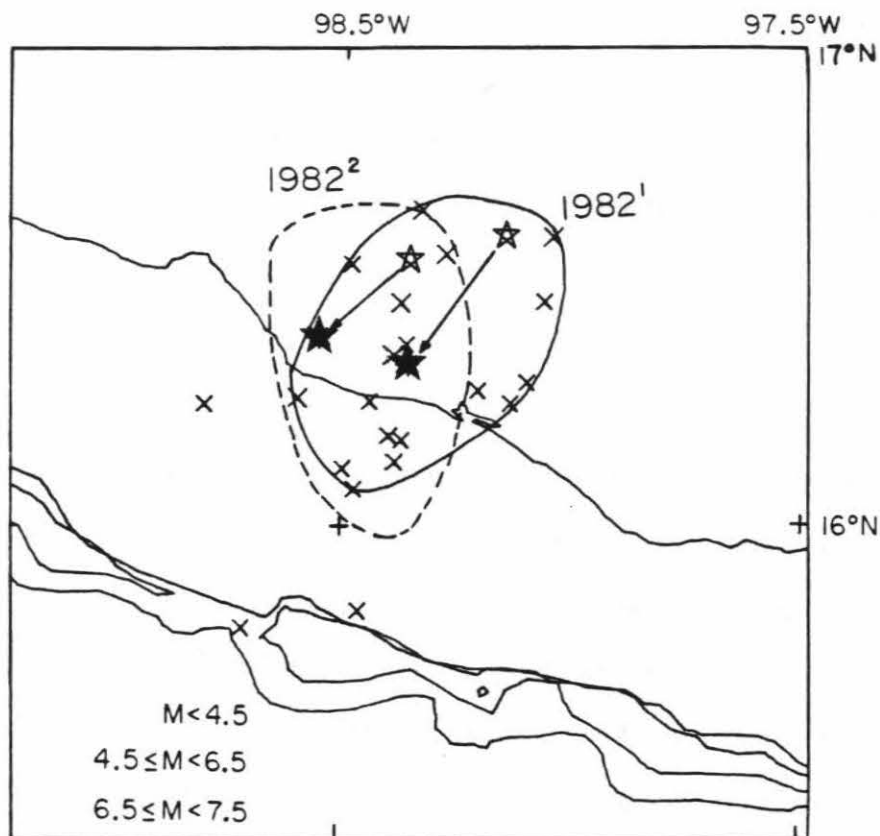
Figure 2.1: The heavy solid curve indicates the Ometepec doublet aftersock area shown in Figure 2.2. The dashed curve indicates the first week aftershock area and the solid stars the Ometepec doublet epicenters determined by Nava (1983) using a local network. Only events located within 20 km of each other are included in the aftershock areas.

Ometepec region is slightly shorter than in the adjacent segments of the Guerrero-Oaxaca regions. It is shown that these features can be explained by a heterogeneous strength distribution in the fault zone along the Middle America trench. These results, together with those of previous investigators, suggest that the fault zone heterogeneity as characterized by its asperity distribution (Lay and Kanamori, 1981) plays a key role in determining the recurrence time and the triggering mechanism of large earthquakes.

The 1982 Ometepec Doublet

Singh et al. (1981) identified a seismic gap on the Ometepec region based on aftershock areas and recurrence intervals of large earthquakes. Figure 2.2 shows the aftershock area of previous earthquakes in the Guerrero-Oaxaca region with dashed lines (after Kelleher et al, 1973, Singh et al., 1980b, and Valdés et al., 1982). Shaded areas correspond to more recent events. The location of the 1982 Ometepec doublet and the aftershock distribution of events $m_b \geq 3.6$ during the first week of activity as reported by the Preliminary Determination of Epicenters of the U.S. Geological Survey (P.D.E.) are shown by the heavy solid curve (Figure 2.2). The aftershock area is about 3200km^2 ($78 \times 41 \text{ km}^2$). The dashed curve in Figure 2.1 indicates the first week aftershock area and the solid stars are the Ometepec doublet epicenters given by Nava (1983). The locally determined aftershock area is about 3300km^2 ($82 \times 40 \text{ km}^2$). Only events that were located within 20 km of another event were considered in determining the aftershock areas. Large interplate earthquakes in the Ometepec region occurred on December 2, 1890 ($M_S = 7.3$), December 23, 1937 ($M_S = 7.5$), and December 14, 1950 ($M_S = 7.3$), suggesting average recurrence interval of 30 years.
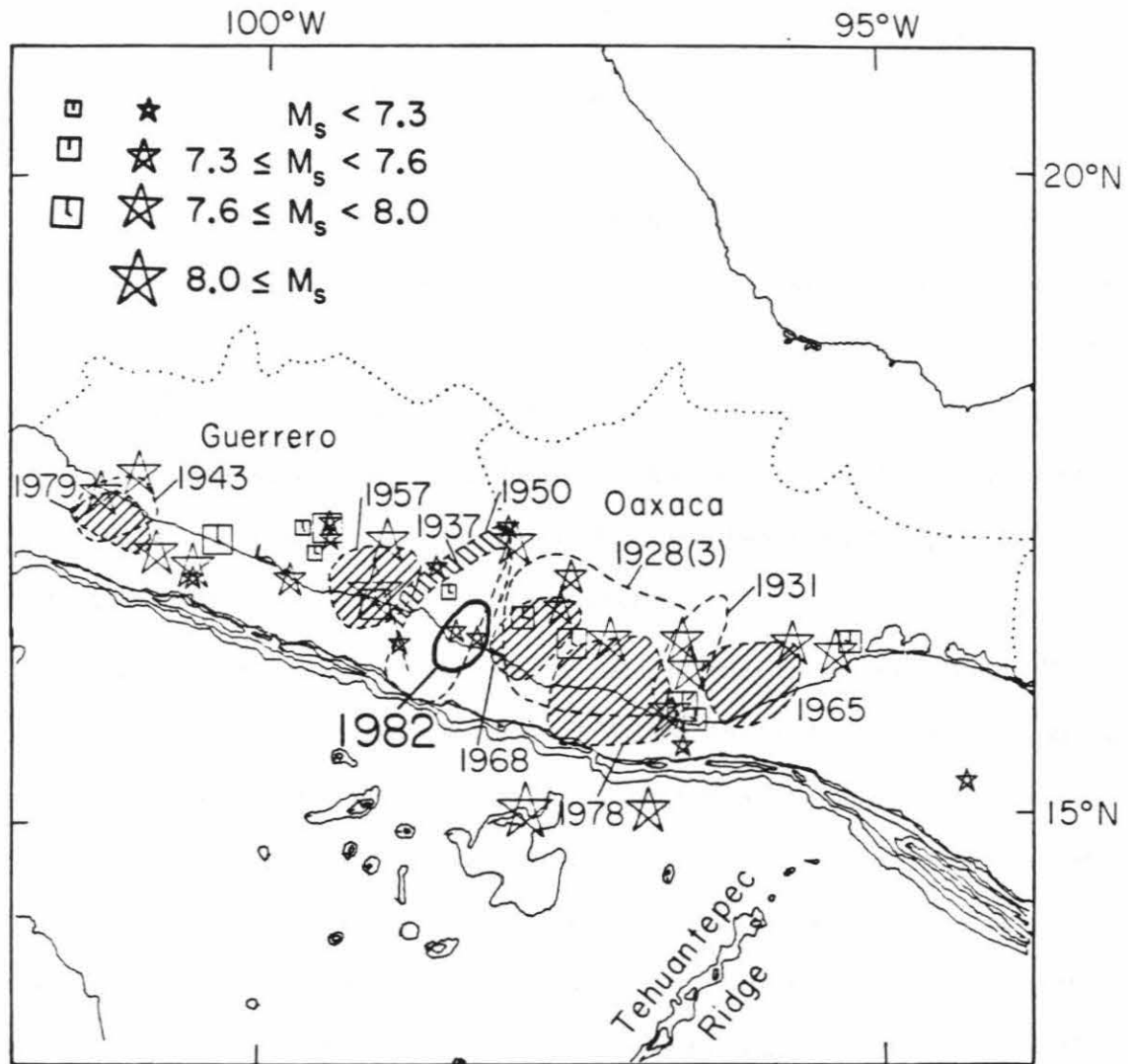
Figure 2.2: Aftershock areas of large shallow interplate earthquakes along the Mexican subduction zone, between the Orozco fracture zone and the Tehuantepec Ridge (after Kelleher et al.,1973; Singh et al., 1980b and Valdeś et al.,1982). Shaded areas correspond to more recent events. The Ometepec doublet aftershock area defined by the events with $m_b \geq 3.6$ (from P.D.E.), which occurred during the first week of activity, is shown by the heavy solid curve.

Miyamura (1976) reports a $M_S=7.0$ event in this region on December 28, 1951; however, Figueroa (1970) assigns this event $M_S=6.5$. In either case, the 1950 earthquake and the 1951 event can be considered part of the same seismic sequence. Notice that the 1957 Acapulco ($M_S=7.5$) and the 1968 Oaxaca ($M_S=7.4$) earthquakes did not break the Ometepec segment.

Seismic reflection and geologic surveys of the region during 1977 and 1978 by Shipley et al. (1980) reveal significant variations in structure over short distances, suggesting that the extent of aftershock activity may be controlled by structural features. The Ometepec Canyon is right-laterally displaced seaward of the trench, suggesting oblique subduction along the Middle-America trench. During this survey, sediments on the Ometepec Canyon appeared undisturbed along the trench, indicating that this segment had not been broken recently.

Long-period recordings of the 1982 Ometepec, Mexico doublet by the World Wide Standardized Seismograph Network (WWSSN), the Global Digital Seismograph Network (GDSN) and the International Deployment of Accelerograph (IDA) are used in the present study. Station distribution around the doublet epicentral area (16.5° N, 98.2° W) is shown in Figure 2.3 and the stations used for body and surface wave analysis for both events are listed in Table 2.1. Surface-wave analysis for these large events gives estimates of source orientation and seismic moment at 180 to 350 s periods (e.g., Kanamori and Given, 1981, 1982; Lay et al., 1982). Body-wave modeling that can determine the depth, the detailed source time history of the event, and the seismic moment at shorter periods (e.g. Kanamori and Stewart, 1976) are presented in Section 2.3.
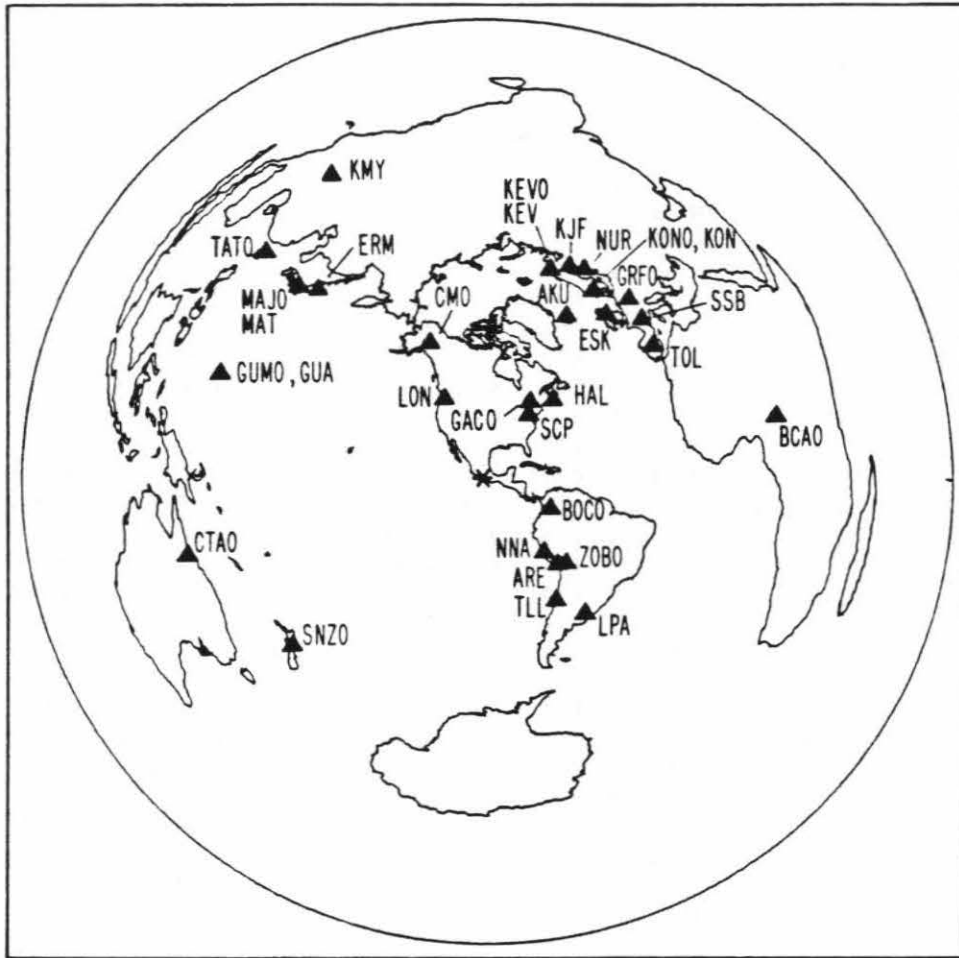
Figure 2.3: Azimuthal equidistant world map centered at the Ometepec, Mexico, doublet epicentral area (16.5°N,98.2°W). The triangles indicate the location of WWSSN, GDSN and IDA stations used in this study.

Table 2.1: Stations used in the Body and Surface Wave Analysis

Station	Location	type	Δ	Az		1982[1]			1982[2]	
			(deg)							
KEVO	Kevo, Finland	DWWSS	86.0	16.5	P			P		
KEV	Kevo, Finland	WWSS	86.0	16.5	P	.		P		
KJF	Kajaam, Finland		89.6	20.7	P			P		
NUR	Nurmijarvi, Finland	WWSS	90.9	24.4	P			P		
AKU	Akureyri, Iceland	WWSS	71.2	25.5				P		
GACO	Glen Almond, Canada	SRO	34.9	28.4	P	R2,R3	G3	P		G3
SSB	Saint-Sauveur, France	IDA	87.4	43.4		R1,R2			R2	
KONO	Kongsberg, Norway	ASRO	84.8	28.9	P	R1,R2	G1,G2	P	R2,R3	G1,G2
KON	Kongsber, Norway	WWSS	84.8	28.9	P			P		
SCP	State College PA, USA	DWWSS	30.2	31.9	P			P		
ESK	Eskdalemuir, Scotland	WWSS	79.6	35.3	P			P		
GRFO	Grafenberg, Germany	SRO	89.8	37.6	P	R2,R3	G3	P	R2,R3	G2,G3
HAL	Halifax, N.S., Canada	IDA	40.3	38.7		R2,R3			R2	
TOL	Toledo, Spain	WWSS	82.9	50.5	P			P		
BCAO	Bangui, Central Afr. Rep.	SRO	114.3	77.1			G1			G1
BOCO	Bogotá, Colombia	SRO	26.5	113.5		R2,R3	G2		R2,R3	G2,G3
ZOBO	Zongo Valley, Bolivia	ASRO	44.1	135.8	P		G2	P		G2
ARE	Arequipa, Peru	WWSS	42.1	139.5	P			P		
NNA	Nana, Peru	WWSS,IDA	35.4	143.4	P			P		
LPA	La Plata, Argentina	WWSS	63.9	143.4	P			P		
TLL	Tololo, Chile		53.3	150.0	P					
SNZO	South Karori, New Zealand	SRO	98.3	229.6	P	R2	G1,G2	P	R1,R2	G1,G2
CTAO	Charters Towers, Australia	ASRO	118.8	255.9	P	R1,R2	G2,G3		R1,R2	G1,G2
GUA	Guam, Mariana Island	IDA	110.7	291.8		R2			R2	
GUMO	Guam, Mariana Island	SRO	110.7	291.8		R1,R2	G2,G3	P	R1,R2	G2,G3
TATO	Taipei, Taiwan	SRO	123.3	315.8	P	R1,R2		P	R1,R2	G3
MAJO	Matsushiro, Japan	ASRO	105.0	315.9	P	R2	G1,G2	P	R2,R3	G2,G3
MAT	Matsushiro, Japan	WWSS	105.0	315.9	P			P		
ERM	Erimo, Japan	IDA	98.8	318.5		R2			R2	
LON	Longmire WA, USA	DWWSS	36.0	332.4	P			P		
KMY	Kunming, PRC	IDA	133.8	333.1		R1,R2			R1,R2	
CMO	College, Alaska, USA	IDA	58.6	337.6		R2,R3			R2,R3	

2.2 Surface-wave Inversion

We use the inversion method described by Kanamori and Given (1981) for long-period surface waves to determine the source parameters from Rayleigh and Love waves recorded on the GDSN and IDA network. We filter all phases R1-R3 and G1-

G3 between 60 and 1500 seconds, and discard the R1 and G1 waves contaminated by nonlinear transients. We first compute the amplitude and phase spectra of both Rayleigh and Love waves at a period of 256 s. Redundant pairs (e.g., R1 and R3) give consistent results in most cases, ensuring the good quality of the data.

We then invert the spectral data to obtain the five moment tensor elements M_{xx}, M_{yy}, M_{xy}, M_{zx} and M_{zy}, assuming that the isotropic component is zero. However, as discussed by Kanamori and Given (1981), two of the five elements, M_{zx} and M_{zy} become indeterminate for shallow (d $\leq$ 30 km) events. In order to overcome this difficulty we invert the data, using three different sets of constraints.

First, following Kanamori and Given (1981), we set $M_{xz}=M_{yz}=0$, which is equivalent to restricting the solution either to a 45° dip-slip or to a vertical strike-slip fault. Despite this restriction, the solutions obtained with these constraints provide useful gross estimates of fault geometry and seismic moments. In the following, these solutions are called "constrained moment tensor solutions."

An alternative method is to use the P-wave first-motion data to determine the source parameters that are not resolvable by surface-wave data. Implicit in this method is the assumption that the same fault geometry is responsible for both P and surface-wave radiations. It is often possible to determine one of the nodal planes by P-wave first-motion data. In such a case, we constrain the parameters (dip angle and strike) of this nodal plane and invert the surface-wave data to determine the other nodal plane and the seismic moment. We call this type of solution "fault constrained solution."

When the P-wave data do not completely constrain one of the nodal planes, we use a third method described in detail by Kanamori (1983). In this method, we
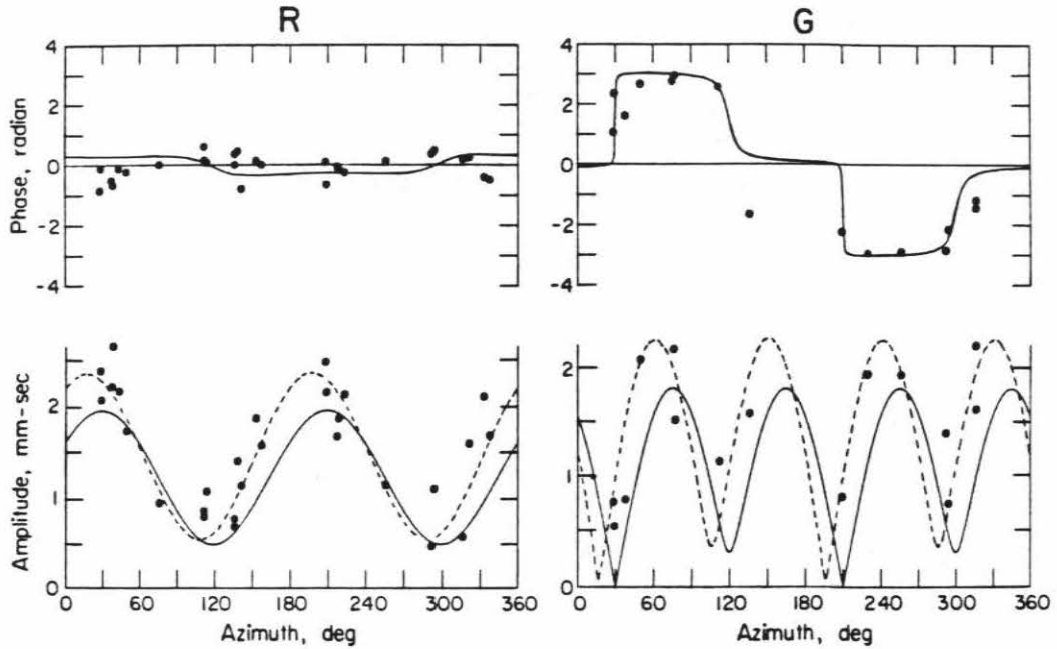
Figure 2.4: Phase and amplitude spectra of Rayleigh and Love waves at 256 sec period of the 1982[1] Ometepec earthquake (June 7, 1982, 06^{h}52^m). The phase spectra have been corrected for source finiteness using τ=12sec. The solutions are listed in Table 2.3. The solid curves are for the solution obtained by inversion of the amplitude and phase data and the dotted curves are for the solution obtained from the amplitude data alone.
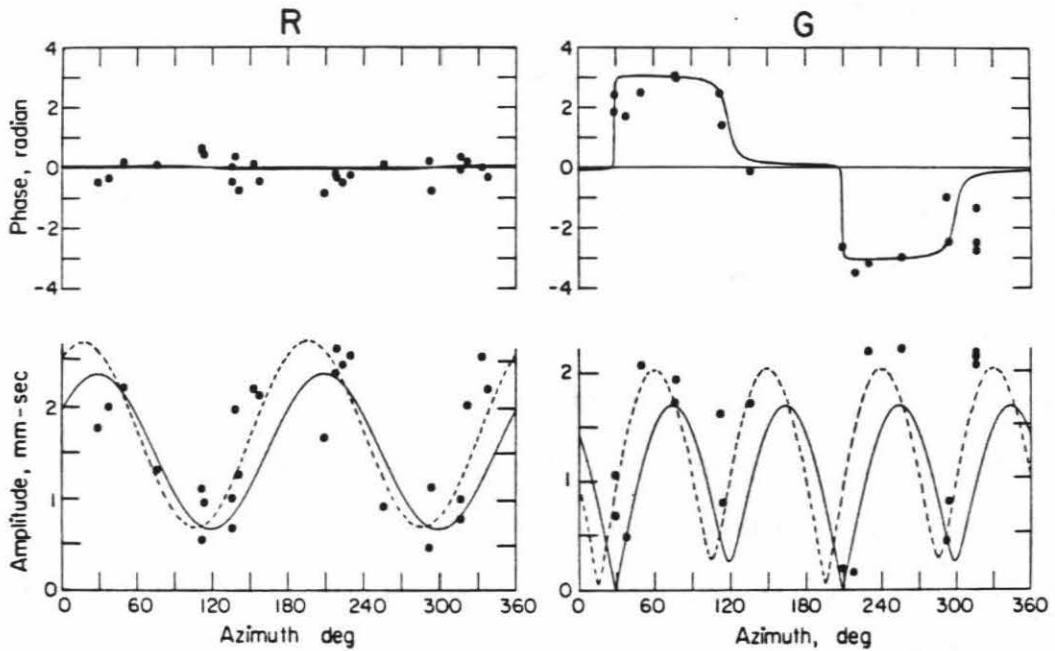
Figure 2.5: Phase and amplitude spectra of Rayleigh and Love waves at 256 sec period of the 1982[2] Ometepec earthquake (June 7, 1982, 10^h59^m). The phase spectra have been corrected for source finiteness using $\tau=16$sec. The solutions are listed in Table 2.3. The solid curves are for the solution obtained by inversion of the amplitude and phase data and the dotted curves are for the solution obtained from the amplitude data alone.

constrain M_{zx} and M_{zy} with respect to the moment tensor element with the largest absolute value, M_r, (i.e., $M_r = M_{xy}$, $M_{xx} + M_{yy}$ or $M_{xx} - M_{yy}$) such that the ratios $\alpha = M_{zy}/M_r$ and $\beta = M_{zx}/M_r$ are consistent with P-wave first-motion data. Hereafter, we call this solution "P-wave constrained solution."

The fault finiteness and the finite rise time of the source dislocation function introduce a source phase delay. For events with fault lengths less than 100 km, this effect can be included by use of a source process time τ, which can be empirically estimated from the earthquake magnitude (Kanamori and Given, 1981, Nakanishi and Kanamori, 1982). The source process times τ obtained from Table III of Kanamori and Given (1981) for the first and second events of the Ometepec doublet are 12 and 16 seconds, respectively. For the inversion, we use a point source at a depth of 33 km for the first event and 16 km for the second event. Although the source depth cannot be resolved in detail by long-period surface waves, they do indicate that both events are shallow. Results of the inversion using the three methods described above are listed in Tables 2.2 and 2.3. Table 2.2 presents a comparison of the constrained solution and the P-wave constrained solution for which the two fault planes are listed. The source parameters determined by inversion of surface-wave data with the steeply dipping nodal plane (dip and strike) constrained by the P-wave first-motion data are given in Table 2.3 and shown in Figures 2.8 and 2.10. In this inversion, the depth and source process time τ are the same as those used in the moment tensor inversions.

The solutions obtained by all three methods have about the same strike and slip angle that are consistent with subduction of the Cocos plate beneath Middle America. The similarity of these solutions indicates that the surface waves and the body waves are radiated from sources with similar geometry for these two earthquakes. Since the

Table 2.2: Constrained Solutions of Moment Tensor Inversion

DATA	1982^1		1982^2	
	$T = 256$ s,d $= 33$ km,$\tau = 12$ s		$T = 256$ s,d $= 16$ km,$\tau = 16$ s	
Inversion Constraints	$M_{xz}=M_{yz}=0$	$\alpha=-0.42$ $\beta=+0.96$ $M_r=M_{xx}+M_{yy}$	$M_{xz}=M_{yz}=0$	$\alpha=+0.16$ $\beta=-1.96$ $M_r=M_{xx}+M_{yy}$
M_{xy} #	0.041 ± 0.007	0.041 ± 0.007	0.035 ± 0.008	0.036 ± 0.008
$M_{xx}-M_{yy}$	0.046 ± 0.012	0.046 ± 0.012	0.044 ± 0.013	0.049 ± 0.013
$M_{xx}+M_{yy}$	-0.126 ± 0.010	-0.119 ± 0.011	-0.113 ± 0.011	-0.114 ± 0.014
M_{yz}	0.0	0.051 ± 0.0	0.0	0.008 ± 0.0
M_{xz}	0.0	-0.115 ± 0.0	0.0	-0.096 ± 0.0
$M_o(10^{26}$dyne–cm$)$	1.26	1.76	1.13	1.53
Dip (δ)	$45.0°$	$21.2°$, $68.9°$	$45.0°$	$25.8°$, $66.1°$
Strike (ϕ)	$300.3°$	$303.6°$, $115.5°$	$298.9°$	$307.2°$, $103.5°$
Slip (λ)	$90.0°$	$97.5°$, $87.1°$	$90.0°$	$111.5°$, $79.9°$
% minor D-C	7.86 %	12.79 %	7.62 %	7.83 %

unit of the moment tensor elements is in 10^{27}dyne–cm

Table 2.3: Fault Constrained Solutions

DATA	1982^1 T$=256$ s, d$=33$ km, $\tau = 12$ s		1982^2 T$=256$ s, d$=16$ km, $\tau = 16$ s	
	Ampl. - Phase	Amplitude	Ampl.- Phase	Amplitude
M_o (10^{26} dyne-cm)	2.35	2.82	2.42	2.75
Dip (δ)	$77.0°,13.0°$	$77.0°,13.0°$	$78.0°,12.0°$	$78.0°,12.0°$
Strike (ϕ)	$116.0°,296.7°$	$116.0°,277.2°$	$116.0°,302.4°$	$116.0°,274°$
Slip (λ)	$88.3°,97.0°$	$94.3°,69.5°$	$88.7°,96.0°$	$94.9°,68.0°$
R.M.S.	0.47	0.05	0.53	0.12
M_W	6.85	6.90	6.86	6.89

steeply dipping nodal plane is very tightly constrained by the body-wave data, we prefer the fault constrained solutions given in Table 2.3, which include the results of inversion of the amplitude data alone, which show slightly higher moments than those obtained by inversion of both amplitude and phase data. This trend is caused by a slight mismatch of the phase data due to the lateral heterogeneity of the earth, and is commonly seen in this type of inversion (see Lay et al., 1982, Nakanishi and Kanamori, 1982). The comparison of the data with the calculated amplitude and phase spectra is shown in Figures 2.4 and 2.5. The continuous line is the result of the amplitude and phase data inversion and the dashed line is the result of the amplitude inversion. In view of the good fit to the amplitude data, we use the results obtained by inversion of amplitude data in the following discussion.

As a check on the source models obtained from the inversion of amplitude and phase data from surface waves (Table 2.3), synthetic seismograms of Rayleigh and Love waves were computed following the method described in Kanamori and Cipar (1974). The first 100 fundamental spheroidal and toroidal modes were used in the calculation, assuming a step dislocation and a point source at 33 and 16 km for each event of the doublet, respectively. Figures 2.6 and 2.7 show the agreement between the observed and synthetic waveforms, filtered from 120 to 1500 sec, for the stations used in the inversion (Table 2.1). The fit between the Rayleigh waves is better than that of the Love waves, since at 120 sec period the latter are more affected by the shallow lateral heterogeneities in the upper mantle than Rayleigh waves. The average seismic moment for the first event from Rayleigh waves is $2.4 \pm 1.1 \times 10^{26}$ dyne cm and from Love waves it is $4.5 \pm 2.3 \times 10^{26}$ dyne cm . For the second event it is $2.1 \pm 0.7 \times 10^{26}$ dyne cm from Rayleigh waves and from Love waves is $5.3 \pm 3.0 \times 10^{26}$
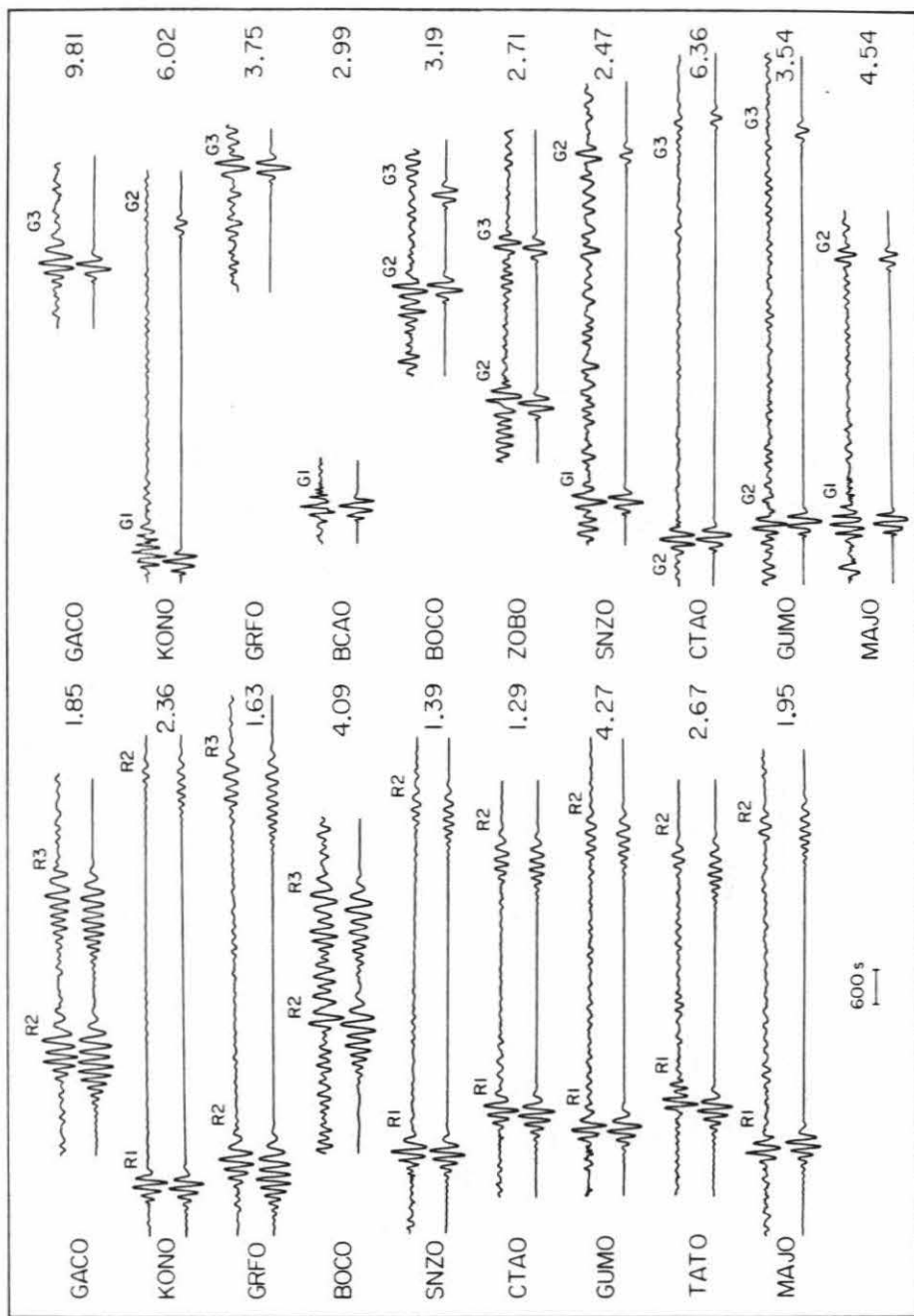
Figure 2.6: Rayleigh and Love waves observed (upper) and synthetic (lower) seismograms, filtered between 120 and 1500 sec period for the 1982[1] Ometepec earthquake (June 7, 1982, 06^{h}52^m). The fault parameters used to calculate the synthetics are those listed in Table 2.3 for the inversion using amplitude and phase data. The numbers to the right of each record pair indicate the seismic moment, in units of 10^{26} dyne cm, that would be obtained using that record alone.
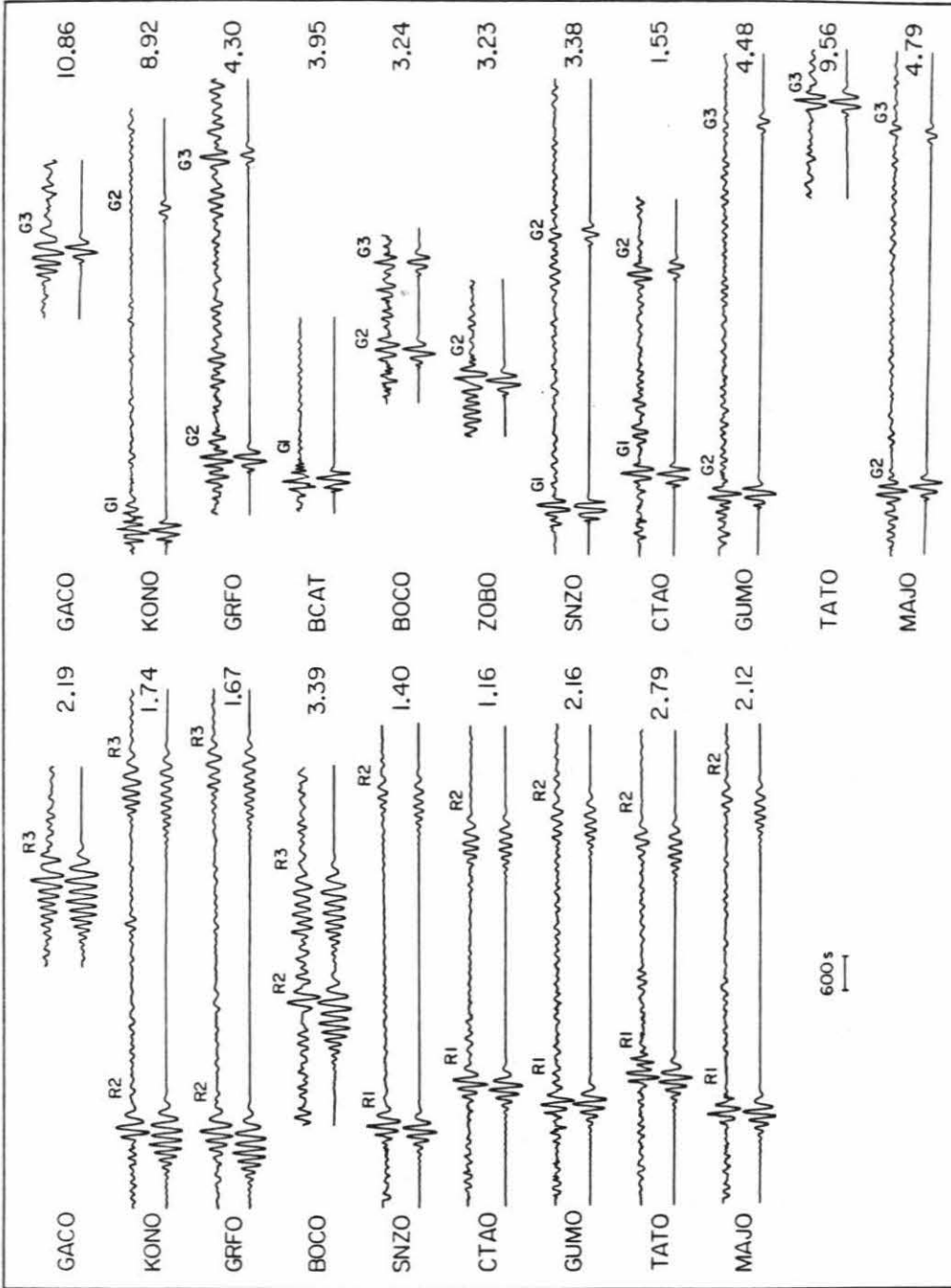
Figure 2.7: Observed and calculated surface waves for the 1982[2] Ometepec event (June 7, 1982, 10^{h}59^m). Fault parameters used are listed in Table 2.3 for the amplitude and phase data inversion. The numbers are the seismic moment determined from each record pair in units of 10^{26} dyne cm.

dyne cm . Overall the agreement observed between the waveforms is good and gives us confidence in the results of the inversion.

In 1982, as part of the U.S.G.S. monthly listing of epicenters, a preliminary moment tensor solution is given for all events $M > 5.5$ (Dziewonski et al., 1981). The fault parameters listed for the Ometepec doublet are: $M_o = 2.9 \times 10^{26}$ dyne cm, $\phi_1 = 268°$, $\delta_1 = 10°$, $\lambda_1 = 48°$, $\phi_2 = 130°$, $\delta_2 = 83°$ and $\lambda_2 = 9°$ for the first event and $M_o = 2.7 \times 10^{26}$ dyne cm, $\phi_1 = 286°$, $\delta_1 = 12°$, $\lambda_1 = 76°$, $\phi_2 = 121°$, $\delta_2 = 79°$, and $\lambda_2 = 93°$ for the second event. Our solutions agree reasonably well with these results.

2.3   Modeling of Body Waves

P-waves recorded by long-period seismographs of 22 WWSSN and GDSN stations (Table 2.1) are modeled for each event of the 1982 Ometepec doublet. Some of the P-waves modeled were recorded by stations of both seismic networks at the same location.

We compute synthetic seismograms using the method described in detail by Langston and Helmberger (1975) and Kanamori and Stewart (1976). First, the response of a homogeneous half-space to a point double-couple source with a trapezoidal time function defined by three time constants (t_1, t_2, t_3) (see Figure 9, Kanamori and Stewart, 1976) is computed. The direct P and surface-reflected phases pP and sP are included. Then the attenuation operator and the instrument response are convolved to obtain the synthetic seismogram. Using the synthetic seismograms thus computed, we determine the source orientation, depth and the dimensions of the trapezoidal time function. Near-nodal stations are important to determine the source

orientation. Although there is some trade-off between the source depth and time func-
tion in fitting the observed seismogram at a particular station, use of many stations
distributed over a large azimuthal range reduces this trade-off significantly.

In order to compare the fault parameters of the Ometepec doublet directly with
those of other large earthquakes along the Middle America trench, we use the same
velocity model as that used by Chael and Stewart (1982): $v_p = 6.1$ km/s, $v_s = 3.5$
km/s and $\rho = 2.6$ g/cm^3 . The Ometepec doublet has simple waveforms, like other
large shallow earthquakes ($M_S > 7$) along the Middle-America trench (Figure 1.3) and
also the smallest peak-to-peak amplitudes of the events displayed on the figure.

Figure 2.8 shows the observed and synthetic P-waves recorded at 22 WWSSN
and GDSN stations for the 1982[1] Ometepec event (June 7, 1982, 06^{h}52^m). The
source orientation can be resolved within a few degrees since near-nodal records are
available. The source time function obtained is (2,6,8) for a point source depth of 20
km. The depth and rupture time can be resolved within $\pm$ 3 km and $\pm$ 1 sec for a
given velocity model. The seismic moment at each station is given in Figure 2.8 and
the average moment at non-nodal stations within teleseismic distances (30° to 90°) is
$M_o = 1.5 \pm 0.4 \times 10^{26}$ dyne cm.

The second event of the Ometepec doublet is slightly more complicated than the
first one. This relative complexity is seen in the first pulse of WWSSN records, sug-
gesting a double source for this event. Initially the P-wave data were modeled with a
single source at a depth of 15 km and a source time function (7,10,17). The synthetic
seismograms fit the overall waveform of the observed records at most stations, but
not the near-nodal stations. A double-source model fits all the stations better. A
comparison of the single and the double-source model for a station near the radiation
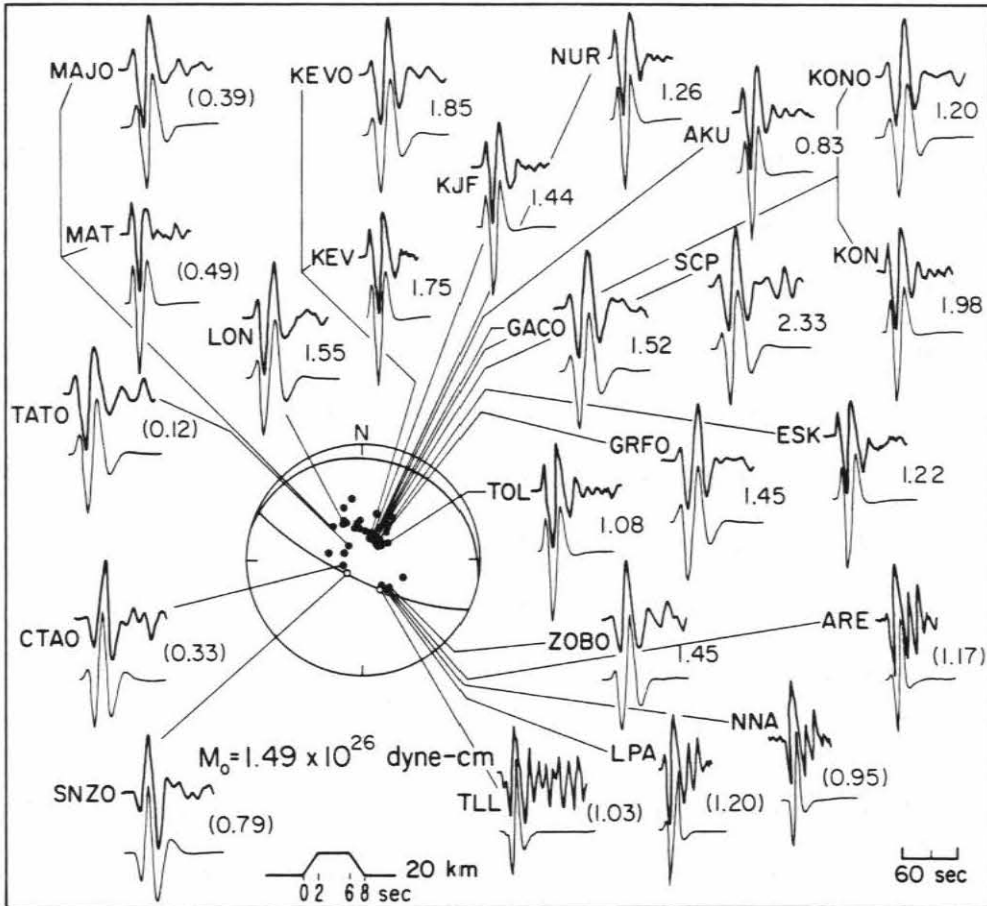
Figure 2.8: Observed (upper) and synthetic (lower) P-waves seismograms of the 1982[1] Ometepec event (June 7, 1982, 06^{h}52^m). The synthetics correspond to the focal mechanism, depth and source time function shown. The seismic moment at each station is given in 10^{26}dyne–cm. The average, M_o=1.49×10^{26}dyne–cm, is computed with the values of non-nodal stations within a distance range from 30° to 90°. Values in parentheses are excluded.

pattern maximum, KEV, and a near-nodal station, ARE, clearly shows (Figure 2.9) that the double source is better. The observed and synthetic P-waves recorded at 22 WWSSN and GDSN stations for the 1982^2 Ometepec event (June 7, 1982, 10^h59^m) are shown in Figure 2.10. The first source is at a depth of 15 km with a source time function (3,6,8) and contributes 25 % of the total seismic moment. The second source is located at 10 km depth with source time function and contributes 75 % of the total seismic moment of the event. The orientation of the sources is similar. The separation between the two sources can be resolved to within 1 second, the time constants of the source time function are determined to $\pm$ 1 second, and the contribution of each source to the seismic moment is accurate to 10 %. The depth of the first source is resolvable to within $\pm$ 3 km and the second source within $\pm$ 5 km. The orientation of the second source is controlled by the near-nodal stations (ZOBO, ARE, NNA, LPA) and its contribution to the total seismic moment by the waveforms at all stations. The seismic moment estimated at each station is given in Figure 2.10 and the average moment from non-nodal stations within 30° and 90° is $M_o=2.8\pm0.6\times10^{26}$ dyne cm.

Table 2.4: Results of Body Wave Modeling for the Ometepec Doublet

Event	Source time delay (s)	function (s)	% M_o	Depth (km)	Strike (ϕ)	Dip (δ)	Slip (λ)	M_o (10^{26}dyne–cm)
1982^1	0	(2,6,8)	100%	20	293°	13°	78°	1.49
1982^2	0	(3,6,8)	25%	15	296°	12°	90°	
	6	(2,6,10)	75%	10	285°	11°	66°	2.75
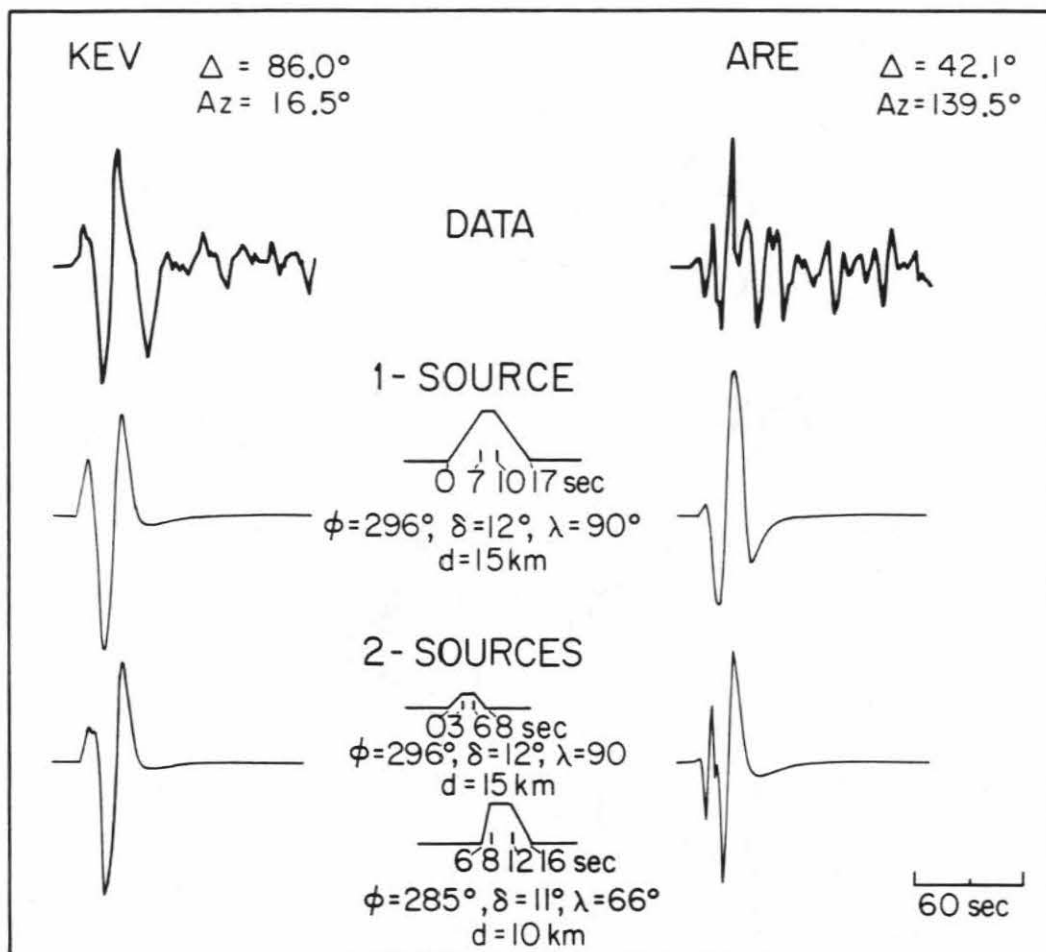
Figure 2.9: Comparison of 1-Source and 2-Source models for KEV and ARE. Notice that the 1-Source model can explain the overall waveform observed at KEV, but it fails to match that of ARE (near-nodal). The 2-Source model can fit the waveforms at both stations.
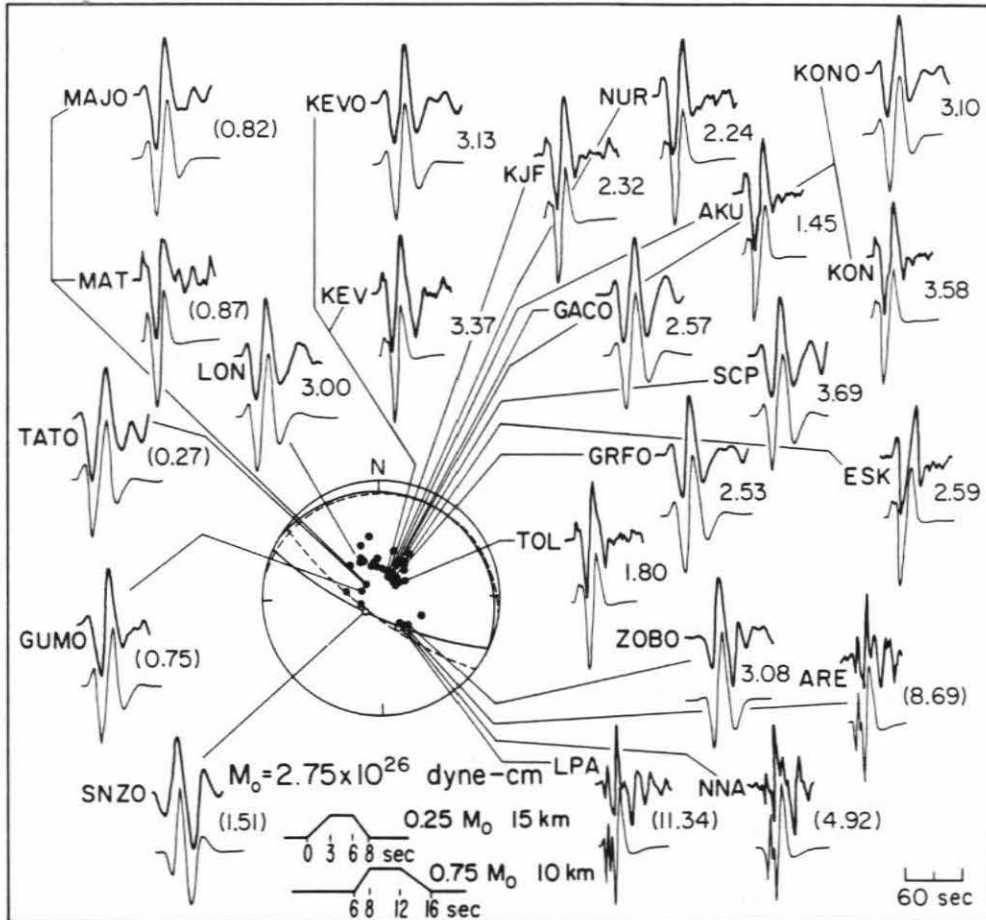
Figure 2.10: Observed (upper) and synthetic (lower) P-waves from of the 1982[2] Ometepec event (June 7, 1982, 10^h59^m). The focal mechanism in the middle indicates the geometry of the first source (continuous line) and the second source (dashed line) used for the P-wave modeling. The source time function, depth and the seismic moment ratio for each source are shown. The seismic moment at each station is given in 10^{26}dyne–cm. The values at non-nodal stations within a distance range from $30°$ to $90°$ are used to calculate the average seismic moment, $M_o=2.75\times10^{26}$dyne–cm . Values of stations in parentheses are not included.

Table 2.4 summarizes the results from the body-wave modeling. Although the absolute depths determined by the modeling of body waves are shallower than those reported by the U.S.G.S. (40.5 and 33.8 km, respectively), the trend that the first event is deeper than the second is consistent with the U.S.G.S. results. Our depths are in good agreement with those determined by a local network 25 and 8 km, respectively.

2.4   Tectonic Implications of the 1982 Ometepec Doublet

The results obtained by inversion of surface waves are in general consistent with those obtained by P-wave modeling. The seismic moments determined by the two methods are about the same for the second event of the doublet. However, for the first event the seismic moment determined by P-wave modeling is about half that obtained by surface-wave inversion (Tables 2.3 and 2.4).

The focal mechanisms indicate thrusting of the Cocos plate under the North America plate in a northeasterly direction, with a small right lateral component (Figures 2.8 and 2.10). These results are consistent with the relative plate motion (Minster and Jordan, 1978) and with local structures in the area, namely, the right lateral displacement of the Ometepec Canyon (Shipley et al., 1980). The source time function of the events is simple, as are those of other large events along the Middle America trench (Chael and Stewart, 1982).

An important aspect of the doublet occurrence is the triggering mechanism. Both of the Ometepec events have about the same seismic moment, 2.8×10^{26} dyne
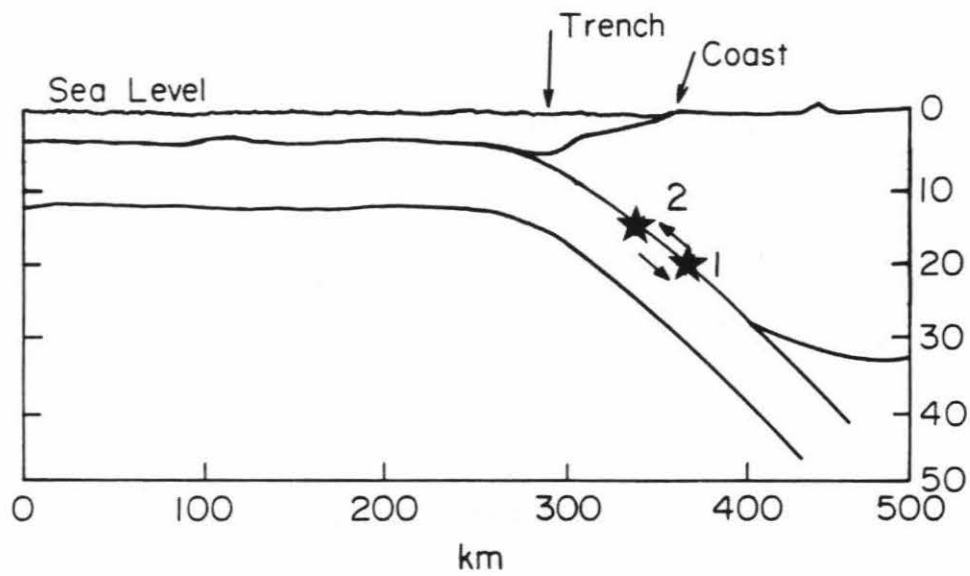
Figure 2.11: Profile of the Middle America trench near the Ometepec region after Couch and Woodcock (1981). Stars show the locations of the Ometepec doublets. Arrows indicate the relative motion between the plates. Note that the first event of the doublet is deeper than the second.

cm. The hypocenter of the first event is deeper and its source time function is shorter by a factor of two, suggesting that the first event represents failure of a smaller and deeper asperity, and the failure of the deeper asperity triggered the shallower one (Figure 2.11). The slip direction of the first event is perpendicular to the trench, forming a 13° angle with the convergence direction of the Cocos plate at the Ometepec region, whereas the slip direction of the main source of the second event is parallel to it. A similar difference between the slip vectors of the doublet events is also observed for the Solomon Islands doublets. The difference, however, is small, since the subduction along this boundary is not as oblique as in the Middle America trench. This difference may indicate that the first event of doublets reflects more local stress heterogeneities on the fault plane than the second one.

2.5 Doublets along the Middle-America Trench

Along the Middle-America trench, seismic doublets similar to the 1982 Ometepec doublet are relatively frequent. Here we define a doublet by a pair of large events with magnitude difference of no more than 0.2 units, spatial separation of less than 100 km, and temporal separation of less than 3 months. Table 2.5 lists doublets according to this definition along the Middle-America trench. Note that under this definition the first event of a doublet has smaller magnitude than the subsequent event, since in the other case the second event will be considered an aftershock of the first one and thus it becomes a matter of semantics. There are several regions in the world where doublets or multiplets occur frequently; the Solomon Islands region (Lay

and Kanamori, 1980; Wesnousky et al., 1986) and the South-West Japan (Ando, 1975) are among typical examples.

Table 2.5: Seismic 'Doublets' along the Middle America Trench

Region	Date	Time Hr.Min.	Location lat(°N)	Location long(°W)	Depth	M_S	Time Interval (hours)
6	May 11, 1962	1411	17.25	99.58	40	7.0	
	May 19, 1962	1458	17.12	99.57	33	7.2	192
7	June 7, 1982	0652	16.348	98.368	25	6.9	
	June 7, 1982	1059	16.399	98.538	8	7.0	4
8	Aug. 4, 1928	1828	16.83	97.61	S	7.4	
	Oct. 9, 1928	0301	16.34	97.29	S	7.6	1584
18	Apr.24, 1916	0802	11	85	S	7.3	
	Apr.26, 1916	0221	10	85	S	7.3	42

Lay and Kanamori (1980) argue that the existence of relatively large isolated asperities (areas with increased strength) on the fault contact plane is responsible for the frequent occurrence of doublets in the Solomon Islands region. Other important features observed for the Solomon Islands region include a relatively high plate convergence rate (11 cm/yr), and short (30 yr) recurrence times for large earthquakes. The subduction zone along the Middle-America trench exhibits many of these features as discussed in the previous section. Also, Singh et al. (1982b) found that the number of large earthquakes ($M_S \geq 7$) that have occurred since 1904 along the Mexican subduction zone is significantly larger than expected from the conventional magnitude-frequency relation. They suggest that the asperities responsible for these events have about the same size. This relatively uniform asperity size may be a favorable factor for the occurrence of doublets.

Chapter 3

The Rupture of the Michoacan Seismic Gap: 1981-1986

3.1 Introduction

The Michoacan seismic gap was originally identified by Kelleher et al. (1973). Later, however Singh et al. (1980a) reassessed the seismic potential of the Michoacan gap to suggest that, due to the presence of the Orozco fracture zone, this segment of the Cocos-North American plate boundary may be aseismic or may have longer recurrence periods than adjacent segments along the Mexican subduction zone. In recent years several large earthquakes have occurred in the Michoacan gap: The Playa Azul (M_S=7.3) earthquake on October 25, 1981 (18.048° N, 102.084° W Havskov et al., 1983), which occurred in the center of the Michoacan Gap; then on September 19, 1985, the Michoacan (M_S=8.1) earthquake occurred to the northwest of this seismic gap, and on September 21, another large (M_S=7.5) event occurred to the southeast of the gap; the latest large event (M_S=7.0) of this sequence occurred on April 30, 1986, close to the northwest boundary of the former Michoacan gap.

The September 19, 1985 Michoacan, Mexico earthquake with M_S=8.1, was the most serious natural disaster to date in Mexico's history; the earthquake caused over 10,000 deaths in Mexico City and left an estimated 250,000 homeless. The epicenter from the National Earthquake Information Center (NEIC) in Golden, CO, is 18.27°N, 102.31°W, with an origin time of 13h 17m 48.1s U.T. The major aftershock, itself a

large earthquake with $M_S=7.5$, occurred 115 km southeast of the main shock on September 21 at 01h 17m 13.6s U.T., at 17.81°N, 101.65°W. Another large aftershock occurred on April 30, 1986 ($M_S=7.0$), about 50 km northwest of the main event at 7h 7m 18.8s, at 18.405°N, 102.979°W. These locations are for a fixed depth of 33 km (Figure 3.1). The epicenters given by the local network are for the main shock 18.141°N, 102.707°W, and for the September 21 aftershock 17.618°N, 101.815°W, both hypocenters are fixed at 16 km depth (UNAM Seismology Group, 1986). The 1981 Playa Azul earthquake local epicenter is 17.75°N, 102.25°W with the depth fixed at 20 km (Havskov et al., 1983).

The most severe damage from the earthquake occurred in Mexico City, 350 km away from the epicenter, where over 800 buildings suffered severe structural damage, including several collapses. The structural damage was concentrated in a well-defined area of the city, where ground accelerations of 0.2 g were recorded with a strong spectral peak centered at a frequency of 0.5 Hz (Prince et al., 1986). Apart from Mexico City, severe damage also occurred in the town of Ciudad Guzman in Jalisco, 250 km from the epicenter. Damage in the epicentral area consisted of landslides in road cuts and river canyons, bent railroad tracks, and structural damage to bridges and to the Morelos Dam curtain. Other coastal cities were relatively undamaged. The unprecedented amount of damage in Mexico City raised the question of whether the earthquake source was inherently different from typical Middle-America subduction zone events. Amplifications of intensities and ground accelerations had been observed in Mexico City from other earthquakes, and had been attributed predominantly to a site effect caused by an old lake basin that underlies the city (Bufaliza, 1984; Duke and Leeds, 1959).

Chapter 3 presents a detailed analysis of the teleseismic source characteristics of the recent events that occurred in the Michoacan gap. We infer the slip and stress distribution in this region and determine the differences between the September 19, 1985 earthquake and previous events occurring along the Mexican trench. In addition, we summarize the faulting mechanism and seismic moment results by other investigators and the historic seismicity in this region.

3.2 Summary of Historic Seismicity near the Michoacan Gap

Figure 3.1 shows the aftershock areas of all large (M≥7) shallow thrust events that have occurred offshore coastal Mexico since 1950. Segments of the plate interface immediately adjacent to the Michoacan gap have experienced recent events at short and regular intervals. To the northwest, the Colima area recently had events in 1941 and 1973 (a 32 year interval). In 1957, the Acapulco earthquake (M_S=7.5) occurred in southern Guerrero. This event was also damaging in Mexico City, but the number of structures experiencing complete collapse was far less than for the September 1985 earthquake. South of the Acapulco event, the plate interface is fairly well filled in with recent large earthquakes: the 1982 Ometepec doublet, and the Oaxaca earthquakes of 1968 (M_S=7.5), 1978(M_S=7.8) and 1965(M_S=7.6). The dashed region shown in Figure 3.1 is the aftershock zone of the 1932 Jalisco earthquake (M_S=8.1), the largest earthquake in Mexico prior to 1985 (Singh, et al., 1985a). This event ruptured the interplate boundary between the Rivera and North American plates and has a longer recurrence interval.
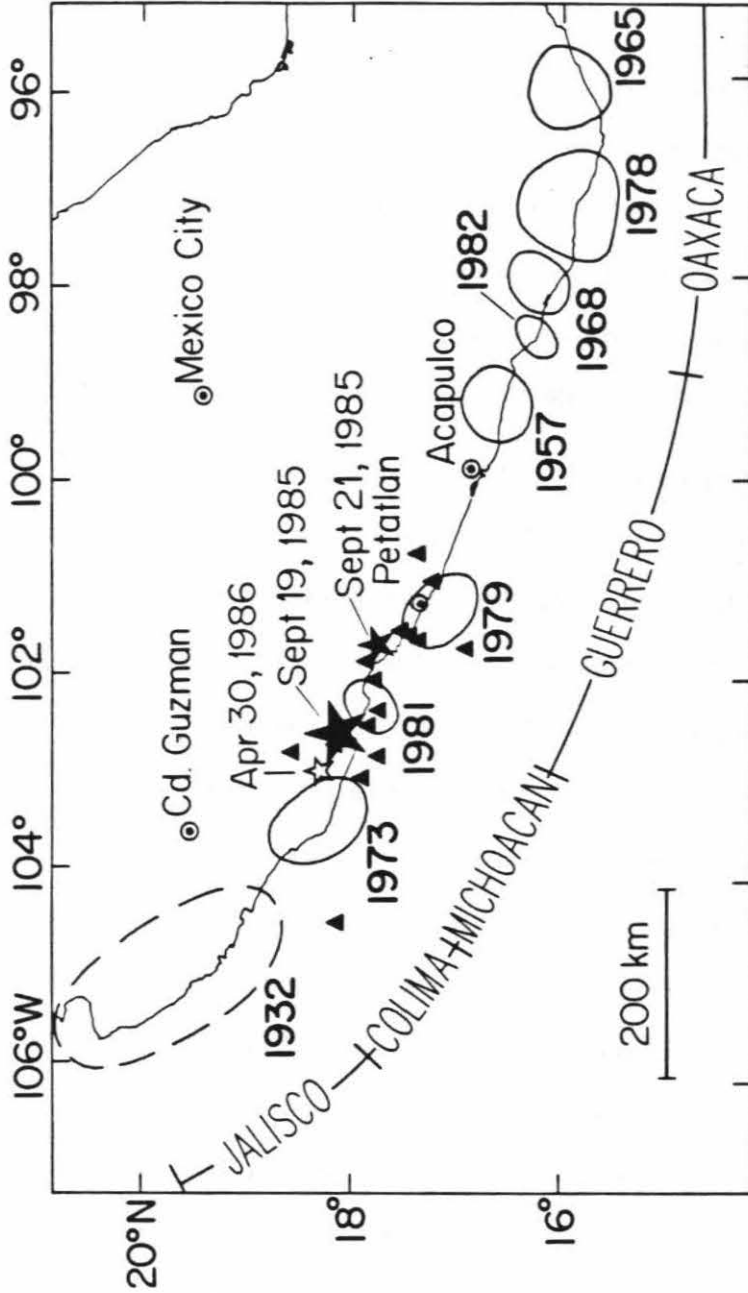
Figure 3.1: Map of central Mexico showing the aftershock areas (ellipses) of interplate thrust events since 1950 with M>7. The September 1985 Michoacan earthquake is plotted as a filled star, and its $M_S=7.5$ aftershock as a smaller star. The epicenter of the $M_S=7.0$ aftershock of April 30, 1986 is shown as an open star. Other plotted symbols are preliminary locations of the one-month aftershocks from NEIC. The dashed region is the aftershock area of the $M_S=8.1$ 1932 Jalisco earthquake.

The area between the 1973 Colima earthquake and the 1957 Acapulco earthquake had been designated a seismic gap in several studies of global earthquake activity (Figure 1; Kelleher et al., 1973; McCann et al., 1979). Depending on consideration of a large earthquake in 1943 in the center of this segment, the area was discussed as either a single gap of large dimensions ($\approx$400 km), or two separate gaps to the north and south of the 1943 event. In 1979 the Petatlań earthquake occurred in the center of the segment at the same location as the 1943 event, clearly separating the region into two quiescent zones designated the Michoacan and the Guerrero gaps, each approximately 150 km long (Singh et al., 1981).

The last large earthquake (M_S=7.9) in the Michoacan gap was in 1911; its location had been determined by Gutenberg and Richter (1954). On the basis of damage reports of the 1911 earthquake and the relocation of an aftershock, Singh et al. (1980a) suggested that the event was not located offshore Michoacan but about 200 km further northwest in Jalisco (19.7° N, 103.7° W). This suggestion and the lack of other large Michoacan earthquakes in the historic record (see Figure 1.2) led several researchers to consider that the Michoacan area might be a "permanent" seismic gap due to the influence of the Orozco fracture zone (Singh et al., 1980a; McNally and Minster, 1981). Locally, the fracture zone is a broad area of disturbed seafloor that intersects the Middle-America trench for about 150 km in the Michoacan area. One possible explanation of the lack of large earthquakes in Michoacan was that the Orozco fracture zone was affecting the subduction process locally such that the area was subducting aseismically, or at least more slowly than adjacent regions of the plate boundary. In southern Oaxaca where the Tehuantepec Ridge is subducting, there are likewise no known large (M>7) earthquakes in the historic record since at

least 1800 (Figure 1.2, region 11). Alterations of subduction characteristics such as local decrease in seismicity, a local change in the dip and depth extent of the Benioff zone, and a local change in the stress axes of earthquakes have been observed in many other circum-Pacific regions where ridges, fracture zones, and other areas of topographically anomalous seafloor are subducting (Kelleher and McCann, 1976; Vogt et al., 1976). The occurrence of the great earthquake in Michoacan in 1985 suggests that the seismic potential of areas similar to the previous Michoacan gap, such as southermost Oaxaca near the Tehuantepec Ridge, should be carefully examined.

3.3 Earthquakes in the Michoacan Region

In 1981, the Playa Azul earthquake (M_W=7.3) occurred in the center of the Michoacan gap (Figure 3.1). Its aftershock area, seismic moment and inferred slip indicated that the event was not large enough to fill the gap (Havskov et al., 1983; LeFevre and McNally, 1985). This event was widely felt in southern Mexico, causing damage in the state of Michoacan and in Mexico City, where 11 people were injured and one person died.

The epicenter of the September 19, 1985 earthquake was located in the northern segment of the Michoacan gap between the 1973 and the 1981 aftershock zones, as shown by the large star in Figure 3.1. Preliminary locations from NEIC of aftershocks that occurred within one month of the earthquake are indicated by filled triangles. Events are shown only if 10 or more arrival times were reported and magnitude was ≥3.5. The aftershocks generally lie between the limits of the 1973 and 1979 zones, and there is some indication that there was less aftershock activity within the

small zone that slipped in the Playa Azul earthquake. The largest aftershock $(M_S=7.5)$ occurred approximately 36 hours after the main shock, on September 21 (small filled star), in the southern portion of the gap between the 1981 and 1979 aftershock zones. A portable seismic network was installed near the epicentral area a few hours after the main shock occurred by the Seismology Group of the National University of Mexico (UNAM). They determined that the one-week aftershock areas for the September 19 and 21 events were 170×50 km^2 and 66×33 km^2, respectively. They noticed that all the aftershocks associated with the main shock were shallower than 30 km and defined a plane dipping at a shallow angle (10 to 15°) northeastward from the trench. Some of these events fell within the rupture area of the 1973 Colima earthquake, but only a few aftershocks were located within the 1981 Playa Azul aftershock zone. The aftershocks of the September 21 event partially overlap with the 1979 Petatlań rupture zone; however, they were located predominantly updip of the Petatlań aftershocks (UNAM Seismology Group, 1986). After several months of decreasing seismic activity in the Michoacan region, a large aftershock $(M_S=7.0)$ occurred on April 30, 1986. This event was located about 50 km northwest of the September 19 earthquake (open star in Figure 3.1).

Coseismic coastal uplift from the great Michoacan earthquake was evidenced by large scale mortality of intertidal organisms. The uplift was of the order of 100 cm in the northern part of the main shock rupture zone was measured by Bodin and Klinger (1986), and decreased to only 15 to 30 cm toward the southeast along the coast of Guerrero, probably because the trench axis is farther from the coast in this region; however, they saw no evidence of subsidence. Ortega et al. (1985), after reconnaissance of the epicentral area, reported fractures on a NW-SE direction, local

collapses of about 100 cm and liquefaction and mud volcanoes associated with the intensely fractured regions. The local tsunami was about 2.5 m at Zihuatanejo, Guerrero, causing only minor damage to coastal structures.

In light of the September 1985 Michoacan earthquake, we reconsidered the location of the 1911 event, placed offshore Michoacan by Gutenberg and Richter (1954) and in Jalisco by Singh et al. (1980a). The literature indicates that the intensity pattern of the 1911 event is similar to the 1985 earthquake, suggesting a similar epicenter near coastal Michoacan. For example, the "center of disturbance" in terms of deaths, damage to homes, and strong shaking from the 1911 event was placed near Ciudad Guzman in Jalisco (Branner, 1912; Figueroa, 1959). This town was also severely impacted by the 1985 Michoacan earthquake in terms of damaged homes and deaths. Further, the 1911 event caused fatalities in Mexico City and had the highest intensity in the city (VIII) of any earthquake during the reporting period of 1900-1959 (Figueroa, 1959). Thus, the 1911 event may have been felt as strongly in Mexico City as the 1985 earthquake, but was less damaging there because of the smaller population and smaller degree of urban development in 1911. We reexamined the supporting material for Gutenberg's epicenter determination (Goodstein et al., 1980) and found that time difference between S and P waves from 3 stations in Mexico (Mazatlan, Oaxaca and Merida) and one direct P-time from Tacubaya (Mexico City) were included among the 20 arrival times used to determine their epicenter. The conclusion of Singh et al. (1980a) that the event had actually occurred in Jalisco was strongly based on the earthquake's destructive effects in Ciudad Guzman. Considering the similarity of the intensity patterns of the 1911 and 1985 events, and the fact that arrival times from nearby stations had been used in the original location, we take the

Michoacan location of Gutenberg and Richter (1954) as the more likely epicenter for the 1911 earthquake. This epicenter is at 17.5°N, 102.5°W, 87 km south of the September 1985 Michoacan earthquake. With the 1911 event, the estimate of the recurrence period of large subduction earthquakes in the Michoacan area is 74 years. Astiz and Kanamori (1984) determined observed recurrence periods for the Colima and Petatlań segments adjacent to the Michoacan segment at 21.3 ± 10.5 yr and 35.5 ± 0.7 yr, respectively.

Last century the large earthquake of November 23, 1837 ($M\approx7\ 3/4$) may have occurred near or in the Michoacan gap region. The epicenter listed by Singh et al. (1981) is 20.0°N, 105.0°W, in the Jalisco region; however, damage reports gathered by Singh (written communication) and Orozco y Berra (1887) indicate that this event was widely felt in southern Mexico, especially in the states of Michoacan and Guerrero. This earthquake caused considerable damage to the cities of Guadalajara and Mexico (Figure 3.1), where it was described as "extraordinary for its strength and duration." In Acapulco the motion was described as "ondulatory type" and it was suggested that it may have occurred elsewhere. This event was also felt strongly in the city of Oaxaca. Note that the population density in the early 1800's in the Michoacan coast was scarce; thus, if this earthquake actually occurred in this region it may have gone unnoticed. To the north, in the coastal cities of Manzanillo and Puerto Vallarta, it was reported only as "felt" but there were no reports of extraordinary damage or tsunami. The September 19, 1985 earthquake was also widely felt throughout southern Mexico, especially in the states of Guerrero and Michoacan, suggesting that the 1837 earthquake may have occurred in or near the Michoacan gap region. If we assume that the 1837, 1911 and 1985 events broke a similar segment of

the Middle-America trench, then the recurrence period for this region is 74 years; however, location errors for the 1837 and 1911 events are at least of the order of 1°.

3.4 Teleseismic Source Characteristics from Body-wave Modeling

Forward modeling of teleseismic P waves over a wide azimuthal range was done to determine the focal mechanism, point source depth, and source time function of the recent earthquakes that occurred in the Michoacan gap, using the geometric ray approach described in Langston and Helmberger (1975) and Kanamori and Stewart (1976). Initial control on the focal mechanism was provided by numerous P-wave first motion data read from long-period WWSSN seismograms. The first motion data constrain one steeply dipping nodal plane in most cases and the orientation of the second plane was resolved with waveform modeling. Three rays (P, pP and sP) were used and half-space velocities of v_P=6.2km/s and v_S=3.5km/s with a density of ρ=2.6g/cm^3 were assumed.

The Playa Azul Earthquake

Modeling of 17 long-period WWSSN P-waves of the October 25, 1981 Playa Azul earthquake indicates that this event has two point sources at 27 km depth with a total duration of 15 s as shown in Figure 3.2. The first source contributes to 15% of the total seismic moment. The fault parameters determined from the P-waves are theta=285°, δ=11°, λ=75° and are consistent with previous studies (Havskov et al., 1983; LeFevre and McNally, 1985). The average seismic moment recovered from non-diffracted P-wave is 7.2×10^{26} dyne cm. The epicenter given by Havskov et al (1983) for the Playa Azul event (17.75°N, 102.25°W) had a fixed depth at 20 km;
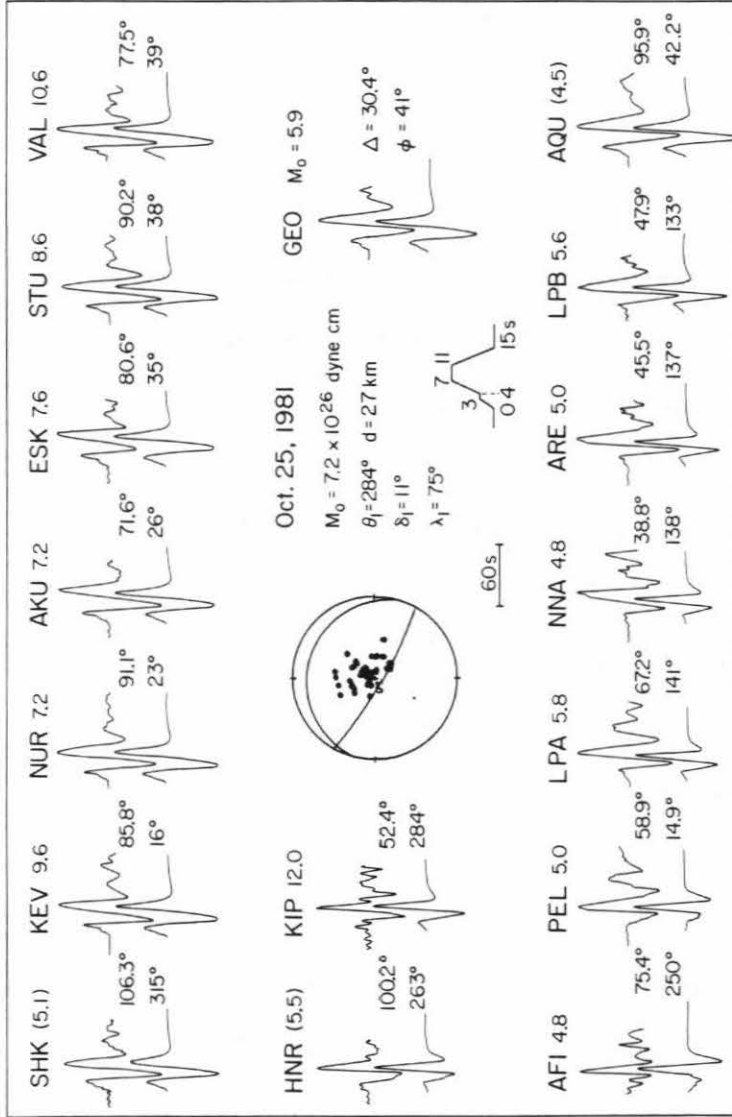
Figure 3.2: Upper traces (observed) are long-period WWSSN P-waves of the October 25, 1981 Playa Azul (M_w=7.3) earthquake. The synthetic seismograms (lower traces) are for a double source 27 km deep, and the shallow thrust fault mechanism shown. The first source contributes to 15% of the total seismic moment M_o=7.2×10^26 dyne cm.

however, the aftershocks with good depth determinations were as deep as 26 km. They also point out that the aftershocks are clustered in two groups on either side of the mainshock location, suggesting the presence of two asperities. This is also consistent with the source time function determined above.

The September 19, 1985 Michoacan Earthquake

The focal mechanism of the great Michoacan earthquake that occurred on September 19, 1985, was constrained by numerous P-wave first motion data read from long and short-period WWSSN seismograms that were offscale for most stations with large magnification, but mostly the first motion direction was clear. First motion data are plotted in Figure 3.3 and listed in Table 3.1. The first motion data constrain one steeply dipping nodal plane with dip 81° and strike 127°.

Figure 3.3 shows observed P wave seismograms from 12 WWSSN stations and one GEOSCOPE station (SSB) and synthetic seismograms calculated for the focal mechanism, point source depth, and time function that provided optimal waveform fit for the mainshock. The time function is a multiple source consisting of two trapezoids of equal duration (16 s) and seismic moment, with the second source beginning 26 s after the first on average. The point source depth is 17 km, and the focal mechanism shows an overall thrust geometry on a low-angle plane ($\delta=9°$, $\theta=288°$, $\lambda=72°$). The horizontal projection of the slip vector orientation is N39°E, which agrees with the local convergence direction of the Cocos plate calculated at the epicenter from the RM2 pole of rotation (Minster and Jordan, 1978). The seismic moment estimated from the P wave amplitudes is $7.2 \pm 1.6 \times 10^{27}$ dyne cm. Many of
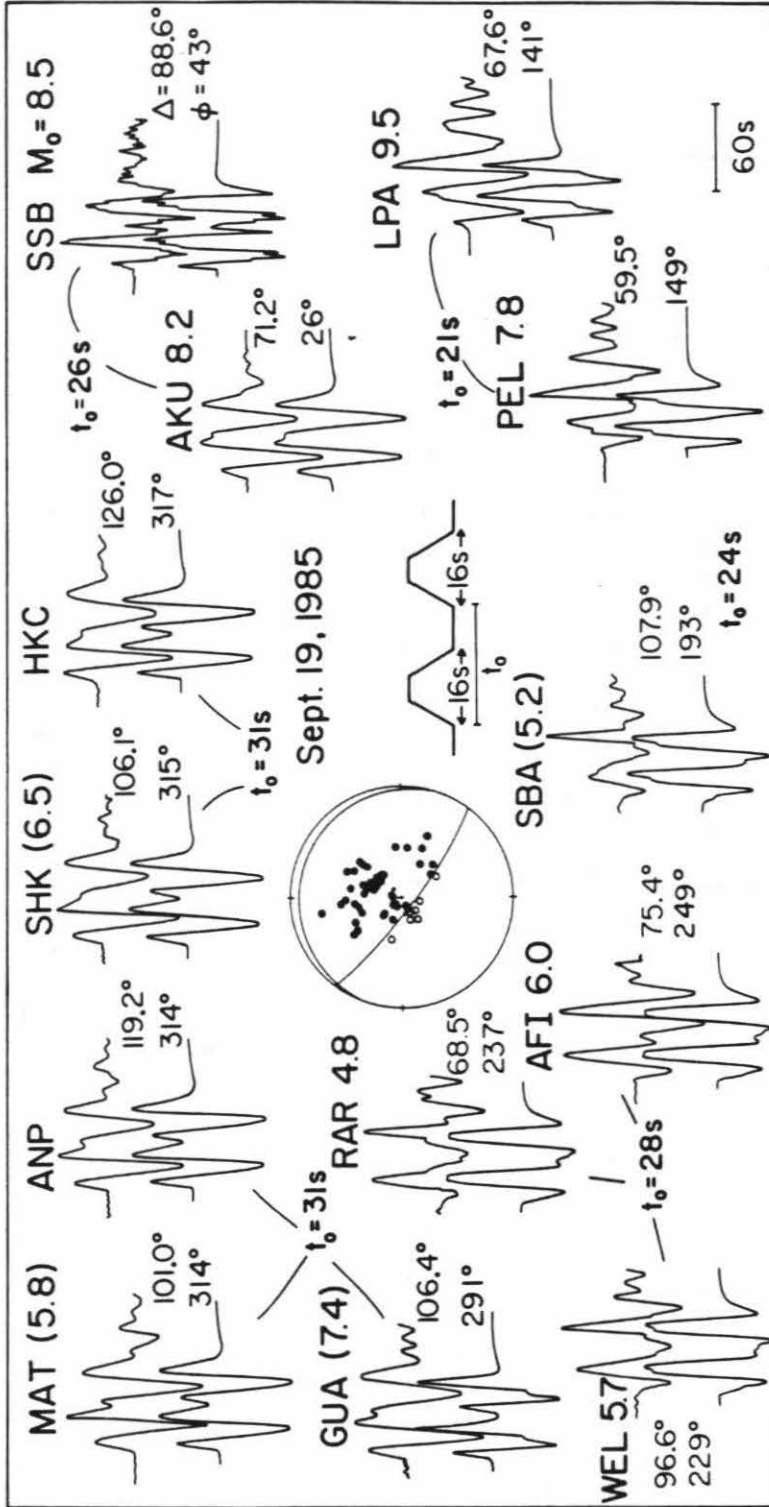
Figure 3.3: P waves of the September 19, Michaoacan earthquake at teleseismic distances. Observed (above) and calculated waveforms shown are from long-period WWSSN recordings and one GEOSCOPE station. The synthetic seismograms are for a shallow thrust fault subparallel to the Mexican trench ($\theta=288°$, $\delta=9°$, $\lambda=72°$) with a point source depth of 17 km, and a two-source time function whose time separation t_o varies systematically with azimuth, indicating source directivity. The value next to the station code is the amplitude ratio of observed to synthetic seismogram from which the average seismic moment is $M_o=7.2\times10^{27}$ dyne cm. Values in parentheses are not considered in determining this value.

the P waves were diffracted arrivals ($\Delta > 100°$) and these were not used in the estimate of seismic moment.

Table 3.1: P-wave Data from WWSSN Stations for the September 19 Event

	Station	Distance (deg)	Azimuth (deg)	P	A_{P1} (cm)	A_{P2} (cm)	t_o (sec)
AKU	Akureyri, Iceland	71.2	25.8	C	30.2	23.5	26
ESK	Eskdalemuir, Scotland	80.3	34.9	C	27.1	23.5	26
LPA	La Plata, Argentina	67.6	141.5	D	6.7	9.8	21
PEL	Peldehue, Chile	59.5	149.1	D	4.1	7.1	21
SBA	Scott Base, Antarctica	107.9	192.9	D	1.2	2.1	(24)
WEL	Wellington, New Zealand	96.6	228.8	D	3.7	4.8	28
RAR	Rarotonga, Cook Islands	68.5	237.6	D	7.2	9.2	28
ADE	Adelaide, Australia	123.5	239.8	D	0.5	0.6	(29)
AFI	Afiamalu, Western Samoa	75.4	249.8	D	4.8	6.4	28
CTA	Charters Towers, Australia	115.5	256.0	D	0.9	0.7	(29)
GUA	Guam, Mariana Islands	106.4	290.6	C	2.2	1.6	31
DAV	Davao, Philippines	126.3	293.6	C	1.0	0.8	-
BAG	Baguio, Philippines	125.4	306.5	C	1.1	1.0	-
ANP	Anpu, Taiwan	119.2	313.9	C	1.8	1.3	(31)
MAT	Matsushiro, Japan	101.0	314.3	C	4.8	4.0	31
SHK	Shiraki, Japan	106.1	315.2	C	3.9	2.7	31
HKC	Hong Kong, China	126.0	316.9	C	0.7	0.6	(31)

A_{P1} - Peak-to-peak amplitude at Mag=750 of the first P-wave pulse
A_{P2} - Peak-to-peak amplitude at Mag=750 of the second P-wave pulse
P - Polarity of the P-wave
t_o - Time delay between the first and second source

It was necessary to adjust the time separation t_o between the two sources as a function of azimuth to obtain the best waveform fit. The time separations range from a minimum of 21 s for South American stations in southeast azimuths to a maximum of 31 s for Japanese and mid-Pacific stations in northwest azimuths (Figure 3.4). European stations (northeast azimuths), South Pacific and Australian stations (southwest azimuths), and Antarctica (to the south) have intermediate time
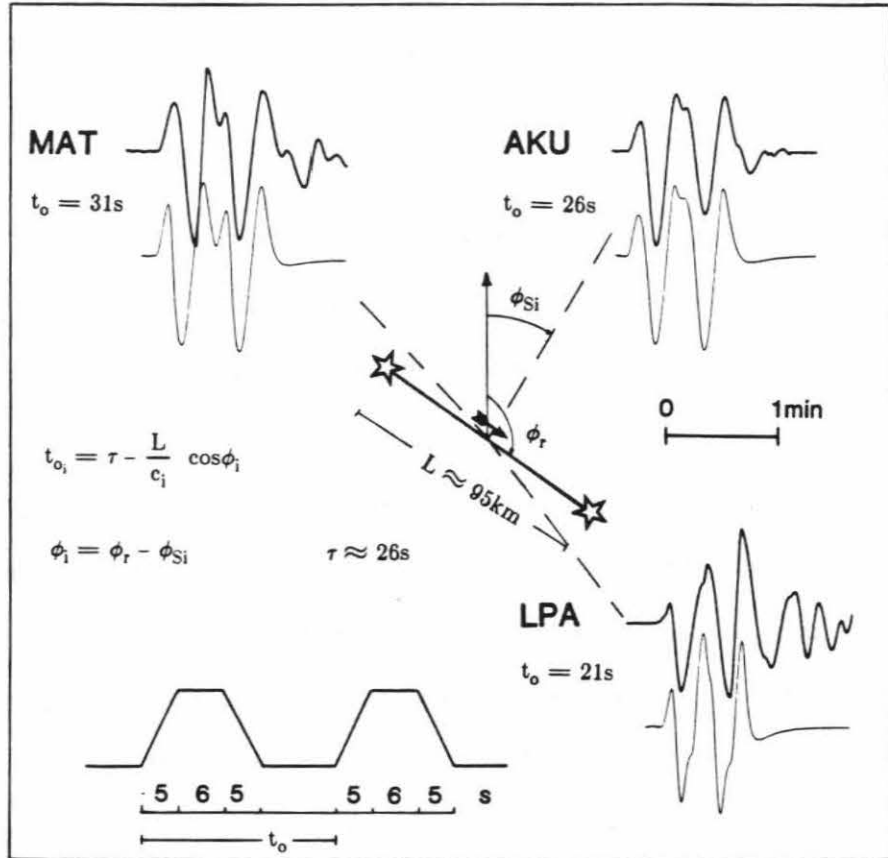
Figure 3.4: Observed and synthetic P-wave traces from three selected long-period WWSSN stations. The time separation t_o between the trapezoidal source time functions decreases from northwest to southeast, indicating directivity. From the azimuthal variation of t_o, the spatial and temporal separation between the two sources (stars) and the rupture direction (arrow) can be estimated.

separations of 26 s, 28 s, and 24 s, respectively. This systematic variation indicates that the second source was located to the southeast of the first. The actual time separation τ at the source and spatial separation L of the subevents can be estimated from the azimuthal variation of t_o, which is given by

$$t_{o_i} = \tau - \frac{L}{c_i} \cos\phi_i. \tag{1}$$

Here c_i is the P-wave phase velocity for the i-th station and $\phi_i = \phi_r - \phi_{Si}$, where ϕ_{Si} is the azimuth to the station and ϕ_r is the rupture direction. Using (1), the data listed in Table 1, and assuming $\phi_r = 120 \pm 5°$, which is the local strike of the trench, we obtained $\tau = 26s$ and $L = 95km$.

The multiple source and southeast rupture direction have been noted by many studies of the source of the Michoacan earthquake. Two subevents or distinct durations of energy release were observed in strong motion accelerograms near the epicenter (Anderson et al., 1986). These records suggest that the second source occurred approximately 95 km southeast of the first (UNAM Seismology Group, 1986). Houston and Kanamori (1986) obtained a source time function similar to our results with two sources of equal seismic moment followed by a smaller third source, using teleseismic broad-band records from the Global Digital Seismic Network (GDSN). From the directivity they estimated that the second source began 26 s after and 82 ± 7 km eastsoutheast of the first at azimuth 114°. Ekstrom and Dziewonski (1986) determined that the second source began 28 s after and approximately 70 km east-southeast of the first at azimuth 97°, using a broad-band GDSN data set similar to that used by Houston and Kanamori (1986). Priestley and Masters (1986) estimated a time separation of 25 s with the second source located 70 km southeast of the first. These results

are all consistent with the picture that the rupture began in the northern portion of the Michoacan gap (first source), propagated with low moment release through the rupture area of the 1981 Playa Azul earthquake, and then broke the remaining asperity in the southern segment of the gap (second source). The source depth and focal mechanism of the Michoacan earthquake are essentially the same as those of all other large Mexico interplate subduction events studied to date, but the double source time function is unusual. Most of the large Mexico subduction events have very simple time functions [Chael and Stewart, 1982], and for the few events that show a complex time function, the dominant moment release still occurs in one simple pulse (Astiz and Kanamori, 1984; Singh et al., 1984). The exception is the 1932 Jalisco earthquake, which had a second event of equal size approximately 30 s after the first and a total seismic moment of about 1.0×10^{28} dyne-cm, similar to the source of the Michoacan earthquake (Singh et al., 1984; Wang et al., 1982). Earthquakes with larger seismic moments such as those in 1932 and 1985 in general have larger rupture zones, so that if the asperity distribution of the Mexico subduction zone is fairly homogeneous with moderate-sized asperities, a large $(M > 8)$ earthquake will likely break through several asperities to create a multiple-source time function.

The September 21, 1985 Aftershock

Only a few P waveforms of the large M_S 7.5 aftershock on September 21 are available. The waveforms are consistent with a mechanism identical to the main shock, with a slightly greater source depth of 22 km (Figure 3.5). The aftershock time function is a single source with a duration of 13 s. The seismic moment recovered from the body waves is 1.2×10^{27} dyne cm.
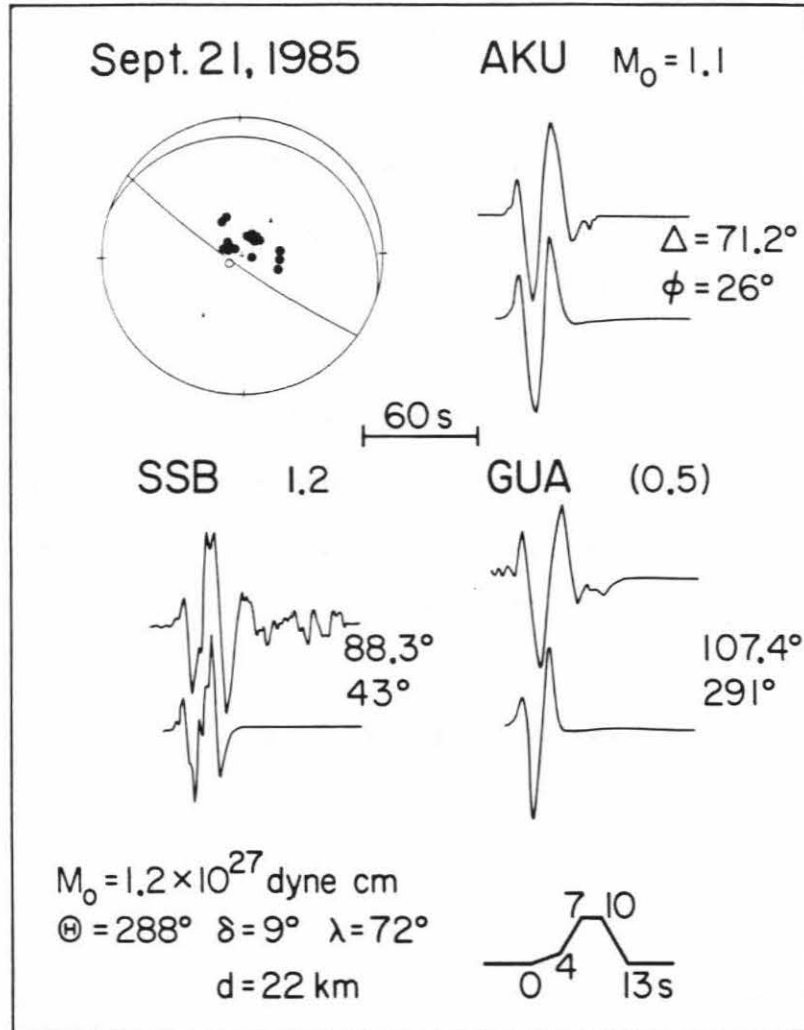
Figure 3.5: Observed (above) and calculated P waves for the aftershock of September 21. The recordings are from a broad-band GEOSCOPE and long-period WWSSN stations at teleseismic distances. The observed waveforms are matched with the focal mechanism shown and a simple 13 s long trapezoidal source time function at 22 km depth.

The April 30, 1986 Aftershock

Long-period P-waves of the aftershock of April 30, 1986 from 15 WWSSN stations are shown in Figure 3.6. The synthetic seismograms are calculated for a point source 21 km deep and source time duration of 10 s. First motion data constrain only one of the nodal planes as is common for most large Mexican subduction events. The second fault plane was resolved from waveform modeling. The fault parameters determined are $\theta=280°$, $\delta=12°$, $\lambda=70°$. The seismic moment is given next to the station code; values within parentheses are obtained from diffracted P-arrivals that are not included to determine the average seismic moment that is 2.0×10^{26} dyne cm. This value is consistent with that obtained from long-period centroid moment tensor inversion 3.1×10^{26} dyne cm (Dziewonski and Woodhouse, 1983).

3.5 Seismic Moment from Long-period Surface Waves

Long-period surface waves recorded by the GDSN, RSTN and IDA networks are used to determine the seismic moment of the Michoacan earthquakes. We use the amplitude and phase spectra at a period of 256 s from multiple passages of Rayleigh and Love waves with an inversion method described by Kanamori and Given (1981). Table 3.2 shows the stations and phases used for the September Michoacan earthquakes. The moment tensor source representation was not used, since the M_{zx} and M_{zy} moment tensor components are poorly constrained for shallow source earthquakes. Instead, we use the fault model inversion, where the orientation of one nodal plane is constrained and the surface-wave data are inverted for the best fitting values of seismic moment and slip angle λ. In this case, we hold the steeply dipping
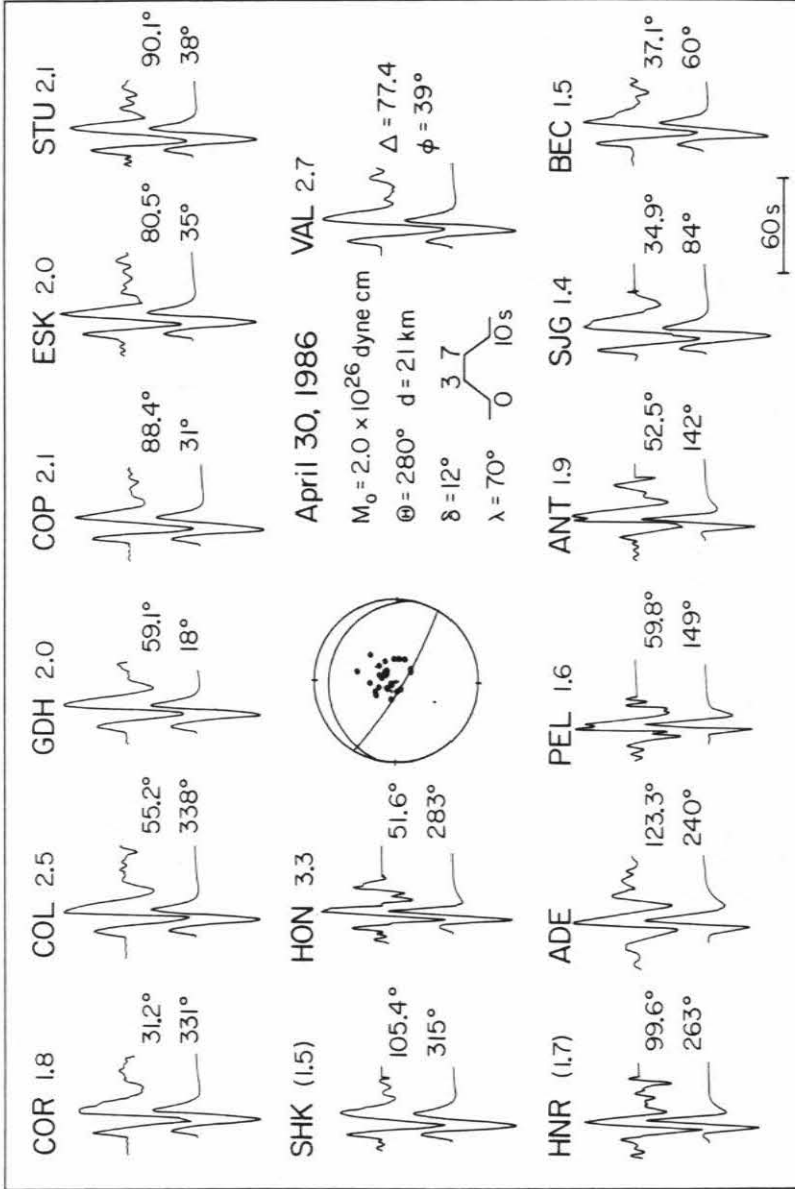
Figure 3.6: Long-period WWSSN recordings of P waves of the April 30, 1986 (M_w=6.9) earthquake are shown by the upper traces. Distance and azimuth to each station are indicated as well as the seismic moment obtained. The synthetic seismograms (lower traces) are calculated using the fault parameters shown and a point source at 21 km depth an a 10 s long source time function.

auxiliary plane fixed at the orientation determined from the P-wave first motion solution ($\delta_a = 81°$, $\theta_a = 127°$). A data set of 42 Rayleigh-wave phases with a good azimuthal coverage gave a solution with $\lambda_a = 91.9°$ and $M_o = 1.70 \times 10^{28}$dyne–cm with an assumed source depth of 16 km. The fault plane parameters are then $\delta = 9.2°$, $\theta = 295°$, and $\lambda = 78°$. This is very close to the body-wave focal mechanism, with a difference of only $7°$ in fault strike and $6°$ in slip angle. Figure 3.7 shows the fit between the

Table 3.2: Stations used in the Surface-wave Inversion

	Station	Distance (deg)	Azimuth (deg)	Sept. 19, 1985	Sept. 21, 1985
ALE	Alert, Canada	66.1	5.3	R3,R4	R2,R3
RSON[+]	Red Lake, Canada	33.3	10.2	R2,R3,G2,G3	
ESK	Eskdalemuir, Scotland	80.3	34.9	R2,R3	R2,R3
RSNY[+]	Adirondack, New York	35.1	35.6	R2,R3	
SCP[*]	State College, Pennsylvania	30.8	38.1	R2,R3	
HAL	Halifax, Canada	41.7	42.3	R2,R3	R2,R3
SJG	San Juan, Pto. Rico	34.5	84.4	R2,R3	R2,R3
SUR	Sutherland, RSA	127.4	117.1	R3,R4	R2,R3
BDF	Brasilia, Brasil	63.4	118.6	R2,R3	R2,R3
NNA	Nana, Peru	39.3	138.0	R2,R3	R2,R3
RAR	Rarotonga, Cook Is.	68.5	237.6	R3,R4	R2,R3
TWO	Adelaide, Australia	123.7	239.7	R3,R4	R2,R3
HON[*]	Honolulu, Hawaii	49.8	280.3	R2,R3,G2,G3	
KIP	Kipapa, Hawaii	52.1	283.2	R2,R3	R2,R3
GUA	Guam, Mariana Is.	106.4	290.6	R2,R3	R2,R3
ERM	Erimo, Japan	94.8	317.0	R2,R3	R2,R3
BJT	Bejin, China	111.7	328.9	R3,R4	R2,R3
COL[*]	College, Alaska	55.5	338.4	R2,R3,G2,G3	
ANMO[*]	Alburquerque, New Mexico	17.0	348.8	R2,R3	
RSNT[+]	Yellowknife, Canada	45.0	352.1	R2,R3,G2,G3	
RSSD[+]	Black Hills, S.Dakota	25.8	357.4	R2,R3,G2,G3	

[*] GDSN (Global Digital Seismic Network)
    IDA (International Deployment of Accelerographs)
[+] RSTN (Regional Seismic Test Network)
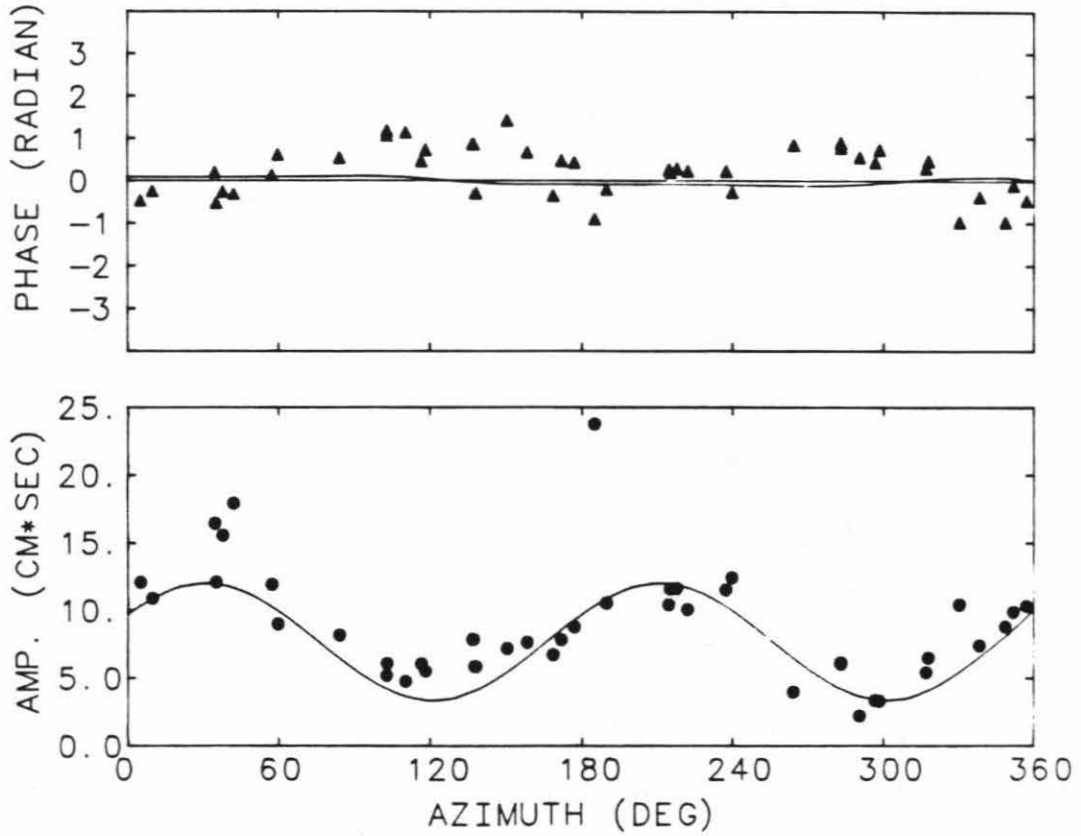
Figure 3.7: Observed phase (triangles) and amplitude (circles) spectral values as a function of azimuth of Rayleigh wave data used in the surface wave inversion from GDSN, IDA and RSTN stations, compared with the theoretical pattern for the best fitting solution for the September 19, 1985 Michoacan earthquake. Spectral values are for a period T = 256 s.

observed Rayleigh-wave radiation pattern and that calculated for this solution. When 10 Love-wave phases were included, the solution was virtually identical. Due to the large size of the earthquake, the fault finiteness and finite rise time of the source dislocation function may introduce a source phase delay. Following Kanamori and Given (1981), this effect can be included, assuming the rate of moment release to be constant with time, by introducing a source process time τ. We find that the errors in the inversion are minimized with a source process time $\tau=100$s for a period of 256 s. A simultaneous inversion of long-period surface waves at different periods (150 - 300 s) gives $\tau=80$s for the Michoacan earthquake (Zhang and Kanamori, 1987).

For the aftershock, we used 26 Rayleigh-wave phases from the IDA network, again holding the auxiliary plane fixed as determined from the main shock first-motion data. The inversion gives a fault orientation of $\delta=9.5°$, $\theta=289°$, $\lambda=73°$, essentially the same as the mainshock, with a seismic moment of 4.7 x 10^{27} dyne cm, 28 % that of the mainshock, and a source process time $\tau=60$s. Figure 3.8 shows the observed and calculated Rayleigh-wave radiation pattern for the aftershock.

Because the auxiliary plane is tightly constrained to have a steep dip from the first-motion data, the fault plane given by the inversion will have a shallow dip for any mechanism that is predominantly thrust. By relaxing this constraint, the inversion for the long-period source might return a fault plane orientation with a slightly different dip angle that will sensibly modify the moment estimate. For shallow thrust events, the seismic moment determined from the surface-wave inversion, M_o, depends on the dip angle δ as $M_o = M_{o_{min}}/ \sin 2\delta$, where $M_{o_{min}}$ is the minimum seismic moment (Kanamori and Given, 1982). Thus, for a dip of 15° instead of 9° the moment is smaller by about a factor of 1.6. For a mechanism with a maximum fault plane dip
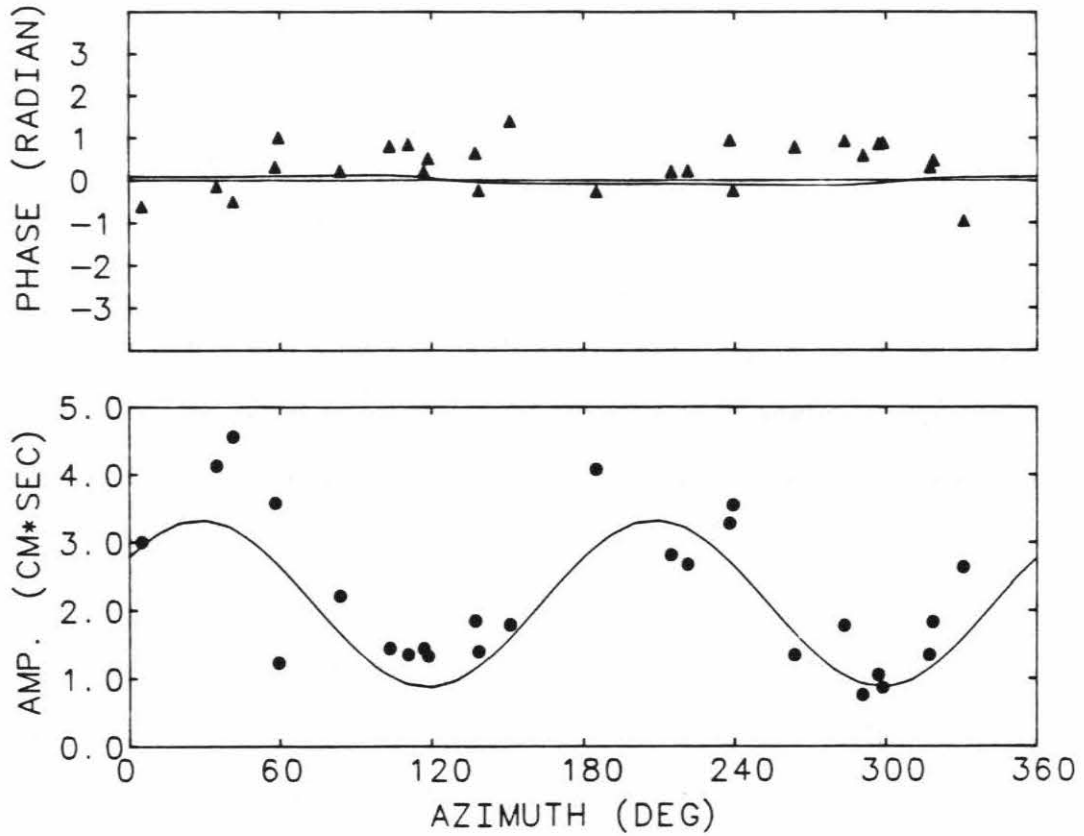
Figure 3.8: Observed phase (triangles) and amplitude (circles) spectral values as a function of azimuth of Rayleigh wave data from IDA stations used in the surface wave inversion, compared with the theoretical pattern for the best fitting solution for the large September 21 aftershock. Spectral values are for a period T = 256 s.

of 15° and a minimum of 9°, for the mainshock the moment ranges from 1.05 to 1.70×10^{28}dyne–cm or M_W=7.9–8.1, respectively. Locations of aftershocks from local networks define a dip of approximately 12° to 14° (Stolte et al., 1986; UNAM Seismology Group, 1986), indicating that the lower end of the range is more appropriate. For the aftershock, the moment range is 2.9 to 4.7×10^{27}dyne–cm, or M_W=7.6–7.7.

Results of other studies of the long-period source of the 1985 Michoacan earthquake are summarized in Table 3.3 and compare favorably with those presented here. Details of the solutions vary due to differences in the data sets, techniques, constraints on the solutions or Earth models used. In particular, different approaches can be taken to provide control on the poorly determined components of the moment tensor. All the studies found an overall thrust geometry (rake angles deviating from 2° to 17° from pure thrust) on a fault plane striking parallel to the Middle-America trench (N289°E - N302°E). Shallow dip angles ($<20°$) were determined or inferred in all the studies; for example, Priestley and Masters (1986) fixed the dip at 15°, while Riedesel et al. (1986) left the dip unconstrained and resolved it to be 19±15°. In view of the dependence of the seismic moment value on fault-plane dip angle, we correct the values in Table 3.3 to correspond to a dip angle of 15° for comparison. Values of seismic moment are then very consistent, varying from 1.03–1.32x10^{28}, with an average value of 1.17x10^{28} dyne cm or M_W=8.0.

Riedesel et al. (1986) determine the characteristic time τ_c for the September earthquakes from the scalar-moment algorithm of Silver and Jordan (1983) and obtain τ_c=49±7s for the main event and 30±11s for the aftershock. This compares favorably with the source process times τ resolved above because τ=1.73τ_c (Silver and Jordan, 1983).

Table 3.3: Results of Long-period Studies

	δ	ϕ	λ	M_o $\times 10^{28}$dyne–cm	M_o at $\delta = 15°$ $\times 10^{28}$dyne–cm
This Study	9°	295°	78°	1.70	1.05
Ekstrom and Dziewonski (1986)	18°	302°	107°	1.10	1.29
Priestley and Masters (1986)	15° (fixed)	298°	88°	1.03	1.03
Riedesel et al. (1986)	19±15°	289°	76°	1.07	1.32

3.6   Rupture of the Michoacan Gap

The rupture pattern of the Michoacan gap during the period 1981 to 1986 can be characterized by a sequential failure of five distinct asperities, as schematically shown in Figure 3.9. Before 1981 the Michoacan region had not experienced a large earthquake since 1911, when an $M_S = 7.8$ earthquake occurred. The recent sequence started in October 1981 with the Playa Azul ($M_w = 7.3$) earthquake that broke the central part of the Michoacan gap, which had not experienced a large earthquake since 1911. Body-wave modeling indicates that the Playa Azul event is slightly deeper than the recent Michoacan earthquakes in September 1985 and April 1986. In addition, the stress drop of this event is relatively higher, suggesting a higher stress level at depth in the middle of the Michoacan gap.

Analysis of records from the September 19, 1985 ($M_w = 8.1$) earthquake indicate that the seismic moment of this event was released in two main events, with the rupture starting in the northern portion of the seismic gap and propagating to the southeast with low moment release through the area already broken by the 1981 Playa Azul earthquake. Then on September 21, 1985, the rupture propagated farther
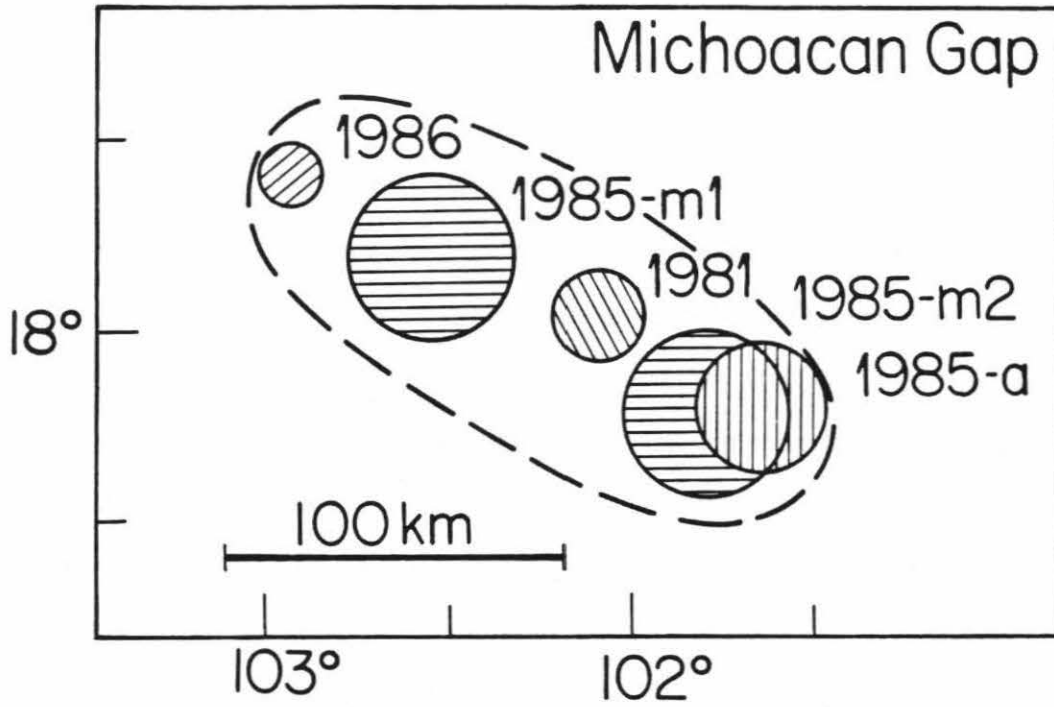
Figure3.9: The Michoacan earthquake sequence is shown schematically. The circles represent the location of the asperities on the fault plane. The radius of the circle is pproportional to $M_o^{1/3}$.

southeast with a $M_w=7.5$ event that may have broken the shallower portion of the subduction zone up-dip of the 1979 Petatlań ($M_w=7.6$) earthquake (UNAM Seismology Group, 1986). The April 30, 1986 ($M_w=6.9$) location to the northwest of the great Michoacan earthquake epicenter (Figure 3.1), suggests that this event released the remaining stress between the 1973 Colima ($M_w=7.6$) earthquake and the September 1985 events.

Although this distribution of asperities is considered characteristic of the Michoacan gap, whether the temporal sequence exhibited by the 1981-1986 sequence is also characteristic of this gap or not is unclear. In fact, there is no obvious evidence that the 1911 event occurred in a similar sequence. It is probable that, depending on the state of stress in each asperity, the entire gap may fail in either a single large event with a complex time history or a sequence of moderate-to-large events spread over a few years. If a similar model is applicable to the adjacent Guerrero gap, we should expect a similar variation in the failure mode of the next Guerrero earthquake.

The spectral peak of the ground acceleration of 0.5 Hz in the damaged zone agrees with the resonance frequency predicted from the structure of the lake sediments under Mexico City (Beck and Hall, 1986). Fortunately the source spectrum of the earthquake was actually depleted in frequencies between 0.1 Hz and 1.0 Hz relative to globally averaged source spectra of other large interplate thrust earthquakes at teleseismic distances (Houston and Kanamori, 1986). Thus, the extensive damage to Mexico City on September 19, 1985 could be due to the long duration of the source rupture.

Chapter 4

Implications from Recent Earthquakes for Middle America

4.1 Introduction

In recent years, many detailed studies have been conducted on individual earthquakes that occurred on the Middle-America trench (e.g., Chael and Stewart, 1982; Guendel and McNally, 1982; Singh et al., 1984), as well as on its regional seismicity (e.g., LeFevre and McNally, 1985). These studies, together with the results presented in the previous two chapters for the most recent large Mexican subduction earthquakes, suggest that these events occur repeatedly at locations with increased mechanical strength, which have been called asperities in the recent literature. A relatively homogeneous asperity size distribution along the Mexican subduction zone has been inferred from magnitude-frequency relations for large earthquakes (Singh et al., 1982b). It seems likely that the fault zone heterogeneity, characterized by the asperity distribution, plays a key role in controlling the recurrence time and triggering mechanisms of large subduction earthquakes.

Relations of seismic parameters for large subduction events in Middle America are presented in Chapter 4, which may help us assess the future seismic and tectonic activity for this plate boundary. First we compare the range of stress drop values for recent large subduction earthquakes in the Mexican subduction zone by estimating fault area and seismic moment M_o for each event. The relation between M_S and M_o,

which is determined from surface wave studies, would allow an estimate of seismic moment for events for which seismic records are not available. A reassessment of the recurrence interval, T, for individual regions along the Middle America is also presented, which permits a test of the relation between T and M_o derived from a simple asperity model. Finally, implications for present seismic gaps along the Middle-America plate boundary are examined.

4.2   Stress Drop of Large Mexican Subduction Events

Stress drop is a useful parameter to characterize earthquakes that may reflect the state of stress in the interplate boundary. Earthquake stress drops are usually estimated from the seismic moment M_o and the fault area. However, as discussed above, M_o of shallow thrust earthquakes depends on the dip angle assumed. The fault area S is often estimated from the aftershock area, but its definition varies for different investigators. Due to these uncertainties it is hard to estimate the error associated with a single stress drop value, to compare the published values of stress drops for different events.

To circumvent this difficulty, we compare the seismic moments and the fault areas estimated for large earthquakes in the Mexican subduction zone and examine the overall trend. Figure 4.1 shows the data we used. The horizontal bars attached to each data point indicate the range of seismic moment estimated from body- and surface-waves for events listed in Table 4.1. The fault dimensions correspond, in most cases, to the one-week aftershock area. The vertical bars indicate the range of the values calculated for a rectangular and elliptic shape for S. Closed symbols
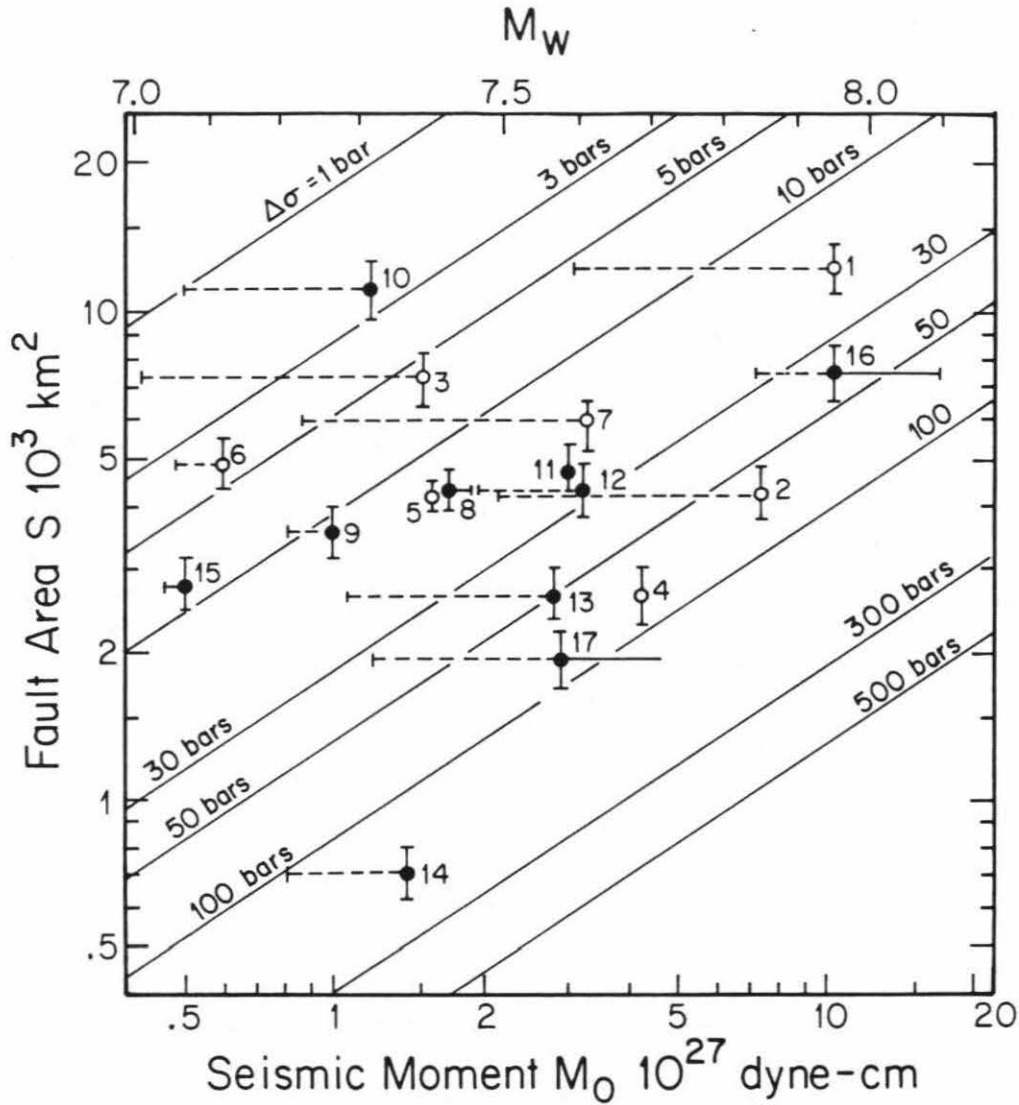
Figure 4.1: Plot of seismic moment M_o, versus fault area S, for large Mexican subduction earthquakes since 1932. The range of values determined from body and surface waves for M_o are indicated by the error bars. Error bars for S are for rectangular and elliptical areas. Open symbols are events before the installation of the WWSSN stations. Event numbers correspond to those in Table 4.1. Lines are constant static stress drop ($\Delta\sigma$) calculated for a circular crack. Uncertainties in the data are too large to assign a unique stress drop value to each event.

Table 4.1:Source Parameters of Large Shallow Interplate Mexico Earthquakes

N	Date	Lat. (°N)	Long. (°W)	Depth (km)	M_S	M_W	M_{ob}	$M_{\alpha S}$	L x W (km²)
							: (10^{27} dyne-cm)		
	April 15, 1907	16.70	99.20[v]	S	8.0[b]	7.8		5.9[j]	
	June 17, 1928	16.33	96.7[g]	S	7.8[b]	7.7		3.9[d]	
1	June 3, 1932	19.57	104.42[a]	16[c]	8.2[b]	7.9	3.12[c]	9.1[d]	170x80[e]
2	June 18, 1932	19.50	103.50[f]	13[c]	7.8[b]	7.8	2.10[c]	7.3[d]	60x80[e]
3	Dec. 23, 1937	17.10	98.07[g]	16[c]	7.5[f]	7.4	0.44[c]	1.53[c]	120x70[g]
4	Apr. 15, 1941	18.85	102.94[g]	S	7.7[f]			4.4[h]	60x50[g]
5	Feb. 22, 1943	17.62	101.15[g]	16[c]	7.5[f]	7.4	0.45[c]	1.59[c]	75x60[g]
6	Dec. 14, 1950	17.22	98.12[g]	20[c]	7.3[f]	7.1	0.48[c]	0.60[c]	80x70[g]
7	July 28, 1957	17.11	99.10[g]	16[c]	7.5[l]	7.6	0.85[c]	3.3[j]	100x65[g]
8	Aug. 23, 1965	16.02	95.93	25[k]	7.6[l]	7.5	1.9[l]	1.7[l]	105x46[k]
9	Apr. 2, 1968	16.39	98.06	21[k]	7.1[f]	7.3	0.8[l]	1.0[l]	50x82[k]
10	Apr. 29, 1970	14.52	92.60	33	7.3[f]	7.4	0.5[l]	1.2[l]	130x96[m]
11	Jan. 30, 1973	18.39	103.21	32[n]	7.5[f]	7.6		3.0[l]	90x63[n*]
12	Nov. 29, 1978	15.77	96.80	18[k]	7.8[f]	7.6	1.9[l]	3.2[l]	82x60[k]
13	Mar. 14, 1979	17.45	101.45	14[o]	7.6[f]	7.6	1.0[l]	2.7[l]	65x45[p]
14	Oct. 25, 1981	17.75	102.25	27[t]	7.3[f]	7.3	0.72[t]	1.4[r]	40x20[q]
15	June 7, 1982*	16.40	98.54	S	7.0[f]	7.1	0.40[s]	0.50[s]	78x41[f]
16	Sep. 19, 1985	18.27	102.31[f]	17[t]	8.1[f]	8.0	7.2[t]	10.5[t]	170x50[u]
17	Sep. 21, 1985	17.81	101.65[f]	22[t]	7.5[f]	7.6	1.2[t]	2.9[t]	66x33[u]
18	Apr. 30, 1986	18.41	102.98	21[t]	7.0[f]	6.9	0.20[t]	0.31[f]	

N , Event number in Figure 4.1

M_{ob} , Seismic moment from body waves

$M_{\alpha S}$, Seismic moment from surface waves

LxW , Fault length and width for 1 week aftershock area

M_W , determined from $M_{\alpha S}$

* , Doublet event

(References: [a] Eissler and McNally, 1984; [b] Geller and Kanamori, 1977; [c] Singh, et al., 1984; [d] Wang, et al., 1982; [e] Singh, et al., 1985a; [f] NOAA; [g] Kelleher, et al., 1973; [h] determined from M_S ; [l] Abe and Kanamori, 1980; [j] Singh, et al., 1982a; [k] Tajima and McNally, 1983; [l] Chael and Stewart, 1982; [m] Yamamoto, 1978 (12 hr. aftershock area); [n] Reyes, et al., 1979 (* 2.5 weeks aftershock area); [o] Gettrust, et al., 1981; [p] Valdés, et al., 1982; [q] Havskov, et al., 1983; [r] LeFevre and McNally, 1985; [s] Astiz and Kanamori, 1984; [t] Astiz et al., 1987; [u] Seismology Group, UNAM, 1986; [v] Figueroa, 1970)

indicate the events for which the moment determination was made from at least several WWSSN seismograms (i.e., events after 1963). Lines in Figure 4.1 are equal static stress drop calculated for a circular crack model. If a rectangular dip-slip model is used, with an aspect ratio (length/width) of 1.5 (the average for the Mexican subduction-zone events), the stress drop values in Figure 4.1 should be multiplied by 0.4.

Although the uncertainties in M_o and S are large, Figure 4.1 suggests that some events near the Orozco fracture zone have larger stress drops ($>$50 bars). Those events are the Petatlań earthquakes in 1941 and 1979 (events 4 and 13), the September 21, 1985 Michoacan earthquake aftershock (event 17), and the 1981 Playa Azul earthquake (event 14). This may be due to an increased interplate interaction as the seafloor of the Orozco fracture zone, which is probably more buoyant than the adjacent seafloor, subducts in this area. The September 19 main shock (event 16) has a lower stress drop than these events. The Ometepec doublet (event 15) has a low stress drop value ($<$ 10 bars), similar to most other large subduction events in Mexico.

Anderson et al. (1986) determined from strong ground motion records that the apparent stress drop (Aki, 1966) of the main 1985 Michoacan earthquake, which is a measure of the average stress drop on the fault, is 6 bars. They also determined that effective dynamic stress drop (Brune, 1970) varies from 6 to 12 bars for the main event. Although the apparent stress and the effective stress cannot be directly related to the static stress drop, these low values are generally consistent with the low static stress drop inferred from Figure 4.1. These low stress drop values correlate with the low amplitude strong ground motions ($\approx$.15g on the NS and EW components)

recorded at hard rock sites in the epicentral area (Anderson et al., 1986). For the 1981 Playa Azul (M_S=7.3) earthquake larger accelerations (.24 g on the EW component, Havskov et al., 1983) were recorded at hard rock sites near the epicenter. Figure 4.1 shows a relatively higher stress drop value for the Playa Azul event (14) than for the 1985 Michoacan main event (16). This observation suggests that possible variations in stress drops need to be considered for estimating strong ground motions from future Mexican subduction-zone earthquakes. Note also that the depth determined for the 1981 Playa Azul event in Chapter 3 was deeper relative to other events along the Mexican subduction zone, a fact that may also influence the higher stress drop value for this event.

4.3 A Test of the Asperity Model

Now we consider a simple asperity model in which the fault contact plane is held by discrete asperities (places with increased strength), each surrounded by weak regions. For simplicity, we assume that the slip on the asperities is completly seismic, and the slip in the weak zone is aseismic during the inter-seismic period. When an asperity breaks, causing a seismic event, some coseismic slip accompanies in the surrounding region. Hence, the rupture zone that is responsible for seismic radiation is larger than the asperity. A simple mechanical model corresponding to this situation has been considered by Madariaga (1977) and Rudnicki and Kanamori (1981). We let u, A and D be the amount of slip on the asperity, the area of the entire rupture zone and the slip averaged over the rupture zone, respectively. The seismic moment, M_o , measured by surface waves is then given by

$$M_o = \mu \, D \, A, \tag{1}$$

and since the gross stress drop in large earthquakes is constant (e.g., Kanamori and Anderson, 1975), then

$$M_o \approx D^3, \tag{2}$$

where μ is the rigidity of the medium, D is the average displacement on the fault and A is the fault area. In this model, the slip on the asperity is equal to the slip accumulated by plate motion $u = VT$, where V is the plate convergence rate and T is the repeat time. The ratio of the seismic slip averaged over the entire rupture zone to the total plate motion during the interseismic period is

$$\eta = \frac{D}{u} = \frac{D}{V}T = \frac{M_o}{\mu}AVT; \tag{3}$$

then combining the expressions above the repeat time is given by

$$T = \frac{u}{V} = \frac{D}{\eta V} \approx \frac{1}{\eta V} M_o^{1/3}. \tag{4}$$

If the convergence rate, V, and η, are approximately constant for a given subduction zone, it follows that

$$\log T \approx \frac{1}{3} \log M_o. \tag{5}$$

Although the location, size, and rupture length of historical events along the Middle-America trench are somewhat uncertain, we attempt to test this relation with the presently available data. Event locations are taken from a recompilation made by Singh et al. (1981) for the Mexico region and from Stoiber and Carr (1977) and McNally and Minster (1981) for Central America. Note that misslocations of last century events (squares in Figure 4.3) can be at least of the order of $\pm 1°$ (Singh,

personal communication; Stoiber and Carr, 1977). Events that occurred early this century could also have considerable location errors as seen in Section 3.3. Focal parameters for some large, shallow interplate Middle-America events are listed in Table 4.1. The moment-magnitude relation for these events is shown in Figure 4.2, where the heavy line is

$$\log M_o = 1.5 \ M_S + 16.0. \tag{6}$$

The data approximately follow this line. Seismic moment of events that have not been determined from seismic recordings are therefore estimated, using this relation.

A time-distance plot of large shallow events $(M > 7)$ along the Middle America trench is shown in Figure 4.3. The events in parenthesis are listed by Miyamura (1976) as M=7; however, Singh et al. (1981) show that these events are likely to have smaller magnitude, and they are neither listed in Table 4.2 or considered in calculating the recurrence time for each region. The entire Middle America region is subdivided into 21 regions (Figure 4.3). This division is made mainly on the basis of the distribution of aftershock areas of recent events (Kelleher et al., 1973; Reyes et al., 1979; Singh et al., 1980b; Valdés et al., 1982; Guendel and McNally, 1982; Havskov et al., 1983). Three dotted regions corresponding to the Orozco Fracture zone (3), the Tehuantepec (11) and Cocos (19) Ridges are defined on the basis of high or anomalous seafloor topography. Note that earthquakes of $M \approx 7$ have occurred in the middle of the Cocos ridge region (19) about every 30 years during this century (Figure 4.3, Table 4.2). However, no large earthquakes have occurred in the Tehuantepec region during this century, and it is considered aseismic or seismic with anomalously large recurrence intervals (McCann et al., 1979, Singh et al., 1981). The Orozco Fracture zone was the locus of the recent large Michoacan earthquakes studied in Chapter
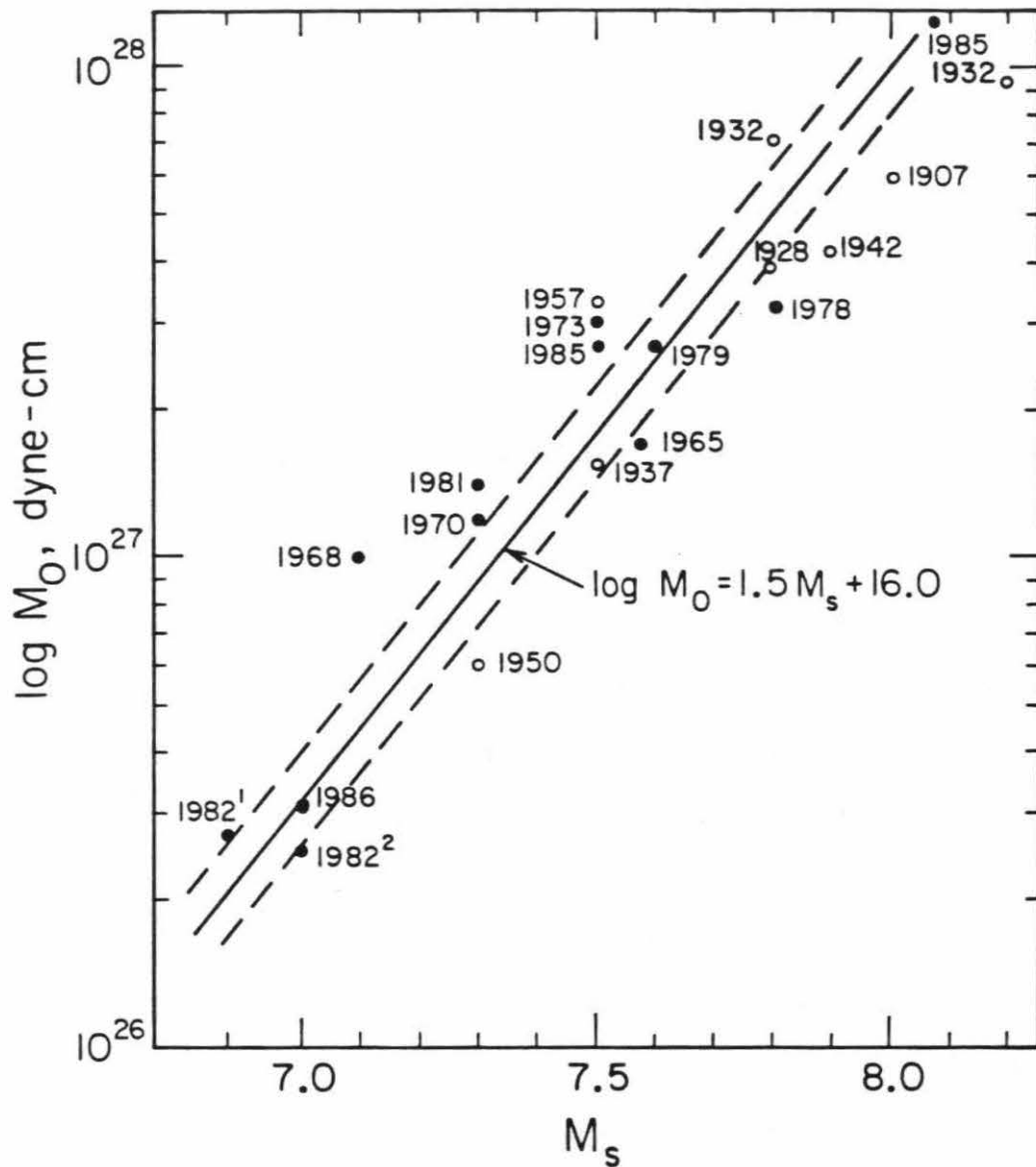
Figure 4.2: Relation between M_S (20 s surface wave magnitude) and M_o (seismic moment) for events that have occurred along the Middle-America subduction zone (Table 4.1). The dashed lines correspond to $\log M_o = 1.4 M_S + (16.0 \pm 0.1)$. Open circles are estimates of M_o from one station and solid circles indicate estimates from several stations.

3. Regions where no large, shallow interplate earthquake has occurred for more than 30 years are indicated in hatched pattern in Figure 4.3. These regions are considered seismic gaps with high potential, since the average recurrence interval for this type of earthquake along the entire plate boundary is 33 ± 8 years (McNally and Minster, 1981). The Jalisco (1), Guerrero (5), Guatemala (14), El Salvador (15), Nicaragua (16) and West Panama (20) gaps fall in this category. Special attention should be directed to these areas, as well as to the regions where the Tehuantepec and the Cocos ridges are subducting.

Table 4.2 shows the year and magnitude of the events that occurred in each region. The average recurrence interval, T, is calculated from $\frac{1}{n}\sum_{i=1}^{n}t_i$, where n is the number of intervals and t_i is the time interval in years between consecutive events. Events not used to estimate T are in brackets. Only those events that occurred after 1820 are used to estimate the average recurrence intervals for each region. If the interval between two consecutive events is less than 3 years, the events are grouped together as a single sequence. In the Jalisco region (1), the events that occurred in 1900(7.4) and 1934(7.0) are probably aftershocks of the 1900(7.9) and 1932(8.2) earthquakes, respectively. In the Acapulco region (6), the 1962 doublet is considered to be part of the activity associated with the 1957(7.5) Acapulco earthquake. Only the time of occurrence of the first event of those listed as doublets in Table 2.5 is used to estimate the average recurrence interval in the Ometepec (7), West Oaxaca (8), Central Oaxaca (9) and Costa Rica (18) regions. In the East Panama region (21), the 1962(7.0) earthquake is probably a foreshock of the 1962(7.4) event. The Guerrero region (5) has not experienced a major earthquake in almost 80 years; since most of the historic events are clustered in a 22 year-period, no reliable recurrence period can be

Table 4.2: Observed Recurrence Period T, Large Subduction Earthquakes along Middle America

	Region	Year of Earthquake (M_S)					T (years)
1.	Jalisco		1875(7.4)	1900(7.9) [1900(7.4)]	1932(8.2) [1934(7.0)]		31.7 ± 6.5
2.	Colima	[1806(7.5)]	[1818(7.7)]		1932(7.8)	1941(7.7)	1973(7.5) 21.3 ± 10.5
3.	Michoacan		1837(7.8)		1911(7.9)		1981(7.3) 1985(8.1) 73.0± 1.0
4.	Petatlán				1908(7.5)	1943(7.5)	1979(7.6) 35.5 ± 0.7
5.	Guerrero	1887(7.2) [1889(7.2)]	1899(7.9)	1908(7.8) [1909(7.4)]			-----
6.	Acapulco	[1820(7.6)]	1845(7.9)	1907(8.0)		1957(7.5) [1962(7.0)] [1962(7.2)]	56.0 ±8.5*
7.	Ometepec		1890(7.2)		1937(7.5)	1950(7.3)	1982(6.9) [1982(7.0)] 30.6 ± 17.0
8.	West Oaxaca	1854(7.7)	1894(7.4)		1928(7.6) [1928(7.4)]	1968(7.4)	38.0 ± 3.5
9.	Central Oaxaca		1870(7.9) [1872(7.4)]		1928(7.8)		1978(7.8) 53.0 ± 4.2
10.	East Oaxaca		1897(7.4)		1928(7.5)	1965(7.6)	34.5 ± 3.6
11.	Tehuantepec						-----
12.	Chiapas			1902(8.2)	1944(7.0)	1970(7.3)	34.0 ± 11.3
13.	W. Guatemala				1919(7.0)	1950(7.1)	31.5
14.	E. Guatemala	1862(L)	1902(7.9)			1942(7.9)	40.0 ± 0.0
15.	El Salvador	1859(L)	1901(7.9)	1926(7.1)			33.5 ± 12.0
16.	W. Nicaragua	1850(G)	1901(7.6)	1921(7.3)			35.5 ± 21.9
17.	E. Nicaragua	1881(L) 1885(L)	1898(7.5)			1956(7.3)	25.0 ± 28.9
18.	Costa Rica	1851(G)	1916(7.3) [1916(7.3)]	1939(7.3)	1950(7.7)	1978(7.0)	20.7 ± 8.7
19.	Cocos				1924(7.0)	1952(7.2)	1983(7.2) 29.5 ± 2.1
20.	West Panama		1904(7.6)	1941(7.5)			37.0
21.	East Panama		1934(7.7)			[1962(7.0)] 1962(7.4)	28.0

[ ] - events not used to estimate the recurrence time T

(L)-large earthquake, (G)-great earthquake from Carr and Stoiber (1977)

* - T for events with $M_S \geq 7.4$

determined. Note that Astiz and Kanamori (1984) considered the January 30, 1931 earthquake in the Central Oaxaca region (9) as a shallow thrust event; however, it is known now that this event is a normal fault earthquake at intermediate depth (Singh et al., 1985b). Recently, Gonzàlez-Ruiz (1986) has suggested that the event that occurred on March 27, 1872 may be similar to the 1931 event. If this were true, the recurrence period for the Central Oaxaca region (9) would not change significantly.

The average seismic moment, $\overline{M}_o$, for each region is obtained from events that occurred during this century from $\dfrac{1}{n} \sum\limits_{i=1}^{n} M_{o_i}$, where n is the number of events and M_{o_i} is the seismic moment for each event. If the seismic moment of the event is known as listed in Table 4.1, it is used for calculating the average. If not, it is estimated from the M_S using Equation (6). If consecutive events occur less than 3 years apart, they are treated as a single event and their moments are added and considered a single value. Table 4.3 gives the average seismic moment, $\overline{M}_o$, for regions along Mexico. However, the data are insufficient for Central America regions, since most of large earthquakes in the region occurred near the turn of this century. Then, for each region the corrected recurrence time period, T_c , is calculated for a uniform velocity of 6.4 cm/yr, since the M_o - T relation given by (5) assumes constant V. This velocity is that of the Guerrero gap (Table 4.3) and will be useful in the forthcoming discussion. Thus, the recurrence period, T, for each region is multiplied by V/6.4, where V is the corresponding plate velocity for each region. Note that this correction is of the order of 15% for the Guerrero-Oaxaca (4-10) regions. The plate velocities given for each region are computed for the Cocos plate pole (Minster and Jordan, 1978).

The value of η given in Table 4.3 for each region was determined, using expression (3) above. The source parameters for the most recent events (Table 4.1) in each region are used to estimate η, where T is the time between the last and the previous event in each region. Although this estimate is quite crude, since it involves only the most recent events in each region the variation of η is a factor of only two for the Mexican subduction zone. The source of error to estimate η comes from the fault area dimension: e.g. Valdés et al. (1982) calculated η ranging from 0.3 to 0.5 in this way for the 1979 Petatlań earthquake. These values of η indicate moderate seismic coupling in the Cocos-North America plate boundary, and the assumption of a constant η for the Mexican subduction zone seems reasonable. However, south of the Tehuantepec ridge large discrepancies between the convergence and seismic slip have been observed, indicating rather weak coupling between the Cocos and Caribbean plates (McNally and Minster, 1981). Since 1902 there have been no truly great events along the El Salvador and Nicaragua coasts (Figure 4.3). Kanamori (1977) compared the seismic slip with the rate of plate motion for various subduction zones and concluded that the ratio of the seismic slip to total slip, η, varies significantly from place to place and is probably a good indicator of strength of interplate seismic coupling. For example, $\eta \approx 1$ for Chile and possibly Alaska, $\eta \approx 1/4$ for the Kurile Islands and Northwestern Japan, and $\eta \approx 0$ for the Marianas subduction zone. Similarly, Sykes and Quittmeyer (1981) found that η ranges from 0.3 to 0.9 for various subduction zones, if it is computed with the time-predictable model of earthquake occurrence (Shimazaki and Nakata, 1980).
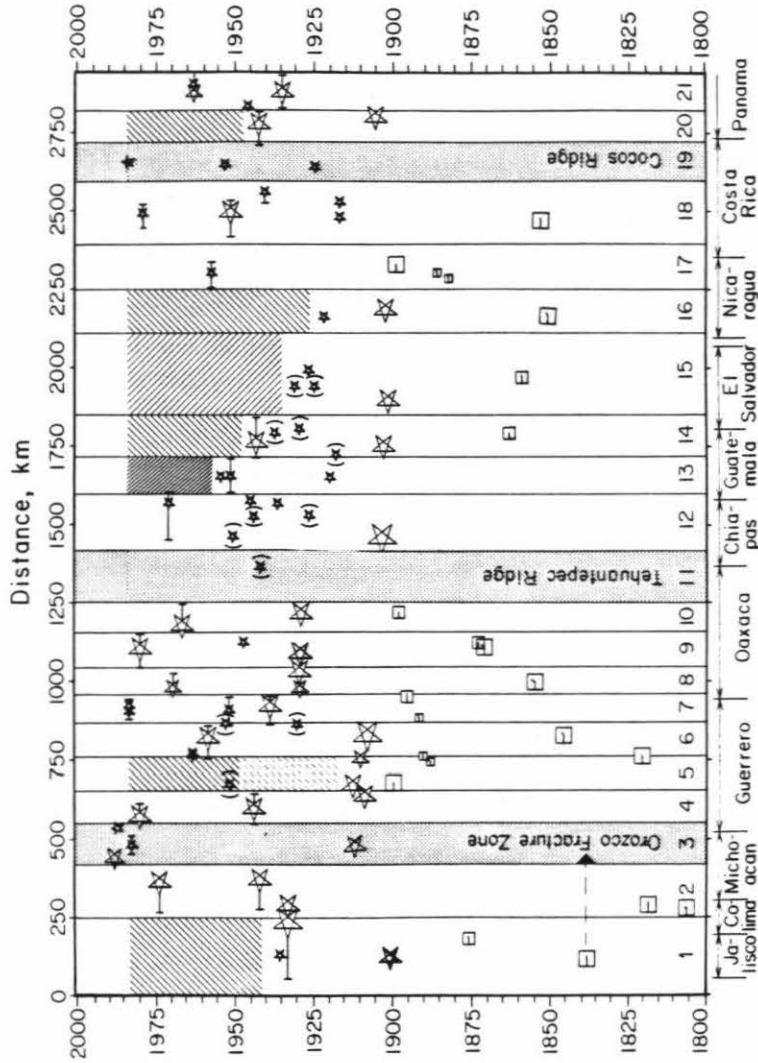
Figure 4.3: Time-distance plot of large earthquakes (M>7) along the Middle-America trench. Stars are large events that occurred during this century. Squares indicate last century events. Bars indicate the extent of aftershock areas for recent events. Names at the bottom refer to Mexican coastal states and Central American countries. Numbers at the bottom refer to regions determined from aftershock distribution of recent earthquakes. Dotted regions correspond to the Orozco Fracture zone (3), and the Tehuantepec (11) and Cocos (19) Ridges, where anomalous seafloor is being subducted. Hatched sections indicate seismic gaps: Jalisco (1), Guerrero (5), West and East Guatemala(13-14), El Salvador(15), Nicaragua(16) and West Panama(20). Notice that the 1982 Ometepec doublet broke the preexisting seismic gap and that the former Michoacan Gap (3) was ruptured during the September 1985 earthquakes.

Table 4.3: Average Seismic Moment $\overline{M}_o$,

for regions along the Mexican Subduction Zone

	Region	$\overline{M}_o$ (10^{27} dyne-cm)	V (cm/yr)	T (years)	η	T_c (years)
1.	Jalisco	8.75 ± 0.92	5.14	31.7 ± 6.5		25.4 ± 5.2
2.	Colima	4.95 ± 1.80	5.27	20.5 ± 11.5	0.52	16.9 ± 9.5
3.	Michoacan	8.50 ± 1.50	5.74	73.0 ± 1.0	0.44	65.5 ± 1.0
4.	Petatlan	2.24 ± 0.54	6.22	35.5 ± 0.7	0.45	34.5 ± 0.7
5.	Guerrero	8.5 ± 1.5	6.40			
6.	Acapulco	5.08 ± 1.16	6.71	56.0 ± 8.5	0.26	58.7 ± 8.9
7.	Ometepec	0.88 ± 0.56	7.00	30.6 ± 17.0	0.25	3.5± 18.6
8.	W.Oaxaca	2.39 ± 1.95	7.07	38.0 ± 3.5	0.23	42.0 ± 4.2
9.	C.Oaxaca	5.25 ± 2.89	7.30	53.0 ± 4.2	0.30	60.4 ± 4.8
10.	E.Oaxaca	1.74 ± 0.05	7.50	34.5 ± 3.6	0.20	40.4 ± 4.2
11.	Tehuantepec					

$\overline{M}_o$ - Average seismic moment for each region

V - Plate convergence rate calculated from Minster and Jordan (1978)

T - Observed average recurrence period from Table 4.2

η - Ratio of seismic slip, D, to total slip, u, between the plates

T_c - T corrected assuming a constant V=6.4 km/s

The relation between $\overline{M}_o$ and T_c is shown in Figure 4.4 for regions along the Mexican subduction zone. The heavy line has a slope of 1/3. Despite the relatively large error bars associated with each region, the data for the Guerrero-Oaxaca regions (4-10) follow the relation given (5) and fit the following empiric relation

$$\log T = \frac{1}{3}\log M_o - 7.5, \tag{7}$$

thus supporting the simple asperity model (Lay and Kanamori, 1981). The events in the Jalisco and Colima regions do not follow the trend for the Guerrero-Oaxaca region. The plate geometry is more complex northwest of the Michoacan gap than in the Guerrero-Oaxaca region, and factors other than the asperity size may have to be
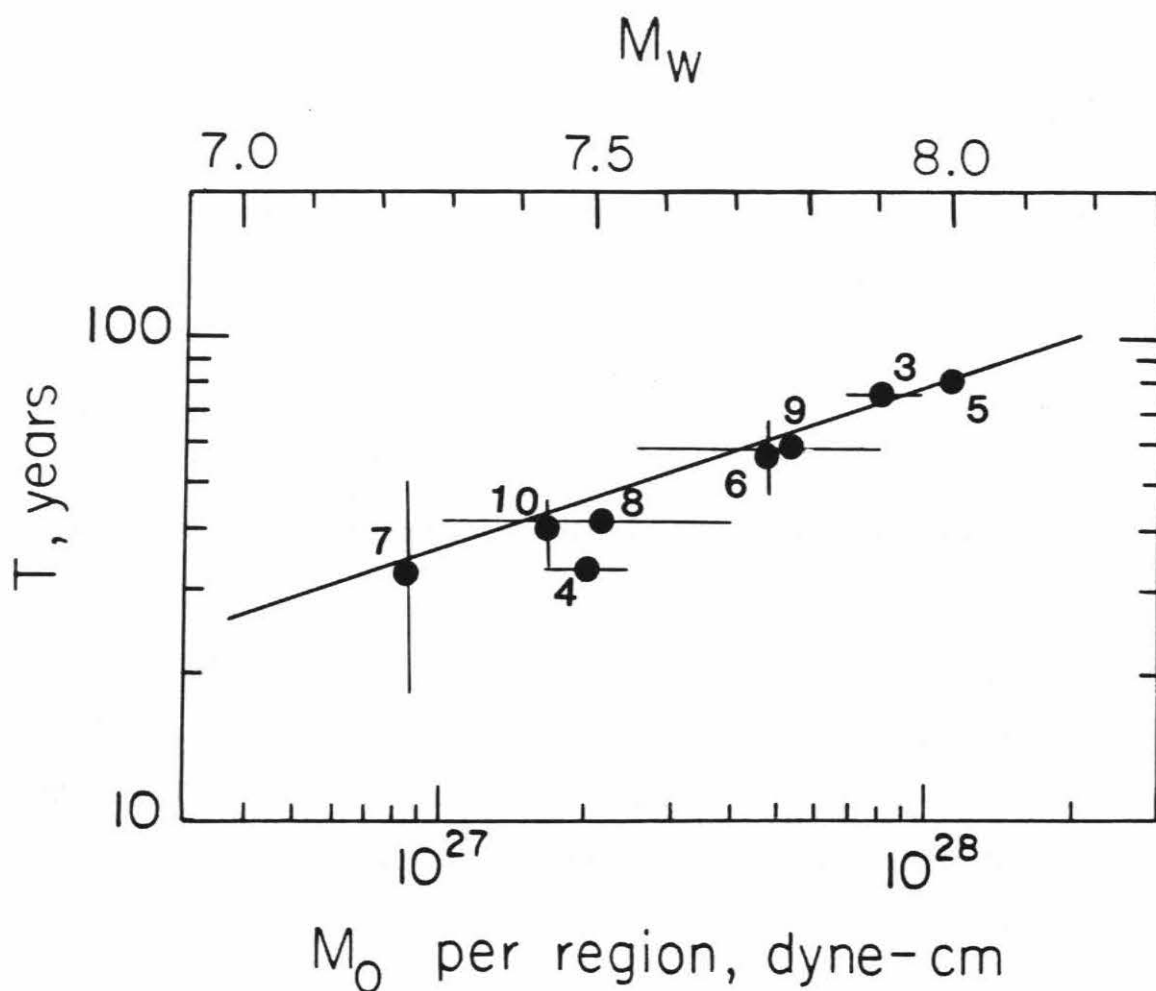
Figure 4.4: Plot of log of average moment per region $\overline{M}_o$, versus log of recurrence period T, along the Mexican subduction zone. Numbers correspond to regions in Figure 4.1. The line has a slope of $1/3$, suggesting that the relation $\log T = 1/3 \log M_o$ holds for events that have occurred along the zone from Michoacan to Oaxaca. The 1985 Michoacan earthquake (region 3) fits the general trend.

considered in estimating the repeat time. However, last-century event location of events in these regions is very uncertain (Singh et al., 1985a) and consequently, their average recurrence times are also uncertain. Nevertheless, this relation suggests that the high convergence rate, which produces rapid strain accumulation and short recurrence intervals for large earthquakes, and the smooth seafloor subducted may contribute to the homogeneous distribution of comparable size asperities along the Middle-America trench.

4.4 Implications for Present Seismic Gaps in Middle America

Although several large earthquakes have occurred in the last 20 years along the Middle America plate boundary, about 40% of its length has not been broken in over 30 years. These regions have a high seismic potential and are shown hatched in Figure 4.3: Jalisco(1), Guerrero(5), Guatemala (13-14), El Salvador(15), Nicaragua(16), and West Panama (20).

Recurrence intervals of large subduction earthquakes in Central America are somewhat uncertain, probably due to the fact that no large earthquakes have occurred there recently and that historic seismic data are more uncertain than for Mexico. Similar size earthquakes have occurred at regular intervals in the Cocos Ridge(19) and those regions adjacent to it in the last 100 years (Table 4.2), and the West Panama region (20) is a seismic gap. On the other hand, the region south of the Tehuantepec Ridge from Chiapas, Mexico, to Nicaragua (Figure 4.3) may have been broken last at the turn of the century in a series of great earthquakes (M_S=7.9–8.2). Since then only earthquakes with $M_S \approx 7.2$ have occurred there, with

the exception of the 1942 Guatemala earthquake (M_S=7.9). The Middle-America trench offshore this area is wider and more pronounced than adjacent regions (Chase et al., 1970). The subducting seafloor is also older, and presumably more dense, increasing the dip of the slab and consequently decreasing the coupling between the Cocos and the Caribbean plates (Ruff and Kanamori, 1983). Since the Benioff zone is more steeply dipping in this area than in the region north of the Tehuantepec Ridge (Molnar and Sykes, 1969) and the convergence rate is similar, of the order of 7 cm/yr (Minster and Jordan, 1978), then longer recurrence periods will be expected. In any case, most of this region has not experienced a truly great earthquake in more than 80 years making this region offshore Central America, about 650 km in length, the largest seismic gap in the Middle-America trench. A crude estimate of the seismic moment accumulated in this region is given by $M_o = \mu\ \eta\ u\ L\ W$, where u=595 cm is the total displacement accumulated in 85 years from the convergence rate from Minster and Jordan (1978). Assuming μ=3×10^{11}dyne/cm^2, η=0.4, L = 650 km, and W = 40 km, then M_o=1.8×10^{28} dyne cm, which is a conservative estimate. This seismic moment could be released in three M_w=7.8 earthquakes similar to those events that occurred during the 1898-1902 period.

In the Tehuantepec Ridge (11) no large earthquake has occurred during this century and perhaps for as long as 200 years. This region is either aseismic or has extremely long recurrence intervals (Singh et al., 1981). The location of earlier events in the Jalisco and Colima regions are uncertain; thus, the recurrence times in Table 4.2 for these two regions are unreliable. Singh et al. (1985a) suggested that if the 1932 Jalisco (M_S=8.2) earthquake is characteristic of this region, then the expected recurrence time would be about 95 years, if the convergence between the Rivera and

North-American plates is completely seismic.

The Guerrero seismic gap (5) is a region of great concern, since the last events occurred there around the turn of the century, from 1899 to 1909, and because the 1957 Acapulco (M_S=7.5) earthquake, in the region to the south, caused considerable damage to Mexico City (see Section 3.2). Equation (7) was derived for the Mexican subduction zone and implies that an impending event in the Guerrero gap would have a large seismic moment similar to the Michoacan earthquake. In deriving the T - M_o relation, seismic moments of earthquakes occurring within three years of each other were added together and considered as one event, approximately 10% of the average recurrence period in the region (McNally and Minster, 1981). Thus, the relation does not distinguish between single large earthquakes or sequences of smaller events closely spaced in time. Using 1907 as the last date for an event in Guerrero, the relation predicts that the moment for a future event would be 1.6×10^{28} dyne cm. This is equivalent to one earthquake with a moment magnitude of 8.1, or alternatively, three of M_w=7.8. Both scenarios have serious implications for damage in Mexico City. Another consideration is that the Acapulco region (6) can be considered almost a seismic gap, since the last event occurred in 1957. Nishenko and Singh (1987) suggest that the Acapulco-Ometepec regions broke simultaneously during the 1907 San Marcos (M_S=8.0) earthquake and that this region has a variable rupture mode. It should be emphasized that the boundaries between the regions delineated in Figure 4.3 are somewhat arbitrary, since they reflect only the rupture areas of recent events. This in no way precludes the possibility that a great earthquake may break adjacent regions. However, most regions in the Mexican subduction zone seem to be associated with a characteristic earthquake that breaks more or less the same region successively.

Conclusion to Part I

Since 1980 several large earthquakes have occurred along the Mexican subduc-
tion zone, in regions that had been previously identified as seismic gaps. The telese-
ismic source characteristics of these events have been analyzed to understand the rup-
ture processes of these events in the context of the Middle-America trench tectonics.

On June 7, 1982, an earthquake doublet occurred near Ometepec, Guerrero. The
second event occurred within five hours of the first. The first event of the doublet is
slightly smaller (M_S=6.9) than the second event (M_S=7.0). Both events had rela-
tively simple fault processes reflecting subduction of the Cocos plate underneath
North America. Source parameters of the first event are θ=116°, δ=77°, λ=88° and
M_o=2.8×10^{28} dyne cm, and for the second event, θ=116°, δ=78°, λ=78° and
M_o=2.8×10^{28} dyne cm. The first event had a single source 20 km deep, whereas the
second one consisted of two point sources located at 15 and 10 km depth, respec-
tively. These results suggest that the rupture of the Ometepec region started at
depth, with the first event breaking a deeper asperity, causing an incremental stress
change at shallower depth that triggered the second event.

The 1985 Michoacan, Mexico earthquake occurred in a region of the Mexico sub-
duction zone that had been devoid of large (M > 7.5) earthquakes since 1911. From
long-period teleseismic P-waveforms, we resolved that its focal mechanism and focal
depth were basically identical to those of other recent shallow interplate thrust events
in neighboring regions of the subduction zone. The seismic moment determined from
256 s period surface-waves is between 1.05 and 1.70×10^{28}dyne–cm, depending on the
assumed dip angle of the fault plane with a source process time τ=100s. A dip of 15°

yields the lower value of moment, more consistent with results of other studies of the earthquake. This corresponds to $M_W=7.9$ and is thus among the largest known earthquakes in Mexico. A comparison of four long-period source studies yields an average seismic moment of 1.17×10^{28}dyne–cm ($M_W=8.0$). The last event of comparatively size with a reliable instrumental estimate of seismic moment was the great Jalisco earthquake of 1932 ($M_o \sim 1 \times 10^{28}$dyne–cm ; Singh et al., 1985).

The source time function of the Michoacan earthquake consisted of two main episodes of moment release with the second source starting about 26 s after the origin time. From observed directivity in the body waves we estimate that the second event was located 95 km southeast of the first. This observation and evidence from the aftershock distribution implies that the earthquake broke the two remaining asperities in the Michoacan gap to the northwest and southeast of the rupture zone of the 1981 Playa Azul earthquake ($M_W=7.3$). The extended time duration of the source (of at least 42 s) was likely an ingredient in the severity of structural damage in Mexico City. The fault parameters determined from long-period P-waves are $\phi=288°$, $\delta=9°$ and $\lambda=72°$, consistent with the convergence direction of the Cocos plate in the region.

The large aftershock on September 21 was found to have the same focal mechanism as the mainshock and a slightly larger source depth (22 km) with a seismic moment of $2.9 - 4.7 \times 10^{27}$ ($M_W = 7.6 - 7.7$). This event occurred 125 km southeast of the main event, and ruptured the updip area of the 1979 Petatlán aftershock zone. Another large aftershock occurred on April 30, 1986, 50 km northwest of the mainshock epicenter. The fault parameters determined for this event are $\theta=280°$, $\delta=12°$, $\lambda=70°$, with a point source at 21 km depth and $M_o=2.0–3.1 \times 10^{26}$

dyne cm (M_w=6.9). Analysis of the 1981 Playa earthquake indicates that this event was deeper than the other events, d = 26 km, and also had a larger stress drop, ≈50bars, in contrast with most events along the Mexican subduction, some that are between 5 and 10 bars. The rupture of the Michoacan gap is then complex, since it was a sequence of events that started with the 1981 Playa Azul event that broke a small deep asperity and then continued on September 19, 1985, breaking the shallower asperities in the region.

A review of seismicity along the Middle-America trench shows that some regions, along Jalisco, Guerrero, Guatemala, El Salvador, Nicaragua and West Panama have not had a large earthquake for more than 30 years, and are considered seismic gaps with high seismic potential. The Tehuantepec region may not have had an earthquake for as long as 200 years, meaning that this area either is aseismic or has unusually long recurrence times for Middle America. The region south of the Tehuantepec Ridge, from Chiapas, Mexico, to Nicaragua, is the largest seismic gap in the Middle-America trench. A series of great earthquakes occurred there at the turn of the century; only smaller (M≈7) events have occurred thereafter with the exception of the 1942 Guatemala (M_S=7.9) earthquake. This region is considered to have a high seismic potential.

An empirical relation between M_o and T was derived for the Mexican subduction zone $\log T = \frac{1}{3} \log M_o - 7.5$, where T is the average repeat time and M_o is the average moment of the characteristic events of a sequence that occurred at approximately the same place. This relation suggests that the scale length of asperities controls the repeat time, if other factors, such as the plate convergence rate and the seismic slip, η, are approximately the same. Applying this relation to the Guerrero seismic gap

predicts an event with $M_o = 1.6 \times 10^{28}$ dyne cm, similar in size to the great 1985 Michoacan earthquake, which caused very large damage to Mexico City.

References to Part I

Abe, K., 1973, Tsunami and mechanism of great earthquakes; *Phys. Earth and Planet. Int., 7,* 143-153.

Abe, K. and H. Kanamori, 1980, Magnitude of great shallow earthquakes from 1953-1977; *Tectonophysics, 62,* 191-203.

Aki, K., 1966, Generation and propagation of G waves from the Niigata earthquake of June 16, 1964. 2. Estimation of earthquake movement, released energy and stress-strain drop from G wave spectrum; *Bull. Earthquake Res. Inst. Tokyo Univ., 44,* 23-88.

Anderson, J.G., P. Bodin, J.N. Brune, J. Prince and S.K. Singh, R. Quaas, M. Onate, 1986, Strong ground motion and source mechanism of the Mexico earthquake of September 19, 1985 (M_S=8.1); *Science, 233,* 1043-1049.

Ando, M., 1975. Source mechanisms and tectonic significance of historical earthquakes along the Nankaido Trough, Japan; *Tectonophysics, 27,* 119-140.

Astiz, L. and H. Kanamori, 1984, An earthquake doublet in Ometepec, Guerrero, Mexico, *Phys. Earth Planet. Int., 34,* 24-45.

Astiz, L., H.K. Eissler and H. Kanamori, 1987, Source characteristics of the Michoacan, Mexico earthquakes sequence: 1981-1986; *submitted to Bull. Seis. Soc. Am.*

Aubouin, J., J.F. Stephan, V. Renard, J. Roump and P. Lousdale, 1982, Subduction of the Cocos plate in the Mid America Trench; *Nature, 294,* 147-150.

Beck, J.L. and J.F. Hall, 1986, Factors contributing to the catastrophe in Mexico city during the earthquake of September 19, 1985; *Geophys. Res. Lett., 13,* 593-596.

Bodin, P. and T. Klinger, 1986, Coastal uplift and mortality of intertidal organisms caused by the September 1985 Mexico earthquakes; *Science, 233,* 1071-1072.

Branner, J., 1912, in *Reviews, Bull. Seismol. Soc. Am., 3,* 12.

Brune, J.N., 1970, Tectonic stress and the spectra of seismic shear waves from earthquakes; *Jour. Geophys. Res., 75,* 4997-5009.

Bufaliza, M., 1984, Atenuación de intensidades sismicas con la distancia en sismos mexicanos; *M.S. Thesis, Fac. de Ingeniería, U.N.A.M.* 94 p..

Carr, M.J. and R.E. Stoiber, 1977, Geologic setting of some destructive earthquakes in Central America; *Geol. Soc. Am. Bull., 88,* 151-156.

Chael, E. P. and G. S. Stewart, 1982, Recent large earthquakes along the Middle-American trench and their implications for the subduction process, *J. Geophys. Res., 87,* 329-338.

Chase, T.F., H.W. Menard and J. Mammerickx, 1970, Bathymetry of the North Pacific; *Map from Scripps, Inst. of Oceanogr. and Inst. of Mar. Resour., Univ. of Calif., San Diego.*

Couch, R. and S. Woodcock, 1981, Gravity and structure of the continental margins

of southwestern Mexico and northwestern Guatemala; *J. Geophys. Res., 86,* 1829-1840.

Dean, B.W. and C.L. Drake, 1978, Focal Mechanism solutions and tectonics of the Middle America Arc; *J. Geol., 86,* 111-128.

Demaint, A., 1978, Caracteristicas del Eje Neovolcanico Transmexicano y sus problemas de interpretacion; *Rev. Inst. Geolo. U.N.A.M., 2,* 172-187.

Duke, C.M. and D.J. Leeds, 1959, Soil conditions and damage in the Mexico earthquake of July 28, 1957; *Bull. Seis. Soc. Am., 49,* p. 179-191.

Dziewonski, A.M., Chou,T.-A. and Woodhouse, J.H., 1981, Determination of earthquake source parameters from wave-form data studies of global and regional seismicity; *J. Geophys. Res., 86,* 2825-2852.

Dziewonski, A.M. and J.H. Woodhouse, 1983, An experiment in the systematic study of global seismicity; centroid-moment tensor solution for 201 moderate and large earthquakes of 1981; *Jour. Gephys. Res., 88,* 3247-3271.

Eissler, H. and K. McNally, 1984, Seismicity and tectonics of the Rivera plate and implications for the 1932 Jalisco, Mexico earthquake; *Jour. Geophys. Res., 89,* 4520-4530.

Eissler, H., L. Astiz and H. Kanamori, 1986, Tectonic setting and source parameters of the September 19, 1985 Michoacan, Mexico, earthquake; *Geophys. Res. Lett., 13,* 569-572.

Ekstrom, G. and A.M. Dziewonski, 1986, A very broad band analysis of the Michoacan, Mexico, earthquake of September 19, 1985 Geophys. Res. Lett., 13, p. 605-607.

Espindola, J.M., S.K. Singh, J. Yamamoto and J. Havskov, 1981, Seismic moments of large Mexican subduction earthquakes since 1907; EOS, 62, 948.

Figueroa, J. A., 1959, New seismic chart of Mexico, *Anales del Instituto de Geofísica, Universidad Nacional Autonoma de México, 5,* 45-162.

Figueroa, J., 1970, Catálogo de sismos ocurridos en la Republic Mexicana, *Report 272, Instituto de Ingenieria, U.N.A.M., Mexico*

Fisher, R.L., 1961, Middle America Trench: topography and structure; *Geol. Soc. Am. Bull., 72,* 703-720.

Geller, R.J. and H. Kanamori, 1977, Magnitude of great shallow earthquakes from 1904-1952; *Bull. Seis. Soc. Am., 67,* 587-598.

Gettrust, J.F., V. Hsu, C.E. Helsley, E. Herrero and T. Jordan, 1981, Patterns of local seismicity preceding the Petatlan earthquake of March 14, 1979; *Bull. Seis. Soc. Am., 71,* 761-769.

González-Ruiz, J.R., 1986, Earthquake source mechanics and tectonophysics of the Middle America subduction zone in Mexico; *Ph.D. Thesis, U. of Calif., Santa Cruz.*

Goodstein, J.R., H. Kanamori and W. Lee, 1980, Seismology microfiche publications from the Caltech archives; *Bull. Seis. Soc. Am., 70,* 657-658.

Guendel F. and K.C. McNally, 1982, The foreshock-mainshock-aftershock sequence of

the 1978 ($M_s=7.0$) Samara, Costa Rica earthquake: A unique data set.; *Abstracts with Programs Seism. Soc. Am., 53;* 81.

Gutenberg, B. and C. F. Richter, 1954, *Seismicity of the Earth and Associated Phenomena,* Princeton University Press, Princeton, NJ., 135 pp.

Havskov, J., S.K. Singh, E. Nava, T. Dominguez and M. Rodriguez, 1983, Playa Azul, Michoacan, Mexico, earthquakes of 25 October, 1981 ($M_S=7.3$); *Bull. Seis. Soc. Am., 73,* 449-458.

Houston, H. and H. Kanamori, 1986, Source characteristics of the 1985 Michoacan, Mexico earthquake at short periods; *Geophys. Res. Lett., 13,* 597-600.

Kanamori, H., 1977, Seismic and aseismic slip along subduction zones and their tectonic implications; *Maurice Ewing series 4, 4,* 163-174.

Kanamori, H., 1983, *Summaries of Technical Reports XVI,* Open-file report 83-525.

Kanamori, H. and J. Cipar, 1974, Focal process of the Great Chilean earthquake May 22, 1960. *Phys. Earth Planet. Int., 9,* 128-136.

Kanamori, H. and D.L. Anderson, 1975, Theoretical basis of some empirical relations in Seismology; *Bull. Seism. Soc. Am., 65,* 1073-1093.

Kanamori, H. and G.S. Stewart, 1976, Mode of strain release along the Gibbs fracture zone, Mid-Atlantic Ridge; *Phys. Earth Planet. Int., 11,* 312-332.

Kanamori, H. and J. W. Given, 1981, Use of long-period surface waves for rapid determination of earthquake source parameters, *Phys. Earth Planet. Inter., 27,* 8-31.

Kanamori, H. and J. W. Given, 1982, Use of long-period surface waves for rapid determination of earthquake source parameters, 2. Preliminary determination of source mechanisms of large earthquakes ($M_S \geq 6.5$) in 1980, *Phys. Earth Planet. Inter., 30,* 260-268.

Kelleher, J., L. Sykes, and J. Oliver, 1973, Possible criteria for predicting earthquake locations and their application to major plate boundaries of the Pacific and the Caribbean, *J. Geophys. Res., 78,* 2547-2585.

Kelleher, J. and W.R. McCann, 1976, Buoyant zones, great earthquakes and unstable boundaries of subduction; *Jour. Geophys. Res., 81,* 4885-4896.

Langston, C.A. and D.V. Helmberger, 1975, A prodedure for modeling shallow dislocation sources; *Geophys. J.R. Astr. Soc., 42,* 117-130.

Lay, T. and H. Kanamori, 1980, Earthquake doublets in the Solomon Islands; *Phys. Earth Planet. Int., 21,* 283-304.

Lay, T. and H. Kanamori, 1981, An asperity model of large earthquakes sequences; *Maurice Ewing Series 4, Earthquake Prediction Research , 1,* 3-71.

Lay, T., J. Given and H. Kanamori, 1982, Long period mechanism of the 8 November 1980 Eureka, CA earthquake; *Bull. Seism. Soc. Am., 72,* 439-456.

LeFevre, L. V., and K. C. McNally, 1985, Stress distribution and subduction of aseismic ridges in the Middle America subduction zone, *J. Geophys. Res., 90,* 4495-4510.

Madariaga, R., 1977, Implications of stress-drop models of earthquakes for the

inversion of stress drop from seismic observations; *Pure Appl. Geophys., 115,* 301-316.

Mammerickx, J., S.M. Smith, I.L. Taylor and T.E. Chase, 1975, Topography of the south Pacific; *Carte Bathymetrique,* Scripps Institution of Oceanography, La Jolla, Calif.

McCann, W.R., S.P. Nishenko, L.R. Sykes and J. Krause, 1979, Seismic gaps and plate tectonics: seismic potential for major boundaries; *Pageoph., 117,* 1082-1147.

McNally, K. C., and J. B. Minster, 1981, Nonuniform seismic slip rates along the Middle America Trench, *J. Geophys. Res., 86,* 4949-4959.

Minster, J.B. and T.H. Jordan, 1978, Present day plate motions; *Jour. Geophys. Res., 83,* 5331-5354.

Miyamura, S., 1976, Provisional magnitudes of Middle American earthquakes not listed in the magnitude catalogue of Gutemberg-Richter; *Bull. Int. Inst. Seism. Earthquake Eng., 14,* 41-46.

Molnar, P. and L. Sykes, 1969, Tectonics of the Caribbean and Middle America regions from focal mechanisms and seismicity; *Geol. Soc. Am. Bull., 80,* 1639-1684.

Mooser, F., 1972, The Mexican Volcanic Belt: structure and tectonics; *Geof. Internal., 17,* 55-70.

Nakanishi, I. and H. Kanamori, 1982, Effects of lateral heterogeneity and source process time on the linear moment tensor inversion of long-period Rayleigh waves; *Bull. Seism. Soc. Am., 72,* 2063-2080.

Nava, E.A., 1983, Estudio de los temblores de Ometepec del 7 de junio de 1982 y sus réplicas. *Tesis Profesional, Facultad de Ingeniería, UNAM.*

Nishenko, S.P. and S.K. Singh, 1987, The Acapulco-Ometepec, Mexico earthquakes of 1907-1982: Evidence for a variable recurrence history; *submitted to Bull. Seis. Soc. Am.*

Ohtake, M., T. Matumoto and G. V. Latham, 1977, Seismic gap near Oaxaca, southern Mexico as probable precursor to a large earthquake; *Pageoph., 115,* 375-385.

Orozco y Berra, J., 1887, Journal of seismic activity in Mexico (in Spanish); *Jour. Sci. Soc. "Antonio Alzate, "* 1.

Ortega, F., R. Corona, J. Martínez and O. Quintero, 1985, Isosistas preliminares de la región epicentral del sismo del 19 de septiembre de 1985 y fenómenos geológicos y destructivos associados; *Unión Geofísica Mexicana, Reunión Anual 1985,* abstract.

Plafker, G., 1976, Tectonic aspects of the Guatemala earthquake of 4 February 1976; *Science, 193,* 1201-1208.

Priestley, K.F. and T.G. Masters, 1986, Source mechanism of the September 19, 1985 Michoacan earthquake and its implications; *Geophys. Res. Lett., 13,* 601-604.

Prince, J., R. Quaas and E. Mena, 1986, The Michoacan-Guerrero earthquake of September 19, 1985: Strong ground motion in Mexico City; *EOS, 67,* 85.

Reyes, A., J.N. Brune and C. Lomnitz, 1979, Source mechanism and aftershock study of the Colima, Mexico earthquake of January 30, 1973; *Bull. Seism. Soc. Am.*, *69*, 1819-1840.

Riedesel, M.A., T.H. Jordan, A.F. Sheehan and P.G. Silver, 1986, Moment-tensor spectra of the 19 Sept. 85 and 21 Sept. 85 Michoacan, Mexico, earthquakes; *Geophys. Res. Lett.*, *13*, 609-612.

Rudnicki, J.W. and H. Kanamori, 1981, Effects of fault interaction on moment, stress drop and strain energy release; *J. Geophys. Res.*, *86*, 1785-1793.

Ruff L.J. and H. Kanamori, 1983, Seismic coupling and uncoupling at subduction zones; *Tectonophysics, 99*, 99-117.

Shimazaki, K. and T. Nakata, 1980, Time-predictable recurrence model for large earthquakes; *Geophs. Res. Lett.*, *71*, 279-282.

Shipley, T., K.J. McMillen, J.S. Watkins, J.C. Moore, J.H. Sandoval-Ochoa and J.L. Worzel, 1980, Continental margin and lower slope structures of the Middle America trench near Acapulco (Mexico); *Marine Geol.*, *35*, 65-82.

Silver, P.G. and T.H. Jordan, 1983, Total-moment spectra of fourteen large earthquakes; *Jour. Geophys. Res.*, *88*, 3273-3293.

Singh, S.K., J. Yamamoto, J. Haskov, M. Guzmán, D. Novelo, and R. Castro, 1980a, Seismic gap of Michoacan, Mexico, *Geophys. Res. Lett.*, *7*, 69-72.

Singh, S.K., J. Havskov, K. McNally, L. Ponce. T. Hearn and M. Vassiliou, 1980b, The Oaxaca, Mexico earthquake of 29 November 1978: A preliminary report on aftershocks; *Science, 207*, 1211-1213.

Singh, S.K., L. Astiz and J. Havskov, 1981, Seismic gaps and recurrence periods of large earthquakes along the Mexican subduction zone: A reexamination; *Bull. Seis. Soc. Am.*, *71*, 827-843.

Singh, S.K., J.M. Espindola, J. Yamamoto and J. Havskov, 1982a, Seismic potential of Acapulco-San Marcos region along the Mexican subduction zone; *Geophys. Res. Lett.*, *9*, 633-636.

Singh S.K., M. Rodriguez and L. Esteva, 1982b, Statistics of small earthquakes and frequence of occurrence of large earthquakes along the Mexican subduction zone; *EOS, 63*, 1040.

Singh, S.K., T. Dominguez, R. Castro, and M. Rodriguez, 1984, P waveform of large, shallow earthquakes along the Mexican subduction zone, *Bull. Seism. Soc. Am.*, *74*, 2135-2156.

Singh, S.K., L. Ponce and S. P. Nishenko, 1985a, The great Jalisco, Mexico earthquakes of 1932: Subduction of the Rivera plate, *Bull. Seismol. Soc. Amer.*, *5*, 1301-1314.

Singh, S.K., G. Suárez and T. Dominguez, 1985b, The Oaxaca, Mexico, earthquake of 1931: lithospheric normal faulting in the subducted Cocos plate; *Nature, 317*, 56-58.

Stewart, G.S., E.P. Chael and K. McNally, 1981, The November 29, 1978, Oaxaca, Mexico earthquake. A large simple event; *Jour. Geophys. Res.*, *86*, 5053-5060.

Stoiber, R.E. and M.J. Carr, 1977, Quaternary volcanic and tectonic segmentation of Central America; *Bull. Volcanol.*, *37*, 304-325.

Sykes, L.R. and R.C. Quittmeyer, 1981, Repeat times of great earthquakes along simple plate boundaries; *Maurice Ewing series 4*, 217-247.

Stolte, C., K.C. McNallyu, J. Gonzalez-Ruiz, G.W. Simila, A. Reyes, C. Rebollar, L. Munguia, and L. Mendoza, 1986, Fine structure of a post failure Wadati-Benioff; *Geophys. Res. Lett.*, *13*, p. 577-580.

Tajima, F. and K. McNally, 1983, Seismic rupture patterns in Oaxaca, Mexico; *Jour. Geophys. Res.*, *88*, 4263-4276.

Tajima, F., 1984, Study of source processes of the 1965, 1968 and 1978 Oaxaca, earthquakes using short-persod records; *Jour. Geohphys. Res.*, *89*, 1867-1873.

UNAM Seismology Group, 1986, The September 1985 Michoacan earthquakes: aftershock distribution and history of rupture; *Geophys. Res. Lett.*, *13*, 573-576.

Valdés, C., R.P. Meyer, R. Zúñiga, J. Havskov and S.K. Singh, 1982, Analysis of the Petatán aftershocks: number, energy release and asperities; *Jour. Geophys. Res.*, *87*, 8519-8527.

Vogt, P. R., A. Lowrie, D. Bracey, and R. Hey, 1976, Subduction of aseismic oceanic ridges: Effects on shape, seismicity, and other characteristics of consuming plate boundaries, *Geol. Soc. Amer. Spec. Pap.*, *172*.

Wang, S., K. McNally and R.J. Geller, 1982, Seismic strain release along the Middle America trench, Mexico; *Geophys. Res. Lett.*, *9*, 182-185.

Wesnousky, S.G., L. Astiz and H. Kanamori, 1986, Earthquake multiplets in the Southeatern Solomon Islands; *Phys. Earth. Planet. Int., in press*

Yamamoto, J., 1978, Rupture processes of some complex earthquakes in southern Mexico; *Ph. D. Thesis, Saint Louis University, MO*, 203 pp.

Zhang, J. and H. Kanamori, 1987, Source finiteness of large earthquakes measured from long-period surface waves (in preparation).

Abstract to Part II

Chapter 1 explores the relation of intermediate-depth earthquakes to the shallower seismicity, especially if these events may reflect the state of inter-plate coupling at subduction zones. First, we consider the historic record of the largest earthquakes ($m_B \geq 7.0$) that occur within the subducting lithosphere to provide a general background for a more detailed study of recent large events. The largest number of large intraplate events is observed at the New Hebrides and Tonga subduction zones. Regions associated with bends in the subducted lithosphere also have many large events (e.g., Altiplano and New Ireland). The profiles of earthquake magnitude versus depth of these historic large intraplate earthquakes give an estimate of the seismic energy released within the subducting lithosphere for different regions (Appendix 1).

Secondly, a catalog of earthquake focal mechanisms was gathered. The catalog includes all events listed by NOAA and ISC catalogs with $M > 6$ and depth between 40 to 200 km, which occurred between 1960 and 1984. The final catalog includes only intermediate-depth earthquakes, a total of 335 events, for which 47 were determined by this study (Appendix 2), and it is probably complete for earthquakes with $m_B > 6.5$ from 1960 to 1984. Focal mechanism solutions for intermediate-depth earthquakes with $M > 6.8$ can be grouped into four: 1) Normal-fault events (44%), and 2) reverse-fault events (33%), both with a strike nearly parallel to the trench axis. 3) Normal or reverse fault events with a strike significantly oblique to the trench axis (10%), and 4) tear faulting events (13%). The focal mechanisms of Type 1 events occur mainly along strongly or moderately coupled subduction zones. However, these events also occur in the Tonga trench, where they may be related to the subduction

of the Louiville ridge that may cause an increased coupling of the subducting litho-
sphere. Thus, these events may be interpreted as evidence for strong or moderate cou-
pling between plates. Simple models of plate coupling and geometry suggest that
Type 1 events occur at strongly coupled plate boundaries, where a down-dip exten-
sional stress prevails in a gently dipping plate. Continental loading may be another
important factor. In contrast, subduction zones that are considered to be decoupled
great normal fault earthquakes occur at shallow depths, for example, the 1933 San-
riku earthquake in northeast Japan and the 1977 Sumbawa earthquake in Indonesia.
In summary, strongly coupled plates will have normal-fault earthquakes at the base of
the coupled zone, while uncoupled subduction zones will have them near the trench
axis. Type 2 events with strike subparallel to the subduction zone, most of them
with near vertical tension axis, occur mainly in regions that have partially coupled or
uncoupled subduction zones and the observed continuous seismicity is deeper than
300 km. In terms of our simple model, the increased dip of the downgoing slab asso-
ciated with weakly coupled subduction zones and the weight of the slab may induce
near vertical tensional stress at intermediate depth and, consequently, the change in
focal mechanism from Type 1 to Type 2 events. Events of Type 3 occur where the
trench axis bends sharply causing horizontal (parallel to the trench strike) extensional
or compressional intraplate stress. Type 4 are hinge-faulting events. We determine
the number of aftershocks reported by the NOAA and ISC catalogs of the
intermediate-depth events with $M \geq 6.5$ that occur within one week of the mainshock.
About 48% of the events had no aftershocks, 37% of the events had between 1 and 5
aftershocks and only 15% more than 5 aftershocks. There is a slight correlation
between mainshock magnitude and number of aftershocks. However, events with

more than 10 aftershocks are located in regions associated with bends in the subducted slab.

Chapter 2 discusses the temporal variation of the mechanism of large intermediate-depth earthquakes in relation to the occurrence of large underthrusting earthquakes in Chile. Focal mechanisms were determined for three large events (March 1, 1934: M=7.1, d=120 km, April 20, 1949: M=7.3, d=70 km and May 8, 1971: M_w=7.2, d=150 km), which occurred down-dip of the great 1960 Chilean earthquake (M_w=9.5) rupture zone. The 1971 event is down-dip compressional: θ=12°, δ=80°, λ=100° . The 1949 earthquake focal mechanism is θ=350° , δ=70° and λ=-130°. The data available for the 1934 event are consistent with a down-dip tensional mechanism. Thus, the two events that occurred prior to the great 1960 Chilean earthquake are down-dip tensional. Published fault plane solutions of large intermediate-depth earthquakes (March 28, 1965 and November 7, 1981), which occurred down-dip of the Valparaiso earthquakes of 1971 (M_w=7.8) and 1985 (M_w=8.0), are also down-dip tensional. These results suggest that before a major thrust earthquake, the interplate boundary is strongly coupled and the subducted slab is under tension at intermediate depths; after the occurrence of an interplate thrust event, the displacement on the thrust boundary induces transient compressional stress at intermediate depth in the down-going slab. This interpretation is consistent with the hypothesis that temporal variations of focal mechanisms of outer-rise events are due to changes of interplate coupling.

Chapter 3 investigates the variation of focal mechanisms of moderate and large intermediate-depth earthquakes in relation to local variations of the strength of interplate coupling in a region. Temporal changes due to the occurrence of large

underthrusting earthquakes are also explored. The stress axis orientation of the intermediate-depth events shows that most regions have either dominant down-dip tensional stresses at intermediate depth or a mixed pattern. The exception is Tonga, where down-dip compressional stresses are dominant. Along Middle and South America, where the interplate boundary varies from moderate to strongly coupled, intermediate-depth earthquakes are generally normal-fault events that occur before and down-dip of future large subduction earthquakes. In most regions along Middle and South America, we observe a reduction only in the number of large intermediate-depth events after a large subduction occurs in the region. However, down-dip compressional events have been observed down-dip and after the 1960 Chile and the 1974 Peruvian large thrust earthquakes. In the Caribbean and Scotia arcs, which have weakly coupled plate boundaries, most intermediate-depth events have nearly vertical tension axis induced by the negative buoyancy of the downgoing lithosphere. After the 1964 Alaska earthquake, only one tear fault event has occurred at intermediate-depth. Down-dip of the large 1957 Aleutian earthquake, the few events located there indicate coupling at the interplate boundary. This region was very active at intermediate-depth before 1957, when the interplate boundary broke. In addition, one of these events occurred before and down-dip of the large 1986 Andreanof earthquake. Down-dip of the 1952 Kamchatka earthquake aftershock zone, a down-dip compressional event occurred in 1960. After 1969, only events with down-dip tensional axis have occurred indicating that this region is again moderately coupled. Large intermediate-depth events under Japan and the south Kurile trench reflect the complexity of the subducting lithosphere in this region, which has been very active throughout this century. Subduction zones in the Philippine Sea region

are either weakly coupled as the Philipine and Ryukyu trenches or uncoupled as the Mariana and Izu-Bonin subduction zones. All of these regions have nearly vertical tensional stresses. Along the southern boundary of Indonesia, the coupling of the Indo-Australian and Eurasia plates changes from weakly coupled to uncoupled, and intermediate-depth events exhibit nearly vertical tension axis. The Timor trench, where bending of the lithosphere is observed, is very active. The subduction zones from New Britain to New Hebrides have moderately to partially coupled interplate boundaries. Temporal changes of focal mechanisms are observed associated with the 1971 New Ireland doublet events, whereas intermediate-depth events in New Hebrides have nearly vertical tension axis induced by the weight of the slab. Under the Tonga trench, mostly down-dip compressioanal events are observed; however, the events located down-dip of the Louiville ridge have down-dip tensional mechanisms and occurred before the large 1982 Tonga thrust event. Temporal changes in the focal mechanisms are also observed with the occurrence of the 1976 Kermadec doublet events.

Chapter 1

Intermediate-depth Earthquakes and Interplate Seismic Coupling

1.1 Introduction

In the theory of Plate Tectonics, subduction of the oceanic lithosphere plays a primary role, with the contact zone between subducting and overriding plates being the locus of large underthrusting earthquakes. Such large interplate thrust earthquakes have been extensively studied, and are basically well understood within the context of the tectonic convergence process. However, while most large earthquakes in subduction zones involve interplate thrusting (event A in Figure 1.1), a significant number are intraplate events within the subducting lithosphere. These intraplate ruptures occur as shallow events near the trench axis (e.g., 1933 Sanriku, 1977 Sumba) or in the outer-rise region (e.g., 1981 Chile, event B in Figure 1.1), or they occur as deeper events located down-dip from the plate interface within the subducting slab (e.g., 1982 San Salvador, event C in Figure 1.1). Intraplate events also occur well removed from subduction zones, in the interior of oceanic plates (e.g., 1965 Nazca, event D in Figure 1.1). In general, our understanding of the process producing the intraplate activity is very limited, principally because the tectonic context of intraplate events is much more difficult to interpret than for interplate events.

It is generally believed that intraplate subduction zone events are infrequent and less important than interplate thrust events for evaluating regional seismic hazard.
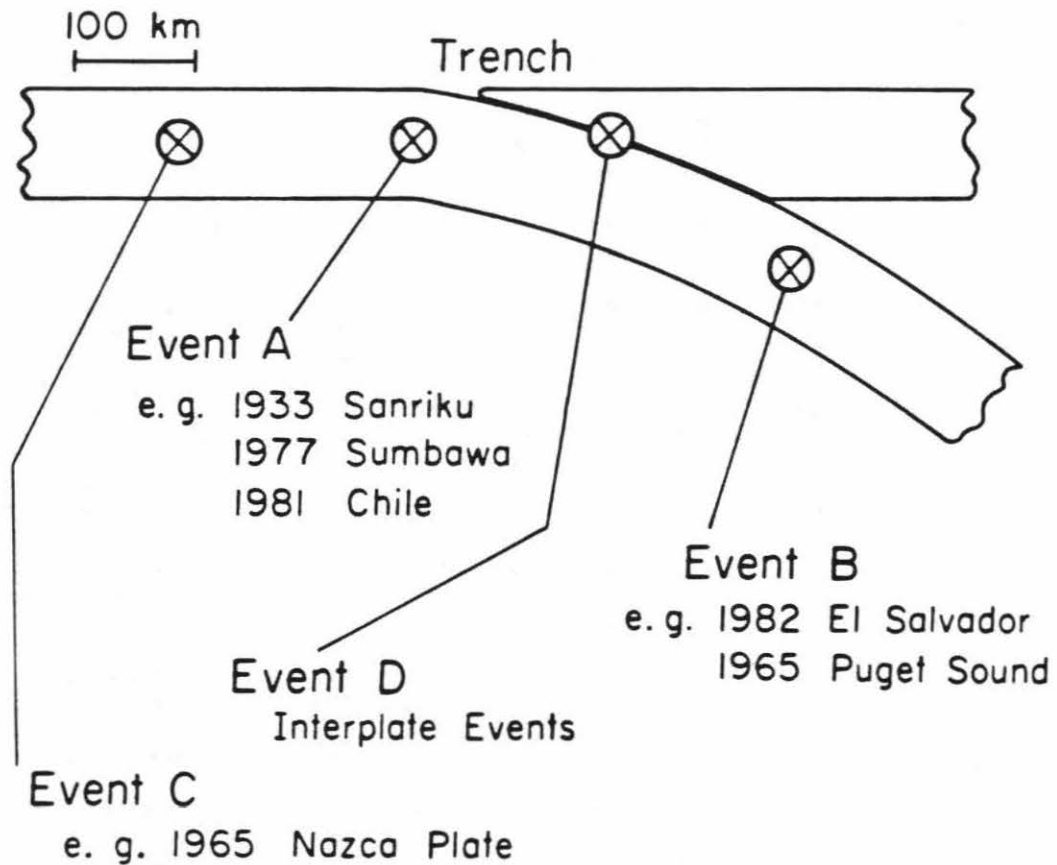
Figure 1.1: A schematic figure showing the location of the seismic events near a subduction boundary. Event A: thrust events on the interplate boundary. Event B: trench and outer-rise events. Event C: intermediate-depth events occurring in the subducted plate. Event D: oceanic intraplate events. Also indicated are examples of events for some of these categories.

Table 1.1: Characteristics of Subduction Zones

Region SP-OP	Subduction Zone Name	Age (m.y.)	Dip (deg)	TAz (deg)	TLg (km)	Depth (km)	Plate Convergence Rate (cm/y)	Azimuth (deg)	V_N (cm/y)
South America									
NA-SA	1-Colombia	<20	35[1]	30	800	250	7.9	81	6.2
	2-Ecuador	20	30[1]	0	600	200	8.0	82	7.9
	3-Peru	35	8[1]	335	1000	220	8.7	82	8.3
	4-Altiplano	50	28[1]	750	325	300	9.2	80	8.3
	5-North Chile	40	30[1]	2	720	300	9.3	80	9.1
	6-Central Chile	35	10[1]	10	600	200	9.1	81	8.6
	7-South Chile	<20	27[1]	8	1250	160	9.0	81	8.6
SA-Sw	8-Scotia	70	70[2]	135	500	200	5.4[3]	260	4.4
Middle America									
Ri-NA	-Rivera	2-10	10[4]	305	300	90	2.3[26]	39	2.1
Co-NA	9-Mexico	20-40	15[4]	300	900	200	7.0	37	6.9
Co-Cb	10-C. America	35-45	60[5]	314	1500	280	8.0	34	7.8
Caribbean									
Cb-NA	11-Greater Antilles	125?	75[6]	85	300	180	0.2	NS?	0.2
NA-Cb	12-Lesser Antilles	80	65[7]	150	800	250	2.0	282	1.5
North Pacific									
JF-NA	13-Juan de Fuca	10	22[8]	350	500	100	3.8[9]	45	3.1
Pc-NA	14-Alaska	45	45[10]	210	2000	160	7.2	329	6.3
	15-Aleutians	60	63[10]	260	3000	280	8.0	320	6.9
Western Pacific									
Pc-EU	16-Kamchatka	90	50[10]	216	450	540	8.8	305	8.8
	17-North Kuriles	95	50[10]	216	500	600	9.0	298	8.9
	17-South Kuriles	100	45[10]	230	500	625	9.2	298	8.5
	18-NE Japan	100	40[11]	236	900	580	9.4	294	8.0
Pc-Ph	19-Izu-Bonin	135	45[12]	165	1000	560	6.5[13]	278	6.0
	20-North Marianas	>150	80[14]	135	350	640	4.7[13]	295	4.1
	20-South Marianas	>150	80[14]	235	400	640	3.5[13]	305	3.3
Philippine Sea									
Ph-EU	-Nankai	9-20	35[15]	250	800	60	4.0[13]	310	3.5
	21-Ryukyu	45	65[12]	210	1000	220	5.6[13]	310	5.5
	22-North Taiwan	65	70[12]	20	120?	300	6.0[13]	130	5.6
EU-Ph	23-Luzon	20-35	60[16]	5	500	640	7.3[13]	130	5.2
Ph-EU	24-Philippines	55	60[16]	165	1500	640	8.3[13]	295	6.4
EU- ?	25-Sulawesi	60?	62[15]	268	350	190	-	NS?	?
Indonesia									
In-EU	26-Burma	-	60[17]	0	900	200	6.0	20	2.1
In-EU	27-Andaman	55	50[18]	335	1000	100	6.3	21	4.5
	28-Sunda	80	47[19]	320	1500	300	7.0	25	6.3
	29-Java	135	60[19]	280	1700	650	7.7	22	7.5
	30-Timor	90	70[20]	255	1100	690	7.8	20	7.7
Southwest Pacific									
Bi-In	31-New Guinea	30?	55[21]	118	550	200	3.3[22]	203	3.3
So-Bi	32-New Britain	30?	60[21]	254	500	200	9.2[22]	343	9.2
So-Pc	33-New Ireland	30?	75[21]	300	400	550	10.1[22]	34	10.1
In-Pc	34-Solomon	60	50[21]	300	1000	200	10.0	79	7.7
	35-New Hebrides	65	70[23]	348	1500	320	10.0	85	9.9
Pc-In	36-Tonga	100	55[24]	200	1500	650	9.2	280	9.1
	37-Kermadec	100	70[24]	200	600	600	7.2	278	7.1
	38-New Zealand	90	67[25]	200	500	350	5.0	275	4.8

SP-OP Subducted and overriding plates names (Bi-Bismark, Cb-Caribbean, Co-Cocos, EU-Eurasian, In-Indian, JF-J. Fuca, NA-North America, Pc-Pacific, Ph-Philippine, Ri-Rivera, SA-South America, Sw-Sandwich, So-Solomon)

However, recent studies by several investigators (Abe, 1972a, b; Malgrange et al., 1981) indicate that these events occur frequently in some subduction zones, and intermediate-depth events are often very damaging (e.g., 1965 Puget Sound, Washington; 1973 Orizaba, Mexico; 1979 Colombia earthquake). It is clearly a difficult task to appraise the seismic hazard posed by intraplate activity since we cannot even reliably assume that long-term plate motions will drive repeated failure on the same fault. However, the events must be controlled by the regional stress environment, and many studies have attempted to extract information about the state of stress within the subducting plate by analyzing the intraplate focal mechanisms. These investigations reveal that the subducting slab acts like a complex stress guide (e.g., Isacks and Molnar, 1969, 1971).

This offers the possibility that the characteristics of large intermediate-depth earthquakes may reflect the state of interplate coupling at various subduction zones, in addition to the conventional interpretations of unbending, sagging, detachment, and penetration resistance.

Age of the SP from Sclatter and Parsons, 1981; and Moore, 1982

Dip of the SP at intermediate depth

TAz Trench Azimuth from Moore, 1982

TLg Approximate Trench Length from Moore, 1982

Depth of maximum extent of continous observed seismicity. Note that there are deep events in South America but the seismicity is not continous

Plate Convergence (Rate, Azimuth) calculated from RM2 model of Minster and Jordan, 1978

V_N convergence velocity normal to the trench axis

References: 1. Barazangi and Isacks, 1979; 2. Frankel and McCann, 1979 ; 3. Barker, 1972; 4. Molnar and Sykes, 1969, LeFevre and McNally, 1985; 5. Dewey and Algermissen, 1974, Dean and Drake, 1978; 6. Frankel, et al., 1980; 7. McCann and Sykes, 1984; 8. Clowes et al., 1983; 9. Nishimura et al., 1984; 10. Enghdal, et al., 1977; 11. Ishida, 1970; 12. Shiono, et al., 1980; 13. Seno, 1977; 14. Katsumata and Sykes, 1969; 15. Kanamori and Tsumura, 1971; 16. Cardwell, et al., 1980; 17. Fitch, 1970b; 18. Eguchi, et al., 1979; 19. Fitch, 1970a; 20. McCaffrey et al., 1985, Cardwell and Isacks, 1978; 21. Pascal, 1979; 22. Johnson and Molnar, 1972; 23. Pascal et al., 1978; 24. Billington, 1980, Giardini and Woodhouse, 1984; 25. Ansell and Smith, 1975; 26. Reid, 1976.

In order to improve our understanding of the nature of intermediate-depth seismicity, Chapter 1 presents a review of the spatio-temporal distribution of large (M≥7) intermediate and deep focus earthquakes that occurred during this century in the subduction zones listed in Table 1.1. Given our relative ignorance of the causes of intermediate-depth events, as well as their hazard potential, we conducted a global investigation of the focal mechanisms of these events. In particular, we explored the interaction between the shallow seismically coupled region where thrust events occur and the deeper uncoupled region in subduction zones. This analysis was motivated in part by the recent suggestion that outer rise intraplate events may, under some conditions, respond to variations in interplate coupling (Christensen and Ruff, 1983). A comprehensive catalogue of focal mechanisms of large (M>6) intermediate-depth earthquakes that occurred between 1960 and 1984 was gathered as our primary data base. This is used in the development of qualitative models relating gross tectonic properties to the intraplate earthquake activity. Achieving an understanding of the relationship between interplate and intermediate-depth seismic activity is particularly important for seismic gap regions and for zones of uncertain seismic potential such as the Juan de Fuca plate, where large intermediate-depth earthquakes have occurred recently.

1.2 Earthquakes within the Subducting Lithosphere: An Overview

Earthquakes occurring below 40 km depth near convergent plate margins form inclined zones of seismicity known as Benioff zones, which presumably delineate the

location of the colder, subducting lithosphere to as deep as 650 km depth (e.g. Isacks et al., 1968; Sleep, 1973; Richter, 1979).

Many studies of deep and intermediate-depth earthquakes have focused on understanding the stress distribution within the subducting lithosphere by relating the orientation of the compressional and tensional axis of earthquake focal mechanisms to the orientation of the seismic zone. Based on a global study of individual focal mechanism solutions of deep and intermediate-depth earthquakes Isacks and Molnar (1969, 1971) concluded that the descending slab acts like a stress-guide, in which compressional stresses are dominant below 300 km, and either down-dip tensional or compressional stresses are observed between 70 and 300 km depth. They attributed down-dip tensional events to extensional stresses induced by the slab's own negative buoyancy, but they also argue that the slab encounters more resistant material as it sinks into the mantle so that the stresses at intermediate depth become compressional for plates that extend to 650 km depth. Oike (1971) made similar observations by contouring pressure and tension axes for events in various subduction zones. Moment tensor inversions of recent earthquakes (Vassiliou, 1984) also indicate that down-dip compressional stresses are dominant below 300 km depth, but the behavior of intermediate-depth events is much more complicated as discussed below.

Richter (1979) suggests that the occurrence of down-dip compressional events below 300 km is an evidence of the inability of the subducted material to penetrate below 700 km depth. Vassiliou et al. (1984) conducted numerical modeling to test whether the observed stress pattern within the subducted slab (transition from down-dip tension to compression with increasing depth) is the result of the slab encountering a penetrable viscosity increase or an impenetrable chemical discontinuity

in the mantle. Either hypothesis can explain the gross characteristics of the stress orientation. Vassiliou et al. (1984) suggest that an observed decrease in seismic activity between 250 and 400 km depth may be due to the olivine to spinel phase transition at 400 km depth (Anderson, 1967) and that the lack of seismicity below 670 km depth indicates that either the slab cannot penetrate below this depth or that a change of the subducted lithosphere rheology occurs, which prevents brittle earthquake failure.

The non-uniform stress pattern observed at intermediate depths could be related to the existence of double seismic zones. Well-located hypocenters in the Kanto district in Japan (Tsumura, 1973) and composite focal mechanisms of small events in the region indicate that the upper seismic zone is under in-plate compression whereas the lower layer is under in-plate tensional stresses (Hasegawa and Umino, 1978). The two layers of seismicity are separated by about 35 km and extend in depth from 60 to 190 km. Double seismic zones have been observed beneath most of the Japanese arc (e.g., Yoshii, 1979; Suzuki and Motoya, 1978; Ishikawa, 1985) and also in the Kuriles-Kamchatka subduction zone (Sykes, 1966; Fedotov, 1968; Fedotov et al., 1971; Veith, 1974, 1977; Stauder and Maulchin, 1976). However, double seismic zones are not found in every subduction zone (Fujita and Kanamori, 1981). Some regions exhibit stress-segmented seismic zones where regions of compression and tensional events are in close proximity and may give the impression of a double-seismic zone in cross section, as is the case for the central Aleutian arc (Engdahl and Scholz, 1977; Fujita and Kanamori, 1981). Some of the mechanisms proposed to explain double seismic zones include stresses associated with phase changes (Veith, 1974), unbending of the lithosphere (Engdahl and Scholz, 1977; Samowitz and Forsyth, 1981; Kawakatsu, 1986a),

sagging of the subducted plate (Yoshii, 1977; Sleep, 1979), and thermo-elastic stresses (House and Jacob, 1982; Molnar et al., 1979; Goto et al., 1985).

Fujita and Kanamori (1981) interpreted published focal mechanism solutions of intermediate-depth earthquakes as a function of the slab age and convergence rate as follows. Stresses at intermediate depth of old and slow slabs are tensile and induced by the slab's own weight, whereas those of old and fast slabs are generally mixed resulting in double seismic zones. Intermediate-depth stresses in young and slow slabs are also mixed, but instead exhibit stress-segmented zones. Young and fast slabs are tensile, specifically under South America, probably due to continental loading. Their results are interpreted in the context of the global variation of interplate coupling at subduction zones, which is predominantly controlled by slab age and convergence rate (Ruff and Kanamori, 1980).

Mogi (1973) studied the relationship between shallow and deep seismicity in the western Pacific region and concluded that temporal changes in the seismic activity at depth associated with the occurrence of large thrust events are not fortuitous, but may indicate an integral part of the earthquake cycle. Mogi's observations suggest that the descending lithosphere may act as a visco-elastic body under gradually increasing load, rather than as a rigid elastic plate (Kawakatsu, 1986a). Seno and Pongswat (1981) and Kawakatsu and Seno (1981) defined a third seismic zone in northern Japan, and suggested that the focal mechanisms of the events in this zone change in response to stress changes on the interplate boundary. Recently, McNally et al. (1986) and González-Ruiz (1986) constructed a composite spatio-temporal cross section of shallow and intermediate-depth events that occurred along the Mexican subduction zone, which suggests that stress transfer between the shallow interplate

boundary and the intraplate seismic activity takes place. Furthermore, temporal variations in the focal mechanisms of intraplate earthquakes in relation to the occurrence of large thrust earthquakes have been observed in southern Chile, both in the outer-rise region (Christensen and Ruff, 1983, 1987) and at intermediate depths (Astiz and Kanamori, 1986).

Large Intermediate and Deep Focus Earthquakes: 1904-1984

To provide a general context for a detailed investigation of intermediate depth earthquakes, we first consider the historic record of the largest events within the sub-ducting slabs. Figure 1.2 shows the world-wide distribution of large ($M \geq 7$) inter-mediate and deep focus earthquakes that occurred from 1904 to 1984. Most inter-mediate and deep focus earthquakes occur at major active plate boundaries (Figure 1.2), with only a few events apparently being unrelated to presently subducting plates. Examples of the latter include the 1954 deep Spanish event (Chung and Kanamori, 1976) or the 1915 event located offshore western Australia, which may be mislocated. These events are listed by region in Table A.1. Appendix 1 shows the depth and time distribution for each region in Figure 1.2.

The most active region at intermediate depths is New Hebrides(35). Tonga(36) is the most active below 400 km depth but has also relatively high intermediate-depth seismic activity. Regions with large number of intermediate-depth earthquakes with $m_B \geq 7.0$ are the Altiplano(4), Timor(30), Sulawesi(25), Scotia(8), and New Ireland(33), which are associated with bends in the subducted lithosphere. Other regions with a large number of large intermediate-depth events are North Chile(5), Kuriles(17), Ryukyu(21), and Philippines(24). The Nankai and Rivera regions where the
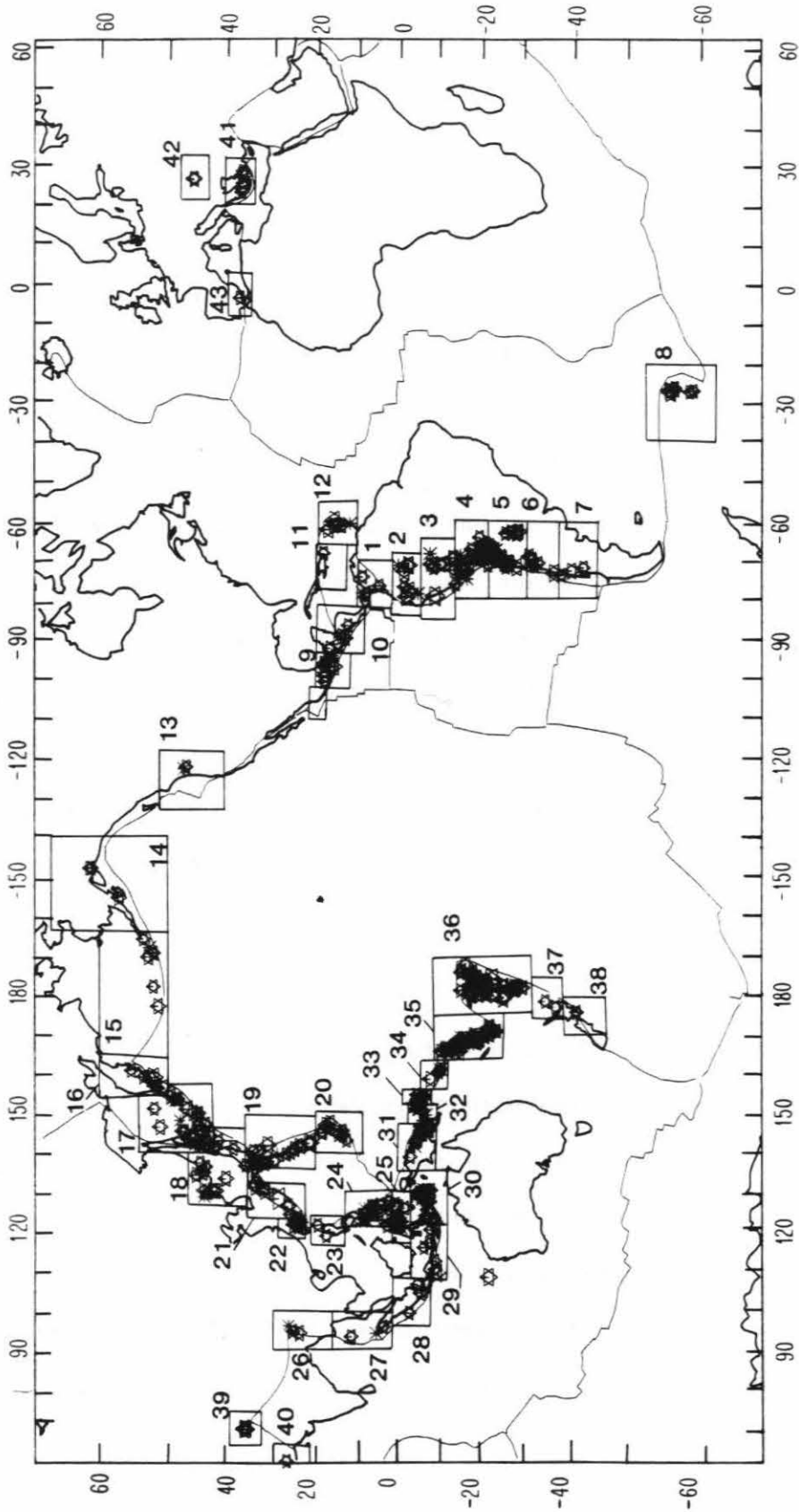
Figure 1.2: Global distribution of large ($M \geq 7$) intermediate and deep focus earthquakes that occurred between 1904 and 1984. Symbol sizes are proportional to the earthquake magnitude which are m_B for events that occurred before 1975 and M_w for later events. Boxes encompass regions (Table 1.1) in the depth-magnitude profiles in Appendix 1.

subducting lithosphere is young, and the observed seismicity shallower than 100 km do not have large intraplate earthquakes. Some regions such as Luzon(23) and New Zealand(38) had very few intrplate events in this century.

Comparing the time distribution of large earthquakes in this century versus the time distribution of these events after 1960, we can get an idea of how well seismicity after 1960 represents the intraplate activity of different subduction zones. Regions where seismicity within the subducting plate has been relatively constant in the last 80 years are the Altiplano(4), North Chile(5), Kuriles(17), Northeast Japan(18), Timor(30), New Hebrides(35), Tonga(36) and the Hindu-Kush(39). However, seismic activity in some other regions has changed during this century. For example the Ryukyu(21) and Sulawesi(23) regions were especially active in the early part of the century, whereas other regions such as Peru(3), Philippines(24) and New Guinea(31) seem to be more active recently. These temporal changes in activity may be related either to changes in the regional subduction process (e.g., the shallow interplate earthquake cycle) or to global changes like the Chandler wobble (Abe and Kanamori, 1979).

Vassiliou et al. (1984) determined the variation of the number of $m_b \geq 5$ events between 1964 and 1980 from the NOAA catalog. They observed that for the world seismicity, the number of intraplate events decreased with depth to about 300 km. It remained constant to about 500 km depth, where an increase in the number of events was observed to about 600 km depth. They assumed that this distribution reflected the level of stress within the plate with increasing depth. However, Giardini (1987) determined the b value for deep seismic regions and found large regional variations, from 0.33 in South America to 1.22 in Tonga. The b value for most regions is about

Table 1.2: Largest Earthquake Magnitude by Seismic Depth

Subduction Zone Name	Maximum Observed Magnitude				Seismic Depth (km)
	M_w d<40km	m_B 40<d<260	m_B 260<d<400	m_B d>400km	
South America					
1-Colombia	8.8	7.0			250
2-Ecuador	(8.8)	7.5		7.5	200
3-Peru	8.2	7.8		7.3	220
4-Altiplano		7.6			300
5-North Chile	(8.5)	7.7		7.4	300
6-Central Chile	8.5	7.5			200
7-South Chile	9.5	7.5			160
8-Scotia	7.0	7.6			200
Middle America					
9a-Rivera	8.2				90
9-Mexico	8.1	7.7			200
10-C. America	(8.1)	7.4			280
Caribbean					
11-Greater Antilles	(8.0)	7.0			180
12-Lesser Antilles	7.5	7.5			250
North Pacific					
13-Juan de Fuca		7.1			100
14-Alaska	9.2	7.3			160
15-Aleutians	9.1	7.4			280
North Pacific					
16-Kamchatka	9.0	7.8			540
17-Kuriles	8.5	7.6	7.5	7.4	625
18-NE Japan	8.2	7.5	7.4	7.4	580
Western Pacific					
19-Izu-Bonin	7.2	7.9	7.7	7.2	560
20-Marianas	7.2	7.3	7.0		640
21a-Nankai	(8.2)				60
21-Ryukyu	8.0	8.1			220
22-North Taiwan		7.6			300
23-Luzon		7.0			640
24-Philippines	(8.3)	7.3	7.4	7.2	640
25-Sulawesi	(8.0)	7.8			190
Indonesia					
26-Burma		7.4			200
27-Andaman	(8.0)	7.2			100
28-Sunda	7.9	7.3		7.2	300
29-Java	7.1	7.6	7.0	7.2	650
30-Timor	(8.5)	7.8	7.2	7.0	690
Southwest Pacific					
31-New Guinea	(8.0)	7.3			200
32-New Britain	(8.1)	7.2			200
33-New Ireland		7.3	7.2		550
34-Solomon	8.1	7.3			200
35-New Hebrides	7.9	7.9	7.3		320
36-Tonga	8.3	7.7	7.5	7.6	650
37-Kermadec	8.1	7.0	7.0		600
38-New Zealand	7.8	7.1			350

M_w are mostly taken from Ruff and Kanamori (1980); values in parenthesis are M_s from Abe (1981).
m_B values are body-wave magnitude at $T \approx 8s$ (Table A.1)

0.6. These results indicate that a profile of a number of intraplate events with depth for the world's seismicity would be biased by the high seismic activity in Tonga at depth. Chung and Kanamori (1980) investigated the variation of earthquake source parameters with depth and concluded that the stress drop of intermediate and deep events ranges from 20 bars to about 4.6 kbars. This variation is generally associated with an increase in the earthquake depth; however, events with comparable depth closer to bends in the subducting lithosphere would have higher stress drops than events located in relatively simple subducting slabs. The relation of stress within the plate and earthquake stress drop is unclear. However, since most of the seismic energy is released in large earthquakes, the profiles shown in Appendix 1 should reflect the seismic energy released within the plate for each subduction zone during this century.

If we divide the large intraplate earthquakes into three depth ranges $(40 \leq d \leq 260, 260 < d \leq 400,$ and $d > 400$ km) that correspond to different stress regimes within the downgoing slab and assign a maximum observed earthquake magnitude, m_B, to each depth range, then we observe that the maximum m_B decreases with depth for most regions (Table 1.2) with the exception of the Sunda(28), Java(29) and Tonga(36) regions for which the observed magnitude m_B increases for the deepest range and the Philippines(24) for which the middle range $(260 < d \leq 400$km) has the largest observed m_B. The deepest range $(d > 400$ km) corresponds to the region with down-dip compressional events (e.g., Isacks and Molnar, 1971). In the middle range, 260 to 400 km, down-dip tensional events mainly occur (Vassiliou et al., 1984) with the exception of Tonga, where down-dip compressional events are commonly observed to shallow depths (Giardini and Woodhouse, 1984). At the shallower

range (40 to 260 km) many events have nearly down-dip tensional axes; however, the focal mechanisms of these events exhibit a large variation as shown in the following sections. The above observations suggest that the occurrence of large intraplate events may be influenced not only by the slab's rheology but also by other factors such as lateral thermal variations in the surrounding mantle.

1.3 Catalog of Intermediate-depth Earthquakes

There is evidence that subducted plates are uncoupled from the overriding plate below 40 km depth, where a steepening of the Benioff zone is generally observed (e.g., Engdahl, 1977; Isacks and Barazangi, 1977; Billington, 1980). This bend in the sub-ducting plate has been related to the phase change in the oceanic crust from basalt to eclogite at approximately 35 km depth, whtich causes an increase in the average den-sity of the slab (Wortel, 1982; Pennington, 1983; Ruff and Kanamori, 1983; Fukao et al., 1983). Also, most large thrust events appear to have rupture zones constrained to depths less than 40 km (Schwartz and Ruff, 1987). Thus, earthquakes deeper than 40 km depth are believed to occur within the subducting plate, since it is no longer in contact with the overriding plate. An analysis of intraplate events in the depth range 40 to 200 km should provide us with a better understanding of the interaction between the state of stress in the deeper uncoupled region and the degree of coupling of the interplate boundary at subduction zones. Such a study requires a detailed cata-log of events that are reliably identified as being intraplate.

We gathered a catalog of intermediate-depth earthquakes (Table 1.3). First, all earthquakes with $m_b \geq 6.0$ that occurred from 1960 to 1984 between 40 and 200 km depth were identified by sorting the NOAA and ISC (International Seismic Centre) catalogs. Then, a search for published focal mechanisms for these earthquakes was undertaken. Some events have been studied by several groups of researchers. However, only the focal mechanism solution that was considered the most reliable is listed in Table 1.3. Reliability was determined on the basis of the most recent study (that generally referred to earlier works) or on the basis of studies in which the authors picked the first-motion and S-polarization data themselves. Although there is a considerable variation in the confidence attached to individual focal mechanisms, the general character of the solutions is reliable. If the studies included epicentral relocation then we list these hypocenters in Table 1.3 instead of the location reported by NOAA. In surveying the literature, numerous intermediate-depth events given depths less than 40 km or missing in the NOAA and ISC listings were identified and included in Table 1.3. Published focal mechanism solutions were not available for nearly 140 of the earthquakes in the initial list.

A preliminary focal mechanism solution was determined from first-motion data in the ISC bulletin for those events lacking a published solution. Most of these mechanisms were not very well constrained. If the depth of the event was shallower than 60 km, with no depth phases being reported in the ISC bulletin, and if the preliminary focal mechanism solution was relatively reliable and consistent with an interplate thrust orientation in the direction of local subduction (Table 1.1), we assumed that the event was probably interplate, and it was removed from the initial catalog. In this way, we eliminated about 30 events. Then we picked first-motion data from

short and long-period records of the World Wide Seismograph Standard Network (WWSSN) for over a hundred events to determine better constrained focal mechanisms. Recordings for 25 events of the catalog were very small, and no reliable focal mechanism could be determined for them from WWSSN seismograms. Most of these events occurred in the early 1960's and their magnitudes may have been overestimated. These events were removed from the catalog as well. After timing depth phases in short-period WWSSN records, we found that 40 events were clearly shallow, and these were not included in the intermediate-depth earthquake catalog either. Some of these events may be outer-rise events, for which a comprehensive catalog has been compiled by Christensen and Ruff (1987). These events were eliminated from our catalog. Finally, we determined 40 new focal mechanism solutions of intermediate-depth earthquakes, which are shown in Appendix 2. First-motion data were insufficient to constrain both fault planes for half of these events, but we determined the depth and one of the focal mechanism parameters by modeling long-period body waves. Only a few critically oriented stations were modeled for each of these events, but generally this provided adequate resolution of the source depth and mechanism. The asterisk (*) in Table 1.3 indicates which parameter was constrained by the synthetic seismograms or by timing of pP-P phases in short period records to determine the event depth.

The final catalog, listed in Table 1.3, contains 335 hypocenters, magnitudes and focal mechanism solutions of earthquakes that occurred between 40 and 200 km depth. Event numbers are chronological, hypocenters are given in degrees (latitude north and longitude east are positive), depth is given in km. The magnitude M listed is m_b for most events that occurred before 1977 except for the larger events, for

which m_B from Abe (1981) is given. For events that occurred after 1977, M_w was determined from Kanamori's (1977a) relation $M_w = \frac{2}{3}\log M_o - 10.73$. Note that the magnitudes included in Table 1.3 are intended to reflect the real size of the event. Figure 1.3 shows that there is a large scatter between m_b and either M_w or m_B for the intermediate-depth events in Table 1.3, indicating that m_b is not a very reliable measure of large ($M \geq 7$)intermediate-depth events. Relations between m_B and seismic moment, M_o, or M_w are given by Kanamori (1983). The fault parameters, azimuth (ϕ), dip (δ), and rake (λ) , of one of the planes are given as well as the pressure (P), tension (T) and intermediate (B) stress axes. Azimuth is measured clockwise from the north. Abbreviations are references that are listed at the bottom of Table 1.3.

This catalog probably includes most intermediate-depth earthquakes with $M \geq 6.5$ that occurred within the subducting slab between 1960 and 1984. However, some intermediate-depth events that were originally listed by NOAA and ISC as shallow may be missing, particularly if they have compressional mechanisms. Also, a few of the events listed in the catalog may actually be interplate events with slightly anomalous depths and mechanisms. This is a significant expansion of the data base of 210 events in the same period compiled by Fujita and Kanamori (1981). However, they compiled an additional 33 mechanisms for events prior to 1960, most of which are based on ISS reports.

Table 1.3: Catalog of Intermediate-depth Earthquakes

No.	Date	Lat. N+,S-	Long. E+,W-	Depth	M	Fault Plane $\phi°$	$\delta°$	$\lambda°$	P $Az°$	$Pl°$	T $Az°$	$Pl°$	B $Az°$	$Pl°$	Ref.
1	07/10/60	1.00	98.00	150.0	6.50	299.0	16.0	90.0	209	29	29	61	119	0	FK
1'	07/25/60	54.00	159.00	100.0	6.90	340.0	35.0	41.0	301	46 ·	182	26	73	57	FK
2	03/11/61	48.70	155.20	50.0	6.20	237.0	20.0	109.5	132	26	296	63	39	6	FK
3	08/17/61	46.40	149.30	160.0	6.70	271.5	18.7	-25.0	275	50	130	35	27	18	FK
4	08/03/62	-23.30	-68.10	108.0	7.30	142.0	32.8	-123.7	307	66	76	16	171	17	S73
5	01/01/63	56.60	-157.70	50.0	6.50	156.0	23.5	58.9	88	25	291	61	185	12	SB
6	01/29/63	49.70	155.00	143.0	6.20	159.2	17.5	42.2	108	32	317	55	206	13	SMa
7	02/13/63	24.50	122.10	67.0	7.25	259.0	29.0	90.0	169	16	349	74	79	0	KS
8	02/26/63	-7.60	146.20	182.0	7.3B	267.0	21.9	-180.0	105	41	249	41	355	20	IM
9	03/10/63	-29.90	-71.20	70.0	6.30	82.5	11.5	-158.9	250	48	51	40	151	11	S73
10	03/30/63	-19.11	169.00	156.0	6.30	278.1	48.9	13.4	235	20	130	36	348	40	IM
11	04/02/63	53.10	-171.70	140.0	6.38	6.4	36.9	-54.6	349	65	252	13	157	20	SB
12	04/13/63	-6.30	-76.70	125.0	6.10	20.0	31.2	-63.7	49	69	271	16	177	13	SB
13	05/01/63	-19.00	168.90	142.0	7.1B	296.5	41.4	23.8	250	20	138	46	356	37	IM
14	05/22/63	-8.20	115.70	76.0	6.10	96.0	6.0	90.0	6	39	186	51	276	0	F72
15	06/17/63	-4.10	102.20	69.0	6.30	330.0	10.0	90.0	240	35	60	55	150	0	F72
16	06/19/63	4.70	126.50	83.0	6.20	174.0	10.0	90.0	84	35	264	55	354	0	F72
17	07/04/63	-26.30	-177.70	190.0	6.50	122.4	62.8	-151.1	339	39	71	1	164	51	ISO
18	07/30/63	-55.90	-27.50	55.0	6.20	168.0	40.0	160.0	32	23	146	44	283	37	F75
19	09/15/63	-10.30	165.60	43.0	6.30	280.0	40.0	-90.0	10	85	190	5	280	0	JoM
20	09/17/63	-10.80	-78.20	61.0	6.70	187.1	43.8	-60.0	186	69	76	5	344	20	S75
21	09/24/63	-10.60	-78.00	80.0	6.00	90.8	24.9	-141.0	261	56	39	27	139	19	S75
23	10/24/63	-4.90	102.90	65.0	6.10	298.0	16.0	90.0	208	29	28	61	118	0	F72
24	11/04/63	-15.14	167.38	123.0	6.40	5.0	40.0	90.0	275	5	95	85	185	0	IM
25	11/04/63	-6.86	129.58	100.0	7.8B	80.0	48.0	52.0	16	3	279	63	108	27	OA
26	11/15/63	44.30	149.00	50.0	6.00	96.5	14.0	-84.6	179	59	2	31	271	1	SMa
27	12/18/63	-24.80	-176.60	46.0	6.50	270.0	0.1	-180.0	92	45	272	45	2	0	ISO
28	01/15/64	29.10	140.80	80.0	6.40	219.6	37.5	55.0	154	12	35	66	249	20	KS
29	01/20/64	-20.70	169.90	141.0	6.10	97.6	39.0	-50.0	93	63	340	12	244	24	IM
30	01/22/64	22.40	93.60	88.0	6.10	238.0	18.9	0.0	220	42	76	42	328	19	LTM
31	01/26/64	-16.30	-71.70	116.0	6.10	203.0	37.6	-16.4	181	43	64	26	313	36	IM
32	01/28/64	36.48	70.95	197.0	6.30	340.0	80.0	90.0	70	35	250	55	160	0	New
33	02/27/64	21.70	94.40	102.0	6.40	263.3	19.6	30.8	220	33	76	52	321	17	LTM
34	04/07/64	0.10	123.20	184.0	6.30	169.2	60.3	-179.2	30	21	128	20	258	60	So73
35	04/24/64	-5.10	144.20	106.0	6.30	356.3	10.0	-87.3	83	55	264	35	172	1	IM
36	05/26/64	-56.45	-27.70	114.0	7.5B	179.3	52.7	162.0	41	14	156	36	297	49	A72
37	05/27/64	-56.40	-28.40	61.0	6.00	281.0	48.2	44.7	221	6	125	57	315	32	IM
38	06/23/64	43.30	146.10	77.0	6.20	200.5	13.4	38.9	152	36	351	52	249	9	SMa
39	07/06/64	18.30	-100.40	45.0	7.3B	87.0	46.0	-116.0	279	72	15	2	106	18	MS
40	07/08/64	-5.50	129.80	165.0	7.0B	4.4	26.1	157.3	225	31	357	49	119	25	FM

No.	Date	Lat. N+,S-	Long. E+,W-	Depth	M	Fault Plane ϕ^o	δ^o	λ^o	P Az^o	Pl^o	T Az^o	Pl^o	B Az^o	Pl^o	Ref.
41	07/09/64	-15.50	167.60	127.0	7.4B	353.0	36.0	90.0	263	9	83	81	173	0	IM
42	07/12/64	24.90	95.30	155.0	6.70	258.0	61.2	-9.0	219	26	122	14	6	60	O71
43	09/12/64	-4.40	144.00	120.0	6.30	305.0	2.0	90.0	215	43	35	47	125	0	IM
44	09/15/64	8.90	93.03	89.0	6.30	263.6	29.4	43.9	207	22	75	59	306	21	LTM
45	11/01/64	3.10	128.10	89.0	6.30	220.4	52.3	146.3	94	7	192	48	358	41	F72
46	11/02/64	-4.10	-76.90	91.0	6.00	144.9	43.2	-95.8	299	85	59	2	149	4	IM
47	11/17/64	-5.70	150.70	65.0	6.70	266.0	32.5	90.0	176	13	356	78	86	0	So73
48	11/24/64	-6.80	107.40	130.0	6.00	230.0	70.0	0.0	187	14	93	14	320	70	KS
49	01/02/65	19.10	145.40	136.0	6.50	235.2	28.7	-133.7	43	60	177	22	275	19	IM
50	01/16/65	-56.60	-27.40	101.0	6.10	158.0	15.0	90.0	68	30	248	60	338	0	S73
51	02/23/65	-25.70	-70.50	80.0	7.25	138.8	12.8	-144.6	291	51	93	37	193	10	O71
52	03/04/65	-5.40	147.00	191.0	6.40	284.6	56.7	-32.6	252	45	158	4	63	45	O71
53	03/14/65	36.42	70.73	205.0	7.5B	270.0	22.0	84.0	184	23	10	67	276	2	ISO
54	03/22/65	-15.30	-173.40	44.0	6.50	10.0	31.8	-174.0	212	40	339	34	93	30	ISO
55	03/28/65	-32.40	-71.20	72.0	7.30	348.0	80.0	-100.0	246	54	86	34	350	10	MDM
56	03/31/65	38.60	22.40	78.0	6.75	348.4	35.0	127.2	235	17	29	60	137	18	IM
57	04/29/65	47.40	-122.40	63.0	6.88	344.0	70.0	-75.0	277	62	62	24	159	14	LB
58	05/17/65	22.41	121.26	72.0	6.00	196.5	56.5	4.7	155	20	55	26	278	56	KS
59	05/26/65	-56.10	-27.60	120.0	6.70	175.9	57.2	140.7	52	0	146	50	322	41	IM
60	06/12/65	-20.50	-69.30	102.0	6.50	95.0	18.2	-145.0	260	53	49	33	149	15	S73
61	07/02/65	53.10	-167.60	60.0	6.90	121.5	9.4	-34.3	138	50	339	39	246	8	IM
62	07/30/65	-18.10	-70.80	72.0	6.00	232.6	24.6	-2.6	211	41	77	39	325	25	S73
63	08/05/65	-5.20	151.60	50.0	6.50	44.0	50.0	96.8	129	5	357	83	220	5	JoM
64	08/20/65	-18.90	-69.00	128.0	6.50	206.0	15.2	-30.6	221	51	67	36	328	13	S73
65	08/20/65	-22.80	-176.20	79.0	6.10	313.0	5.0	55.1	263	40	93	50	357	6	ISO
66	09/16/65	7.10	126.60	183.0	6.00	115.6	56.6	36.9	60	2	328	48	152	42	FM
67	09/17/65	-1.50	-77.70	191.0	6.50	82.6	13.4	-143.0	242	52	38	36	135	11	IM
68	09/21/65	29.00	128.10	199.0	6.75	139.1	34.7	-149.0	329	52	90	22	193	30	KS
69	10/25/65	44.20	145.30	181.0	6.50	178.0	16.8	26.1	139	36	346	50	237	14	IM
70	11/12/65	30.70	140.10	65.0	6.75	10.0	42.8	-75.8	15	80	270	3	180	10	KS
71	11/20/65	-7.30	129.20	132.0	6.10	233.4	29.4	136.1	110	22	241	59	10	22	FM
72	11/21/65	-6.30	130.30	132.0	6.60	236.4	32.3	149.9	104	24	235	52	3	25	FM
73	12/07/65	-6.40	146.30	116.0	6.10	339.0	67.8	-2.2	297	17	202	14	77	68	R74
74	12/08/65	-37.10	177.50	156.0	6.20	117.5	29.5	56.2	52	19	275	65	148	16	IM
75	12/13/65	-56.10	-27.60	153.0	6.30	215.0	55.0	138.7	94	2	180	51	2	38	O71
76	12/26/65	-5.40	151.60	76.0	6.10	331.0	24.6	-180.0	174	40	308	40	60	25	IM
77	02/03/66	0.10	123.50	165.0	6.00	270.0	9.0	90.0	180	36	0	54	90	0	FM
78	05/01/66	-8.40	-74.30	154.0	6.75	248.2	26.7	-33.9	251	54	117	27	15	22	S75
79	07/01/66	24.80	122.40	119.0	6.75	304.0	27.0	90.0	214	18	34	72	124	0	KS
80	08/10/66	-20.10	-175.40	95.0	6.50	110.3	23.8	-145.4	282	54	62	29	163	19	ISO

No.	Date	Lat. N+,S-	Long. E+,W-	Depth	M	Fault Plane $\phi°$	$\delta°$	$\lambda°$	P $Az°$	$Pl°$	T $Az°$	$Pl°$	B $Az°$	$Pl°$	Ref.
81	08/21/66	8.50	126.60	67.0	6.75	158.0	26.0	90.0	68	19	248	71	338	0	F72
82	09/08/66	2.40	128.30	71.0	7.2B	326.7	41.3	98.1	231	4	2	83	140	4	FM
83	10/07/66	-21.60	170.60	160.0	6.30	9.5	69.3	157.6	59	0	328	30	149	60	IM
84	11/10/66	-31.90	-68.40	113.0	6.00	49.7	46.2	-35.9	28	52	284	11	186	36	S73
85	12/01/66	-14.00	167.10	132.0	6.00	335.7	42.1	85.3	249	3	122	86	339	4	IM
86	12/14/66	-4.89	144.00	70.0	6.00	122.0	30.0	90.0	32	15	212	75	302	0	IM
87	01/19/67	-11.85	166.40	156.0	6.00	162.0	37.8	74.6	83	8	317	78	174	9	IM
88	02/19/67	-9.13	113.05	94.0	6.75	147.1	8.0	-83.2	229	53	51	37	320	1	F72
89	03/11/67	-10.77	166.26	49.0	6.25	290.4	29.3	-52.3	309	63	173	20	76	17	JoM
90	04/12/67	5.26	96.40	55.0	6.10	98.0	28.0	90.0	8	17	188	73	278	0	F72
91	05/11/67	-20.26	-68.69	79.0	6.75	190.6	25.2	-46.2	209	59	68	25	330	17	S73
92	05/21/67	0.97	101.35	172.0	6.70	323.1	20.0	76.4	244	25	77	65	335	5	FM
93	06/17/67	-58.30	-26.60	140.0	6.10	147.0	22.6	-114.4	272	64	73	24	170	9	IM
94	07/29/67	6.80	-73.00	161.0	6.00	289.9	30.0	13.5	254	32	127	44	4	29	MS
95	08/12/67	-24.70	-177.50	134.0	6.50	37.5	26.7	43.7	342	24	204	58	81	19	CK80
96	08/26/67	12.18	140.80	53.0	6.10	68.9	40.2	-83.1	115	83	334	5	244	4	KS
97	10/12/67	-7.10	129.80	86.0	6.20	84.8	56.1	37.7	29	2	296	49	122	41	F72
98	10/15/67	11.90	-86.00	162.0	6.20	304.2	18.1	67.5	232	28	68	61	326	7	IM
99	10/25/67	24.50	122.20	65.0	7.0B	33.3	42.7	133.4	274	10	18	60	180	28	KSe
100	12/27/67	-21.20	-68.30	135.0	7.0B	163.0	37.2	-73.1	195	76	61	9	329	10	S73
101	03/11/68	-16.20	-173.90	112.0	6.00	2.8	47.7	-30.6	339	48	234	12	137	39	IM
102	05/28/68	-2.91	139.32	65.0	7.2B	118.9	39.0	94.1	26	6	180	84	296	3	F72
103	07/25/68	-30.77	-178.35	60.0	6.40	192.0	30.0	90.0	102	15	282	75	12	0	JoM
104	08/05/68	33.29	132.18	41.0	6.30	11.0	20.0	-90.0	101	65	281	25	11	0	New
105	09/09/68	-8.73	-74.52	120.0	6.00	97.6	17.0	-152.3	265	51	57	36	159	15	S75
106	09/20/68	10.73	-62.67	103.0	6.20	71.0	85.0	95.0	156	40	346	50	251	5	S&al
107	09/28/68	-13.16	-76.38	70.0	6.00	122.0	16.6	-125.5	257	57	59	32	156	10	S75
108	10/28/68	-12.47	166.46	60.0	6.50	282.7	47.2	36.3	228	10	125	52	325	36	JoM
109	11/17/68	9.55	-72.65	172.*	6.63	240.0	60.*	90.0	330	15	150	75	60	0	New
110	12/17/68	60.20	-152.80	90.*	6.50	346.0	65.0	70.*	91	18	222	64	355	18	New
111	01/05/69	-7.98	158.91	71.*	7.1B	114.0	76.0	-80.*	37	58	196	30	292	10	New
112	01/11/69	-28.41	-176.96	68.0	6.63	206.0	13.8	90.0	116	31	296	55	26	0	JoM
113	01/19/69	-14.89	167.19	107.0	7.30	175.0	40.6	175.0	31	30	145	35	272	40	CK78
114	01/30/69	4.80	127.44	70.0	7.1B	1.0	22.3	116.7	251	25	48	63	156	4	F72
115	06/14/69	-7.91	158.98	66.0	6.60	318.9	67.8	-5.0	278	19	182	12	57	61	R75
116	07/16/69	52.20	158.98	69.0	6.50	214.6	30.2	138.2	90	22	221	58	351	22	SMa
117	10/17/69	23.05	94.70	124.0	6.00	90.0	15.0	90.0	0	30	180	60	270	0	LTM
118	10/26/69	-16.17	-173.95	127.0	6.70	46.4	45.8	64.7	334	2	239	72	65	18	B80
119	12/25/69	15.79	-59.64	42.0	7.50	168.0	74.0	-105.0	58	58	270	27	172	14	S&al
120	01/08/70	-34.74	178.57	179.0	7.0B	217.1	36.8	131.0	101	16	252	59	2	23	B80

No.	Date	Lat. N+,S-	Long. E+,W-	Depth	M	Fault Plane			P		T		B		Ref.
						ϕ^o	δ^o	λ^o	Az^o	Pl^o	Az^o	Pl^o	Az^o	Pl^o	
121	01/10/70	6.82	126.74	73.0	7.30	179.1	45.7	77.3	98	0	6	81	190	9	F72
122	01/20/70	-25.80	-177.35	82.0	7.2B	60.0	6.0	90.0	330	39	150	51	240	0	B80
123	01/20/70	42.52	142.97	46.0	6.70	13.4	20.9	147.1	239	32	28	53	140	15	SMa
124	02/28/70	52.70	-175.10	159.0	6.10	171.0	27.0	-116.3	313	67	102	20	195	12	S72
125	03/15/70	-29.65	-69.50	119.0	6.00	332.2	25.3	-102.8	90	70	252	20	344	5	S73
126	03/30/70	6.80	126.65	76.0	7.1B	10.4	36.4	124.7	256	13	19	66	162	18	F72
127	05/20/70	-55.89	-28.33	70.0	6.00	262.8	61.0	17.5	216	9	120	32	320	57	Fo75
128	05/31/70	-9.18	-78.82	48.0	7.80	160.0	40.0	-90.0	250	85	70	5	160	0	S75
129	06/11/70	-24.53	-68.50	112.0	6.80	163.6	32.5	-62.7	189	69	54	15	320	14	S73
130	06/17/70	-15.80	-71.80	91.0	6.10	135.6	10.0	-84.6	219	55	41	35	310	1	S75
131	06/19/70	-22.19	-70.52	52.0	6.40	179.1	19.2	-85.8	263	63	86	27	355	1	S73
132	06/25/70	-7.92	158.69	69.0	6.50	263.0	75.0	-90.0	173	60	353	30	263	0	P79
133	07/29/70	26.02	95.40	68.0	6.50	264.4	57.5	-10.3	227	29	128	16	13	56	LTM
134	08/13/70	-8.88	117.98	99.0	6.00	208.1	26.2	66.7	135	20	340	66	229	10	CI
135	08/28/70	-4.57	153.05	76.0	6.20	303.8	30.0	114.5	196	17	339	69	103	12	R75
136	09/29/70	-13.52	166.55	59.0	6.60	344.0	79.0	82.0	81	34	244	55	346	8	New
137	12/08/70	-30.70	-71.21	50.0	6.40	331.2	25.3	78.4	250	20	86	70	342	5	S73
138	12/28/70	-5.16	153.62	61.0	6.50	204.0	80.0	90.0	294	35	114	55	24	0	P79
139	12/29/70	-10.55	161.40	72.0	6.80	154.0	45.1	96.0	60	0	150	86	329	3	R75
140	02/21/71	-23.85	-67.16	169.0	6.80	350.0	78.0	-110.0	236	53	96	30	354	20	New
141	03/13/71	-5.72	145.37	118.0	6.50	223.0	43.7	-130.8	51	62	161	8	256	25	R75
142	03/23/71	-22.88	-176.36	76.0	6.10	278.0	14.3	0.0	268	44	108	44	8	14	B80
143	04/07/71	2.44	129.12	47.0	6.60	327.0	34.0	-90.0	57	79	237	11	327	0	CIK
144	04/08/71	-4.33	102.40	75.0	6.30	338.0	24.0	90.0	248	21	68	69	158	0	New
145	05/08/71	-42.22	-71.69	150.*	6.80	12.*	80.*	100.*	93	34	294	54	190	10	New
146	05/17/71	-1.60	-77.70	176.0	6.50	150.1	20.8	-69.8	209	63	45	26	311	7	S75
147	06/11/71	17.97	-69.78	70.0	6.50	275.0	80.0	90.0	5	35	185	55	95	0	New
148	06/17/71	-25.48	-69.15	93.0	7.2B	2.0	70.0	-104.0	250	62	103	24	7	13	New
149	07/08/71	-7.03	129.70	92.0	7.3B	184.0	20.0	90.0	94	25	274	65	4	0	New
150	07/19/71	-5.69	153.80	42.0	7.10	324.0	80.0	-80.0	246	54	45	34	142	10	New
151	07/27/71	-2.75	-77.43	135.0	7.50	208.2	46.4	-54.7	194	65	94	4	2	25	S75
152	08/02/71	41.38	143.46	51.0	7.00	94.3	40.2	-82.5	135	83	359	5	269	5	SMa
153	09/16/71	-5.92	130.65	115.*	6.20	220.0	78.0	-90.0	130	57	310	33	220	0	New
154	09/25/71	-6.54	146.57	115.0	6.30	320.1	34.4	-47.1	329	61	200	17	103	20	R75
155	09/28/71	-5.57	153.99	107.0	6.60	63.8	40.1	44.2	5	13	255	59	103	28	R75
156	11/21/71	-11.82	166.53	115.*	7.4B	118.0	45.0	116.*	10	3	109	72	279	18	New
157	11/24/71	52.90	159.19	106.0	7.3B	30.0	86.0	90.0	120	41	300	49	210	0	New
158	12/30/71	-4.73	151.87	109.0	6.00	165.3	59.3	-149.0	22	42	112	3	207	50	R75
159	01/08/72	-55.76	-28.72	60.*	6.20	38.0	78.0	-70.*	332	53	112	30	214	20	New
160	01/28/72	-19.38	169.11	124.*	6.60	74.0	62.0	-80.*	6	71	157	16	249	9	New

No.	Date	Lat. N+,S-	Long. E+,W-	Depth	M	Fault Plane ϕ^o	δ^o	λ^o	P Az^o	Pl^o	T Az^o	Pl^o	B Az^o	Pl^o	Ref.
161	02/14/72	-11.36	166.33	102.0	7.0B	15.0	55.0	100.0	98	9	319	77	189	8	New
162	02/26/72	-10.43	161.26	90.0	6.50	220.0	44.2	67.2	146	3	45	74	237	15	R75
163	03/07/72	-28.23	-178.35	200.0	6.70	23.2	52.0	-20.3	352	39	250	14	144	48	B80
164	03/19/72	40.83	141.90	76.0	6.00	93.1	71.8	-163.9	315	24	46	2	140	66	SMa
165	03/22/72	49.06	153.57	134.0	6.80	182.0	17.9	-119.1	311	58	114	30	208	9	SMa
166	03/24/72	56.14	-157.18	71.0	6.00	326.6	38.6	110.6	222	8	342	75	130	13	HJ
167	09/05/72	1.88	128.17	132.0	6.10	153.0	42.0	90.0	63	3	243	87	333	0	CIK
168	12/04/72	33.33	140.68	62.*	7.4B	340.0	57.0	54.0	95	5	194	60	2	30	New
169	01/05/73	-39.00	175.23	150.0	6.20	196.7	38.4	145.9	69	18	184	53	328	31	D77
170	01/18/73	-6.87	149.99	43.0	6.80	253.0	62.0	90.0	343	17	163	73	73	0	P79
171	01/27/73	0.11	123.93	55.0	6.00	174.0	38.0	90.0	84	7	264	83	354	0	CIK
172	03/09/73	6.27	127.34	41.0	6.00	326.1	37.9	-133.2	149	61	266	14	3	25	CIK
173	04/03/73	4.69	-75.63	158.0	6.70	24.0	66.0	-80.0	313	67	106	20	200	9	New
174	04/24/73	4.96	-78.14	50.0	6.50	50.0	32.0	-36.0	48	55	282	22	181	25	New
175	06/09/73	-10.29	161.36	70.*	6.60	354.0	40.0	90.0	264	5	84	85	174	0	New
176	06/17/73	42.71	146.04	50.0	6.00	139.9	22.9	-42.6	158	57	14	28	275	17	SMa
177	08/01/73	-14.26	167.27	200.0	6.50	210.0	46.0	74.0	131	0	41	79	221	11	New
178	08/28/73	18.27	-96.60	80.0	7.3B	326.0	50.0	-75.0	297	78	45	4	136	11	GMR
179	08/30/73	7.34	-72.83	181.0	6.50	182.0	82.0	90.0	272	37	92	53	2	0	New
180	11/30/73	-15.20	167.39	124.0	6.00	16.5	38.4	93.5	284	7	86	83	194	2	CK78
181	12/29/73	-15.12	166.90	47.0	7.20	176.0	51.1	133.0	57	2	151	58	326	32	CK78
182	01/02/74	-22.54	-68.40	105.0	7.1B	146.0	14.0	-90.0	236	59	56	31	146	0	New
183	01/05/74	-12.30	-76.35	98.0	6.60	170.0	74.0	-144.0	35	36	296	12	191	51	New
184	10/08/74	17.30	-62.00	47.0	7.50	250.0	58.0	-90.0	160	77	340	13	250	0	S&al
185	10/09/74	44.72	150.12	55.*	6.70	222.0	14.0	90.0	132	31	312	59	42	0	New
186	10/29/74	-6.88	129.46	156.0	6.60	304.0	51.0	164.0	169	17	272	37	58	48	New
187	11/20/74	-15.12	167.16	62.0	6.20	168.0	37.3	92.0	77	15	248	82	346	1	ISO
188	03/18/75	-4.23	-77.02	75.*	6.50	8.0	65.0	-85.*	288	70	94	20	186	5	New
189	04/09/75	-4.04	152.69	133.0	6.30	272.0	80.0	42.0	36	20	141	36	283	47	New
190	05/27/75	0.77	122.62	74.0	6.10	322.0	16.2	-90.0	52	59	232	31	322	0	CIK
191	07/08/75	21.48	94.70	157.0	6.50	228.0	44.0	29.0	178	16	70	48	280	37	LTM
192	07/10/75	6.51	126.64	86.0	7.00	9.0	41.0	117.3	260	7	14	71	168	18	CIK
193	08/10/75	-22.65	-66.59	166.0	6.20	338.0	74.0	-88.0	251	61	66	29	157	2	New
194	08/23/75	10.01	125.79	66.0	6.00	154.4	35.4	59.3	86	13	318	68	180	17	CIK
195	10/17/75	-7.47	128.73	120.*	6.30	53.0	62.0	108.*	130	15	358	68	224	16	New
196	11/01/75	13.84	144.75	113.*	7.10	132.0	84.0	90.0	222	39	42	51	312	0	New
197	12/25/75	-4.08	142.04	115.*	6.80	75.0	75.0	105.*	153	28	5	57	251	14	New
198	01/24/76	-28.64	-177.59	78.0	6.20	115.7	51.4	34.0	61	8	327	48	158	40	R79
199	03/04/76	-14.74	167.10	90.0	6.40	273.0	77.0	34.0	40	13	139	33	291	54	New
200	06/03/76	-5.20	153.44	72.*	6.20	56.0	50.0	50.*	353	2	259	60	84	29	New

No.	Date	Lat. N+,S-	Long. E+,W-	Depth	M	Fault Plane ϕ^o	δ^o	λ^o	P Az^o	Pl^o	T Az^o	Pl^o	B Az^o	Pl^o	Ref.
201	11/07/76	8.48	126.38	60.0	6.90	180.0	24.4	90.0	90	21	270	69	0	0	CIK
202	11/30/76	-20.52	-68.92	82.0	7.30	342.0	78.0	-108.0	230	54	87	31	346	18	New
203	01/01/77	-7.91	109.01	102.8	6.00	63.0	23.0	-130.0	217	60	3	26	101	15	G84
204	01/12/77	1.58	99.88	186.0	6.00	92.0	46.0	132.0	334	6	75	60	240	29	G84
205	03/04/77	45.77	26.76	94.0	7.40	255.0	76.0	90.0	345	31	165	59	75	0	New
206	03/28/77	-14.68	167.10	111.9	6.07	165.0	53.0	164.0	30	16	132	36	280	50	G84
207	04/02/77	-16.70	-172.10	50.3	7.28	317.0	41.0	45.0	258	12	147	60	354	28	GDW
208	05/21/77	15.70	120.82	188.0	6.12	329.0	48.0	-15.0	298	38	192	20	81	46	G84
209	06/22/77	-22.88	-175.90	59.1	8.04	10.0	13.0	-98.0	111	58	287	32	18	2	G84
210	07/10/77	-56.12	-27.56	116.7	6.03	166.0	56.0	140.0	43	1	134	51	312	39	G84
211	08/04/77	-56.01	-27.79	111.1	5.94	171.0	47.0	143.0	46	10	149	53	309	36	G84
212	10/29/77	-6.22	146.64	110.5	6.06	252.0	62.0	-162.0	110	32	205	8	307	57	G84
213	10/30/77	-14.89	166.95	106.8	6.15	192.0	68.0	166.0	58	6	151	25	316	64	G84
214	12/31/77	-15.30	-71.68	161.4	6.15	224.0	28.0	-7.0	204	42	74	36	322	28	G84
215	01/28/78	-25.92	-177.30	97.6	6.38	110.0	28.0	153.0	334	28	106	51	230	25	G84
216	04/18/78	5.14	127.41	114.0	6.30	346.0	29.0	78.0	265	16	105	73	357	6	G84
217	05/01/78	-21.24	169.80	73.4	7.37	18.0	41.0	-170.0	226	38	339	27	95	40	G84
218	05/13/78	-14.52	167.32	180.4	6.80	178.0	48.0	120.0	67	1	160	68	337	22	G84
219	05/23/78	31.05	130.13	175.9	6.66	229.0	23.0	113.0	121	23	278	65	28	9	G84
220	08/03/78	-26.51	-70.54	69.3	6.83	9.0	72.0	-110.0	252	58	114	24	15	19	New
221	09/02/78	24.90	121.98	89.3	6.26	33.0	28.0	149.0	260	27	32	53	157	24	G84
222	09/06/78	-13.32	167.14	202.3	6.70	306.0	41.0	53.0	242	9	131	65	336	23	G84
223	12/06/78	44.59	146.58	181.0	7.80	64.0	57.0	-172.0	282	28	21	18	140	56	G84
224	02/07/79	5.21	127.29	129.0	6.37	29.0	31.0	96.0	295	14	102	76	204	3	G84
225	02/11/79	5.99	125.92	142.0	6.22	229.0	47.0	132.0	111	6	210	60	17	29	G84
226	02/14/79	-15.56	167.57	126.8	6.05	7.0	29.0	98.0	271	16	77	73	180	4	G84
227	05/20/79	56.65	-156.73	71.0	6.50	123.7	32.8	26.6	78	25	314	50	183	29	HJ
228	06/22/79	17.00	-94.61	117.0	6.91	190.0	47.0	-40.0	169	55	67	9	331	34	G84
229	06/25/79	-4.98	145.58	192.1	6.60	131.0	32.0	-76.0	181	74	31	14	299	7	G84
230	08/05/79	-22.72	-177.49	229.0	6.40	195.0	14.0	-112.0	315	58	123	32	216	5	G84
231	08/22/79	52.27	157.33	126.0	6.50	86.0	32.0	166.0	303	31	67	44	192	31	G84
232	11/05/79	17.83	-68.62	78.3	6.19	93.0	22.0	87.0	5	23	188	67	96	1	G84
233	11/22/79	-24.34	-67.39	181.0	6.22	209.0	44.0	-37.0	191	54	84	12	345	34	G84
234	11/23/79	4.80	-76.22	108.6	7.20	137.0	41.0	-163.0	341	42	94	23	205	39	G84
235	12/11/79	28.88	140.70	124.7	6.64	95.0	38.0	162.0	317	25	74	44	207	36	G84
236	02/29/80	6.30	126.88	79.3	6.34	138.0	35.0	49.0	77	16	314	62	173	22	G84
237	04/13/80	-23.47	-177.30	166.2	7.57	144.0	25.0	-154.0	326	51	102	31	206	22	G84
238	05/14/80	-6.01	154.51	62.0	6.32	131.0	41.0	81.0	47	4	281	83	138	6	GDW
239	05/26/80	-19.36	-69.24	104.0	6.61	177.0	23.0	-83.0	254	68	82	22	351	3	G84
240	06/16/80	-7.35	128.54	160.1	6.00	330.0	44.0	74.0	251	2	151	79	342	11	G84

No.	Date	Lat. N+,S-	Long. E+,W-	Depth	M	Fault Plane $\phi°$	$\delta°$	$\lambda°$	P $Az°$	$Pl°$	T $Az°$	$Pl°$	B $Az°$	$Pl°$	Ref.
241	06/18/80	-15.27	-173.57	72.8	6.35	193.0	23.0	166.0	45	36	183	46	298	22	GDW
242	06/25/80	4.44	-75.78	151.1	6.33	231.0	74.0	14.0	184	2	94	21	279	69	GDW
243	07/08/80	6.63	125.79	164.5	6.52	79.0	32.0	16.0	41	30	276	45	150	31	G84
244	07/16/80	-4.46	143.52	81.9	7.26	276.0	22.0	101.0	178	23	346	66	86	4	GDW
245	07/19/80	-29.00	-69.68	129.3	5.94	306.0	26.0	-77.0	9	70	206	19	114	6	G84
246	07/22/80	-20.30	169.61	132.5	6.31	352.0	23.0	-95.0	91	68	266	22	357	2	G84
247	10/08/80	-1.38	-77.69	192.1	6.00	115.0	16.0	-117.0	243	59	47	30	141	7	G84
248	10/24/80	18.21	-98.24	63.4	7.14	311.0	26.0	-66.0	354	67	203	21	109	10	GMR
249	01/23/81	42.52	142.12	120.9	6.76	86.0	11.0	-65.0	145	55	335	35	241	5	DW
250	02/24/81	-6.06	148.74	77.8	6.56	288.0	37.0	108.0	185	9	315	76	93	11	DW
251	03/26/81	-19.37	-68.96	143.9	6.46	179.0	14.0	-76.0	250	58	77	31	345	3	DW
252	05/13/81	5.83	127.01	133.1	6.32	317.0	39.0	111.0	212	8	332	75	120	13	DW
253	05/22/81	-6.56	132.25	80.0	6.07	72.0	66.0	11.0	27	9	292	24	136	64	DW
254	05/28/81	-14.69	167.28	138.0	6.16	185.0	60.0	150.0	57	3	150	41	324	49	DW
255	06/26/81	-30.27	-178.99	163.8	6.14	169.0	18.0	-119.0	302	60	102	29	197	9	DW
256	07/06/81	-22.26	171.73	58.3	7.54	345.0	30.0	-179.0	191	38	318	37	74	30	DW
257	08/07/81	-5.19	151.67	65.8	6.14	251.0	36.0	71.0	175	10	42	75	267	11	DW
258	08/26/81	-5.34	151.48	63.6	5.94	259.0	29.0	77.0	179	17	20	72	270	6	DW
259	09/03/81	6.49	126.20	83.9	6.02	290.0	29.0	-167.0	126	44	255	33	5	28	DW
260	09/14/81	18.32	-68.89	159.6	6.02	78.0	25.0	85.0	352	20	178	70	83	2	DW
261	10/17/81	-7.10	128.97	185.8	6.39	292.0	51.0	148.0	165	9	264	47	67	41	DW
262	11/04/81	-20.02	-174.39	56.6	6.51	19.0	8.0	-71.0	87	52	272	37	180	3	DW
263	11/07/81	-32.20	-71.34	65.6	6.94	208.0	5.0	-47.0	251	49	78	41	345	3	DW
264	12/02/81	40.91	142.51	83.3	6.28	224.0	69.0	-162.0	85	27	176	3	272	63	DW
265	12/11/81	-6.09	148.18	59.8	6.16	272.0	33.0	85.0	186	12	19	78	276	3	DW
266	12/14/81	-56.36	-26.48	71.1	6.04	234.0	37.0	-155.0	70	48	188	23	294	33	DW
267	01/04/82	-23.05	-177.47	190.5	6.36	181.0	16.0	-120.0	313	58	115	31	210	8	DFiG
268	02/27/82	22.26	143.53	103.6	6.27	91.0	62.0	172.0	315	14	51	25	198	61	DFiG
269	03/10/82	-56.01	-27.26	109.8	6.48	168.0	42.0	145.0	41	15	151	53	301	33	DFiG
270	03/28/82	-12.77	-76.09	108.7	6.31	32.0	17.0	-13.0	27	46	240	39	136	17	DFiG
271	03/29/82	0.10	123.37	164.6	6.00	305.0	31.0	134.0	183	20	313	60	85	21	DFiG
272	04/16/82	-15.68	-173.08	59.3	6.13	223.0	19.0	154.0	82	35	229	50	340	17	DFiG
273	06/11/82	-17.53	-174.46	113.2	6.80	237.0	16.0	-38.0	259	53	105	34	6	13	DFiG
274	06/19/82	13.25	-89.40	51.9	7.28	102.0	25.0	-106.0	224	68	24	21	117	7	DFiG
275	08/14/82	-5.06	143.91	114.1	6.03	30.0	42.0	-15.0	4	40	252	24	140	40	DFiG
276	08/26/82	-2.70	-79.91	92.1	6.01	128.0	54.0	19.0	81	13	341	37	188	50	DFiG
277	09/06/82	29.31	140.28	155.6	6.80	100.0	55.0	-158.0	313	39	52	11	155	49	DFiG
278	09/15/82	-14.52	-70.84	168.6	6.28	109.0	44.0	-128.0	301	64	45	7	138	25	DFiG
279	10/02/82	-14.74	167.28	154.6	6.02	190.0	51.0	147.0	63	8	163	48	326	41	DFiG
280	10/31/82	14.15	-90.19	89.7	6.20	39.0	14.0	-178.0	231	44	24	43	127	14	DFiG

No.	Date	Lat. N+,S-	Long. E+,W-	Depth	M	Fault Plane ϕ^o	δ^o	λ^o	P Az^o	Pl^o	T Az^o	Pl^o	B Az^o	Pl^o	Ref.
281	11/18/82	-1.73	-76.74	190.2	6.54	163.0	29.0	-51.0	180	62	45	21	308	18	DFiG
282	11/18/82	-31.25	-65.86	166.2	6.00	129.0	24.0	-114.0	263	65	57	23	151	10	DFiG
283	12/17/82	24.64	122.62	94.4	6.47	54.0	49.0	152.0	284	12	27	46	183	42	DFiG
284	01/01/83	-17.31	-69.28	171.8	6.27	216.0	32.0	-19.0	201	46	76	29	328	30	DFiW
285	01/08/83	-15.32	-173.40	52.9	6.25	214.0	11.0	-150.0	15	50	176	39	274	10	DFiW
286	01/24/83	16.18	-95.15	35.6	6.60	110.0	54.0	-145.0	320	48	56	5	150	42	DFiW
287	01/24/83	12.95	93.64	72.7	6.76	110.0	54.0	-145.0	320	48	56	5	150	42	DFiW
288	01/26/83	-6.13	150.05	56.8	6.17	81.0	74.0	170.0	307	4	38	18	204	71	DFiW
289	02/13/83	13.84	144.98	108.1	6.10	154.0	36.0	-23.0	138	47	18	24	272	33	DFiW
290	02/25/83	-18.27	-69.44	144.9	6.68	253.0	15.0	-14.0	252	47	100	40	357	15	DFiW
291	03/18/83	-4.86	153.51	69.9	7.71	170.0	49.0	120.0	59	0	150	68	329	22	DFiW
292	03/20/83	-4.73	153.13	65.2	6.34	316.0	34.0	134.0	195	18	319	61	97	23	DFiW
293	03/21/83	-21.67	-175.32	51.5	6.65	357.0	16.0	84.0	272	29	96	61	3	2	DFiW
294	04/04/83	5.73	94.81	71.6	6.96	207.0	51.0	51.0	143	1	52	61	234	29	DFWa
295	04/04/83	-15.02	167.27	119.8	6.08	180.0	34.0	146.0	51	21	173	54	309	28	DFWa
296	04/12/83	-4.89	-78.18	111.1	6.97	339.0	35.0	-86.0	53	80	246	10	156	2	DFWa
297	04/18/83	27.72	62.06	51.3	6.70	81.0	43.0	-68.0	80	75	336	4	245	15	DFWa
298	05/10/83	-5.36	150.92	101.4	6.43	198.0	33.0	-167.0	38	43	161	30	273	32	DFWa
299	05/11/83	2.30	128.35	133.1	6.09	198.0	27.0	153.0	62	29	195	51	318	24	DFWa
300	06/01/83	-17.00	-174.71	185.7	6.51	211.0	24.0	-97.0	315	69	126	21	217	3	DFWa
301	07/24/83	53.85	158.39	177.4	6.18	315.0	11.0	7.0	298	43	139	45	38	11	DFWb
302	08/02/83	20.46	122.17	166.2	6.24	0.0	23.0	-79.0	70	67	262	22	170	4	DFWb
303	08/06/83	-6.56	130.13	172.7	5.94	72.0	9.0	-25.0	88	48	284	41	187	8	DFWb
304	08/17/83	55.79	161.21	77.2	7.01	216.0	41.0	60.0	147	8	36	69	240	19	DFWb
305	08/25/83	33.49	131.43	127.5	6.48	230.0	42.0	123.0	117	7	225	67	24	21	DFWb
306	09/07/83	60.98	-147.50	52.1	6.33	26.0	41.0	-97.0	169	84	301	4	31	5	DFWb
307	09/14/83	18.09	145.81	148.4	6.27	235.0	51.0	-156.0	85	42	186	13	290	45	DFWb
308	09/15/83	16.11	-93.23	121.5	6.29	138.0	9.0	-107.0	248	54	63	36	155	3	DFWb
309	10/27/83	1.05	120.81	60.0	6.44	41.0	38.0	27.0	353	21	237	49	98	33	DFWc
310	10/31/83	-9.11	119.23	98.4	6.38	205.0	18.0	154.0	64	35	212	50	322	16	DFWc
311	11/20/83	-7.53	130.67	78.5	6.09	73.0	60.0	11.0	29	14	291	28	142	58	DFWc
312	11/24/83	-7.55	128.25	157.1	7.40	74.0	39.0	59.0	6	10	250	69	99	19	DFWc
313	12/10/83	14.38	-91.63	55.6	5.98	247.0	45.0	31.0	196	14	89	49	297	37	DFWc
314	12/12/83	-7.70	127.38	164.5	6.35	290.0	38.0	131.0	172	13	288	62	76	24	DFWc
315	12/15/83	-33.09	-70.28	103.6	6.00	202.0	21.0	-78.0	271	65	103	24	11	4	DFWc
316	01/01/84	-3.86	-78.49	125.9	5.68	327.0	35.0	-46.0	328	61	206	17	109	23	DFWd
317	01/24/84	-56.56	-26.63	113.6	5.64	219.0	40.0	151.0	88	19	202	50	345	34	DFWd
318	01/27/84	36.39	71.03	172.0	6.03	68.0	34.0	89.0	339	11	162	79	69	1	DFWd
319	02/16/84	36.43	70.83	204.2	6.37	266.0	34.0	114.0	159	13	292	71	66	13	DFWd
320	02/17/84	-6.60	130.12	172.1	5.96	216.0	26.0	103.0	116	19	279	70	24	6	DFWd

No.	Date	Lat. N+,S-	Long. E+,W-	Depth	M	Fault Plane ϕ^o	δ^o	λ^o	P Az^o	Pl^o	T Az^o	Pl^o	B Az^o	Pl^o	Ref.
321	02/26/84	-17.32	-70.53	115.0	6.09	169.0	21.0	-69.0	224	64	63	25	329	7	DFWd
322	03/08/84	-38.25	177.22	78.5	6.01	310.0	49.0	146.0	184	10	285	50	86	39	DFWd
323	03/23/84	-15.19	-173.74	43.0	5.96	226.0	6.0	-137.0	8	49	179	41	273	4	DFWd
324	04/06/84	-18.90	168.85	175.0	6.80	304.0	14.0	42.0	254	35	95	53	351	10	DFWe
325	04/13/84	-5.65	148.30	170.0	6.09	202.0	31.0	-17.0	187	45	61	30	312	30	DFWe
326	04/18/84	-15.93	-174.35	158.0	6.44	198.0	21.0	-76.0	264	65	97	24	5	5	DFWe
327	05/29/84	3.56	97.14	79.6	5.50	130.0	21.0	-78.0	199	65	31	24	299	4	DFWe
328	07/17/84	-56.39	-27.39	118.0	6.00	348.0	35.0	29.0	300	22	179	51	44	30	DFWf
329	09/30/84	-6.06	148.54	49.9	5.93	258.0	32.0	82.0	174	13	12	76	265	4	EDR
330	10/15/84	-15.86	-173.64	119.7	7.07	161.0	89.0	-105.0	56	44	265	42	161	15	EDR
331	10/20/84	-24.07	-66.83	192.0	6.15	220.0	27.0	-67.0	263	68	113	20	19	10	EDR
332	11/11/84	-12.69	166.74	88.0	5.66	213.0	67.0	96.0	298	22	134	67	31	6	EDR
333	11/17/84	47.52	154.49	42.0	5.70	202.0	84.0	-22.0	156	20	250	11	7	67	EDR
334	11/19/84	51.78	-175.28	47.0	5.65	253.0	31.0	107.0	151	15	299	73	58	9	EDR
335	11/20/84	5.17	125.12	180.7	7.48	335.0	66.0	-97.0	232	68	70	21	338	6	EDR

* parameter constrained by modeling of long-period P waves.

M magnitudes are m_b for events before 1977, if a B appears next to the value, then it is m_B from Abe (1980); magnitudes are M_w from 1977 to 1984.

A72 - Abe, 1972; B80 - Billington, 1980; CI - Cardwell and Isacks, 1978; CIK - Cardwell, Isacks and Kraig, 1980; CK78 - Chung and Kanamori, 1978b; CK80 - Chung and Kanamori, 1980; D77 - Denham, 1977; DW - Dziewonski and Woodhouse, 1983; DFiG - Dziewonski, Friedman, Giardini and Woodhouse, 1983a; DFiW - Dziewonski, Friedman and Woodhouse, 1983b; DFWa - Dziewonski, Franzen and Woodhouse, 1983c; DFWb - Dziewonski, Franzen and Woodhouse, 1984a; DFWc - Dziewonski, Franzen and Woodhouse, 1984b; DFWd - Dziewonski, Franzen and Woodhouse, 1984c; DFWe - Dziewonski, Franzen and Woodhouse, 1985a; DFWf - Dziewonski, Franzen and Woodhouse, 1985b; EDR - Earthquake Data Report, U.S.G.S., 1984; F72 - Fitch, 1972; FM - Fitch and Molnar, 1970; Fo75 - Forsyth, 1975; FK - Fujita and Kanamori, 1981; G84 - Giardini, (personal communication) 1984; GDW - Giardini, Dziewonski and Woodhouse, 1985; GMR - Gonzalez, McNally and Rial, 1984; HJ - House and Jacob, 1983; ISO - Isacks, Sykes and Oliver, 1969; JoM - Johnson and Molnar, 1972; KS - Katsumata and Sykes, 1969; KSe - Kawakatsu and Seno, 1983; LB- Langston and Blum, 1977; LTM - LeDain, Tapponier and Molnar, 1984; MDM - Malgrange, Deschamps and Madariaga, 1981; MS - Molnar and Sykes, 1969; O71 - Oike, 1971; OA - Osada and Abe, 1981; P79 - Pascal, 1979; Ri79 - Richter, 1979; R74 - Ripper, 1974; R75 - Ripper, 1975; So73 - Soedarmo, 1973; S72 - Stauder, 1972; S73 - Stauder, 1973; S75 - Stauder, 1975; SB - Stauder and Bollinger, 1966; SMa - Stauder and Maulchin, 1976; SEWS - Stein, Engeln, Wiens, Speed and Fujita, 1982.
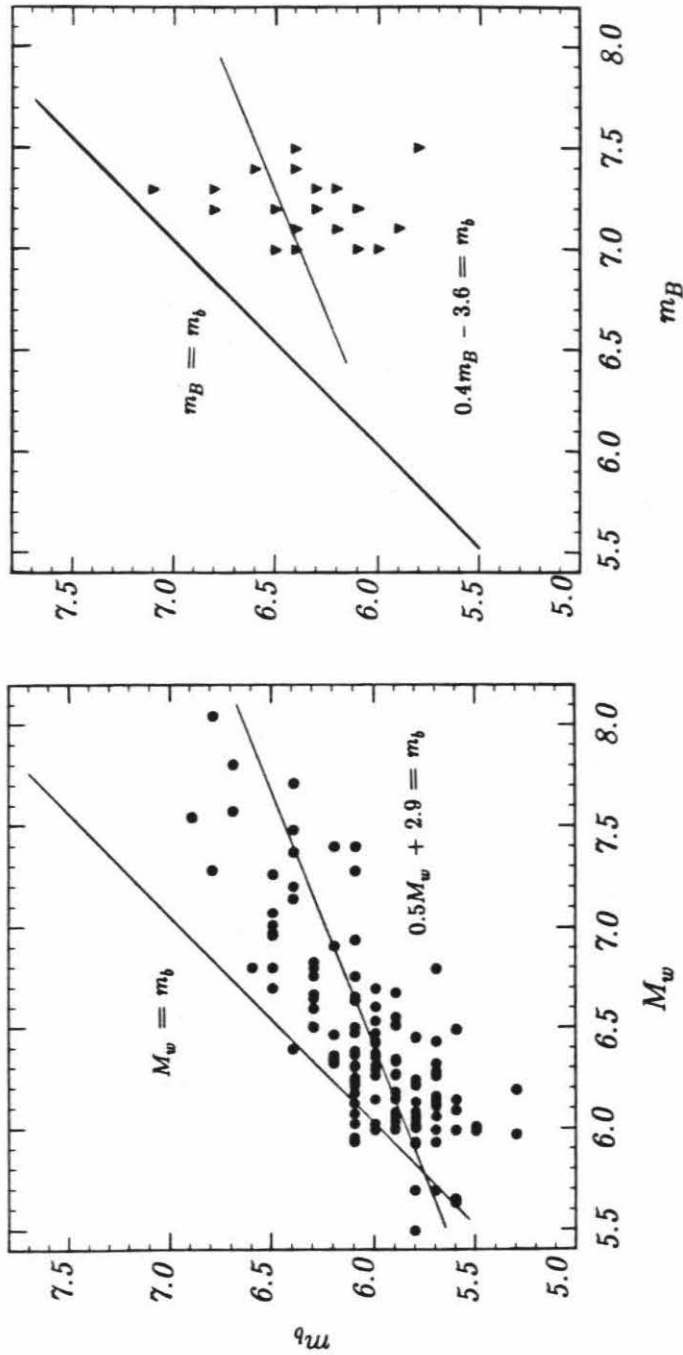
Figure 1.3 Magnitude relations for intermediate-depth events in Table 1.2. All m_b values are from NOAA, M_w is determined from the event seismic moment, M_o, for the events that occurred after 1977, and m_B values are from Abe (1981) for large events between 1960 and 1974.

1.4   Seismic Coupling and Large Intermediate-depth Events

After recognizing a systematic variation in the size of earthquakes in the northwest Pacific, Kanamori (1971) introduced the term seismic coupling to describe the interaction between the two plates in subduction zones. He noticed that in some regions, such as the Aleutians and Alaska, great earthquakes occur along the entire trench, whereas in the Mariana Islands there is no record of great events. Similarly, Kelleher et al. (1974) observed a correlation between earthquake size and width of the contact zone between the two plates at shallow depth in subduction zones. Figure 1.4 shows the epicenters of earthquakes with $M_S > 7.6$ that occurred between 1904 and 1985, with known aftershock areas being shaded. M_S is given in parenthesis and M_w in brackets. M_w is a measure of seismic energy (Kanamori, 1977a), which remains unsaturated even for great earthquakes. Notice the uneven distribution of great ($M_w = 8.5$) earthquakes in Figure 1.4, that together with estimates of seismic and aseismic slip (Kanamori, 1977b; Sykes and Quitmeyer, 1981) suggest a global variation of seismic coupling at plate boundaries.

In an attempt to understand the subduction process, several investigators (e.g. Isacks et al., 1968; Vlaar and Wortel, 1976; Molnar et al., 1978) have studied the interrelation among the physical and geometric characteristics of subduction zones (Table 1.1). For example, Uyeda and Kanamori (1979) characterized subduction zones by whether or not active back-arc spreading is taking place. They constructed an evolutionary model based on the degree of interplate coupling, where the end members are the Chile and Mariana type subduction zones that are respectively under regional compressional or tensional tectonic stresses at shallow depth. Ruff and Kanamori (1983) found a strong correlation between the maximum earthquake size
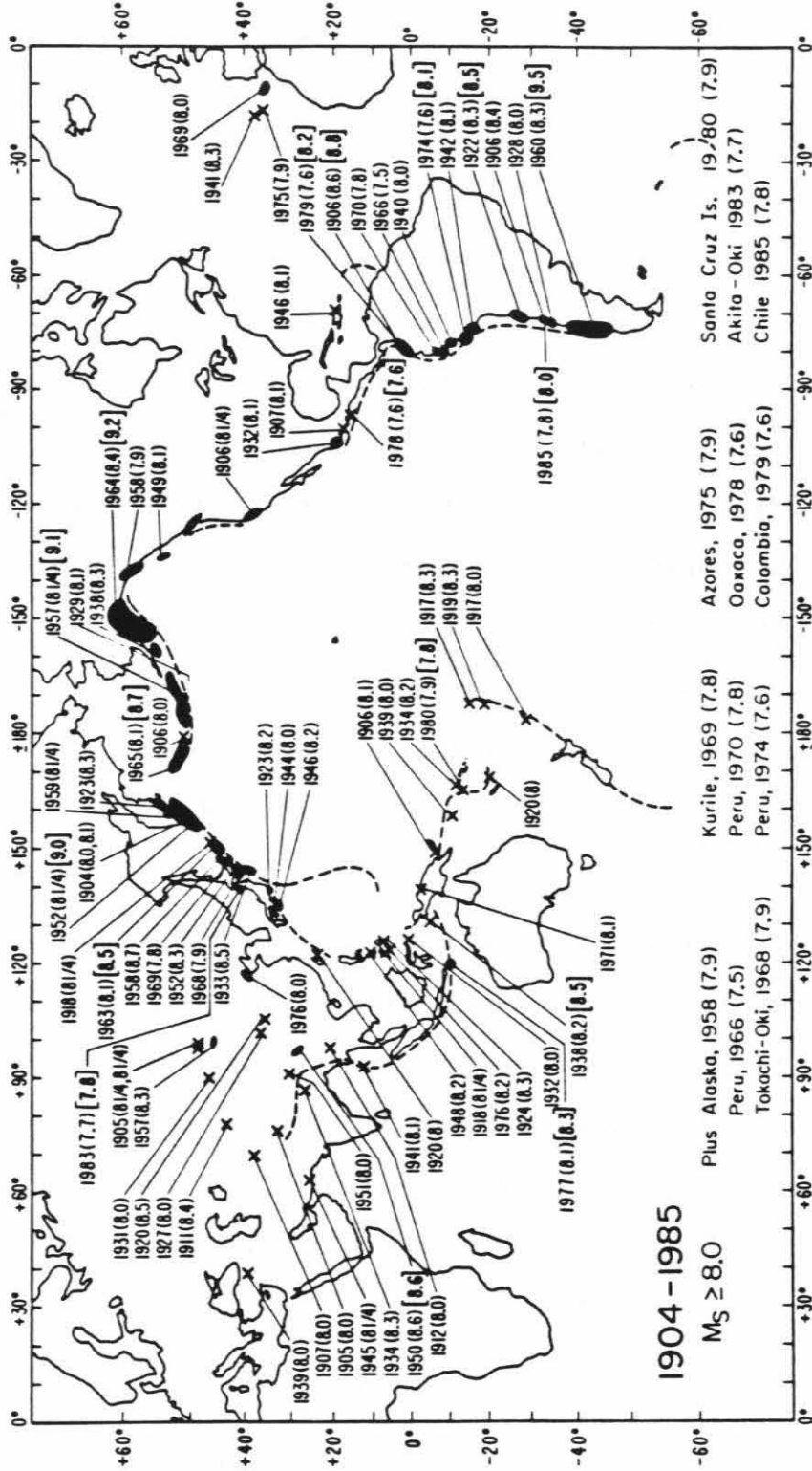
Figure 1.4: Location of large ($M_S \geq 7.6$) shallow earthquakes from 1904 to 1985. M_S is in parenthesis and M_w in brackets. Aftershock areas of recent great earthquakes are shaded. Notice the uneven distribution of great earthquakes ($M_w = 8.5$), suggesting a global variation of interplate coupling at subduction zones. (from Kanamori, 1986)

observed in subduction zones and the convergence rate, and age of the subducting plate; great subduction earthquakes occur where young oceanic lithosphere is being subducted at high convergence rate while smaller events are associated with old plates with slow convergence rates. The above observations suggest that physical characteristics of the contact zone between the subducted and overriding plates can be related to the degree of seismic coupling. Recently, Jarrard (1986) presented an extensive review of the relations among subduction parameters, concluding that interplate coupling is mainly regulated by convergence rate and slab age. In summary, strongly coupled plates produce great earthquakes like the Chile (M_w=9.5) and the 1964 Alaska (M_w=9.1) and the 1952 Kamchatka (M_w=9.0) earthquakes. Weakly coupled zones do not produce large earthquakes as is the case for the Mariana, Bonin and Northeast Japan arcs. Moderately coupled zones do produce large earthquakes but with maximum ruptures less than 500 km long, as is true for the Peru, Middle America, Aleutians and Kurile trenches (Figure 1.4).

In the previous section we compiled a catalog of intermediate-depth earthquake focal mechanisms. If we consider only the largest of these events ($M > 6.8$), a regional pattern in the types of mechanisms emerges, as shown in Figures 1.5 to 1.7. These events can be grouped as follows: (1) Normal-fault events (44%) with a strike sub-parallel to the trench axis (Figure 1.5), (2) reverse-fault events (33%) with a strike sub-parallel to the trench axis (Figure 1.6), (3) normal or reverse fault events with a strike significantly oblique to the trench axis (10%, Figure 1.7) and (4) tear faulting events (13%, Figure 1.7).
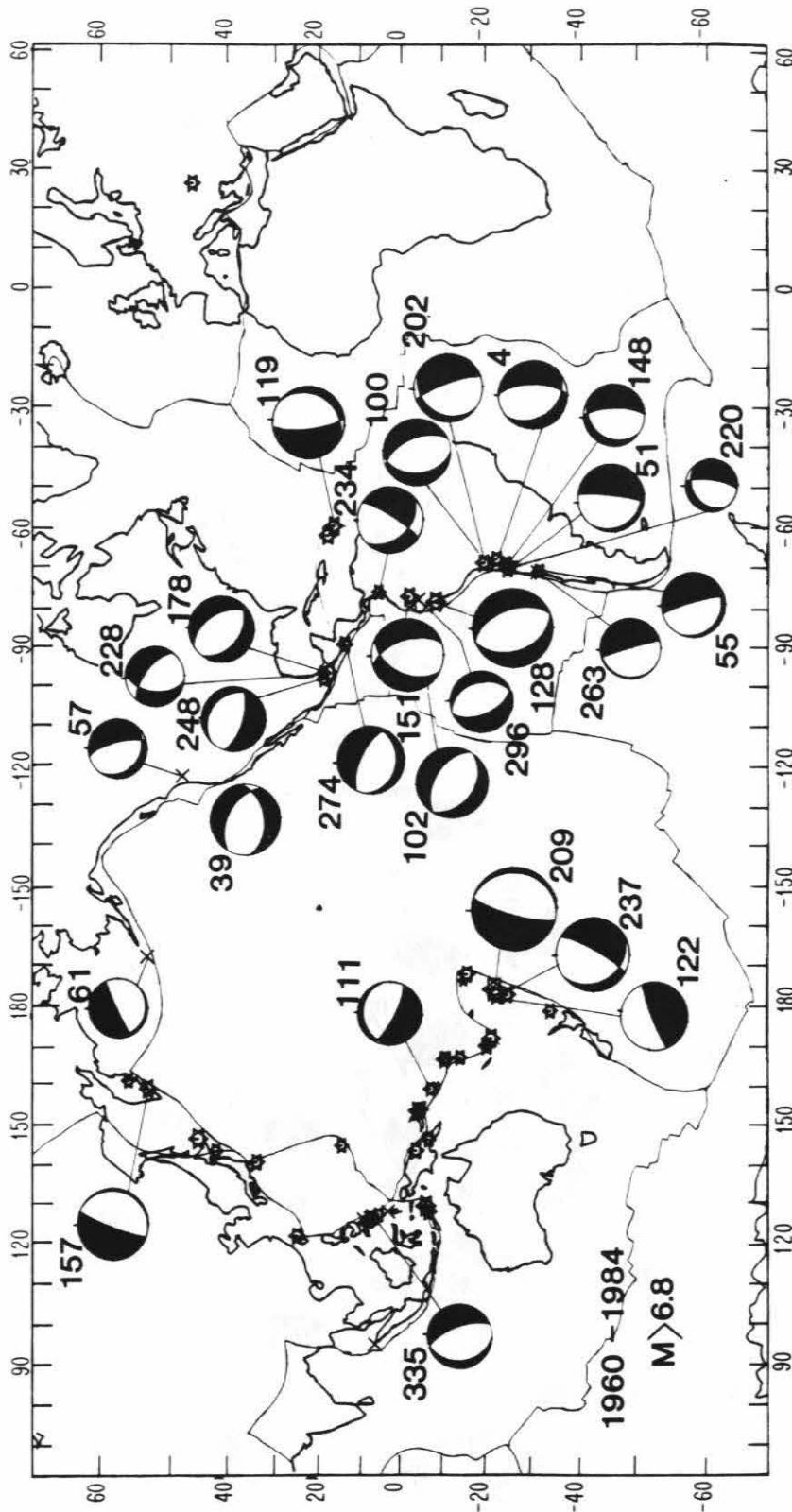
Figure 1.5: Focal mechanisms of Type 1 events (44%) that indicate normal faulting within the subducted plate and strike subparallel to the trench axis. The events shown are large ($M_S > 6.8$) intermediate-depth earthquakes that occurred from 1960 to 1984. The mechanism diagrams are lower hemisphere equal area projections that are proportional in size to the earthquake magnitudes. Dark quadrants are compressional. Numbers identify the events in Table 1.2.
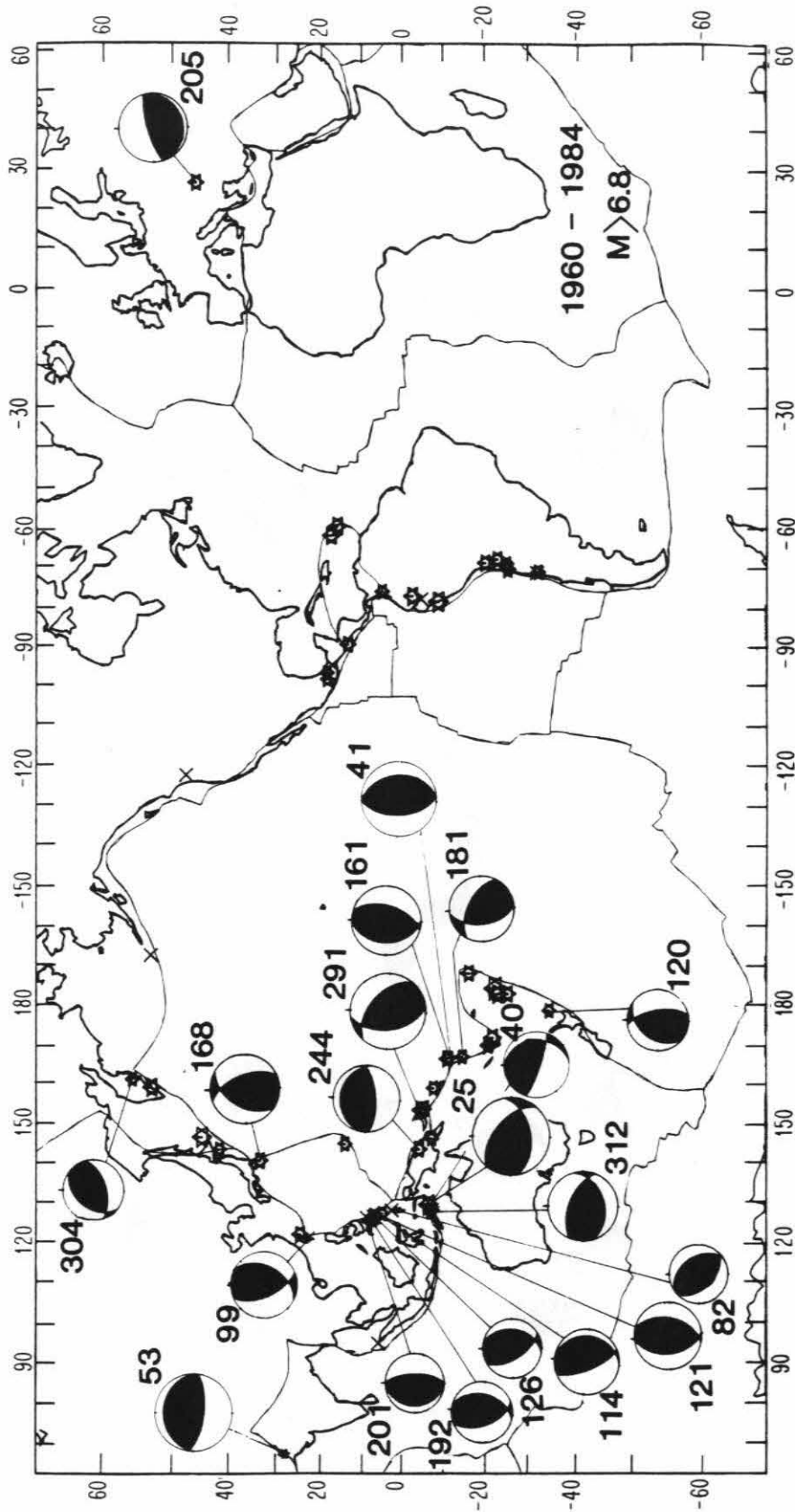
Figure 1.6: Focal mechanisms of Type 2 events (33%) that show reverse faulting within the subducted plate. The strike of these events is also subparallel to the trench axis. Numbers identify the events in Table 1.2. Dark quadrants are compressional. The diagrams are lower hemisphere equal area projections that have sizes proportional to the magnitude of the earthquakes.
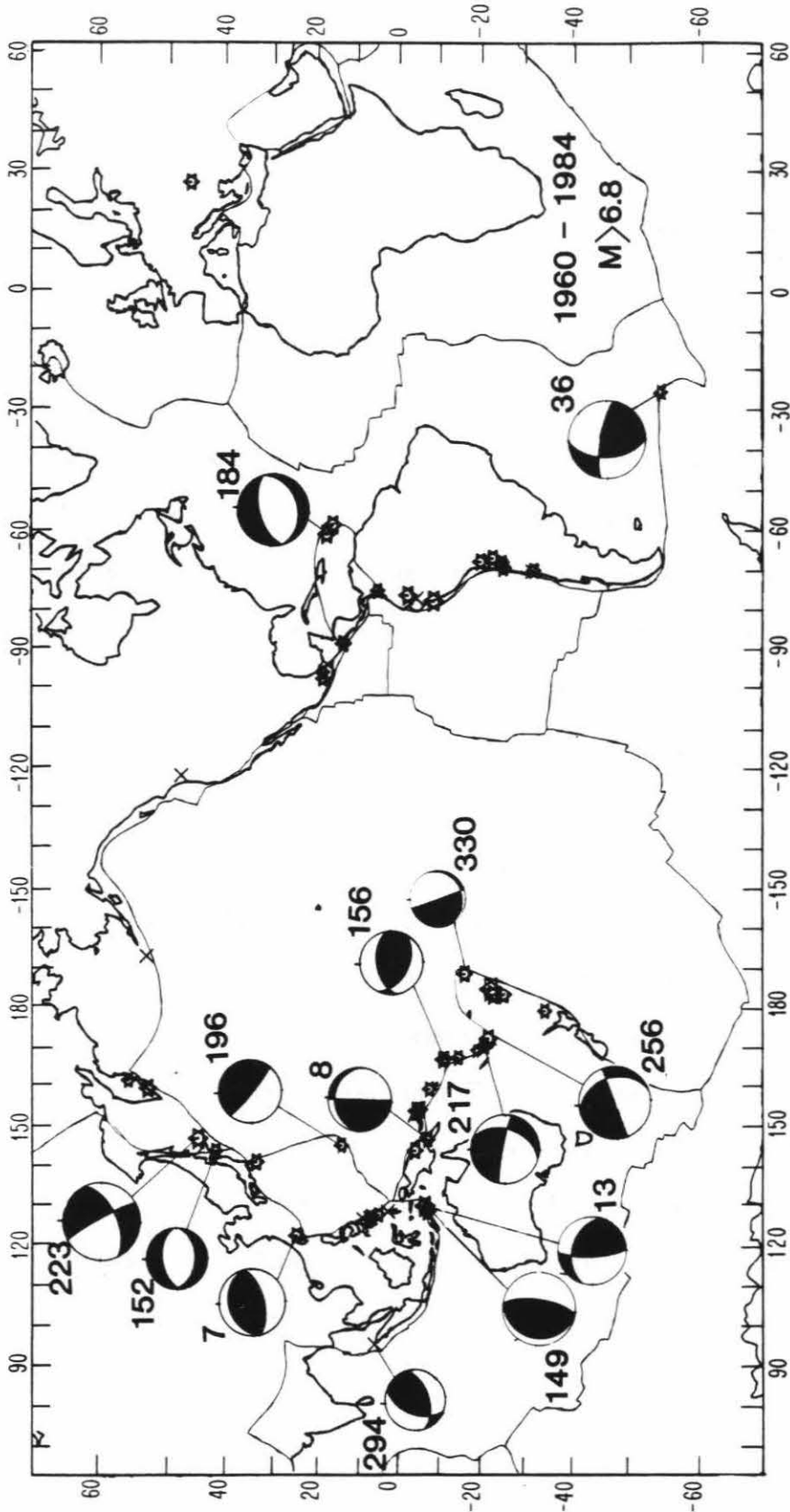
Figure 1.7: Focal mechanisms of Type 3 (10%) and Type 4 (13%) events are shown. These events indicate hinge faulting or contorsions within the subducted slab and tear faulting, respectively. Compressional quadrants are darkened. The mechanism diagrams are plotted in a lower hemisphere equal area projection. Their size is proportional to the earthquake's magnitude. Numbers identify the events in Table 1.2.

Fault plane solutions of Type 1 events (Figure 1.5) indicate a steeply dipping normal fault usually with the "continental" side down-dropped. These events occur mainly along the South and Middle America trenches, but they also occur in the Pacific Northwest, Alaska, and Kamchatka. All of these zones are strongly or moderately coupled subduction zones (Kanamori, 1977b; Uyeda and Kanamori, 1979; Ruff and Kanamori, 1983) in which the focal mechanisms of intermediate-depth events are down-dip tensional. However, the Type 1 events that occur along the Philippine and Solomon Island regions (335 and 111) are down-dip compressional. The Solomon Islands region is the site of numerous large doublet events (Lay and Kanamori, 1980; Wesnousky et al., 1986) that suggest moderate interplate coupling, although no single earthquake with $M>7.7$ has occurred there. Events 122, 209, and 237 in the Tonga trench may be related to subduction of the Louisville ridge, which may cause a localized increase in interplate coupling, in an otherwise uncoupled region. Note that event 209 is down-dip tensional and the largest event ($M_w=8.0$) in the catalog. This event may have fractured and detached the subducted slab at the leading edge of the coupled interplate boundary (Given and Kanamori, 1980). Events 122 and 237, on the other hand, are down-dip compressional and deeper than event 209 (Table 1.3). These events are discussed in more detail below. Simple models of plate coupling and geometry suggest that Type 1 events occur at strongly coupled plate boundaries, where a down-dip extensional stress prevails in a gently dipping plate. Various explanations for the occurrence of these events include (1) bending or unbending stresses, (2) continental loading and (3) down-dip gravitational loading by the leading edge of the plate. The dominant mechanism may vary from region to region, as we will explore in Chapter 3. One possible interpretation is that, at

strongly coupled subduction zones, the stress caused by the negative buoyancy of the subducting plate tends to cause a normal-fault earthquake characterized by down-dip tensional stresses in the downgoing slab near the lower edge of the coupled thrust plane, as shown in Figure 1.8. Thus, the occurrence of Type 1 events may be interpreted as evidence of strong coupling between plates. Although the coupling of the Pacific Northwest is being debated, note that the 1965 and 1949 Puget Sound earthquakes are Type 1 events, which would suggest strong coupling between the Juan de Fuca and North American plates. This study may provide an additional clue to the strength of coupling in this region.

In contrast, if the interplate boundary is weakly coupled, the stress due to negative slab buoyancy is transferred to even shallower depth, causing large normal-fault events near the trench where the curvature of the plate is largest (Figure 1.8). The great 1933 Sanriku earthquake in northeast Japan (Kanamori, 1971; Mogi, 1973), and the 1977 Sumbawa, Java earthquake (Given and Kanamori, 1980; Silver and Jordan, 1983; Spence, 1986), which occurred at weakly coupled subduction zones, are examples of this type.

Type 2 events have reverse-fault plane solutions and strike subparallel to the subduction zone (Figure 1.6). The events that occur in the Philippine, NW Solomon Islands, New Hebrides, and Kermadec regions show near vertical tension and horizontal compression axes. Note that all of these regions are considered partially coupled or uncoupled subduction zones (Kanamori, 1977b; Uyeda and Kanamori, 1979; Ruff and Kanamori, 1983), where the continuous seismicity is deeper than 300 km (see Table 1.1). In terms of our simple model, the increased dip angle of the downgoing slab associated with weakly coupled subduction zones, together with the weight of the
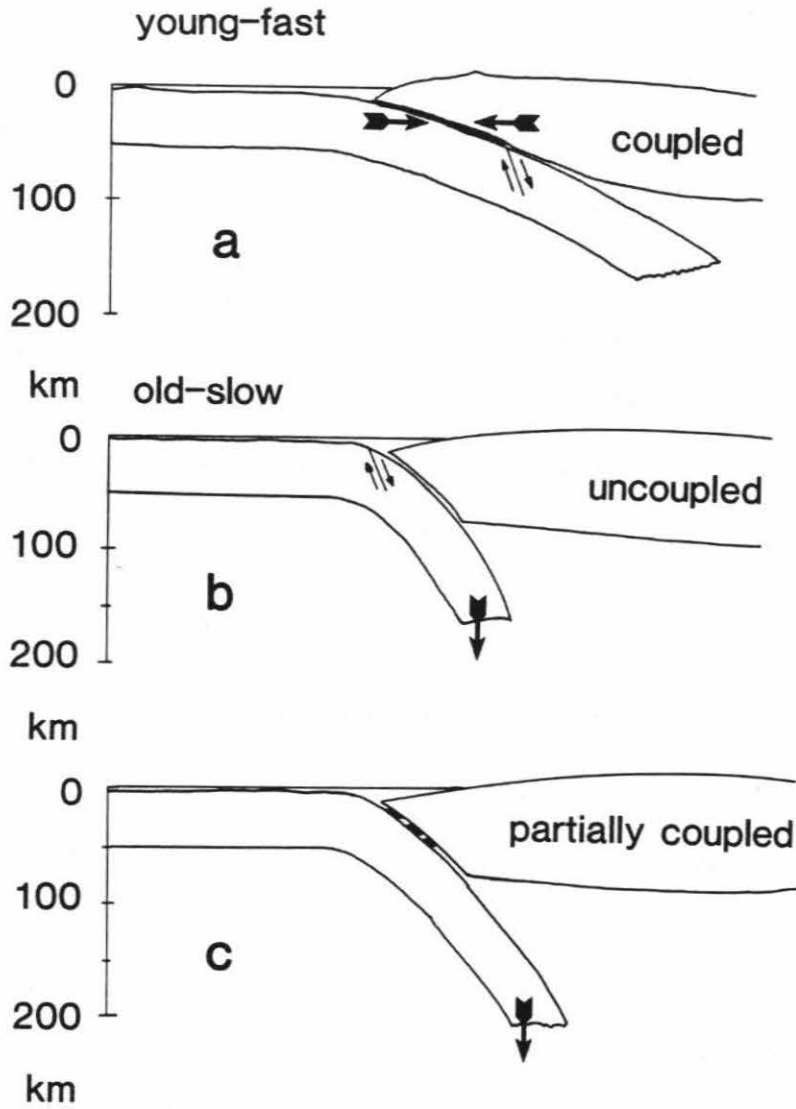
Figure 1.8: A schematic figure showing a) the possible mechanism of Type 1 events at a strongly coupled plate boundary and c) Type 2 events at a moderately coupled boundary. Figure 5b shows the case where the interplate boundary is decoupled to the trench, causing a large normal-fault earthquake.

relatively long subducted plate, induces vertical tensional stresses at intermediate depth, which are responsible for the change in focal mechanism from Type 1 to Type 2 events (Figure 1.8). Exceptions are events 114 in New Guinea, 205 in Rumania, and 244 in the Philippines that show down-dip compressional stresses. We will discuss these three events in detail together with other events in each region.

Events of Type 3 and 4 are shown in Figure 1.7. Type 3 events (7, 149, 152, 156, 184, 294) occur where the trench axis bends sharply, causing horizontal extensional or compressional intraplate stresses. These events indicate hinge faulting within the subducting slab. Type 4 events (8, 13, 36, 196, 217, 223, 256, 330) include all those that do not fall in the above categories. These events occur at plate boundaries with complex features or may be related to tear faulting.

1.5 Seismicity Characteristics of Intermediate-depth Events

Intermediate-depth earthquakes have far fewer aftershocks than shallow subduction events with similar magnitudes. We determine the number of aftershocks of the events with $M \geq 6.5$ in Table 1.3, reported by the NOAA and ISC catalogs within one week after the main event. About 48% of the events had no aftershocks and 37% of the events had between 1 and 5 aftershocks. If we consider a one-month period, the number of aftershocks does not increase significantly. Figure 1.9 shows the variation of the number of one-week aftershocks, N, with characteristics of the subducted slabs where they occur. The events were divided into three magnitude groups, where filled circles are the largest events. The relation of N versus age of the subducted slab at
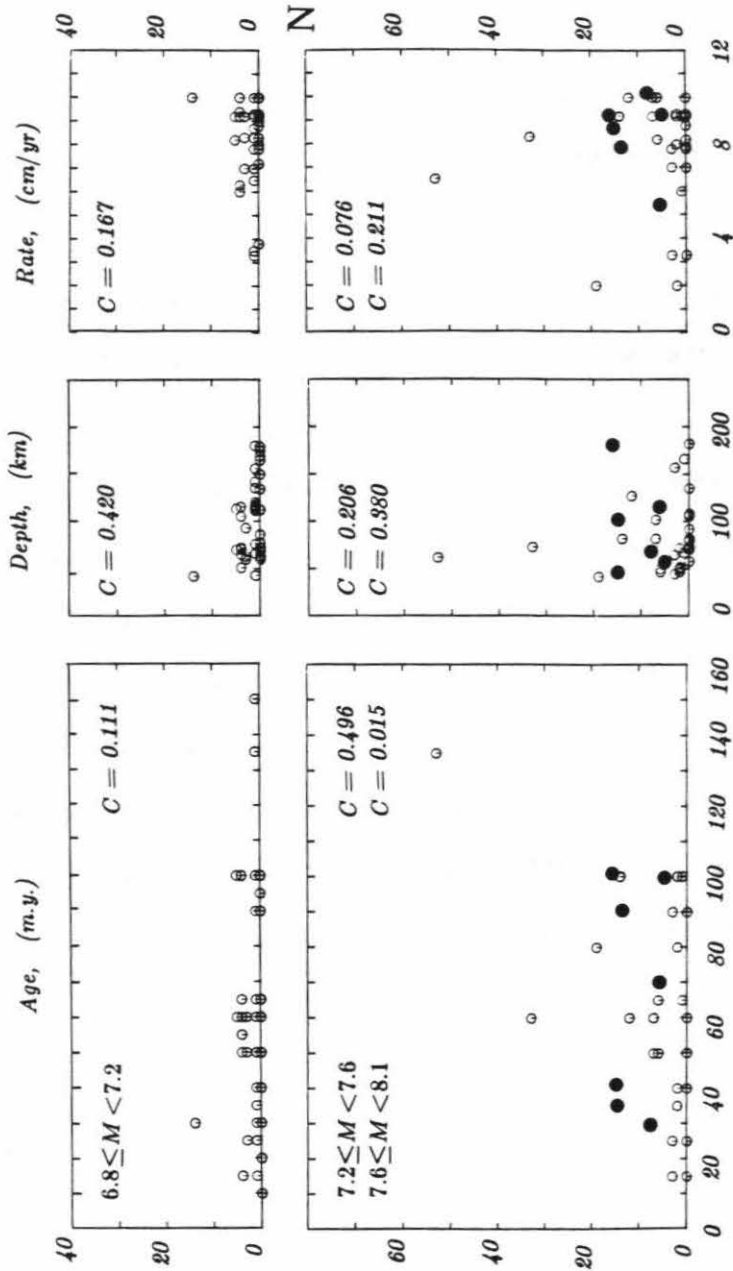
Figure 1.9: Linear relations between age of the subducted slab, depth of continous seismicity and rate of convergence and the number of aftershocks N with M>3.5 that occurred within the first week after an intermediate depth earthquake. The events are grouped by magnitude. Filled circles in the lower diagrams are events with M≥7.6. The correlation coefficients of each group of events is indicated on the figure.

the trench is slightly positive for events with magnitude range 7.2 to 7.6 (correlation coefficient C = 0.5). The relation of number of aftershocks N and depth of the event suggests that shallower intermediate-depth events may have more aftershocks than deeper events; however, the data set may be biased by the inclusion of shallow inter-plate events as aftershocks of these events. Only events with depth larger than 35 km were included in the count. The relation between N and the rate of convergence at the interplate boundary is unclear.

Figure 1.10 shows the distribution of the one-week aftershocks, N, with magni-tude for events with M > 6.5 in Table 1.3. Note that most events have no aft-ershocks or only a few detected. As expected, there is a slight positive correlation between mainshock magnitude and number of aftershocks occurring within one week that could be attributed to detection threshold. However there are some events with particularly large numbers of aftershocks, which are shown on the map in Figure 1.10. Open circles indicate events with N > 5, closed circles N > 10 and stars N > 25 aftershocks. These events are generally large intermediate-depth events that are associated with bends in the subducted slab, or with moderately coupled or uncoupled regions like the December 25, 1969 (event 119, Stein et al., 1982) and the 1972 Izu-Bonin event (168),which had the largest number of aftershocks within a week.
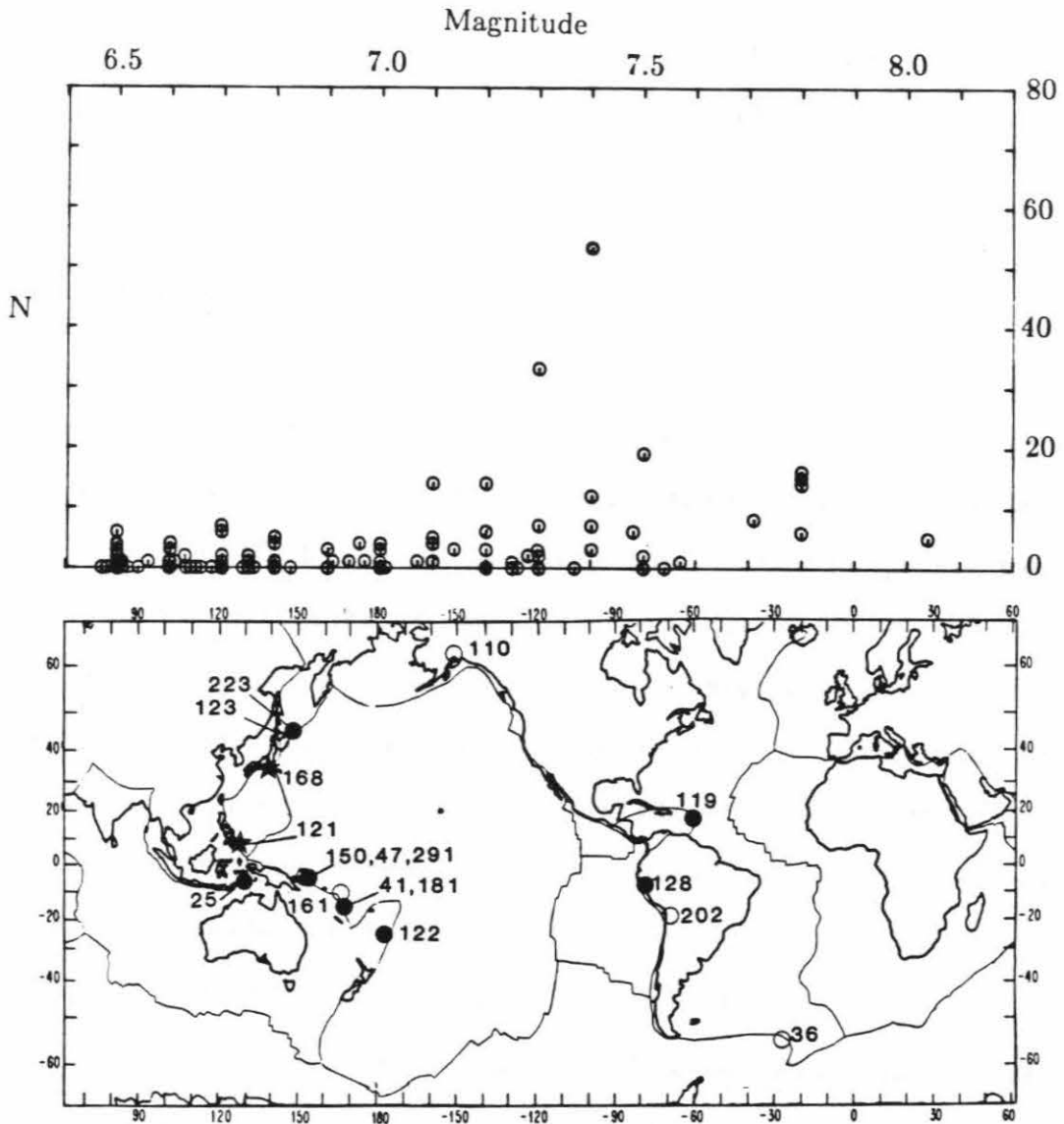
Figure 1.10: The distribution of number of aftershocks with M>3.5 occurred within one week of an intermediate-depth event and the magnitude of the mainshock is shown on the top diagram. Mainshocks are from 1960 to 1984. Note that most events have no aftershocks or only a few. Location of events (Table 1.2) with larger number of aftershocks are indicated in the map. Open circles indicate N > 5, closed circles N > 10, and stars N > 25 aftershocks.

Chapter 2

Temporal Variation of the Mechanism of Large
Intermediate-depth Earthquakes in Chile

2.1   Introduction

Results in Chapter 1 indicate that most large (M>6.8) intermediate-depth earthquakes that occur down-dip of strongly coupled subduction zones have a steeply dipping normal-fault mechanism that is consistent with down-dip tensional stresses within the subducting plate (Figure 1.5). A possible interpretation of this observation is that at strongly coupled subduction zones, the stresses caused by the negative buoyancy of the subducting slab tend to cause (down-dip tensional) normal-fault earthquakes in the downgoing slab near the lower edge of the coupled thrust plane. This suggests that intraplate stress reflects the degree of coupling at the interplate thrust boundary. Similar to Chapter 1, strong and weak seismic coupling is defined in terms of the occurrence and absence of great (M > 8.5) subduction events.

Christensen and Ruff (1983) suggested that the stress axis of outer-rise earthquakes are closely related to the spatio-temporal variation of activity of interplate thrust earthquakes. They found only tensional outer-rise events for uncoupled subduction zones, and suggested that the slab is under tension due to the slab pull. For coupled seismic zones they observed a temporal variation of the stress orientation of outer-rise events associated with the occurrence of large underthrusting earthquakes.

Although most shallow outer-rise events are tensional (normal fault), compressional (thrust) events occur offshore of some seismic gaps. They hypothesized that, for strongly coupled subduction zones, the intraplate stress orientation in the outer-rise region is compressional before a large interplate thrust earthquake; after the occurrence of a large thrust earthquake, and the interplate boundary is temporarily uncoupled, the stress becomes tensional.

In contrast with most South American intermediate-depth events that are down-dip tensional (Barazangi and Isacks, 1976), the mechanism of the May 8, 1971 (M_S=6.8) earthquake is down-dip compressional. This is the only event with M>6.5 to have occurred after the 1960 Chilean (M_w=9.5) earthquake down-dip of its rupture zone. This contrast in the stress orientation may be a result of the large interplate displacement associated with the 1960 Chilean earthquake. To investigate this problem, we examined spatio-temporal variations of large intermediate-depth earthquakes along the Chilean subduction zone.

2.2 Seismicity in Southern Chile

The Chile trench marks the convergence, at about 9 cm/yr, between the South America and the Nazca plates that is laterally segmented as indicated by the spatial distribution of earthquakes that are down-dip tensional (Barazangi and Isacks, 1976). The southern Chile segment (33°–46°S) is bounded by the Juan Fernandez Ridge and the South Chile Rise, and is characterized by subduction of the young (< 40 m.y.) Nazca plate. Quaternary volcanoes lie along the eastern margin of the inland lowlands and thick sediments that mask the Chile trench (Schweller et al., 1981). The shallow

seismicity dips gently (10°), bending at intermediate depths (to 25°) and extending to about 200 km depth (Barazangi and Isacks, 1976). Figure 2.1 shows the rupture zones of the most recent shallow large earthquakes that occurred in southern Chile. These earthquakes occurred on April 6, 1943 (M_t=8.2), July 9, 1971 (M_w=7.8), March 3, 1985 (M_w=8.0), December 1, 1928 (M_t=7.9), January 25, 1939 (M_t=8.3) and May 21, 1960 (M_w=9.5). Here, M_w is the moment magnitude and M_t is the tsunami magnitude defined by Abe, 1973). The 1960 Chilean earthquake is the largest in this century, involving extensive crustal deformation (Plafker and Savage, 1970) and accounting for most of the convergence along the plate boundary (Kanamori and Cipar, 1974). The subduction zone along the rupture zone of the 1960 Chilean earthquake is associated with a young subducting slab and large convergence rate. Ruff and Kanamori (1983) point out that these features are usually associated with strong interplate coupling.

The May 8, 1971 earthquake is the only large event that occurred down-dip of the rupture zone of the 1960 great Chilean earthquake during the period from 1961 to 1985. We searched for possible large, intermediate-depth events that may have occurred during the aftershock sequence of the 1960 Chilean earthquake. Duda (1963) assigns intermediate depths to some of the large 1960 Chilean aftershocks. However, comparing Duda's hypocenters with the International Seismological Centre (ISC) and National Oceanic and Atmospheric Administration (NOAA) hypocentral locations, we found that all of these events are listed as shallow ($<$ 40 km). The largest of these events (Nov. 1, 1960, M_S=7.2) is a shallow complex event (Kanamori and Stewart, 1979).
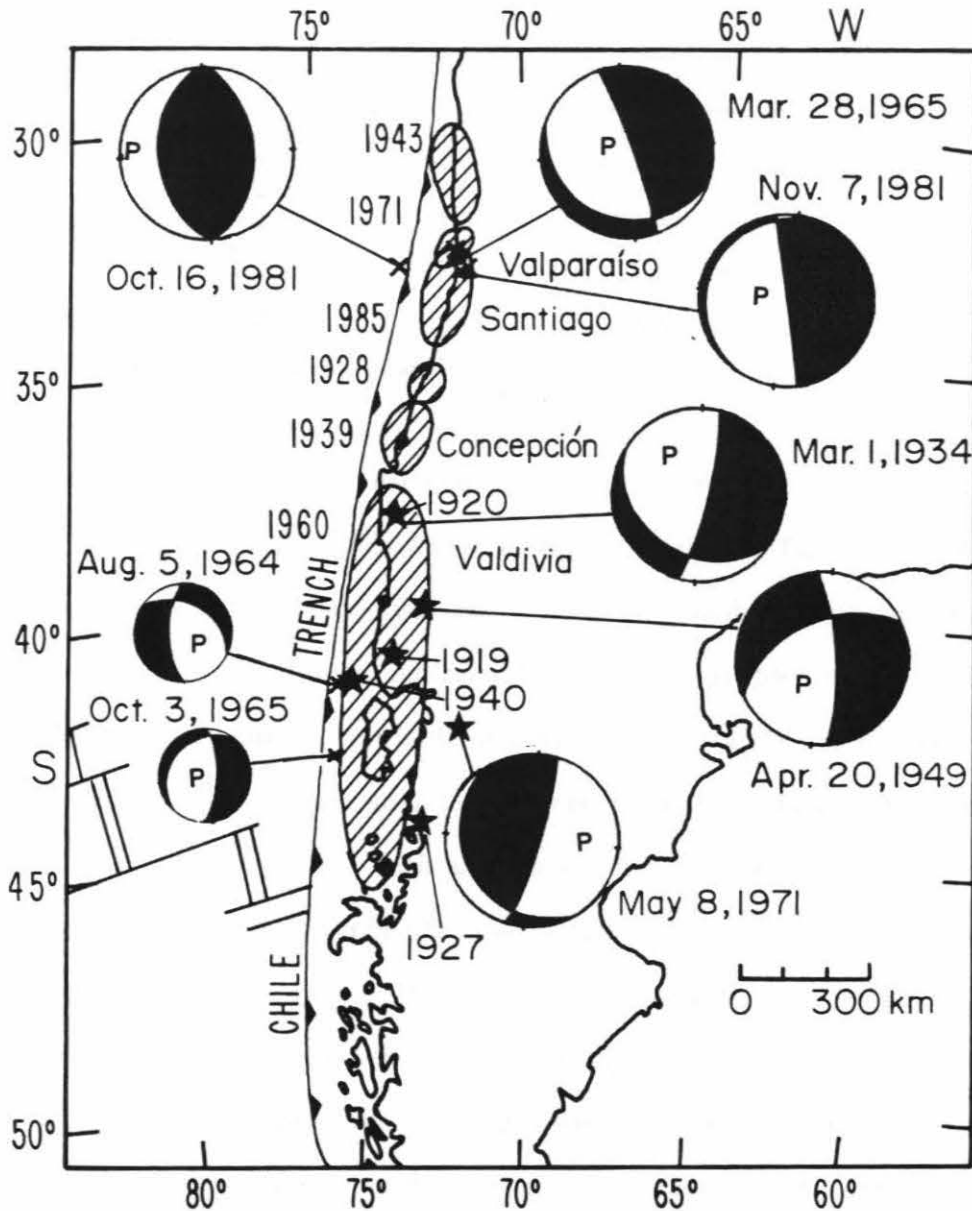
Figure 2.1: The rupture areas of the most recent large shallow earthquakes (Kelleher, 1972; Korrat and Madariaga, 1986), which occurred in central and southern Chile. Dots indicate the location of coastal cities. The epicenters of large (M>7.5) earthquakes that occurred before the 1960 Chile earthquake, south of 37°S, are indicated (Table 1). Fault plane solutions of large (M ≥ 7.0) intermediate-depth earthquakes that occurred from 1930 to 1985, and the solutions for the 1964,1965 and 1981 outer-rise events are also shown. Note that the events occurring before the 1960 Chile earthquake and also those occurring before the 1971 and 1985 Valparaiso earthquakes at intermediate depths are steeply dipping normal faults (down-dip tensional). In contrast, the May 8, 1971 event that occurred after the 1960 earthquake is down-dip compressional. Dark quadrants are compressional.

Table 2.1: Large Earthquakes in Southern Chile before 1960

Date	Time	Lat.°S	Lon.°W	Depth	M$_S$
Mar. 2, 1919	3h 26m	41.0	73.5	40 km	7.2
Mar. 2, 1919	11h 45m	41.0	73.5	40 km	7.3
Dec. 10, 1920	4h 25m	39.0	73.0		7.4
Nov. 21, 1927	23h 12m	44.3	73.0		7.1
Mar. 1, 1934	21h 45m	40.0	73.0	120 km	7.1
Oct. 11, 1940	18h 41m	41.5	74.5		7.0
Apr. 20, 1949	3h 29m	38.0	73.5	70 km	7.3

Hypocenters are taken from Gutenberg and Richter (1954).

We searched for all large earthquakes that occurred before May 21, 1960, between 37° and 47°S in Chile (shown by stars in Figure 2.1, Table 2.1). The 1919 doublet, and the 1920, 1927, and 1940 earthquakes are listed as large shallow earthquakes; however, the ISC Bulletin indicates that the 1919 doublet may be as deep as 130 km. We could not find any records or first motion data for the events prior to 1930; consequently, we could not analyze these events. For the 1940 earthquake, ISC first-motion data are consistent with a shallow (15°) dipping thrust fault, with a strike subparallel to the trench axis (350°) in southern Chile; it probably occurred on the interplate boundary. However, the location of this event (41.5°S, 74.5°W), given by Gutenberg and Richter (1954), is very close to the trench axis (Figure 2.1). If this location is correct, this event could be an outer-rise event with a horizontal compression mechanism. Unfortunately, the data are not good enough to resolve the location and the nature of this event. For the 1949 and 1934 earthquakes we have a few seismograms and also P-wave first motion data reported by ISC. Using these seismograms, we determined orientations of the stress axes with respect to the down-going plate. In the following, we describe our focal mechanism solutions.

2.3 Data Analysis of Intermediate-depth Events

Since the data for old events are incomplete, we combine P-wave first-motion data, S-wave polarization angles and waveform data to determine the mechanisms. We use synthetic seismograms to interpret the observed waveforms. All synthetic seismograms are computed, using the method described by Langston and Helmberger (1975). We assume a half-space with $V_p=7.3km/s$, $V_s=4.1km/s$ and $\rho=3.1g/cm^3$ to determine the source depth, orientation and the source time function. P-wave records are from vertical component recordings and SH-wave records are obtained by rotating the observed horizontal seismograms. SH clockwise motions around the source viewed from above are shown as upward motions (Figures 2.2 to 2.4). Note that for intermediate-depth earthquakes the arrival times of the reflected phases relative to the direct phase provide good constraints on the focal depth, and there is no trade-off between the source time function and the depth of the events. We use a half-space model to compute all synthetic seismograms. Although the absolute amplitude of near nodal phases may be difficult to match between the observed and calculated records because of this simplified structure, the relative amplitude between the direct and reflected phases is used to determine the focal mechanism. Note that stations that are far from the node of the direct P arrival may be near nodal for the surface reflected phases.

The 1971 Earthquake

Figure 2.2 shows the first motion data obtained from short- and long-period vertical seismograms of most WWSSN stations. These data constrain the steeply
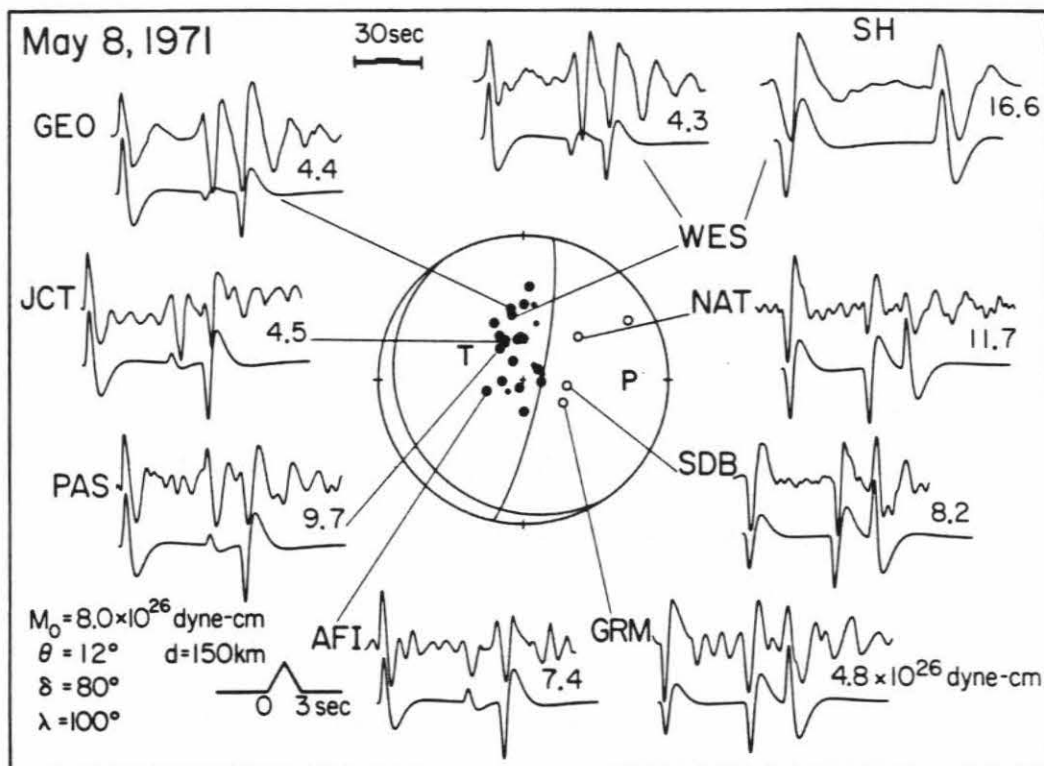
Figure 2.2: Observed P and SH-waveforms for the May 8, 1971 earthquake are shown by the upper traces. P-wave first-motion data from WWSSN stations are plotted on an equal area projection of a lower focal hemisphere. Filled circles are compressions and open circles are dilatations in all figures. The mechanism is reverse type with $\theta=12°$, $\delta=80°$ and $\lambda=100°$. The best fitting synthetics (lower traces) are for a source 150 km deep and 3 seconds long. The amplitude ratio of observed to synthetic seismograms is given for each station. The average seismic moment from P-waves is 8×10^{26} dyne-cm.

dipping fault plane. We modeled long-period P and SH waveforms (upper traces) for Pasadena (T_o=1s, T_g=90s) and WWSSN stations distributed over a large azimuthal range. Note that North American stations (WES, GEO, JCT, PAS) are near nodal for the pP arrival. The fault parameters determined are θ(strike)=12°, δ(dip)=80°, and λ(rake)=100°. Synthetic seismograms constrained the azimuth of the low-angle plane to within 10°. The source time function is 3 seconds long and the depth is 150 km. The seismic moment determined for each station is given in Figure 2.2. The average seismic moment obtained from P waves alone is 8.0×10^{26}dyne–cm (M_w=7.2).

The 1949 Event

This earthquake is the largest (M_S=7.3) analyzed in this chapter (Table 2.1). It caused the death of 57 persons and injury to 150. The damage was centered in the towns of Traiguen and Angol, 560 km south of Santiago, Chile (Seismological Notes, 1949). Nishenko (1985) included this event in a study to estimate the seismic potential of large interplate earthquakes in the Mocha Island region in southern Chile (reg. 3A). However, as is shown below, the mechanism and the depth of this event indicate that it is not an interplate event. First-motion data reported by teleseismic stations in the ISC Bulletin indicate that the tension axis is parallel to the slab dip (Figure 2.3). P waveforms were digitized from Benioff vertical long-period seismograms at PAS (1-90) and TUC (1-77) . The horizontal instruments at Tucson are Wood-Anderson (T_o=8s) and those at Pasadena are long-period Benioff (1-90). The upper traces in Figure 2.3 show P and rotated SH waveforms at these two stations. The P and SH synthetics (lower traces) constrained the source depth to be 63 km with a
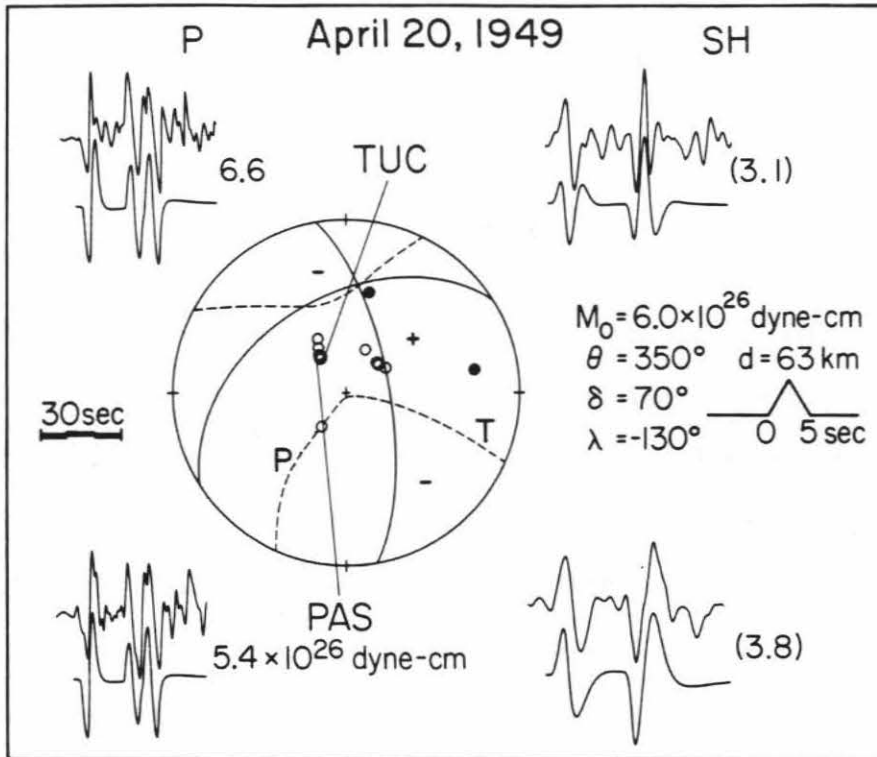
Figure 2.3: Reported first motion data for the April 20, 1949 earthquake from the ISC bulletin are shown on an equal area projection of the lower focal hemisphere where the dashed line is the SH-wave radiation node, + indicates clockwise rotation around the source when seen from above. P and T are the pressure and tension axes respectively. The upper traces are P and SH waveforms recorded at Pasadena and Tucson. The lower traces are synthetic seismograms for a steeply dipping normal fault: $\theta=350°$, $\delta=70°$ and $\lambda=-130°$. The source time function is 5 seconds long and the focal depth is 63 km. The amplitude ratio of observed to synthetic seismograms is given for each station. The seismic moment from P waves alone is 6.0×10^{26} dyne-cm.

simple 5 seconds long source time function. The fault parameters determined using P and S waveform-data are $\theta=350°$, $\delta=70°$, and $\lambda=-130°$. The focal mechanism in Figure 2.3 shows the radiation nodes for both P-waves (continuous line) and SH-waves (dashed line). The average seismic moment obtained from the ratio of observed to synthetic P-waves is 6.0×10^{26}dyne-cm.

The 1934 Earthquake

On March 1, 1934, the cities of Valdivia and Concepcion, 300 km apart along the Chile coast, were severely shaken by an earthquake (Table 2.1), which caused some structural damage in Valdivia (Seismological Notes, 1934). For the 1934 earthquake the ISC Bulletin reports P-wave first-motion data only for the stations in La Plata (LPA-up), Pasadena (PAS-down), Vienna (VIE-up) and Manila (MAN-down). Fortunately, we could retrieve vertical and horizontal records of various Pasadena instruments from the Caltech seismogram library and also recordings of horizontal 8s Wood-Anderson seismographs at Tucson (TUC) and Wenner-horizontal records ($T_o=T_g=10s$) at San Juan, Puerto Rico (SJP), from historic seismograms filmed by the U.S. Geological Survey. Figure 2.4 shows the P waveform recorded at PAS on a Benioff seismograph with $T_o=1s$ and $T_g=12.5s$, and S waves recorded at TUC and SJP by the instruments mentioned above. In spite of the complexity displayed by the P and S waveforms, depth phases can be identified; the expected arrival times of the depth phases shown in Figure 2.4 are computed for a depth of 120 km, based on reported pP-P times from 9 stations listed in Gutenberg's notepads (Goodstein et al., 1980). This depth is consistent with the sS-S times listed in the ISC Bulletin and is considered a good estimate. Although these data are too incomplete to determine the
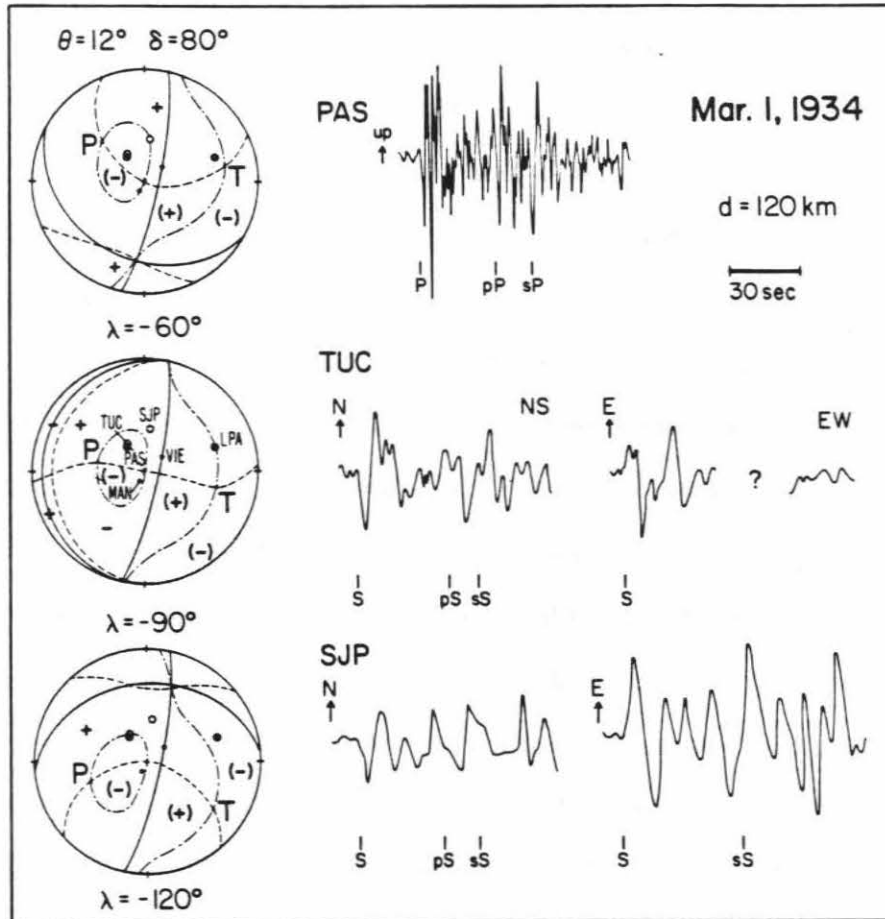
Figure 2.4: Seismograms of the March 1, 1934 earthquake. The P-wave, recorded at Pasadena (PAS) on a vertical seismograph with $T_o=1s$, $T_g=12.5s$ may indicate source complexity. S-waves are recorded at Tucson (TUC) on Wood-Anderson 8 s seismographs and at San Juan, Puerto Rico (SJP), on 10 s Wenner horizontal instruments. The focal mechanisms are for a steeply dipping normal fault ($\theta=12°$, $\delta=80°$) with three different slip angles (λ). The continuous lines are the P-wave nodal planes. First-motion data are from the ISC bulletin. The short-dash lines indicate the SH radiation nodes, where (+) indicates clockwise rotation around the source, viewed from above. The long dash-point lines show the SV radiation nodes, (+) and (-) are directions away and toward the source, respectively. The pressure (P) and tension (T) axes are indicated. The data are consistent with the top focal mechanism.

mechanism, we found a mechanism that is consistent with them in the following manner.

At PAS, P-wave first-motions are down, east and south. S waves are up, east and south, but are emergent and unclear. At TUC, first motion P data are east and south, and those of S waves are clearly east and south. Unfortunately, a portion of the E-W component after the direct S wave is missing and it is not possible to time the sS phase. Nevertheless, we could still determine the S-wave polarization. The peak amplitude of the direct S wave on the EW is similar to that on the NS component. Since, at TUC, the EW and NS components represent approximately SH and SV motions, respectively, we judge the amplitude of the SV component to be comparable to that of SH. We judged the P-wave first motion at TUC to be down, since the horizontal motions are similar to those recorded at PAS. The P-wave first motions at SJP are small and cannot be read, but the S-wave first motions are clearly east and south. The peak amplitude of the E-W component (SH) is twice as large as that of the N-S component (SV). From the SH to SV ratio between TUC and SJP, we consider that SJP is closer to an SV nodal plane than TUC. Note that S-wave polarizations at these three stations are similar. The motion for SH is (+) clockwise rotation around the source and, for SV, it is (-) toward the source. We prefer a steeply dipping ($\delta=80°$) normal fault, with a strike subparallel to the subduction zone ($\theta=12°$). This mechanism is consistent with the available P-wave first motions and with focal mechanism solutions of most recent large South American intermediate-depth earthquakes (Figure 3.5). With this plane fixed, a slip angle $\lambda=-60°$ is consistent with the observed polarization pattern of S waves (Figure 2.4).

2.4 Interpretation

As shown in the previous section, fault plane solutions of the 1949 and 1934 intermediate-depth earthquakes that occurred before the 1960 Chilean earthquake are consistent with steeply dipping normal faults and suggest down-dip tensional stress. Similar steeply dipping normal-fault solutions have been published for two large intermediate-depth events (March 28, 1965, and November 7, 1981) down-dip of the rupture areas of the 1971 (M_w=7.8) and the 1985 (M_w=8.0) Valparaiso earthquakes, respectively (Figure 2.1). Fault parameters for the March 1965 event (M_w=7.4, d=72 km) are θ=350° , δ=80° and λ=–100° (Malgrange et al., 1981) and those for the November 1981 event are θ=345° , δ=86° and λ=–93° (Dziewonski and Woodhouse, 1983). Thus, large intermediate-depth events that occurred before great underthrust earthquakes in southern Chile are down-dip tensional. In the outer-rise region, the focal mechanism of the October 16, 1981 (M_S=7.2) earthquake (θ=0° , δ=45° , λ=90° ; Christensen and Ruff, 1983), that occurred before the 1985 Valparaiso earthquake, shows horizontal compression perpendicular to the trench axis. On the other hand, outer-rise events that occurred after the 1960 Chile earthquake on August 5, 1964 (m_b=6.1) and October 3, 1965 (m_b=6.0), indicate horizontal tension perpendicular to the trench axis (Figure 2.1). The focal mechanisms of the 1964 and 1965 events are θ=181°, δ=68°, λ=–56° and θ=10°, δ=70°, λ=–106° , respectively (Stauder, 1973). If the 1940 event was in fact an outer-rise event, its relation to the 1960 Chilean earthquake is similar to that of the 1981 outer-rise event (horizontal compression) to the 1985 Valparaiso earthquake. The top diagram in Figure 2.5 illustrates the state of stress before a large interplate earthquake described above. The

Stress before and after a large thrust earthquake
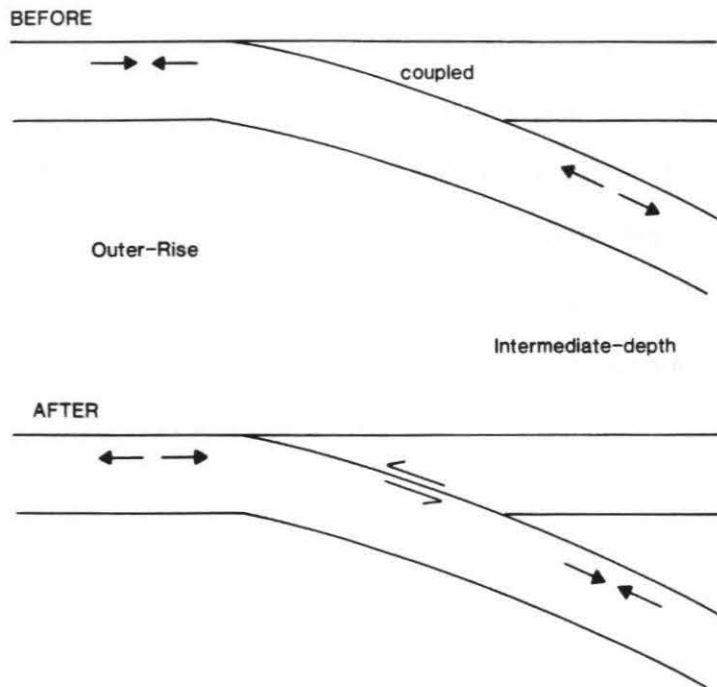
Figure 2.5 A schematic diagram showing the intraplate stress before and after a large thrust earthquake for strongly coupled seismic zones such as the Chile subduction zone.

bottom diagram in Figure 2.5 illustrates our interpretation of the large down-dip compressional event in May 1971. The large interplate displacement associated with the 1960 great Chilean earthquake changed the stress in the downgoing slab to down-dip compression and the 1971 event occurred in response to it. It is known that, after large interplate earthquakes, tensional outer-rise events frequently occur (Sykes, 1971; Stauder, 1973). These observations taken together support the notion that the stress propagation in the slab is rather fast; in our case, it is of the order of 10 km/yr.

The observations above indicate that the interplate boundary is strongly coupled before a major thrust earthquake and the downgoing slab is under tension at intermediate depths; after the interplate event, the displacement at the boundary induces compressional stress in the down-going slab at intermediate depth and causes down-dip compression events. Outer-rise events, on the other hand, experience the opposite phenomenon; shallow, compressional events occur before major underthrusting earthquakes, whereas tensional events occur after them (Figure 2.5). These results suggest that the spatial and temporal variations of focal mechanisms of outer-rise and intermediate-depth earthquakes may be used to infer the strength of interplate coupling.

Chapter 3

Variation of Focal Mechanisms of Intermediate-depth Events

3.1 Introduction

The spatial distribution of focal mechanisms of large intermediate-depth earthquakes in relation to the strength of interplate coupling at subduction zones, studied in Chapter 1, indicates that:

1) Intermediate-depth events that occur down-dip of strongly coupled subduction zones reflect the degree of coupling by producing normal-faulting (down-dip tensional) events at the lower edge of the coupled zone. In general, the continuous seismic zone in these regions is relatively short, less than 300 km.

2) In contrast, subduction zones that are uncoupled produce large normal faulting events at shallower depth near the trench axes, where stresses due to bending of the lithosphere are largest. In these regions seismic zones are larger than 500 km depth.

3) Subduction zones for which weak or moderate coupling at the interplate boundary is inferred, exhibit thrust-type faulting earthquakes at intermediate depth (with near vertical tension axes), probably in response to the negative buoyancy of the subducted slab. These regions have relatively long and steeply dipping seismic zones. However, they may produce double seismic zones in response to other factors such as unbending of the subducted lithosphere (Kawakatsu, 1986a) or the slab's pull (Spence, 1987).

Recently Yamaoka et al. (1986) studied scaled physical models of the downgoing plate in each subduction zone. They showed that the shape of the descending lithosphere, as inferred from the observed intraplate seismicity in most regions, could be explained by modeling the lithosphere by bending an inextensible spherical shell, which shows little deformation under moderate stress. Regions with a poor fit improved greatly by tearing the spherical shell in the region where the lowest seismicity was observed. Their experiments suggest that lateral constraint and bending of the subducted lithosphere are important factors in determining the shape and the strain concentration in local regions. Similarly, numerical models of the downgoing plate calculated by Burbach and Frohlich (1986) suggest that the subducting lithosphere is remarkably cohesive, only rarely breaking or stretching. These studies imply that downdip stresses are dominant for most subduction zones with the exception of the Tonga trench, where down-dip compressional stresses are observed (e.g., Isacks and Molnar, 1969, Giardini and Woodhouse, 1984).

Figure 3.1a shows the static stress distribution near the interplate boundary for the intermediate-depth and outer-rise regions. At intermediate depth the upper seismic zone is in-plate compression stress, whereas the lower seismic zone is in tension (Hasegawa et al., 1979). Note that the stresses due to bending of the lithosphere in the outer-rise region are tensional at shallow depths and compressional at larger depth (Stauder, 1968; Chapple and Forsyth, 1979; Christensen and Ruff, 1987). This simple two-dimensional model does not consider either lateral changes in the subduction zone such as bends in the trench axes, contortion or segmentation of the subducted lithosphere, or subduction of topographic irregularites (e.g., ridges or oceanic platforms), which can presumably change the strength or orientation of the stress
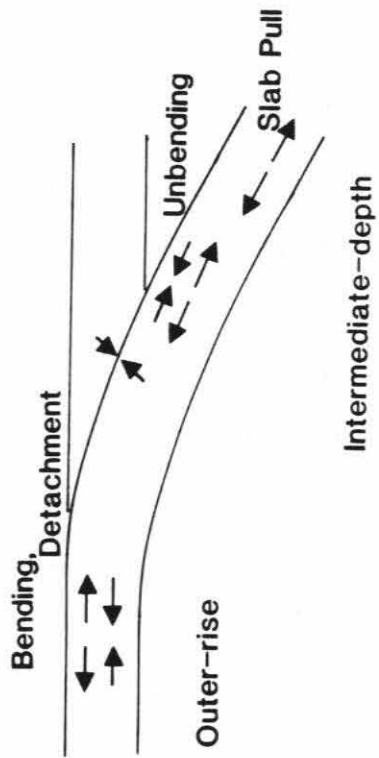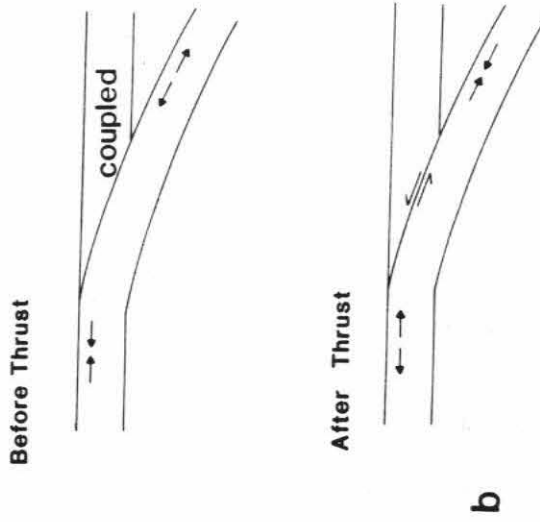
Figure 3.1: a) The diagram to the left shows a two-dimensional model of the stress distribution within the downgoing lithosphere resulting from bending, unbending and the slab's pull in the outer-rise and intermediate-depth region. b) The figures to the right display the dynamic stress model that is observed at strongly coupled regions near the interplate boundary. The change in the observed stress distribution is related to displacement of the interplate boundary after a large thrust event.

field in a region (Burbach and Frohlich, 1986).

Figure 3.1b shows a dynamic model for strongly coupled regions in which, before a major underthrusting earthquake, the interplate boundary is strongly coupled, the down-dip slab is under tension at intermediate depths, and the outer-rise region is under compression. After displacement at the interplate boundary the outer-rise region is under tension, whereas the down-dip slab may be either under compression or with diminished tensional stresses. Observations that support this model are, for example, the temporal variation of focal mechanisms at intermediate depths in southern Chile with respect to the occurrence of the 1960 Chile (M_w=9.5) earthquake (Chapter 2) and the temporal variations of focal mechanisms in the outer-rise region at strongly coupled zones documented by Christensen and Ruff (1987). However, at uncoupled or moderately coupled zones they observed only tensional outer-rise events.

In Chapter 3 we examine the focal mechanisms of moderate and large intermediate-depth earthquakes that occurred from 1960 to 1984 in relation to local variations of the strength of interplate coupling in a region. Temporal changes of focal mechanisms of intermediate-depth events due to large thrust events are also explored. We use Table 1.3 and Table A.2 to study these spatial and temporal variations for different regions. Table 1.3 includes focal mechanisms of all the earthquakes with depth between 40 and 200 km listed by the NOAA and ISC catalogs with $m_b \geq 6.0$, a total of 335 events (see Section 1.3). Table A.2 gives all large (M_S=7.5) shallow events that occurred during this century by region.

3.2   Stress-axis Distribution of Intermediate-depth Earthquakes

In principle, we can obtain the general intraplate stress field orientation of a region by plotting the P and T axis of focal mechanisms of events in that region in a focal sphere together with the downgoing plate orientation at the corresponding depth. This approach has been used by several investigators, for example, Oike, 1971, Fujita and Kanamori, 1981, Vassiliou et al., 1984, Burbach and Frohlich, 1986. Since our data base has been expanded from previous studies we use this same method not only to determine the general characteristics of the stress field in each region but also to help us descriminate "anomalous events."

Figure 3.2 shows equal area lower hemisphere projections of the distribution of compression (P - closed symbols) and tension (T - open symbols) axis for different subduction zones. Circles are used for events located between 40 and 100 km depth and diamonds for deeper events, 100 to 200 km deep. Region names are defined in Figure 1.2 and open arrows indicate the convergence direction of the plates in each region (Table 1.1). The curve indicates the trench azimuth and dip. The dip angle shown in Figure 3.2 is that of the seismic zone at about 100 km depth. Note that an abrupt increase of the seismicity dip angle from 20 to 50° is observed at 40 km depth which is associated with a density increase related to the phase transformation of the oceanic lithosphere from basalt to eclogite (Ruff and Kanamori, 1983). Thus the underthrusting and overriding plates are most certainly uncoupled, and earthquakes that occur below 40 km depth are intraplate events. Seismicity profiles (e.g., Isacks and Barazangi, 1977) show that the dip of the seismic zone increases gently to about 100 km, remaining approximately constant thereafter. We define in-plate tension or
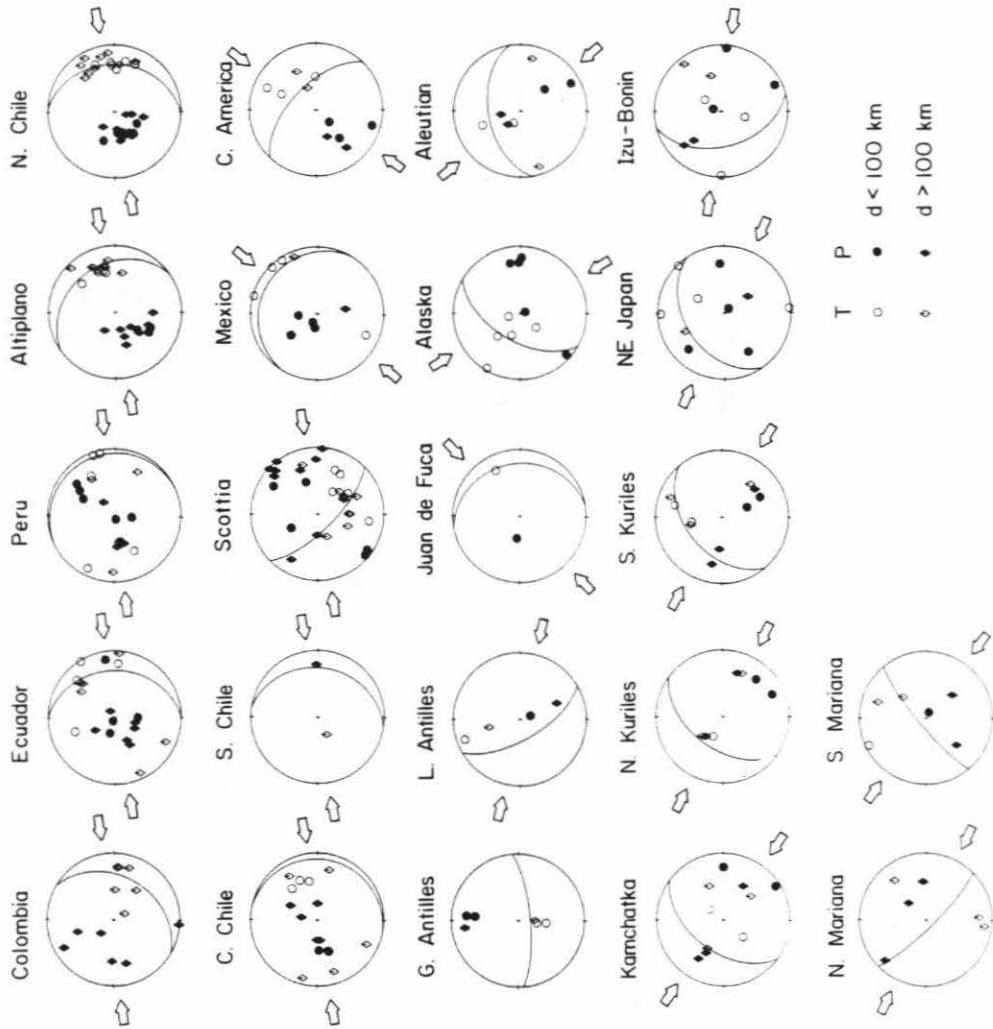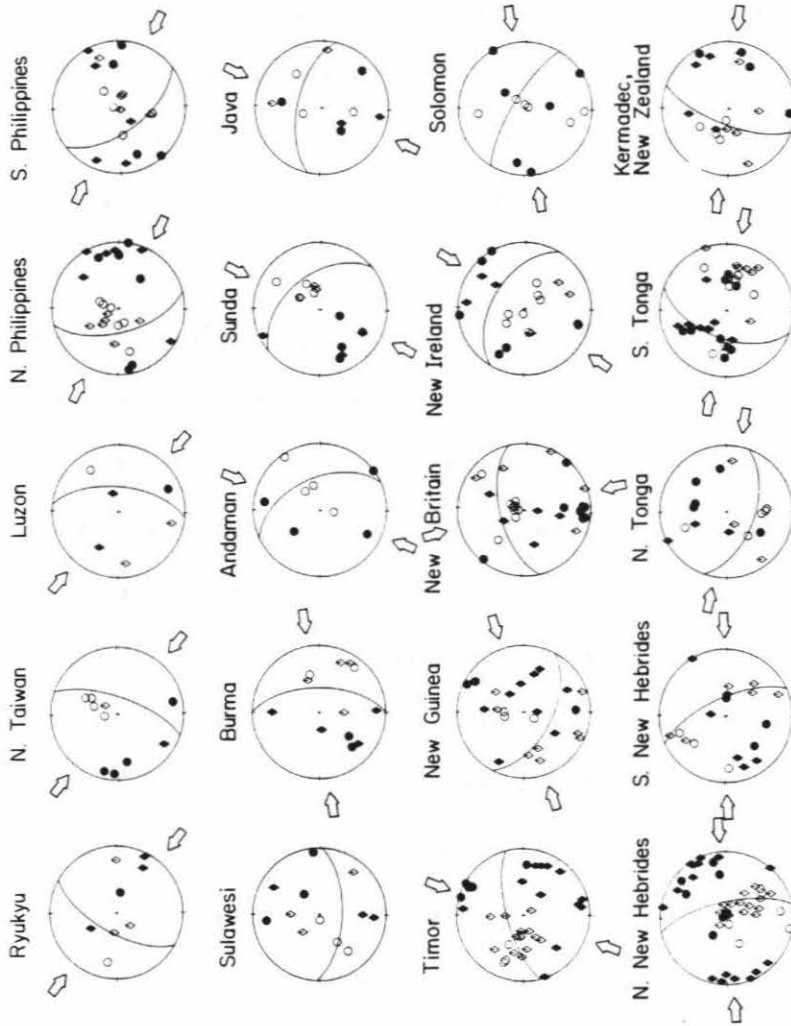
Figure 3.2: Equal area lower hemisphere projection showing P(filled symbols) and T (open symbols) for events in the regions listed in Table 1.3. The curve indicates the trench azimuth and the dip of the seismic zone at intermediate-depth. Open arrows show the direction of convergence across plate boundaries for each region. Diamonds are symbols for events deeper than 100 km and circles for shallower events.

compressional events if the respective stress axes are located within 20° of the down-dip slab location. This method ignores earthquake magnitudes that bias the interpretation of the stress distribution within the downgoing slab; larger events used here reflect the first-order stress distribution in a region, whereas smaller events reflect only secondary or local effects. We will try to overcome this difficulty in the next section by discussing particular events in more detail. Inspection of Figure 3.2 indicates that most regions have either dominant down-dip tensional stresses or a mixed pattern of down-dip tensional and compressional stresses at intermediate depth. Only Tonga has dominant down-dip compressional stresses. Description of Figure 3.2 follows.

Most intermediate-depth events that occur in South America regions (from Colombia to Central Chile) have near in-plate tensional axes. Note also that the tension axis of all events in the Altiplano and North Chile regions are especially well aligned with the subducted plate and the convergence direction. These results agree with those of previous investigators (e.g., Stauder, 1973, 1975). The South Chile region has only one down-dip compression event that occurred on May 8, 1971, and has already been discussed in detail in Chapter 2. A large number of events in the Scotia region have nearly down-dip tensional axis. This result is consistent with the model of weak coupling at the interplate boundary in which near vertical tensional stress is induced as a result of the negative buoyancy of the slab.

The Mexico and Central America regions have mostly shallow-dipping tensional axis in agreement with the observed seismicity dip angle. In the Caribbean region only a few intermediate-depth events have occurred from 1960 to 1984. The Greater Antilles events have nearly vertical tension axis consistent with the weakly coupled

model described earlier. In contrast, the tension and compression axes of events in the Lesser Antilles are aligned with the trench axes. These events are discussed in more detail in the following section.

The 1965 Puget Sound event that occurred in the Juan de Fuca region has down-dip tensional stress axis. The dip angle in this region is shallow, (22°) consistent with a strongly coupled interplate boundary as discussed in Chapter 1. The North Pacific regions are also considered strongly coupled regions and had only a few events at intermediate depth. Alaska has mostly down-dip tensional events, but events that occur in the Aleutians and Kamchatka regions have their stress axis distributed all over the focal sphere.

The Kurile subduction zone is divided into two sections according to differences in the dip and extent of seismicity (see Table 1.1). The stress axis distribution is mixed in both Kurile and the Northeast Japan regions. These two regions have been very active. However, only a few events have occurred within the oldest (>150 m. y.) subducting oceanic lithosphere in the Izu-Bonin and Mariana regions. The deeper events in the Izu-Bonin region have in-plate compression axis; however, the events with depth less than 100 km are mixed. The Mariana region was divided into a northern and southern segments to account for the abrupt change in the trench axis.

Events in the Ryukyu region have a mixed stress axis pattern, but it is aligned with the direction of convergence of the Eurasia and Philippine plates. The North Taiwan region events have mostly down-dip tensional axes which are nearly vertical. Thus, this region is consistent with a rather weakly coupled interplate boundary. In the Luzon subduction plate only 3 events occurred, but the stress axes are distributed randomly that may be reflecting the complexity of this area. The Philippine

subduction zone is among the more active seismic regions at intermediate depth (see Appendix 1). Most events in the northern section show almost vertical tension axes that align with the steeply dipping seismic zone. In the southern segment, however, the tension axes of the events are mostly vertical but are not aligned with the subducted plate.

The Sulawesi region is a complex region and the distribution of the stress axes of intermediate-depth events is sparse. In the Burma subduction zone continental collision is occurring; however, at intermediate depth events may be located within the attached oceanic lithosphere. Tension and compression axes are separated in the diagram but are not easily related to either the seismic zone or the convergence direction in the region. Events that occurred in the Andaman region are all shallower than 100 km, depth but the stress axis distribution is mixed. Most of the events in the Sunda trench have down-dip tensional axes, which are nearly vertical. This observation is consistent with a weakly coupled interplate boundary as described before. The stress axes of intermediate-depth events in the Java region are mixed. In the Timor subduction region; most earthquakes have nearly down-dip tensional axes that are aligned in the direction perpendicular to the convergence direction of the subducting and overriding plates.

The New Guinea region has mixed stress axes. Most events shallower than 100 km that occur in the New Britain region have near vertical tension axes; however, the tension axes of events with depths between 100 and 200 km are nearly horizontal. This pattern certainly reflects the complexity of this region. The New Ireland region is small and very active (see Appendix 1), which may be related to high stress level due to lateral bending of the Solomon plate under this area. The stress axis

distribution of the New Ireland region is mixed. Intermediate-depth events ($M \geq 6$) in the Solomon subduction zone are shallower than 100 km and exhibit a mixed distribution of the stress axis.

The New Hebrides region is the most active area at intermediate depth (see Appendix 1). The trench azimuth changes from the North to the South and events have been divided accordingly. Most events in the northern segment have nearly horizontal compressional axes; the tensional axes of the events located below 100 km depth (open diamonds) are aligned with the plate. The stress axis distribution in the southern New Hebrides segment is mixed.

The Tonga subduction zone is also very active at intermediate depths. The area is divided into two regions that separate the events which occurred near the northern bend from those in the more linear section of the trench. Most of the southern events have down-dip compressional axes with the exception of a few shallower events, which are discussed in detail below. The Kermadec-New Zealand diagram shows a mixed distribution of the stress axis.

3.3 Regional Reexamination of Intermediate-depth Events

Although the regional stress field of intermediate depth events inferred from the focal mechanism catalog in Table 1.3 shows that a large number of events have down-dip or nearly vertical tension axes, as discussed above (Figure 3.2), many regions show a mixed or complex distribution of the tension and compression axes. Figure 3.3 shows the location of intermediate-depth earthquakes with $M \geq 6.0$, which
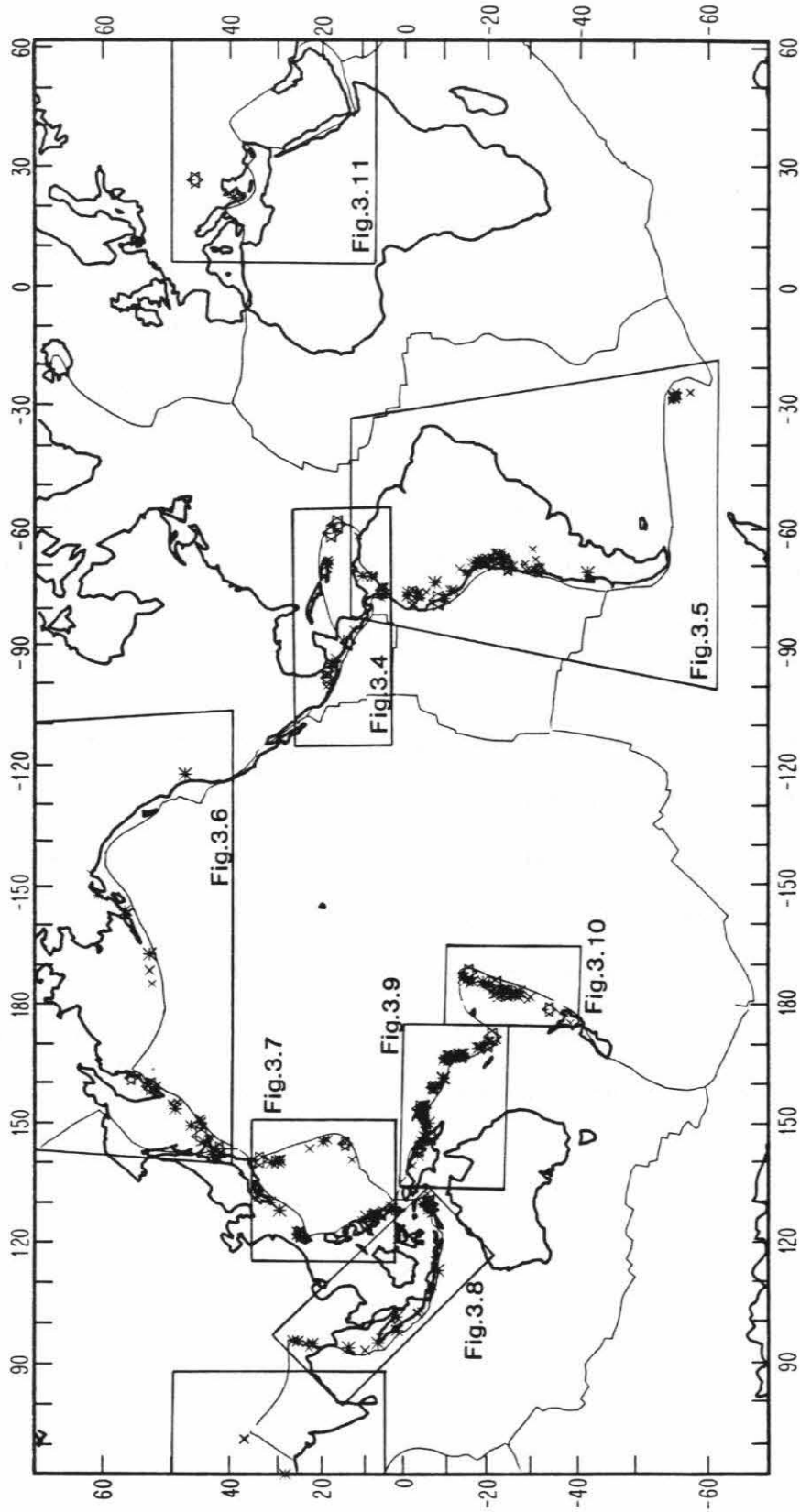
Figure 3.3: Location of intermediate-depth earthquakes (40-200 km) with $M \geq 6.0$ that occurred from 1960 to 1984. Boxes enclose the regions shown in Figure 3.4 to 3.11.

occurred from 1960 to 1984. Boxes enclose the regions shown in Figures 3.4 to 3.11. On the regional maps the plate names, bathymetric features and relative motion between adjacent plates are indicated. Holocene volcanoes are shown as open triangles and close triangles represent active volcanoes in the last 1000 years (Moore, 1982). The fault parameters of the events shown in each regional figure and the event number, next to the lower hemisphere projection of the focal sphere, are given in Table 1.3. Dark quadrants are compressional and numbers within parenthesis indicate the event depth.

In the region by region discussion that follows we describe the characteristics of the downgoing plate as well as those of the interplate boundary for each region. Then we examine individual events or groups of nearby events relative to their location to local physical changes in the subduction, for example, bends or tear of the downgoing plate or subduction of topographic highs. Detailed seismicity profiles and modeling by Yamaoka et al. (1986) and Burbach and Frohlich (1986) for each subduction zone can help us locate the regions where the plate is bending or tearing. Then we explore the relative location, both in space and time, of intermediate-depth events that may be related to the occurrence of large thrust events at the interplate boundary. Large ($m_B \geq 7$) intermediate-depth events that occurred during this century for each region are given in Table A.1 and shallow events with $M \geq 7.5$ are listed in Table A.2, also by region.

Middle-America

North of the Tehuantepec Ridge the Rivera and Cocos plate subduct with a shallow dip (10 to 20°) beneath the North America plate. The seismicity depth

increases eastward to about 150 km. The chain of active volcanoes forms an angle with the trench and is located farther in land than most subduction zones. Large shallow underthrusting earthquakes with rupture lengths of approximately 100 km and short recurrence intervals, 30 to 80 years (Singh et al., 1981) are characteristic of the Mexican subduction zone, suggesting strong-to-moderate coupling along this inter-plate boundary (Figure 3.4). Three large intermediate-depth events occurred from 1960 to 1984 down-dip of future large subduction events. The 1964 event (No. 39) occurred down-dip of the 1979 Petatlán earthquake aftershock area. Similarly, the 1980 Huajuapan event (248) occurred down-dip of the 1982 Ometepec doublet, and the 1973 Orizaba earthquake (178) was located down-dip of the 1978 Oaxaca aft-ershock zone. Although these events are consistent with the dynamic model for strongly or moderately coupled regions explained before (see Section 3.1), no large compressive intraplate events have occurred after these large subduction earthquakes. This suggests that the displacement at the interplate boundary may not be large enough to change the stress characteristics at depth or that this down-dip intraplate compressional events may be small or difficult to identify. González-Ruiz (1986) documented the occurrence of normal faulting events down-dip of the Ometepec region within a few years before four consecutive thrusting episodes. He suggests that the occurrence of normal faulting events at intermediate depth may be an integral part of the earthquake cycle in the Ometepec region. However, the 1931 normal fault event studied by Singh et al. (1985) was located at 45 km depth and down-dip of the region broken in 1928 by four large shallow thrust events offshore Oaxaca (Table A.2). They suggest that this event may have broken the lithosphere, decoupling the Cocos plate from the overriding continental plate. Events 228 and 286 may be

Figure 3.4: Location and focal mechanisms for events with M≥6.0 that occurred in the Middle America subduction zone and in the Greater and Lesser Antilles in the Caribbean during the period of 1960 to 1984. Numbers refer to events in Table 1.3 and those in parentheses indicate event depth in km. Plate names, bathymetric highs and trench names are indicated in the figure. Open triangles are locations of Holocene volcanoes and close triangles are recent active volcanoes (Moore, 1982). Open arrows are convergence rates (Table 1.1) and double arrows indicate strike-slip motion across plate boundaries. The focal spheres are lower hemisphere projections, with compressional quadrants darkened. The sizes of the focal mechanisms are proportional to the magnitude of the events.

associated with subduction of the Tehuantepec ridge, where the arc junction is identified by Yamaoka et al. (1986).

South of the Tehuantepec ridge, the Cocos plate subducts beneath the Caribbean plate with a considerably larger dip angle, which varies from 30° down-dip of Guatemala to 65° beneath Nicaragua. The seismicity is about 250 km deep along Central America, but shallows toward the southeast where a shallower dip is also observed. All events in this region are down-dip tensional. However, events 98 and 313 (M≈6) have a reverse focal mechanism that suggest, under the classification of large events (Section 1.4) an uncoupled interplate boundary. McNally and Minster (1981) observed low seismic slip along Central America, indicating either weak coupling or longer recurrence intervals along this plate boundary. The largest intermediate-depth event is the 1982 San Salvador earthquake (event 274), which occurred down-dip of a region where large subduction events last occurred at the turn of the century (Table A.2, Astiz and Kanamori, 1984).

Atlantic Island Arcs

Caribbean

Subduction of the old, oceanic lithosphere beneath the Caribbean along the Lesser Antilles trench is about 2 cm/yr in a westerly direction. However, as the trench curves to an East-West trend, toward the Greater Antilles, the North America and Caribbean plate boundary becomes mostly oblique and convergence reduces to about 0.2 cm/yr (Figure 3.4). Several studies (e.g., Stein et al, 1982, Yamaoka et al., 1986) indicate that the downgoing slab curves continuously beneath the Caribbean plate. McCann and Sykes (1984), on the other hand, suggest tearing of the plate

based on the focal mechanism of the 1974 earthquake (M_S=7.5, event 184); however, this event is also consistent with in-plate tensional stresses caused by the lateral bending of the lithosphere. The 1969 Christmas Day earthquake (M_S=7.5, event 119) location near the trench axis indicates lithospheric faulting in response to the slab pull in a weakly coupled region (McCann and Sykes, 1984) in agreement with the model shown in Figure 1.8. Note also that this event had a relatively large number of aftershocks with respect to other intermediate-depth events (Section 1.5) that defined faulting along the steeply-dipping plane. This event was studied in detail by Stein et al. (1982). Event 106 indicates tear faulting. Several large intraplate earthquakes are located along the Lesser Antilles arc (Table A.1); however, no large subduction events have occurred there during this century (McCann and Sykes, 1984).

In the Greater Antilles region the 120 m.y. old, oceanic plate subducts along the Puerto Rico trench. At intermediate depth the downgoing lithosphere is nearly vertical (Frankel et al., 1984). Moderate intraplate earthquakes in this area (events 147, 232 and 260) are down-dip tensional events consistent with the model for a weakly coupled region. In this model the dip of the slab is steep and the slab's weight induces tensional stresses at intermediate depth. Frankel (1982) reports that smaller magnitude events in this region are also down-dip tensional.

Scotia Arc

Tectonic studies of the Scotia arc region indicate that back-arc spreading is present (Barker, 1970, 1972) and that the 70 m.y. old, oceanic lithosphere of the South America plate gets younger to the south as it subducts beneath the recently formed (< 10 m.y.) Sandwich plate oceanic floor (Frankel and McCann, 1979). The southern portion of the plate is less active and the focal mechanisms of event 193
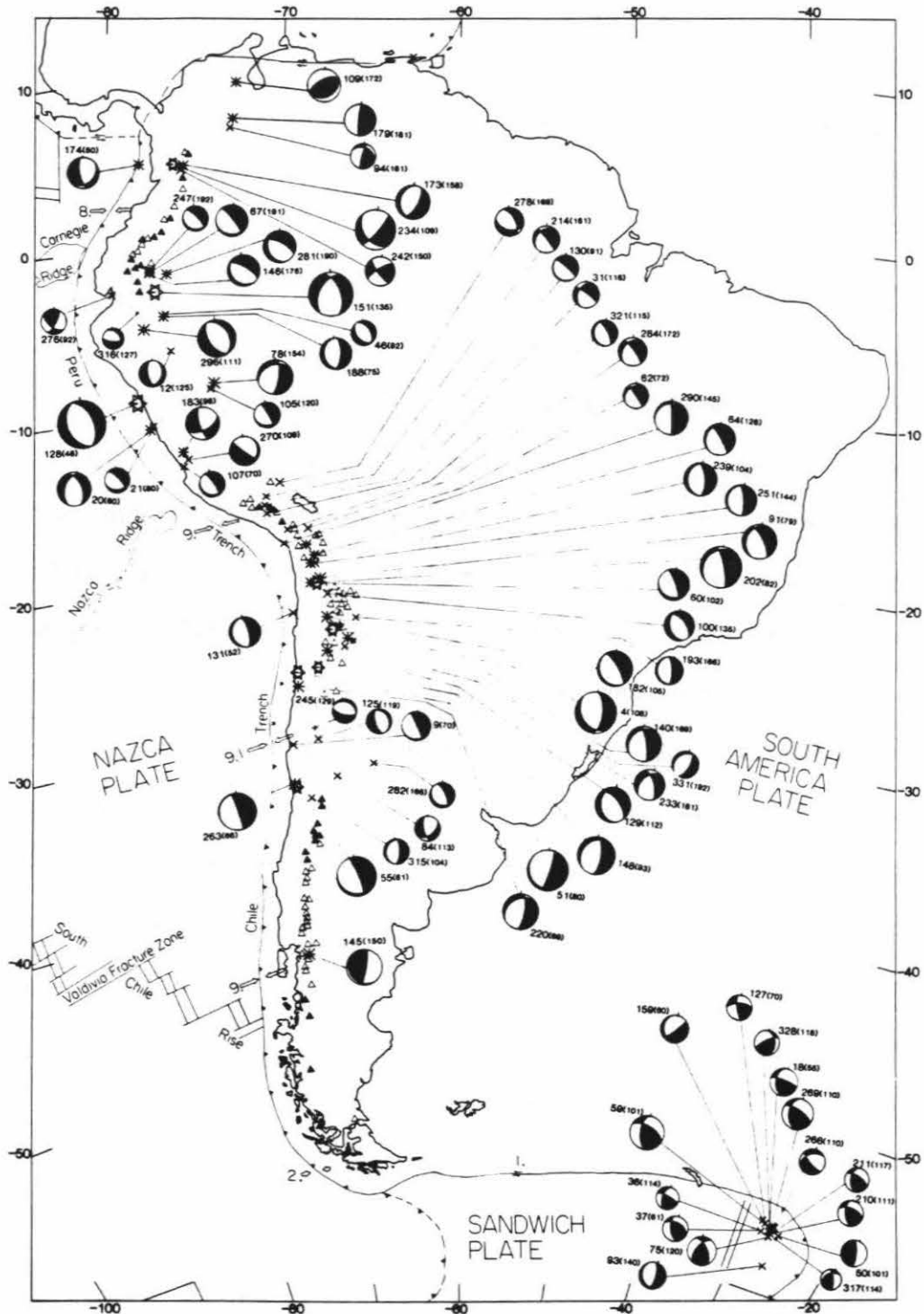
Figure 3.5: Epicenters and focal mechanisms of intermediate-depth earthquakes with M≥6.0 that occurred from 1960 to 1984 (Table 1.3) in South America and the Scotia arc. For symbols, see Figure 3.4.

indicate down-dip compression; however, in the northern segment most events are down-dip tensional (see Figure 3.2). The change from mainly down-dip tensional to down-dip compressive stresses along the Scotia arc is also observed for focal mechanisms of smaller magnitude events by Forsyth (1975), who explains this change as caused by the reduced negative buoyancy forces in the younger, southern half of the subducted plate. Evidence of tearing of the downgoing plate in the northern segment is given by earthquake focal mechanisms (Forsyth, 1975) and a seismicity gap observed at intermediate depth (Yamaoka et al., 1986). Events 159 and 328 indicate tear faulting. Events 266 and 269, which occurred within 3 months of each other, have very different focal mechanisms and may be indicative of internal deformation of the subducting plate. Several large intraplate events have occurred in the Scotia arc in this century (Table A.1). The most recent event on May 26, 1964 (36) was studied in detail by Abe (1972a), who obtained $M_w=7.8$ (from surface-wave seismic moment of 6.2×10^{27} dyne cm) in contrast with $m_b=5.7$. The 1964 event, which is probably the largest event in this region, is consistent with the model described above for weakly coupled regions. Note also that no large $(M>7.5)$ subduction events have occurred in this region.

South America

The Nazca plate subducts eastward along the curving margin of western South America for about 5000 km. The major topographic features being subducted along this oceanic-continental plate boundary are the Chile rise and the Nazca and Carnegie ridges (Figure 3.5). The characteristics of the downgoing lithosphere vary along the trench, defining several segments (Table 1.1, Figure 1.2) that correlate with the

absence or presence of the volcanic chain according to the shallow or steeper dip of the intermediate-depth seismicity (Barazangi and Isacks, 1976). Although intraplate seismicity is high in South America, inaccurate earthquake hypocenters (due to poor station coverage) allow different interpretations for the configuration of the downgoing Nazca plate. For example, Barazangi and Isacks (1976) and Yamaoka et al. (1986) propose a tear in the subducted lithosphere, where the slab dip changes abruptly from 8° to 28° along the Peru-Altiplano border line (see Figure 1.2). In contrast, Hasegawa and Sacks (1981) suggest that the Nazca plate is contorted rather than torn in this region, based on observations from local seismic data. The observed continuous seismicity is as deep as 300 km for all regions; however, events deeper than 500 km are observed in Colombia, Peru and North Chile regions (Appendix 1), which probably occur within a detached segment of the subducted lithosphere (Isacks and Molnar, 1971, Stauder 1975). Most intermediate-depth events in South America (from Colombia to Central Chile, Figure 3.2) have nearly down-dip tensional axis induced from the lithosphere negative buoyancy or may be in response to continental loading

We divide the following discussion into five sections, corresponding to variations of intermediate-depth seismicity and also to the occurrence of recent large subduction earthquakes along the Nazca-South America interplate boundary.

South Chile

Seismicity in this 1250 km long section is 160 km deep and shallow dipping and is dominated by the 1960 Chile (M_w=9.5) earthquake aftershock area. This region, from 34° to 45°S, is considered the typical example of a strongly coupled subduction zone (Uyeda and Kanamori, 1979), since relatively young, 0 to 35 m.y., oceanic

lithosphere is being subducted at about 9.5 cm/yr (see Figure 2.1). Large intraplate (intermediate-depth and outer-rise) earthquakes that occurred in this region during this century have been discussed in Chapter 2, which helped us construct the dynamic model proposed earlier for strongly coupled regions (Figure 3.1b). We should remark that the down-dip compressional event (145) that occurred on May 8, 1971 is the only earthquake with $M \geq 6$ to have occurred to date in this region at intermediate depth. The remaining 250 km long section to the North was broken by the 1939 ($M_S = 7.8$) and the 1928 ($M_S = 8.0$) earthquakes. From 1960 to 1984 no intermediate-depth earthquakes with $M \geq 6$ occurred there.

Central Chile

This region (29° to 34°S) is characterized by a very shallow dipping slab (10°) at intermediate depth, the absence of active volcanism and large underthrusting events with rupture lengths of about 300 km. The northern half is defined by the aftershock area of the 1906 Valparaiso ($M_S = 8.4$) earthquake, which has partially reruptured, about 75% of its length, in two large subduction events that occurred on July 9, 1971 ($M_S = 7.5$) and March 3, 1985 ($M_S = 7.8$). The southern-most segment has not been broken yet (Korrat and Madariaga, 1986).

Stress axes of intermediate depth events in this region are aligned with the convergence direction (Figure 3.2); however, the tension axes of most events (except events 245, 125 and 84) are dipping at about 30° instead of 10°, as inferred by the intraplate seismicity in the region. Events 125 and 245 ($M \approx 6$) occurred near the northern limit of the 1943 aftershock zone. Their focal mechanisms indicate, respectively, internal deformation of the plate and slab segmentation associated with the larger plate dip (30°) farther north as proposed by Isacks and Barazangi (1977).

Event 84 has nearly a horizontal axis. Event 9 (m_b=6.3) occurred in 1963, down-dip of the 1943 thrust event rupture area, suggesting that by this time the interplate boundary was at least moderately coupled, and normal faulting events could occur at the base of the coupled zone. Further investigation, which is beyond the scope of this study, is required to determine if a change in the stress field orientation at intermediate depth occurred downdip of the 1943 rupture area.

Before the occurrence of the recent 1971 and 1985 Valparaiso earthquakes, two normal faulting events occurred down-dip at intermediate depth in 1965 (event 55) and in 1983 (315), respectively, in agreement with the dynamic model for coupled regions (Figure 3.1b). Malgrange et al. (1981) studied the 1965 and 1971 Aconcagua events in detail. In 1981, a large normal faulting event (263, M_w=7.0) occurred down-dip of the 1971 aftershock zone. Although the occurrence of smaller (M<6) down-dip compressional events cannot be ruled out, the occurrence of the 1981 event (263) suggests that displacement at the intraplate boundary was not large enough to change the stress field orientation at depth. It may be possible that the 1981 normal-faulting event may have helped to trigger the 1985 Valparaiso earthquake farther south at the interplate boundary. Note also that in 1983 a compressional outer-rise event occurred offshore the future 1985 Valparaiso earthquake rupture zone (Christensen and Ruff, 1983). Thus, this region agrees with the dynamic model shown in Figure 3.1b in that an outer-rise compressional event and a down-dip tensional event occurred before the thrust event. However, neither a large tensional outer-rise or a down-dip compressional intermediate-depth event has occurred to date. One possibility is that the displacement at the interplate boundary may not be large enough to change the stress orientation, but to somewhat lower the intraplate

seismicity in the region adjacent to the large thrusting earthquake.

Altiplano and North Chile

The downgoing lithosphere dips at about 30°, bending gently along the coasts of southern Peru and northern Chile. Note also that the volcanic chain reappears (Figure 3.5) and that at least since 1922 no large thrust earthquakes have occurred along the entire length of the interplate boundary (Kelleher, 1974; McCann et al., 1979). These regions have been very active at intermediate depth, not only during the 1960-1980 time period but throughout this century (Appendix 1). All of the events in Figure 3.5, from event 278 at the northern boundary of the Altiplano region to event 220 to the south boundary of the North Chile region, have down-dip tensional axes. The compression axes are normal to the downgoing plate and the majority are nearly vertical, suggesting that continental loading may play an important role in the stress distribution at intermediate, depth since the Andes are much broader in the Altiplano-North Chile region. Note also the azimuthal variation of the tension axis along the gently bending Nazca plate, from about 40°N for event 278 to about 120°N for event 220. The focal mechanisms of intermediate-depth events in this region also agree with the model for a coupled interplate boundary, since normal faulting events occur at the base of the coupled region in response to bending of the subducting lithosphere.

Christensen and Ruff (1987) report two compressional outer-rise events offshore the 1922 aftershock area in 1964 and 1969. The earlier event was followed by a $M_S=7.4$ thrust event that occurred on October 4, 1983. Malgrange and Madariaga (1983) documented the variation of focal mechanisms of moderate intermediate-depth events associated with the large 1966 ($M_w=7.7$) thrust event. A down-dip tensional

event occurred on February 1965, and a down-dip compressional event occurred on June 1967. They interpreted their observations as possible evidence of the presence of a double seismic zone in the region. An alternative interpretation is that this event reflects the coupling at the thrust boundary as shown in Figure 3.1b.

Ecuador - Peru

The Ecuador-Peru region, $0°$ to about $16°S$, is bounded to the north and south by the Carnegie and Nazca ridges. This region, albeit complex, offers a good example of the relationship between the coupled interplate boundary and the intraplate seismic activity. Seismicity along this region dips at about $30°$ at shallow depth; at about 100 km depth it becomes almost horizontal for about 300 km (Barazangi and Isacks, 1976). The shallow dip ($\approx 10°$) of the subducting lithosphere at intermediate depth has been associated with the lack of volcanism (Figure 3.5). Two regions can be defined in terms of the absence or presence of large thrust events at the interplate boundary. The northern segment, which may be referred to as the "Peru Quiet Zone" with no known historic large subduction events, extends from $0°$ to $10°S$ (McCann et al., 1979). The oceanic lithosphere is heterogeneous since the Carnegie ridge subducts from $0°$ to $3°S$, and numerous fractures are present farther south seaward from the trench.

A cluster of events (247, 67, 28 and 146) at the northern edge of the subducting Carnegie ridge indicates tear faulting, almost perpendicular to the trench, that may be associated with subduction of the presumably more buoyant lithosphere as proposed by Barazangi and Isacks (1976). Events 151, 46, 188, 296 and 12 are down-dip tensional, consistent with a strongly coupled interplate. Christensen and Ruff (1987) report outer-rise compressional events in this region. Event 316 ($M \approx 6$) may be

associated with internal deformation of the Nazca plate, resulting from the presence of the Carnegie ridge to the north. The compression axes of event 276 are almost horizontal, suggesting that high compressive stresses induced by the subducting ridge may be dominant to about 100 km depth. However, this event could be explained as a result of bending of the downgoing slab as it flattens at intermediate depth (see Figure 8 in Isacks and Barazangi, 1977).

The southern segment, from 10° to about 16°S, is characterized by large thrust events with rupture lengths of about 150 km. The most recent sequence occurred from south to north in 1942, 1974, 1940 and 1966 (e.g., McCann et al., 1979). Along the southern boundary of this region several studies have proposed a major tear of the subducting lithosphere (Isacks and Barazangi, 1977, Yamaoka et al., 1986) to accommodate the sharp increase in the dip angle of the downgoing plate farther south. Note that from 1960 to 1984 no large tearing events occurred in this region at intermediate depth, which favors Hasegawa and Sacks' (1981) interpretation of slab contorsion in this region. No large events ($M \geq 6$) have occurred, either, in this same time period down-dip of the 1940 and 1942 aftershock zones.

The region adjacent to, and down-dip of, the October 1974 (M_w=8.1) event presents an interesting sequence of large intraplate events. Before the thrust event, in 1968 (event 107) a down-dip tensional event occurred. In January 1974 a large event (183, m_b=6.6) occurred at the northern edge of the future 1974 thrust rupture zone, suggesting lateral loading of the interplate boundary. In 1982 (event 270), a down-dip compressional event occurred. These observations agree with the dynamic model shown in Figure 3.1b. However, no large outer-rise events occurred either before or after the large 1974 thrust earthquake (Christensen and Ruff, 1987). Down-dip of the

1966 (M_w=8.1 earthquake aftershock area two down-dip tensional events occurred in 1963 (events 20 and 21).

The largest intraplate earthquake in this region occurred on May 31, 1970 (event 128, M_w=7.8), and has been studied by several investigators (Abe, 1972b, Stauder, 1975). This event is unusual in many ways. For instance, it is located between the "quiet" and "active" Peru regions at shallow depth, also a large number of aftershocks (see Figure 1.10) followed it, defining a steeply dipping plane that almost broke the entire subducting lithosphere (Abe, 1972b). Christensen and Ruff (1987) report that near the northern edge of the 1966 thrust event an outer-rise compressional event occurred on September 1967. Note also that two normal-faulting events (78 and 105) occurred prior to the large 1970 shallower normal-fault earthquake at intermediate depth. The existence of these events before the occurrence of the 1970 (M_w=7.8) earthquake reflects the presence of a strongly coupled interplate boundary, but they may have helped to trigger this large intraplate event as suggested by Christensen and Ruff (1987). Abe (1972b) suggests that this event occurred in response to the gravitational pull exerted by the denser sinking slab.

Colombia

The strongly coupled interplate boundary north of the Carnegie ridge, from 5°N to 0°, has very young oceanic lithosphere that subducts along the shallow Colombia trench at about 8 cm/yr. The seismicity dip is gentle at shallow depth and increases to 35° at intermediate depth. The volcanic chain parallels the coast with numerous active volcanoes (Figure 3.5). The entire length of the earlier 1906 Colombia (M_S=8.7) earthquake has been reruptured by the recent thrust events, which occurred, from South to North, in 1942, 1958 and 1979 (Kanamori and McNally,

1982, Beck and Ruff, 1984).

Events 109, 179 and 94 which occurred in northern Colombia where the trench is not well defined, are consistent with down-dip tensional stresses that are probably induced by the negative buoyancy of the sinking slab. No large ($M \geq 6$) intermediate-depth events occurred between 1960 and 1984 down-dip of the 1942 and 1958 aftershock zones. However, near the northern edge of the 1979 aftershock zone several events occurred. The shallower event 174 that occurred in 1973 may be located near the inferred trench axis; however, the 50 km depth of this event indicates that it occurred at the base of the coupled interplate boundary. Down-dip of the future December 1979 ($M_w = 8.2$) thrust event, two normal-fault events (173 and 234) occurred at intermediate depth. Event 234 occurred on November 1979 ($m_b = 7.2$), a few weeks before the large thrust event. Although event 242 that occurred after the 1979 event is down-dip tensional the focal mechanism, which is a strike-slip, is different from events occurred previously. An outer-rise tensional event was observed on January 1981 (Christensen and Ruff, 1987), suggesting weak coupling at the interplate boundary.

North Pacific

Cascades

Shallow seismicity is almost nonexistent along the 500 km long plate boundary between the Juan de Fuca's young oceanic lithosphere and the North America plate. However, seismicity at intermediate depth defines a plate dipping at about 22° to about 100 km depth (Crosson, 1980). Heaton and Kanamori (1984) infer a strongly coupled interplate boundary along the Juan de Fuca plate (Figure 3.6). The
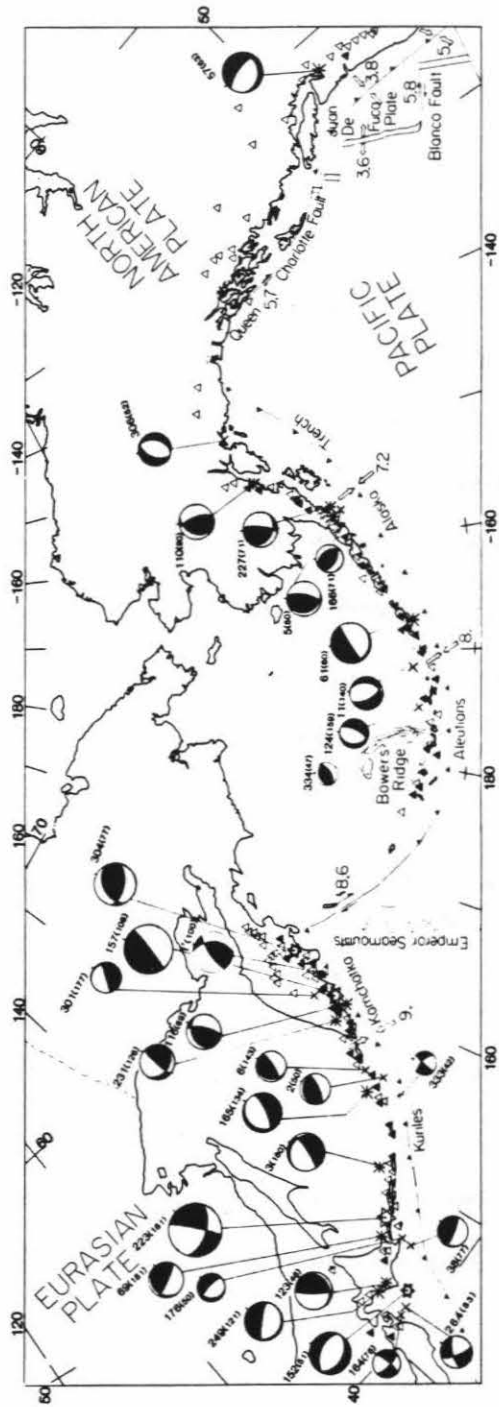
Figure 3.6: Location and focal mechanism of intermediate-depth events with $M \geq 6.0$ that occurred between 1960 and 1984 in the Northern Pacific (Table 1.3). See Figure 3.4 for symbols.

occurrence of the 1965 (event 57, m_b=6.9 and 1949 (m_b=7.1) Puget Sound earth-quakes, both normal-faulting events (Langston and Blum, 1977), at intermediate depth also suggest a strongly coupled interplate boundary as shown in Figure 1.8.

Alaska-Aleutians

Convergence between the North America and Pacific plates occurs along the Alaska-Aleutian trench in a northwest direction. The oceanic plate becomes progressively older to the west along strike from 40 to 65 m.y.. Seismicity defines the down-going slab to a maximum depth of 280 km underneath the Aleutian Arc. The dip of the subducting lithosphere shallows progressively to the east from 65° underneath the Aleutian Islands to about 25° beneath the Cook Inlet, where seismicity is only 150 km depth. Under the Rat Island arc, west of the Bowers ridge, the seismicity depth is only 100 km deep and turns into a transform boundary as it approaches the Kamchatka coast. The volcanic chain that parallels the trench from Alaska to the Rat Island arc is very active (Figure 3.6).

The 1964 Alaska (M_w=9.2), the 1957 Aleutian (M_w=9.1) and the 1965 Rat Island (M_w=8.7) earthquakes, with rupture lengths of over 500 km, are among the largest thrust events that occurred in this century. However, only a few large (m_B>7) intermediate events have occurred in the Aleutian-Alaska region (see Table A.1). Event 306 (m_b=6.3) that occurred near the northern edge of the 1964 Alaska earthquake aftershock area shows in plate horizontal tension and a vertical compressive axis, which suggests that this event may be associated either with deformation in the subducting plate or with continental loading . Only one event with $M \geq 6$ has occurred down-dip of the 1964 Alaska aftershock zone, on December 1968 (event 110, m_b=6.5). This event had many aftershocks and may be associated with the tear

proposed by Burbach and Frohlich (1986) in this region.

Events 5, 166 and 227 occurred down-dip and nearby the northern edge of the 1938 Alaska earthquake aftershock zone (McCann et al., 1979). These three events are down-dip tensional, and events 5 and 227 have steep normal-fault mechanisms that agree with the model for intermediate-depth earthquakes that occur at strongly coupled regions (see Figure 1.8). Hudnot and Taber (1987), using local seismicity data in this region (known as the Shumagin gap), observe a change in the intraplate seismicity pattern, from a single-seismic zone, where events 5, 166 and 227 occur, to a double-seismic zone to the west where no larger intermediate depth events have been observed after 1960. They suggest that this difference may reflect a stress change at the interplate boundary between these two regions that either have different aseismic-to-seismic slip ratio, or are at different stages in the earthquake cycle. Our observations would indicate that coupling at the interplate boundary in the eastern segment is stronger.

Two normal-faulting events, 61 and 334, occurred down-dip of the 1957 Aleutian earthquake aftershock zone. Note that event 334 that occurred in 1984 was located down-dip of the 1986 Andreanof Islands (M_w=8.0) earthquake aftershock zone. Before the 1957 Aleutian event, three large (m_B>7) intermediate-depth earthquakes occurred within the 20 years prior to this event, whereas only one large event (61, m_B=6.9) has occurred thereafter (Table A.1). This suggest that displacement from the 1957 event at the interplate boundary may have only decreased the tensional down-dip tensional stresses at intermediate-depth. Deeper events (11 and 124), however, show a down-dip compressional axis and a near horizontal in-plate horizontal axis, which could be related to lateral bending of the downgoing plate.

Western Pacific

The 95 m. y. old Pacific plate subducts westward at about 9 cm/yr along the
Kamchatka-Kurile-Japan trench under the Eurasia plate. To the south, as the Pacific
plate turns to be over 135 m. y. old, it subducts along the Izu-Bonin-Mariana trench
system beneath the Philippine plate with a slower convergence rate and seismicity,
defining a nearly vertical plate (Katsumata and Sykes, 1969). The chain of active vol-
canoes parallels the trench axis for most of its length as shown in Figures 3.6 and 3.7.
The dip angle and extent of the intraplate seismicity vary along the trench as indi-
cated in Table 1.1. Double seismic zones at intermediate depth have been reported in
the Kurile-Kamchatka region (see Figure 5 of Stauder and Maulchin, 1976) and in
Japan (Hasegawa et al., 1979). The strength of coupling at the interplate boundary,
as inferred from earthquake magnitudes of thrust events (Ruff and Kanamori, 1980),
changes along the trench strike, from considerably strong coupling offshore the Kam-
chatka Peninsula to being uncoupled along the Mariana trench.

Kamchatka

The 1952 Kamchatka (M_w=9.0) earthquake broke the southern 400 km of the
interplate boundary; to the north the 1959 (M_S=7.8) and the 1923 (M_w=8.5) events
ruptured the remaining 150 km. Intermediate-depth earthquakes under Kamchatka
can be divided into 2 depth groups. Events deeper than 125 km (231 and 301) have
down-dip compressional focal mechanisms similar to deeper events in this region
(Stauder and Maulchin, 1976). The shallower events show a temporal change in the
stress axes' orientation, as shown in Figure 3.1b. A down-dip compressional event (1',
m_b=6.9) occurred on July 1960, indicating that displacement at the interplate bound-
ary from the 1952 Kamchatka (M_w=9.0) event induced compressional stresses at

intermediate depth. After July 1969 three normal-faulting events (116, 157 and 304) with $m_b \geq 6.5$) occurred at similar depth, suggesting that the interplate boundary is at least moderately coupled once again. Moreover, Christensen and Ruff (1987) remark that in the outer-rise region, just after the 1952 Kamchatka earthquake, tensional events occurred. However, compressional events have been observed in offshore southern Kamchatka, indicating coupling at the interplate boundary.

Kuriles-Japan

The interplate boundary along northeast Japan and the southern Kurile Island arc has ruptured during recent large thrust earthquakes which occurred northward along the trench in 1952 (M_w=8.1), 1973 (M_w=7.8), 1969 (M_w=8.2), 1958 (M_w=8.3) and 1963 (M_w=8.5) (Schwartz and Ruff, 1987, Beck and Ruff, 1987). However, along the northern 500 km of the Kurile trench, the last shallow earthquake occurred in 1915 (M_S=8.0), but it is unknown if this event broke the entire Kurile gap, (McCann et al., 1979). Christensen and Ruff (1987) observed compressional events offshore this gap suggesting strong coupling at the interplate boundary in this region. Although large intermediate-depth events ($m_b > 6$) down-dip of the Kurile gap are only located close to its northern and southern boundaries, it is unclear if these events could be associated, respectively, with the recent 1952 Kamchatka(M_w=9.0) or the 1963 Kurile Island (M_w=8.5) thrust earthquakes.

Event 2 has a normal-fault mechanism at the base of the strongly coupled interplate boundary. However, event 6 shows down-dip tensional axis, whereas event 165 has a down-dip compressional axis. The relative location of these events is consistent with a double-seismic zone at intermediate depth (Stauder and Maulchin, 1976). Event 333 (M_w=5.6) indicates intraplate deformation, and event 3, which occurred
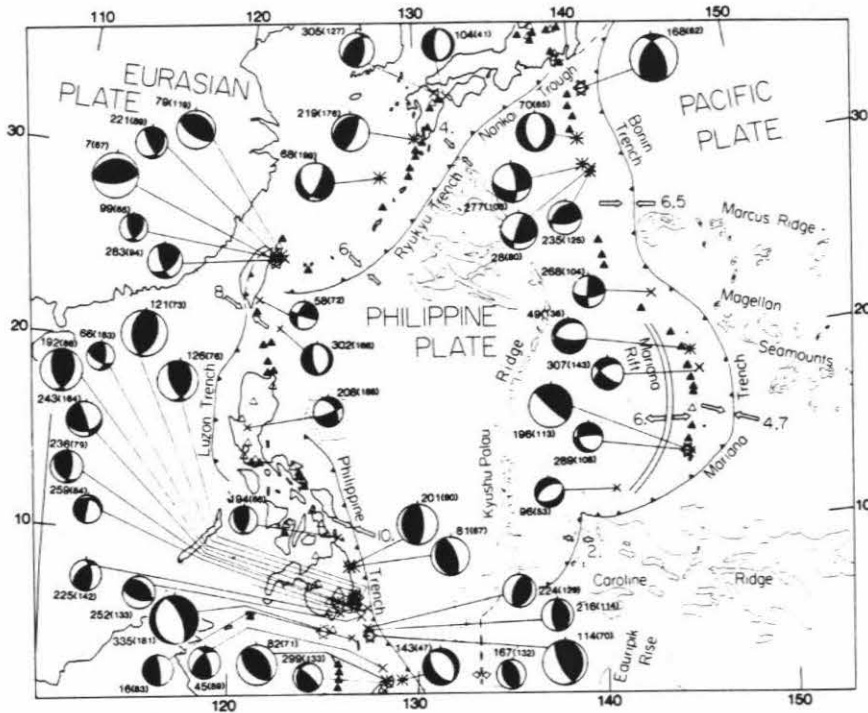
Figure 3.7: Focal mechanisms and location of intermediate-depth earthquakes (M≥6.0) associated with the Philippine Plate that occurred between 1960 and 1984. For symblos, see Figure 3.4.

near the southern edge of the Kurile gap is down-dip compressional.

Large intermediate-depth events that occur from 1960 to 1984 down-dip of the Japan-southern Kurile trench reflect the complexity of the subducting lithosphere in this region (e.g., Burbach and Frohlich, 1986). Most intermediate-depth earthquakes in this region: events 223 (m_b=7.8), 176 (m_b=6.0), 123 (m_b=6.7), 163 (m_b=6.7) and 264 (m_b=6.3) have hinge-faulting mechanisms. Note also that events 223 and 123 had more aftershocks within one week than similar magnitude intermediate-depth events (see Figure 1.10). Event 38, with a normal-fault mechanism, occurred in 1968 at the base of the 1952 (M_w=8.1) aftershock zone, indicating a coupled interplate boundary. Events 69 and 249 are down-dip compressional and tensional, respectively, and may be associated with the double-seismic zone observed underneath Japan (Hasegawa et al., 1979). Event 152 (m_b=7.0) has the compression axis vertical and the tension axis horizontal, reflecting lateral bending of the downgoing plate and consistent with the orientation of stresses induced by a buckling plate (Sasatani, 1976). This suggests that the magnitude of intermediate-depth stresses underneath northeast Japan due to the complex downgoing slab are larger than those induced by the rather uncoupled interplate boundary. However, the fact that the interplate boundary is uncoupled induces bending stresses under the trench axis, which produce large normal-faulting events like the 1933 Sanriku (M_w=8.4) earthquake (Kanamori, 1970). Many large intermediate-depth events have occurred down-dip of the Kurile-Japan trench prior to 1960 (see Appendix 1).

Izu-Bonin

Thrust earthquakes along the Izu-Bonin trench are infrequent and with maximum magnitudes of about 7.4 (McCann et al., 1979). However, many large (m_B>7.0)

earthquakes have occurred during this century (Table A.1). Event 168 (m_B=7.4) has a horizontal compression axis aligned with the plates' convergence direction and down-dip tensional axis, consistent with stresses induced by the negative buoyancy of the downgoing plate. However, event 70 (m_b=6.8) has near vertical compressive stresses and a horizontal tension axis. These events have similar depth but event 168 is located closer to the trench axis, suggesting the presence of a double seismic zone in the region. Moreover, the focal mechanisms of these events are consistent with unbending of the downgoing plate. Earthquakes that occur below 80 km depth are down-dip compressional events (28, 235 and 277).

Figure 1.10 shows that event 168 had more than 25 aftershocks with m_b>3 within a week. If this event was shallower, its focal mechanism's solution would be consistent with a shallow-thrust event in this region. However, timing of pP-P phases constrained the depth of this event, but the possibility of a multiple source shallow event was not considered. A more detailed analysis of this event may be required to resolve its depth.

Marianas

In the Mariana subduction zone, back-arc spreading is taking place, the inter-plate boundary is uncoupled and shallow-thrust earthquakes are infrequent, with maximum magnitudes of about 7.0 (Ruff and Kanamori, 1980). In 1902 a large (M_S=7.9) earthquake occurred in the Mariana Island arc. Although this event is considered a shallow event, there was no tsunami associated with it, perhaps indicating that this event was either an intermediate-depth event (McCann et al., 1979). The focal mechanisms of event 268 that shows in-plate horizontal compression, and events 49 and 307 with in-plate horizontal tension are consistent with lateral bending of the

slab along the trench strike, from convex to concave (Burbach and Frohlich, 1986). Seismicity is poorly defined in the southern Mariana arc, where events 196 ($m_b=7.1$) and 289 ($m_b=6.1$) indicate tear faulting below 100 km depth. Event 96 shows vertical compressive stresses and horizontal tension in the convergence direction. This event may be reflecting the tensional stresses induced by the observed back-arc spreading in this region (Figure 3.7).

Philippine Sea

The Philippine Sea (Figure 3.7) is one of the most complex tectonic areas since the Philippine and Eurasia plates subduct in different directions in this region. The Philippine plate subducts to the northwest along the Nankai Trough and the Ryukyu trench and to the southwest along the Philippine trench. The Eurasia plate subducts eastward along the Luzon trench and farther south along the west coast of Negros Island. The Celebes sea-floor subducts eastward along the Cotabato trench, west of Mindanao Island, and to the south along the Sulawesi trench (Cardwell et al., 1980). Seismicity in the Nankai Trough area is very shallow, about 60 km, and the inter-plate boundary in this region is strongly coupled. In contrast, all other subduction zones in the Philippine Sea region are weakly coupled at the interplate boundary (Ruff and Kanamori, 1980) and only tensional outer-rise events are observed there (Christensen and Ruff, 1987).

Ryukyu- North Taiwan

Many large ($m_B>7$) intermediate-depth earthquakes occurred in the Ryukyu-north Taiwan region before 1960 (see Appendix 1), including the largest known intermediate-depth event, $m_B=8.1$ that occurred in 1911 under the Ryukyu Island

arc. However, after 1960 this region has been relatively quiet at intermediate depth. Seismicity is about 200 km deep along most of the trench.

Event 104 indicates hinge faulting between the younger ocean floor that subducts in the Nankai Trough and that of the older Philippine sea-floor to the west of the Kyushu-Palau ridge. Shiono et al. (1980) indicate that a marked change in the dip and state of stress of intermediate-depth seismicity is observed along the Ryukyu Island arc. North of the Tokaora channel, the slab dips at about 70°, active volcanisms is present (Figure 3.7), and intermediate-depth events with $m_b \approx 5$ have down-dip tensional mechanisms in response to the negative buoyancy of the downgoing plate. Note that events 219 ($m_b = 6.7$) and 305 ($m_b = 6.5$) are down-dip tensional. South of the Tokaora channel, the downgoing plate dips at about 45°, volcanism is scarce, and focal mechanisms of $m_b \approx 5$ events indicate down-dip compression, as in event 68 in Figure 3.7. These changes could be explained in terms of lateral differences in temperature in the surrounding mantle, as reflected by volcanism, which can produce less or more resistance to the subducting lithosphere (Shiono et al., 1980).

A cluster of intermediate-depth events underneath north Taiwan delineates the edge of the down-going Philippine plate. The larger events (7, $m_b = 7.2$ and 79, $m_b = 6.7$) in this region have near vertical tensional axis that reflect the weakly coupled interplate boundary and the negative buoyancy forces exerted by the downgoing plate. Events 99, 221 and 283 are hinge-faulting events.

Luzon

Shallow and intermediate-depth seismicity in this region is scarce and not well defined (Cardwell et al., 1980). During this century only a few large earthquakes have occurred in this region (see Appendix 1). Intermediate-depth events (58, 302 and

208) in the Luzon subduction zone may reflect only in-plate deformation. However, note that event 302 is down-dip compressional suggesting resistance to subduction of the plate at depth.

Philippines

Cardwell et al. (1980) discuss in detail the very complex tectonic setting of the Philippine Island arc, which is bounded to the west by the shallow Negros and Cotabato subduction zones and to the east by the Philippine trench, with earthquakes occurring as deep as 640 km. Frequent large shallow and intermediate-depth earthquakes have occurred in this region during this century (see e.g., McCann et al., 1979 and Appendix 1). In the northern section of the Philippine trench all intermediate-depth events, from event 126 to 225 in Figure 3.7, have either near down-dip tensional mechanisms or vertical tension axes consistent with the model for partially coupled regions (Figure 1.8) in which vertical tensional stresses are induced by the negative buoyancy of the subducting plate. Similarly, events along the south Philippine trench have nearly down-dip tensional axes, with the exception of the deepest event, 335 M_w=7.5, that has a down-dip compressional axis.

Sulawesi

The Sulawesi subduction zone (Figure 3.8) was very active at intermediate depths prior to 1960 (Gutenberg and Richter, 1954). Sequences of large (m_B=7.0 to 7.8) earthquakes occurred mainly in 1905-1907 and 1939-1942. However, seismicity at shallow depth is limited.

Stress axes of intermediate-depth events that occurred after 1960 do not have a preferred orientation (see Figure 3.2). Event 171 has an in-plate horizontal axis, in contrast to events (309, 34, 271 and 77) for which the compression axes are normal to

the slab. Events 190 and 309 are down-dip tensional events. Interpretation of events in this region is difficult since the geometry of the downgoing plate as well as the tectonics of the region are poorly understood.

Indonesia

The Indo-Australian plate subducts along the Sunda arc from Burma to the Banda Sea (Figure 3.8). Various segments are defined by differences in 1) the subducting lithosphere age, 2) the convergence direction between adjacent plates, 3) the seismicity depth (see Table 1.1) and 4) the strength of coupling at the interplate boundary.

Burma

Oblique convergence between India and Eurasia occurs in the Burma region, where strong coupling is reflected by several large shallow events that occurred prior to 1950 (Table A.2). The largest intermediate-depth event in the region occurred in 1954 (m_B=7.4, Table A.1). Most intermediate-depth earthquakes have oblique normal-fault mechanisms (down-dip tensional), consistent with detachment of the denser oceanic lithosphere from the more buoyant continental plate. Event 117 indicates tearing of the subducting plate and may be related to some preexisting structure.

Andaman Sea

Oblique subduction of the 55 m. y. old seafloor persists in the Andaman Sea that produces complex back-arc spreading under this region (Eguchi et al., 1979, Banghar, 1987). Seismicity is about 100 km depth, with most intermediate-depth events (287, 44 and 294 with d>40 km) are down-dip tensional, in agreement with the model for
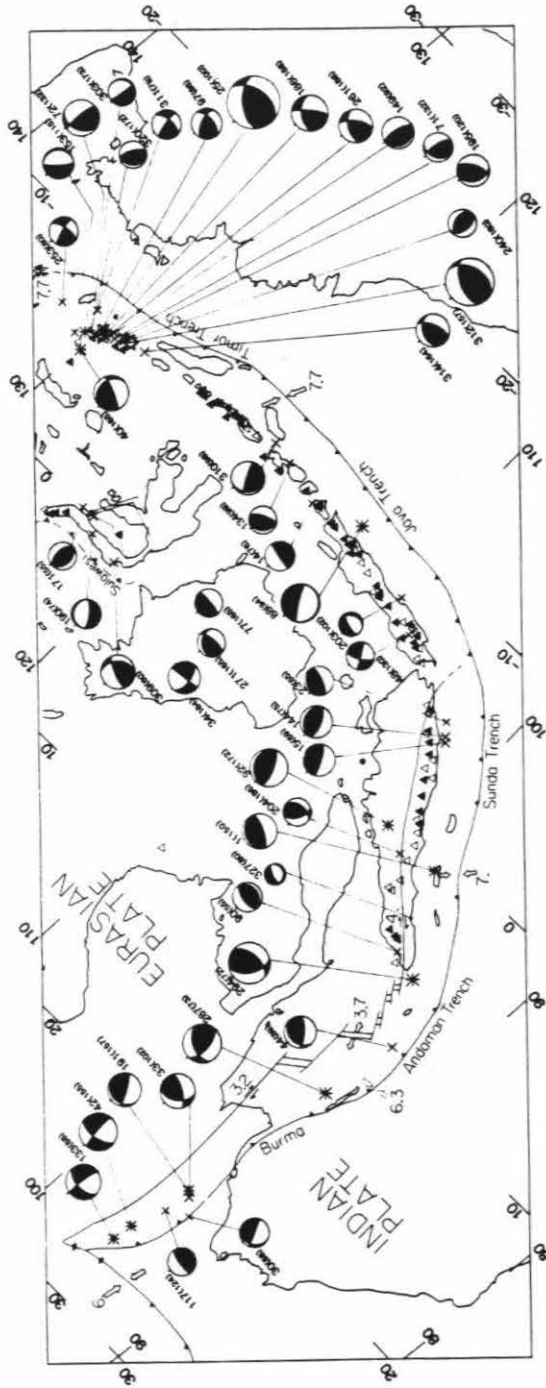
Figure 3.8: Epicentral location and focal mechanisms of intermediate-depth earthquakes associated with the interaction of the Indian and Eurasian plates in Indonesia. Events occurred from 1960 to 1984 (see Figure 3.4).

moderately coupled subduction zones in which down-dip tensional stresses are induced at intermediate depth because of the negative buoyancy of the downgoing plate.

Sunda

Convergence of the subducting Indian plate to the northeast along the Sunda trench is about 7 cm/yr. The volcanic chain parallels the trench and seismicity occurs as deep as 300 km depth. Historic large shallow earthquakes ($M_w \approx 8.7$) have occurred along the Sunda trench (Newcomb and McCann, 1987), suggesting at least a moderately coupled interplate boundary. All intermediate-depth events, from event 327 to the north to event 23 to the south, are down-dip tensional events, and are consistent with the model shown in Figure 1.8 for intermediate-depth events that occur down-dip of a partially coupled interplate boundary. Compressional axes for most events are normal to the subducting plate; the exception is event 204, which has horizontal in-plate compression. Burbach and Frohlich (1986) calculate lateral compression stresses in the region where this event occurs.

Java

South of the Sunda straight the seismicity increases abruptly to 650 km depth, convergence of the 135 m. y. old subducting seafloor occurs and the active volcanic chain parallels the Java trench (Figure 3.8). No large historic shallow earthquakes are known in this region (McCann et al., 1979, Newcomb and McCann, 1987), indicating that subduction is mostly aseismic in this 1700 km long trench. In addition, the 1977 Sumbawa normal-fault earthquake ($M_w = 8.3$) that occured under the trench axis in response to bending of the lithosphere induced by the slab pull (Spence, 1986) was also consistent with an uncoupled interplate boundary (see Figure 1.8). Several large

($m_B \geq 7$) intermediate-depth events occurred prior to 1950 in this region (Table A.1).

Event 48 has an in-plate tension axis that could be induced by the lateral bending of the Indian plate as it subducts in this region (Burbach and Frohlich, 1986). Events 88, 134 and 310 are down-dip tensional, whereas the shallower event, 14, is down-dip compressional. Note the relative location of this event with respect to the trench axis and the stress orientation of these events that suggest the presence of a double-seismic zone.

Timor

In the Banda Sea the subducting lithosphere bends sharply along the Timor trench, where the intermediate and deep seismicity define a highly contorted plate. The fact that the tectonics of the surrounding region is complex, contributes to the different interpretations given to explain the shape of the downgoing plate under the Banda Sea (e.g., Burbach and Frohlich, 1986). During this century, many large intra-plate earthquakes (Table A.1) have occurred in this region, but only a few large shallow events (Table A.2) have occurred there.

All intermediate-depth events in the Banda Sea , from event 314 to the eastern-most event 253, have nearly down-dip tensional focal mechanisms induced by the downgoing plate. Note that the compressional axes, of the Banda Sea events in Figure 3.8, rotate from a nearly north-south direction to a more easterly direction as the subducted plate bends northward. Thus, the compression axis of these events is maintained nearly perpendicular to the downgoing lithosphere. The largest events which occurred recently in the Banda Sea are the 1963 (event 25, m_B=7.8) and the 1983 (312, M_w=7.4) earthquakes. These events are studied in detail by Osada and Abe (1981) and Michael-Leiba(1984), respectively.

Southwest Pacific

The southwest Pacific region is characterized by subduction along deep trenches which parallel a system of island arcs and marginal basins from New Guinea to New Zealand. The interaction between the relatively old seafloor of the Pacific and Indo-Australian plates and the younger Solomon and Bismark plates defines different subduction zones in this complex tectonic region (Figures 3.9 and 3.10). The rupture lengths of most large shallow earthquakes in the southwest Pacific region are less than 150 km long (McCann et al., 1979), indicating weak coupling in the region. However, Christensen and Ruff (1987) observe that in this region compressional and tensional events occur in the outer-rise region, in contrast to subduction zones along Indonesia and around the Philippine Sea which are mostly uncoupled at the interplate boundary in which only tensional outer-rise events occur. They arrived to this conclusion although temporal and spatial variations of focal mechanisms of outer-rise events are difficult to interpret in this region. A regional compressive stress field is required for outer-rise compressional events to occur and some segments along the interplate boundary must be at least moderately coupled.

New Guinea

Subduction of the Bismark plate along the northeast coast of New Guinea defines a downgoing plate to about 500 km depth along the western end of the trench (Pascal, 1979). During this century several large ($M_S > 7.5$) shallow events have occurred along the New Guinea trench (Table A.2) but had very small rupture zones (McCann et al., 1979). A few intermediate-depth events with $m_b \leq 7.2$ have occurred in this region.
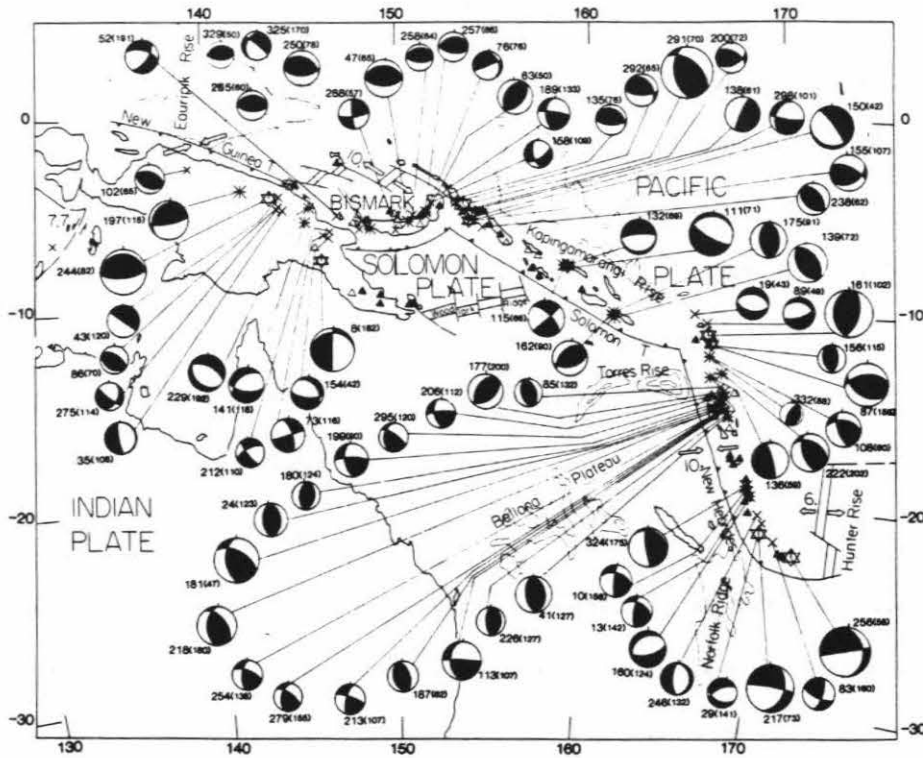
Figure 3.9: Intermediate-depth earthquakes (M≥6.0) in the New Britain, Solomon, and New Hebrides regions, where the Indian and Solomon plates interact with the Pacific plate. Events occurred from 1960 to 1984. See Figure 3.4 for symbols.

Since the shape of the subducting lithosphere under New Guinea is poorly understood and the stress axis distribution of intermediate-depth events in this region do not show a consistent pattern, it is difficult to interpret the intraplate seismicity in this area. Nevertheless, we may emphasize that focal mechanisms of intermediate-depth earthquakes vary rapidly westward along the trench from event 102 to event 73, and that the largest events (8 and 244) with $M \approx 7.3$. may indicate hinge faulting. Mislocation of intermediate-depth events that occur between th New Guinea and New Britain subduction zones may also contribute to confuse the tectonics and the seismic history of this region.

New Britain-New Ireland-Solomon

The Solomon plate subducts northward with an almost vertical dip angle to depths of about 500 km, along the New Britain trench. The chain of volcanoes parallels the trench (Figure 3.9) but follows the 200 km seismicity contour of New Britain. Then it bends abruptly under the New Ireland region and subducts in a northwesterly direction under the Pacific plate (Johnson and Molnar, 1972, Pascal, 1979, Burbach and Frohlich, 1986). Large shallow earthquakes in this region occur as multiplet events, with the most recent sequences occurring after 1966 (Lay and Kanamori, 1980, Wesnousky et al., 1986). The occurrence of large shallow events close occurrence in time and space indicates that this region has moderate coupling at the interplate boundary.

Most intermediate-depth events in the New Britain region have nearly vertical tension axis and the compression axis normal to the plate, consistent with the orientation of stresses induced by the negative buoyancy of the downgoing plate. Exceptions are events 76 and 288, which indicate in-plate deformation. Events 52 and 158,

which are deeper and near the edges of the New Britain subduction zone, have in-plate compressional axis. Christensen and Ruff (1987) report compressional outer-rise events offshore the western segment of the New Britain trench, indicating that the interplate boundary is under compression. Large thrust events occured there in 1945 and 1946 (Table A.2). Note that event 47 with focal depth of 65 km had many aftershocks within a week. If this event was shallower, its focal mechanism is also consistent with subduction in the interplate boundary.

The New Ireland region includes those events located near the corner between the New Britain and Solomon trenches. This small region , between 152.5° and 155°E longitude and 2° and 7°S latitude, had many large intermediate-depth events during this century (Table A.1). The interplate boundary breaks in doublet events (Lay and Kanamori, 1980) that occur about every 30 years (Table A.2), the most recent of which occurred on July 14 (M_w=8.0) and July 26, 1971 (M_w=8.1).

Most events at intermediate depth have down-dip tensional mechanisms consistent with stresses induced by the pull of the slab. Event 138 indicates hinge faulting within the plate. However, event 298 has a down-dip compressional mechanism. This event occurred down-dip, and after, the July 14, 1971 thrust earthquake, and is consistent with the dynamic model shown in Figure 3.1b. Although the normal-fault event 150 (m_b=7.1) that occurred on July 19, 1971 is located down-dip of the July 14 event, it probably helped trigger the July 26 thrust earthquake that broke the adjacent segment near the corner of the New Britain trench (see Figure 3 in Lay and Kanamori, 1980). Christensen and Ruff (1987) report tensional outer-rise events after the occurrence of the 1971 New Ireland doublet. The New Britain-New Ireland region, albeit complicated, agrees with the simple model of partially coupled regions

shown in Figure 1.8, in which vertical tensional stresses are induced at intermediate depth from the slab's weight. Also, temporal changes of focal mechanisms are observed in the outer-rise and intermediate-depth regions associated with the occurrence of large, underthursting earthquakes.

The Solomon trench is the boundary between the Pacific plate and the Solomon and Indo-Australia plates. The Woodlark Ridge subducts along the central part of the Solomon trench, where few large subduction events occur (McCann et al., 1979). However, to the north and south of this topographic high, the interplate boundary has been very active (Table A.2). It is characterized by the occurrence of multiplet events with rupture lengths of about 100 km (Lay and Kanamori, 1980, Wesnousky et al., 1986) Seismicity is at most 200 km deep in this region.

At intermediate depth, events 115, 132 and 111, which occur near the northern edge and down-dip of the Woodlark ridge, indicate hinge faulting and possibly the boundary of the Solomon and Indo-Australian plates at depth. Events 175,139 and 162 have a vertical tension axis induced by the slab pull. Note that these events occurred before the recent 1978-1979 thrust earthquake sequences in this region (Wesnousky et al., 1986).

New Hebrides

The New Hebrides subduction zone dips steeply westward and delineates the boundary between the Indo-Australian plate and the Pacific plates. The volcanic chain parallels the New Hebrides trench for most of its length (Figure 3.9). The inter-plate boundary has been very active during this century (Table A.2, McCann et al., 1979) and it is the most active region at intermediate depth (Table A.1). Seismicity is 300 km deep in New Hebrides. Events 19 and 89, located at the corner of the

Solomon and New Hebrides trenches, have vertical compressive stresses and horizontal tensional stresses aligned with the plate, which reflect the lateral bending of the downgoing Indo-Australian plate (Burbach and Frohlich, 1986). All other intermediate-depth events in the northern segment of the New Hebrides trench, from event 161 to the north to event 41 , have a down-dip tension axis and a compression axis normal to the plate consistent with the orientation of stresses induced by the negative buoyancy of the slab. Events 41 and 181, which may be associated with subduction of the Torres rise, had many aftershocks within a week (see Figure 1.10).

Back-arc spreading occurs in the southern segment of the New Hebrides trench. Intermediate-depth events that occur in this region show a more complex pattern in the stress distribution (see Figure 3.2). Events (324,10 and 13) farther north in this southern segment of the New Hebrides trench have a down-dip tensional axis and a normal compressional axis, similar to events to the north, as discussed above. Event 160 has down-dip compression and a horizontal tension axis within the plate. This event is located in the region where Burbach and Frohlich (1986) computed lateral extension to be present. Event 246 shows intraplate deformation. Events 256, 83, 217 and 29, near the southern bend where the boundary presents left-lateral strike-slip motion, are hinge-faulting events.

Tonga-Kermadec-New Zealand

The Tonga-Kermadec trench system is extremely linear, with seismicity occurring to about 650 km depth. The Pacific plate subducts to the east underneath the Indian plate, delineating a smooth slab to about 400 km depth. However, deep events delineate a highly contorted plate below 400 km depth (Billington, 1980, Giardini and Woodhouse, 1984). The slab dip is 55° under Tonga and increases to 70° farther south
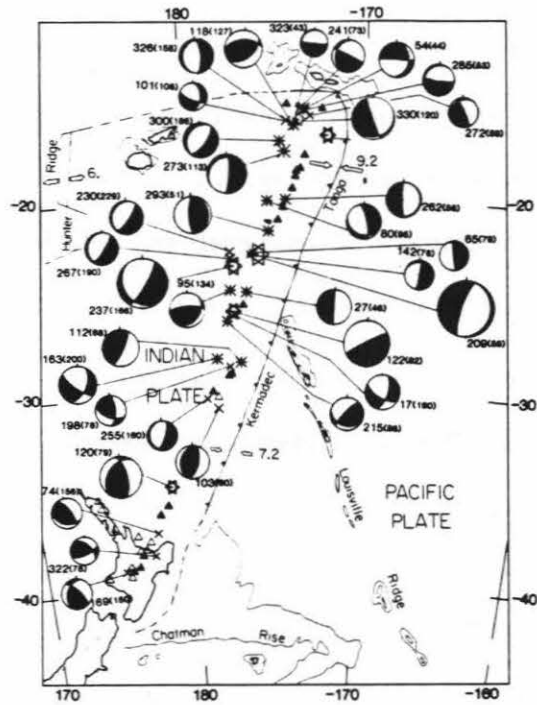
Figure 3.10: Focal mechanisms and epicenters of events occurred in the period 1960 ato 1984 with M≥6.0) in the Tonga, Kermadec and New Zealand regions, where the Pacific plate underlies the Indian plate. For symbols see Figure 3.4.

under the Kermadec and New Zealand trenches. The volcanic chain, which parallels the Tonga trench, disappears in the region where the Louiville ridge is being subducted (Figure 3.10).

Large, shallow events along the northern section of the Tonga trench occurred before 1950 (Table A.2, McCann et al., 1979). Along the northern boundary of the Kermadec trench several thrust events have occurred after 1960. A large thrust event occurred in 1982 (M_S=8.2), where the Louiville ridge intersects the Tonga trench. The interplate boundary along the Tonga-Kermadec region is partially coupled as indicated by the rupture lengths of large shallow thrust events of about 150 km (McCann et al., 1979). Most of the deep seismicity occurs in the Tonga trench (Vassiliou et al., 1984, Giardini, 1987). It is also very active at intermediate depth.

Intermediate-depth events in the northern boundary, where the plate bends, is characterized by in-plate extension in agreement with Burbach and Frohlich's (1986) calculations in this region. Farther south most intermediate-depth events have down-dip compressional stresses, which are transmitted from the deep seismic region to nearly all parts of the Tonga subducting lithosphere. The few down-dip tensional events in this region are associated with subduction of the Louiville ridge which increases the coupling of the interplate boundary locally. Events 262 and 27 with m_b=6.5 are located down-dip of the Louiville ridge at the inferred northern and southern edges of it (Giardini and Woodhouse, 1984). The large normal-fault 1977 Tonga earthquake (event 209) was located down-dip of the large 1982 (M_S=7.7) thrust earthquake. An outer-rise compressional event occurred before 1982 offshore this region (Christensen and Ruff, 1987). This is consistent with the dynamic model shown in Figure 3.1b.

Most events in the Kermadec region have a down-dip tensional axis and normal compression. Event 163, the deepest event in Figure 3.10, which has down-dip compression stresses similarly to deeper events in the region (e.g., Isacks and Molnar, 1969). Event 255 (m_b=6.1) occurred down-dip and after two large subduction events that occurred in 1976 (M_S=7.7,8.0), is down-dip compressional. In 1963, event 103 (m_b=6.4) which is located down-dip of the 1976 aftershock zone, is down-dip tensional. Furthermore, Christensen and Ruff (1987) report that an outer-rise compressional event occurred prior to the 1976 Kermadec doublet.

In New Zealand, the intermediate-depth events (74, 322 and 169) have down-dip tensional events resulting from the negative buoyancy of the downgoing lithosphere.

Alpine-Himalaya Belt

Figure 3.11 shows the intermediate-depth events that occurred between 1960 and 1984 in the Alpine-Himalaya belt.

Hindu-Kush

Seismicity concentrates at about 220 km depth in the Hindu-Kush region, where large m_B>7 events are frequent in this region (Table A.1). Intermediate-depth events have near vertical tensional axis, suggesting that the denser oceanic lithosphere subducted a few million years ago is now being detached from the more buoyant continental lithosphere.

Iran
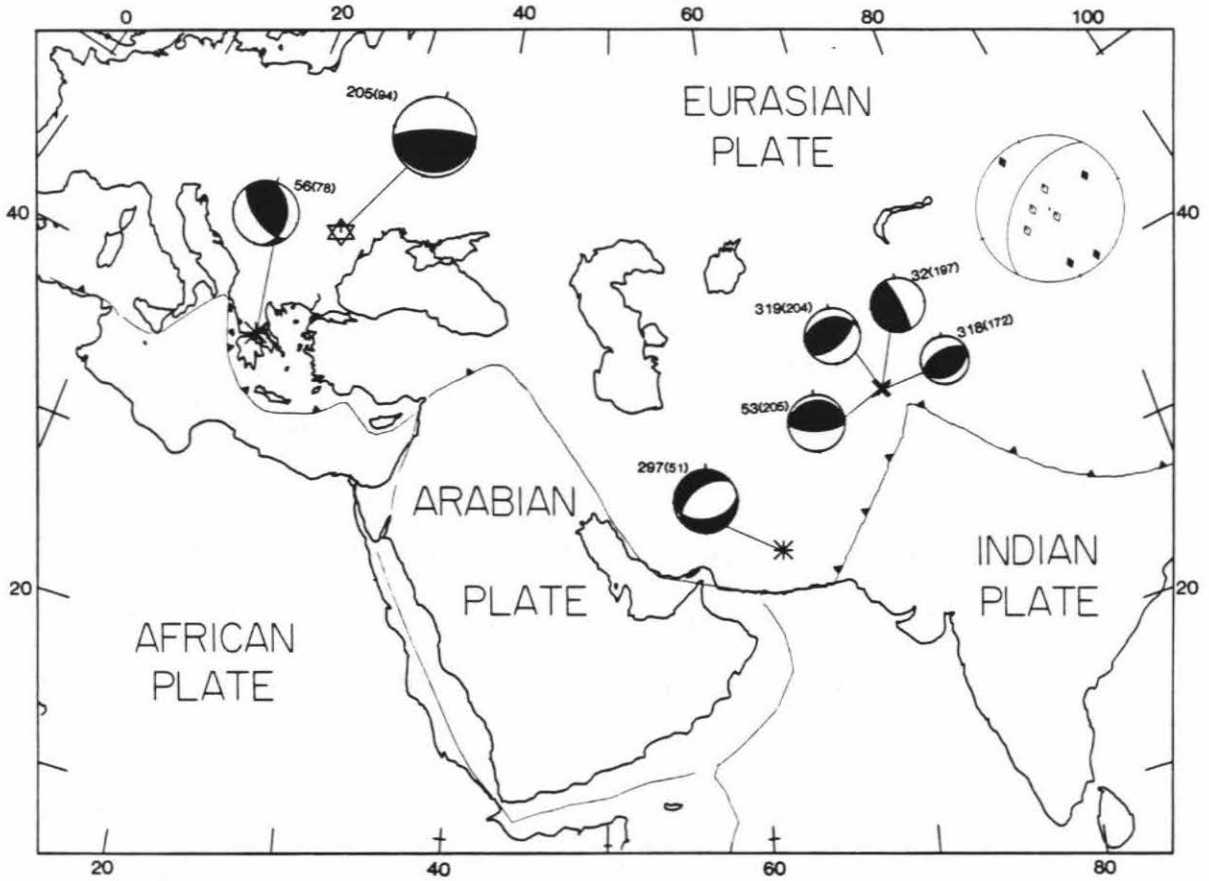
Figure 3.11: Events with M≥6.0 that occurred at intermediate depth between 1960 and 1984 in regions where continental coalitions are taking place. See Figure 3.4 for symbols. The P and T axis closed and open (symbols, respectively) of events that occurred in the Indu-Kush and Hellenic arc regions are shown in a lower hemisphere projection. Circles are events shallower than 100 km and diamonds indicate deeper events.

Jacob and Quittmeyer (1979) review the seismotectonics of the Iran-Paquistan region. Intermediate-depth events occur along the Makran subduction zone, where the Arabian plate is subducting beneath Eurasia at a shallow dip to about 80 km depth. Event 297 (M_w=6.7) has a nearly vertical compression axis and the tension axis nearly horizontal and in the direction of convergence. At larger depth, Jacob and Quittmeyer (1979) report down-dip tensional events in this area.

Rumania

Although the detail structure of the subducting lithosphere under Rumania is poorly defined, it appears that there is an almost vertical slab that strikes to the northeast and dips to the northwest under this region (Isacks and Molnar, 1969). Seismicity concentrates between 100 and 150 km depth. Two large events occurred in these region recently, in 1940 (m_B=7.3) and in 1977 (event 205, M_w=7.4). The later event indicates near vertical tension stresses similarly to events in the Hindu-Kush region.

Greece

The Mediterranean seafloor is subducting eastward along the Hellenic arc under Eurasia at an angle of 60° to about 200 km depth (McKenzie, 1978). Event 56 (m_b=6.7) has down-dip tensional stresses probably induced by the negative buoyancy of the subducting plate. A large earthquake m_B=7.7 occurred in Greece in 1926 at 100 km depth (Table A.1).

Conclusion to Part II

Christensen and Ruff (1987) found that there are spatial and temporal changes in the focal mechanisms of outer-rise events because of variations of seismic coupling at the interplate boundary. Namely, tensional outer-rise events occur offshore most subduction zones, from uncoupled to strongly coupled; however, compressional outer-rise events occur mostly offshore strongly coupled regions. Compressional outer-rise events precede large underthrusting earthquakes and tensional outer-rise events follow them. Unfortunately, seismicity at intermediate depth is more complex than that of the outer-rise region.

A reexamination of the historic record of large ($m_B \geq 7$) events that occurred within the subducting slabs indicates that most intermediate and deep focus earthquakes occur at major active plate boundaries. The most active region at intermediate depth is New Hebrides, and Tonga is the most active below 400 km depth. Other regions with a large number of intermediate-depth events are the Altiplano, Timor, Sulawesi, Scotia, and New Ireland, which are associated with bends in the subducted lithospherre. Other regions with many large intermediate-depth events are North Chile, Kuriles, Ryukyu and Philippines.

Focal mechanism solutions for intermediate-depth earthquakes that occurred from 1960 to 1984 with $M > 6.8$ can be grouped into four: 1) Normal-fault events (44%), and 2) reverse-fault events (33%), both with a strike nearly parallel to the trench axis; 3) Normal or reverse fault events with

a strike significantly oblique. Type 1 events occur at the base of strongly or moderately coupled subduction zones; similar-type events occur near the trench axis in uncoupled zones. Type 2 events with strike subparallel to the subduction zone, most of them with a near vertical tension axis, occur mainly in regions that have partially coupled or uncoupled subduction zones, and the observed continuous seismicity is deeper than 300 km. In terms of our simple model, the increased dip of the downgoing slab associated with weakly coupled subduction zones and the weight of the slab may induce near vertical tensional stress at intermediate depth and consequently, the change in focal mechanism from Type 1 to Type 2 events. Events of Type 3 occur where the trench axis bends sharply, causing horizontal (parallel to the trench strike) extensional or compressional intraplate stress. Type 4 are hinge-faulting events.

Temporal variation of focal mechanisms of large intraplate earthquakes in southern Chile in relation to the occurrence of large thrust events indicates that before a major thrust earthquake, the interplate boundary is strongly coupled and the subducted slab is under tension at intermediate depths; after the occurrence of an interplate thrust event, the displacement on the thrust boundary induces transient compressional stress at intermediate depth in the downgoing slab. This interpretation is consistent with the hypothesis that temporal variations of focal mechanisms of outer-rise events are due to changes of interplate coupling.

The stress axis orientation of moderate and large intermediate-depth events shows that most regions have either dominant, down-dip tensional stresses at intermediate depth or a mixed pattern. The exception is Tonga

where down-dip compressional stresses are dominant. Detailed regional observations of focal mechanisms of moderate and large intermediate-depth earthquakes in relation to spatial or temporal changes of the strength of interplate coupling indicate that the subducting lithosphere acts as a stress guide.

Intermediate-depth earthquakes for uncoupled, weakly or partially coupled regions show thrust-type faulting, with near vertical tension axis. These events occur in response to the negative buoyancy of the subducted slab. These regions have relatively long and steeply dipping seismic zones and may exhibit double-seismic zones in response to other factors such as unbending of the downgoing lithosphere. In these regions no temporal changes in the focal mechanisms of either outer-rise or intermediate-depth earthqukes are observed. Regions that are partially or weakly coupled are Lesser and Greater Antilles, the Scotia arc, south Kurile, Ryukyu, Philippines, Sumatra, Timor, New Hebrides, and Solomon subduction zones. Uncoupled regions are northeast Japan, Izu-Bonin, Mariana, and Java.

Intermediate-depth events down-dip of moderately or strongly coupled regions have normal faulting mechanisms near the base of the interplate boundary in response to bending of the subducting lithosphere. In contrast, regions that are uncoupled produce large normal faulting events near the trench axis, where stresses due to bending of the lithosphere are largest. Temporal changes either in the focal mechanisms of intermediate-depth events, from down-dip tensional to down-dip compressional events, or a reduction in the seismic activity at intermediate depth are observed after the occurrence of large thrust earthquakes.

Along Middle and South America, where the interplate boundary varies from moderate to strongly coupled, intermediate-depth earthquakes are generally normal-fault events that occur before and down-dip of future large subduction earthquakes. In most regions along Middle and South America, we observe a reduction only in the number of large intermediate-depth events after large subduction thrust earthquakes occurs in the region. However, down-dip compressional events have been observed down-dip and after the 1960 Chile and the 1974 Peruvian large thrust earthquakes. After the 1964 Alaska earthquake only one tear fault event has occurred at intermediate depth.

Down-dip of the large 1957 Aleutian earthquake a few events located there indicate coupling at the interplate boundary. This region was very active at intermediate-depth before 1957 when the interplate boundary broke. In addition, one of these events occurred before and down-dip of the large 1986 Andreanof earthquake. Down-dip of the 1952 Kamchatka earthquake aftershock zone, a down-dip compressional event occurred in 1960. After 1969 only events with down-dip tensional axis have occurred. Temporal changes of focal mechanisms of intermediate depth and outer-rise events are also observed to be associated with the 1971 New Ireland doublet events.

Under the Tonga trench mostly down-dip compressioanal events are observed; however, the events located down-dip of the Louiville ridge have down-dip tensional mechanisms and occurred before the large 1982 Tonga thrust event. Temporal changes in the focal mechanisms are also observed with the occurrence of the 1976 Kermadec doublet events.

References to Part II

Abe, K., 1972a, Focal process of the South Sandwich Island earthquake of May 26, 1964; *Phys. Earth and Planet. Int., 5,* 110-122.

Abe, K., 1972b, Mechanisms and tectonic implications of the 1966 and 1970 Peru earthquakes; *Phys. Earth and Planet. Int., 5,* 367-379.

Abe, K.,1973, Tsunami and mechanism of great earthquakes; *Phys. Earth and Planet. Int., 7,* 143-153.

Abe, K., 1981, Magnitudes of large shallow earthquakes form 1904 to 1980; *Phys. Earth of Planet. Int., 27,* 72-92.

Abe, K. and H. Kanamori, 1979, Temporal Variation of the Activity of Intermediate and Deep Focus Earthquakes; *Jour. Geophys. Res., 84,* 3589-3595.

Anderson, D.L., 1967; Phase Changes in the Upper Mantle; *Science, 157,* 1165-1173.

Ansell, J.H. and E.G.C. Smith, 1975, Detailed structure of a mantle seismic zone using the homogeneous station method; *Nature, 253,* 518-519.

Astiz, L. and H. Kanamori, 1984, An earthquake doublet in Ometepec, Guerrero, Mexico; *Phys. Earth Planet. Int., 34,* 24-45.

Astiz, L. and H. Kanamori, 1986, Interplate Coupling and Temporal Variation of Mechanisms of Intermediate-depth Earthquakes in Chile; *Bull. Seis. Soc. Am., 76,* 1614-1622.

Balakina, L.M., 1962, General regularities in the directions of the Principal Stresses effective in the earthquake foci of the seismic belt of the Pacific Ocean; *Acad. Sci. U.S.S.R., Izu, Geophys. Series,* 918-926.

Banghar, A.R., 1987, Seismo-tectonics of the Andaman-Nicobar Islands; *Tectonophysics, 133,* 95-104.

Barazangi, M. and B.L. Isacks, 1976, Spatial Distribution of earthquakes and subduction of the Nazca plate beneath South America; *Geology, 4,* 686-692.

Barazangi, M. and B.L. Isacks, 1979, Subduction of the Nazca plate beneath Peru; evidence from the spatial distribution of earthquakes; *Geophys. J.R. Astr. Soc., 57,* 537-555.

Barker, P.F., 1970, Plate Tectonics of the Scotia Sea region; *Nature, 228,* 1293-1296.

Barker, P.F., 1972, A spreading centre in the East Scottia Sea; *Earth and Planet. Sc. Lett., 15,* 123-132.

Beck, S.L. and L.J. Ruff, 1984, The rupture process of the great 1979 Colombia earthquake: evidence for the asperity model; *Jour. Geophys. Res., 89,* 9281-9291.

Beck, S.L. and L.J. Ruff, 1987, Source process of the 1963 Kurile Islands earthquake; *submitted to Jour. Geophys. Res..*

Billington, S., 1980, The morphology and tectonics of the subducted lithosphere in the Tonga-Fiji-Kermadec region from seismicity and focal mechanism solutions; *Ph.D. Thesis U. of Cornell,* 220 pp.

Burbach G.V. and C. Frohlich, 1986, Intermediate and deep seismicity and lateral

structure of subducted lihtosphere in the Circum-Pacific region; *Rev. Geophs., 24,* 833-874.

Caldwell, J.G., W.F. Haxby, D.E. Karing and D.L. Turcotte, 1976, On the applicability of a universal elastic trench profile; *Earth and Planet. Sc. Lett., 31,* 239-246.

Cardwell, R.K. and B.L. Isacks, 1978, Geometry of subducted lithosphere beneath the Banda Sea in eastern Indonesia from seismicity and fault plane solutions; *Jour. Geophys. Res., 83,* 2825-2838.

Cardwell, R.K., Isacks, B.L. and D.E. Karig, 1980, The spatial distribution of earthquakes, focal mechnism solutions and subducted lithosphere in the Philippine and North Indonesia Island; *in The Tectonic and Geologic Evolution of the southeast Asian Seas and Islands, Gephys. Monogram 23, ed. D.E. Hayes, Washington D.C.,* 1-35.

Chase, C.G., 1978, Extension behind island arcs and motion relative to hot spots; *Jour. Geophys. Res., 83,* 5385-5387.

Chapple, W.M. and D.M. Forsyth, 1979; Earthquakes and bending of plates at trenches; *Jour. Geophys. Res., 84,* 6729-6749.

Chin, D.S. and B.L. Isacks, 1983, Accurate source depths and focal mechanisms of shallow earthquakes in western South America and in the New Hebrides Island arc; *Tectonics, 2,* 529-563.

Christensen, D. and L.J. Ruff, 1983, Outer-rise earthquakes and seismic coupling; *Geophys. Res. Lett., 10,* 697-700.

Christensen, D. and L.J. Ruff, 1987, Outer-rise earthquakes and their relationship to seismic coupling; *preprint*

Chung, W.Y. and H. Kanamori, 1976, Source process and tectonic implications of the Spanish deep-focus earthquake of March 29, 1954; *Phys. Earth and Planet. Int., 13,* 85-96.

Chung, W.Y. and H. Kanamori, 1978a, A mechanical model for plate deformation associated with aseismic ridge subduction in the New Hebrides arc; *Tectonophysics, 50,* 29-40.

Chung, W.Y. and H. Kanamori, 1978b, Subduction process of a fracture zone and aseismic ridges. The focal mechanism and source characteristics of the New Hebrides earthquake of 1969, January 19 and some related events; *Geophys. J. R. astr. Soc., 54,* 221-240.

Chung, W.Y. and H. Kanamori, 1980, Variation of seismic source parameters and stress drop within a descending slab and its implications in plate mechanics; *Phys. Earth and Planet. Int., 23,* 134-159.

Clowes, R.M., R. M. Ellis, Z. Jajnal and I.F. Jones, 1983; Seismic reflections from subducting lithosphere?; *Nature, 303,* 668-670.

Crosson, R.S., 1980, Review of seismicity in the Puget Sound region from 1970 to 1978; *in Proceedings of Workshop XIV, Earthquake Hazards of the Puget Sound Region, Washington, U.S. Geol. Surv., Open-File Report 83-19,* 6-18.

Dean, B.W. and C.L. Drake, 1978, Focal mechanism solutions and tectonics of the

Middle America arc; *Jour. Geology, 86,* 111-128.

Denham, D., 1977, Summary of earthquake focal mechnisms for the western Pacific-Indonesia region 1929-1973; *NOAA, U.S. Dept. of Commerce Report SE-3.*

Dewey, J.W. and S.T. Algermissen, 1974, Seismicity of the Middle America arc-trench systme near Managua, Nicaragua; *Bull. Seis. Soc. Am., 64,* 1033-1048.

Dubois, J., 1971, Propagation of P-waves and Rayleigh waves in Melanesia: structural implications; *Jour. Geophys. Res., 76,* 7217-7240.

Duda, S.J., 1963, Strain release in the Circum-Pacif belt, Chile 1960; *Jour. Geophys. Res., 68,* 5531-5544.

Dziewonski, A.M. and J.H. Woodhouse, 1983, An experiment in the systematic study of global seismicity; centroid-moment tensor solutions for 201 moderate and large earthquakes of 1981; *Jour. Geophys. Res., 88,* 3247 - 3271.

Dziewonski, A.M., A. Friedman, D. Giardini and J.H. Woodhouse, 1983a, Global seismicity of 1982: centroid-moment tensor solutions for 308 earthquakes, *Phys. Earth and Planet. Int., 33,* 76-90.

Dziewonski, A.M., A. Friedman and J.H. Woodhouse, 1983b, Centroid-moment tensor solutions for January-March 1983; *Phys. Earth and Planet. Int., 33,* 71-75.

Dziewonski, A.M., J.E. Franzen and J.H. Woodhouse, 1983c, Centroid-moment tensor solutions for April-June 1983; *Phys. Earth and Planet. Int., 33,* 243-249.

Dziewonski, A.M., J.E. Franzen and J.H. Woodhouse, 1984a, Centroid-moment tensor solutions for July-September 1983; *Phys. Earth and Planet. Int., 34,* 1-8.

Dziewonski, A.M., J.E. Franzen and J.H. Woodhouse, 1984b, Centroid-moment tensor solutions for October-December, 1983; *Phys. Earth and Plant. Int., 34,* 129-136.

Dziewonski, A.M., J.E. Franzen and J.H. Woodhouse, 1984c, Centroid-moment tensor solutions for January-March 1984; *Phys. Earth and Planet. Int., 34,* 209-219.

Dziewonski, A.M., J.E. Franzen and J.H. Woodhouse, 1985a, Centroid-moment tensor solutions for April-June 1984; *Phys. Earth and Planet. Int., 37,* 87-96.

Dziewonski, A.M., J.E. Franzen and J.H. Woodhouse, 1985b, Centroid-moment tensor solutions for July-September 1984; *Phys. Earth and Planet. Int., 38,* 203-213.

Earthquake Data Report, U.S.G.S. 1984

Ebel, J., 1980, Source processes of the 1965 New Hebrides Islands earthquakes inferred from teleseismic waveforms; *Geophys. J. R. astr. Soc., 63,* 381-403.

Eguchi, T., S. Uyeda and T. Maki, 1979, Seismotectonics and tectonic history of the Andaman Sea; *Tectonophysics, 57,* 35-51.

Engdahl, E.R., 1977, Seismicity and plate subduction in the Central Aleutians. *In : M. Talwani and W.C. Pitman III (Editors), Island Arcs, Deep Sea Trenches and Back-arc Basins. Am. Geophysical Union, Washington, D. C.*

Engdahl, E.R. and C.H. Scholz, 1977, A double Benioff zone beneath the central Aleutians: An unbending of the lithosphere; *Geophys. Res. Lett., 4,* 473-476.

Engdahl, E.R., N.H. Sleep and M.T. Lin, 1977, Plate effects in North Pacific subduction zones; *Tectonophysics, 37,* 95-116.

Fedotov, S.A., 1968, On deep structure, properties of the upper mantle, and volcanism of

the Kuril-Kamchatka island arc according to seismic data, *Am. Geophys. Un., Geophys. Monogram; 12,* 131-139.

Fedotov, S.A., S.M., Bagdasarova, I.P. Kuzin and R.Z. Tarakanov, 1971, *Earthquakes and Deep Structure of the South Kurile Island Arc, Israel Program for Scientific Translations, Jerusalem,* vi+ 249 pp.

Fitch, T.J., 1970a, Earthquake mechanisms and island arc tectonics in the Indonesian-Philippine region; *Bull. Seis. Soc. Am., 60,* 565-591.

Fitch, T.J., 1970b, Earthquake mechanisms in the Himalayan, Burmese, and Andaman regions and continental tectonics in central Asia; *Jour. Geophys. Res., 75,* 2699-2709.

Fitch, T.J., 1972, Plate convergence, transcurrent faults and internal deformation adjacent to southeast Asia and the western Pacific; *Jour. Geophys. Res., 77,* 4432-4460.

Fitch, T.J. and P. Molnar, 1970, Focal mechanisms along inclined earthquake zones in the Indonesia-Philippine region; *Jour. Geophys. Res., 75,* 1431-1444.

Forsyth, D.W., 1975, Fault plane solutions and tectonics of the south Alantic and Scotia Sea; *Jour. Geophys. Res., 80,* 1429-1443.

Frankel, A. and W.R. McCann, 1979, Moderate and large earthquakes in the South Sandwich arc: Indications of tectonic variation along a subduction zone; *Jour. Geophys. Res., 84,* 5571-5577.

Frankel, A., W.R. McCann and A.J. Murphy, 1984, Observations from a seismic network in the Virgin Island region: Tectonic structures and earthquake swarms; *Jour. Geophys. Res., 85,* 2669-2678.

Frankel, A., 1982, A composite focal mechanism for microearthquakes along the northeastern border of the Caribbean plate; *Geophys. Res. Lett., 9,* 511-514.

Fujita, K. and H. Kanamori, 1981, Double seismic zones and stresses of intermediate depth earthquakes; *Geophys. J.R. astr. Soc., 66,* 131-156.

Fukao, Y. S. Hori and M. Ukawa, 1983, A seismologica constraint on the depth of basalt-eclogite transition in a subducting oceanic crust; *Nature, 303,* 413-415.

Geller, R. and H. Kanamori, 1977, Magnitude of great shallow earthquakes from 1904 to 1952; *Bull. Seis. Soc. Am., 67,* 587-598.

Giardini, D., 1984, Systematic analysis of deep seismicity: 200 centroid moment tensor solutions for earthquakes between 1977 and 1980; *Geophys. J.R. Astr. Soc., 77,* 883-914.

Giardini, D., 1987, Quantification and frequency distribution of deep earthquakes; *submitted to Jour. Geophys. Res.*

Giardini, D., A.M. Dziewonski and J.H. Woodhouse, 1985, Centroid-moment tensor solutions for 113 large earthquakes in 1977-1980; *Phys. Earth Planet. Int., 40,* 259-272.

Giardini, D. and J.H. Woodhouse, 1984, Deep seismicity and modes of deformation in Tonga subduction zone; *Nature, 307,* 505-509.

Given, J.W. and H. Kanamori, 1980, The depth extent of the 1977 Sumbawa, Indonesia earthquake, *EOS, 61,* 1044.

González, J., K. McNally and J. Rial, 1984, Recent normal faulting in southcentral Mexico: A study of source processes and regional tectonic implications; *preprint.*

González-Ruiz, J.R., 1986, Earthquake source mechanics and tectonophyscis of the Middle America subduction zone in Mexico; *Ph.D. Thesis, U. of Calif., Santa Cruz.*

Goodstein, J.R., H. Kanamori and W. Lee, 1980, Seismology Microfiche Publications from the Caltech Archives (announcements); *Bull. Seism. Soc. Am., 70,* 657-658.

Goto, K., H. Hamaguchi and Z. Suzuki, 1985, Earthquake generating stresses in a descending slab; *Tectonophysics, 112,* 111-128.

Gutenberg, B. and Richter, C.F., 1954, *Seismicity of the Earth. Princeton University Press, Princeton, N.J. 2nd ed.,* 330pp.

Hasegawa, A. and N. Umino, 1978, Focal mechanisms and the distribution of seismicity in northeast Japan; *Progr. Abst. Seism. Soc. Jap., 1,* 34 (in Japanese)

Hasegawa, A., N.Umino, A. Takagi, Z. Suzuki, 1979, Double-planed deep seismic zone and anomalous structure in the upper mantle beneath northeastern Honshu (Japan); *Tectonophysics, 57,* 1-6.

Hasegawa, A. and S. Sacks, 1981, Subduction of the Nazca plate beneath Peru as determined from seismic observations; *Jour. Geophys. Res., 86,* 4971-4980.

Heaton, T.H. and H. Kanamori, 1984, Seismic potential associated with subduction in the Northwestern United States; *Bull. Seism. Soc. Am., 74,* 933-941.

Hilde, T.W.C. and G.F. Sharman, 1978, Fault structure of the descending plate and its influence on the subduction process; *EOS, 59,* 1182.

House, L.S. and K.H. Jacob, 1982, Thermal Stresses in Subductin Lithosphere can explain double seismic zones; *Nature, 295,* 587-589.

House, L.S. and K.H. Jacob, 1983, Earthquakes, plate subduction and stress reversals in the eastern Aleutian arc; *Jour. Geophys. Res., 88,* 9347-9373.

Hudnut, K.W. and J.J. Taber, 1987, Transition from double to single Wadati-Benioff seismic zone in the Shumagin Islands, Alaska; *Gephys. Res. Lett., 14,* 143-146.

Isacks, B.L., J. Oliver and L.R. Sykes, 1968, Seismology and the new global tectonics; *Jour. Geophys. Res., 73,* 5855-5899.

Isacks, B.L., L.R. Sykes and J.Oliver, 1969, Focal mechanism of deep and shalow earthquakes in the Tonga-Kermadec region and the tectonics of island arcs; *Geol. Soc. Am. Bull., 80,* 1443-1470.

Isacks, B.L. and P. Molnar, 1969, Mantle earthquake mechanisms and the sinking of the lithosphere; *Nature, 223,* 1121-1124.

Isacks, B.L. and P. Molnar, 1971, Distribution of stresses in the descending lithosphere from a global survey of focal-mechanisms solutions of mantle earthquakes; *Rev. Geophys. Space Phys., 9,* 103-174.

Isacks, B.L. and M. Barazangi, 1977, Geometry of Benioff zones: lateral segmentation and downward bending of the subducting lithosphere; *Am. Geophys. U., Maurice Ewing Series, 1,* 99-114.

Isacks, B.L., R.K. Cardwell, J.L. Chatelain, M. Barazang, J.M. Marthelot, D. Chim, R. Loutat, 1979, Seismicity and Tectonics of the cental New Hebrides island arc; *Am.*

Geophys. Union, Maurice Ewing Series 4, 93-116.

Ishida, M., 1970, Seismicity and travel-time anomaly in and around Japan; *Bull. Earth Res. Inst., 48,* 1023-1051.

Ishikawa, Y., 1985; Double seismic zone beneath Kysushu, Japan; *Zisin, 38,* 265-269.

Jackson, J. and T.J. Fitch, 1979, Seismotectonic implications of relocated aftershock sequences in Iran and Turkey; *Geophys. J.R. astr. Soc., 57,* 209-229.

Jackson, J., 1980, Errors in focal depth determination and the depth of seismicity in Iran and Turkey; *Geophys. J.R. astr. Soc., 61,* 285-301.

Jackson, J. and T. Fitch, 1981; Basement faulting and the focal depths of the larger earthquakes in the Zagros mountains (Iran); *Geophys. J.R. astr. Soc., 64,* 561-586.

Jacob, K.H. and R.L. Quittmeyer, 1979, The Makron region of Pakistan and Iran: trench-arc system with active plate subduction; *in Geodynamics of Pakistan.*

Jarrard, R.D., 1986; Relations among subduction parameters; *Reviews of Geophysics, 24,* 217-284.

Jimenez-Jimenez, Z., 1977, Mecanismo focal de 7 temblores (mb>5.5) occurridos en al region de Orizaba, Mexico de 1928 a 1973; *Tesis profesional, Fac. de Ciencias, U.N.A.M., Mexico.*

Johnson, T. and P. Molnar, 1972, Focal mechanism and plate tectonics of the southwest Pacific; *Jour. Geophys. Res., 77,* 5000-5032.

Kanamori, H., 1970, Seismological evidence for lithospheric normal faulting: the Sanriku earthquake of 1933; *Phys. Earth and Planet. Int., 4,* 289-300.

Kanamori, H., 1977a, The energy release in great earthquakes; *Jour. Geophys. Res., 82,* 2981-2987.

Kanamori, H., 1977b, Seismic and aseismic slip along subduction zones and their tectonic implications; *Am. Geophys. U., Maurice Ewing Series, 1,* 163-174.

Kanamori, H., 1983, Magnitude scale and quantification of earthquakes; *Tectonophysics, 9,* 185-199.

Kanamori, H., 1984, Global seismicity; *Earthquakes: observation, theory and interpretation;* Bologna, Italia. 596-608.

Kanamori, H., 1986, Rupture process of subduction-zone earthquakes; *Ann. Rev. Earth Planet. Sci., 14,* 293-322.

Kanamori, H. and K. Tsumura, 1971, Spatial distribution of earthquakes in the Kii Peninsula, Japan, south of the Median Tectonic line; *Tectonophysics, 12,* 327-342.

Kanamori, H. and J.J. Cipar, 1974, Focal process of the great Chilean earthquake May 22, 1960; *Phys. Earth Planet. Int., 9,* 128-136.

Kanamori, H. and G. Stewart, 1979, A slow earthquake; *Phys. Earth and Planet. Int., 18,* 167-175.

Kanamori, H. and K.C. McNally, 1982, Variable rupture mode of the subduction zone along the Ecuador-Colombia coast; *Bull. Seism. Soc. Am., 72,* 1241-1253.

Katsumata, M. and L.R. Sykes, 1969; Seismicity and tectonics of the western Pacific: Izu-Mariana-Caroline and Ryuku-Taiwan Region; *Jour. Geophys. Res., 74,* 5923-5948.

Kawakatsu, H., 1986a, Double Seismic Zones: Kinematics; *Jour. Geophys. Res., 91,* 4811-4825.

Kawakatsu, H., 1986b, Downdip tensional earthquakes beneath the Tonga arc: A double seismic zone? ; *Jour. Geophys. Res., 91,* 6432-6440.

Kawakatsu, H. and T. Seno, 1983, Triple seismic zone and the regional variation of seismicity along the northern Honshu arc; *Jour. Geophys. Res., 88,* 4215-4230.

Kelleher, J., 1972, Rupture zones of large South American earthquakes and some predictions; *Jour. Gephys. Res., 77,* 2087-2103.

Kelleher, J., J. Savino, H. Rowlett and W. McCann, 1974, Why and where great thrust earthquakes occur along island arcs; *Jour. Geophys. Res., 79,* 4889-4899.

Korrat, I. and R. Madariaga, 1986, Rupture of the Valparaiso (Chile) gap from 1971 to 1985; *preprint.*

Langston, C.A. and D.V. Helmberger, 1975, A procedure for modeling shallow dislocation sources; *Geophys. J. R. astr. Soc., 42,* 117-130.

Langston, C.A. and D.E. Blum, 1977, The April 29, 1965 Puget Sound earthquake and the crustal and upper mantle structure of western Washington; *Bull. Seism. Soc. Am., 67,* 693-711.

Lay, T. and H. Kanamori, 1980, Earthquake Doublets in the Solomon Islands; *Phys. Earth and Planet. Int., 21,* 283-304.

LeDain, A.Y., P. Tapponier and P. Molnar, 1984, Active faulting and tectonics of Burma and surrounding regions; *Jour. Geophys. Res., 89,* 453-472.

LeFevre, L.V. and K.C. McNally, 1985, Stress distribution and subduction of aseismic ridges in the Middle America subduction zone; *Jour. Geophys. Res., 90,* 4495-4510.

Maki, T., 1984, Focal mechanism and spatial distribution of subcrustal earthquakes occuring in clusters beneath the Kanto district; *Bull. Earth. Res. Inst., Univ. of Tokyo, 59,* 127-196.

Malgrange, M., A. Deschamps and R. Madariaga, 1981, Thrust and extensional faulting under the Chilean coast, 1965, 1971 Aconcagua earthquakes; *Geophys. J. R. astr. Soc., 66,* 313-331.

Malgrange, M. and R. Madariaga, 1983, Complex distribution of large thrust and normal fault earthquakes in the Chilean subduction zone; *Geophys. Jour. Res. astr. Soc., 73,* 489-506.

McCaffrey, R., P. Molnar, S.W. Roecker, Y. Joyodiwiryo, 1985, Microearthquake seismicity and fault plane solutions related to arc-continent collision in the eastern Sunda arc, Indonesia; *Jour. Geophys. Res., 90,* 4511-4528.

McCann, W.R., S.P. Nishenko, L.R. Sykes and J. Krause, 1979, Seismic gaps and plate tectonics: seismic potential for major boundaries; *Pageoph., 117,* 1082-1147.

McCann, W.R. and L.R. Sykes, 1984, Subduction of aseismic ridges beneath the Caribbean plate: implications for the tectonic and seismic potential of the northeastern Caribbean; *Jour. Geophys. Res., 89,* 4493-4519.

McKenzie, D., 1978, Active tectonics of the Alpine-Himalaya belt: the Aegean Sea and surrounding regions; *Geophys. J.R. astr. Soc., 55,* 217-254.

McNally K.C. and B. Minster, 1981, Nonuniform seismic slip ratesd along the Middle America trench; *Jour. Geophys. Res., 86,* 4949-4959.

McNally K.C., J.R. Gonzalez-Ruiz and C. Stolte, 1986; Seismogenesis of the 1985 Great (M_s=8.1) Michoacan, Mexico earthquake; *Geophys. Res. Lett., 13,* 585-588.

Michael-Leiba, M.O., 1984, The Banda Sea earthquake of 24 November 1983: evidence for intermediate-depth thrust faulting in the Benioff zone; *Phys. Earth and Planet. Int., 36,* 95-98.

Minster J.B. and T.H. Jordan, 1978, Present day plate motions; *Jour. Geophys. Res., 83,* 5331-5354.

Mogi, K., 1973, Relationship between shallow and deep seismicity in the western Pacific region; *Tectonophysics, 17,* 1-22.

Molnar, P. and L.R. Sykes, 1969, Tectonics of the Caribbean and Middle-America regions from focal mechanisms and seismicity; *Geol. Soc. Am. Bull., 80,* 1639-1684.

Molnar, P., D. Freedman, and J. Shih, 1979, Lengths of intermediate and deep seismic zones and temperatures in downgoing slabs of lithosphere; *Geophys. J. R. Astr. Soc., 56,* 41-54.

Moore, G.W., 1982, Plate tectonic map of the circum Pacific region, explanatory notes: Tulsa, Okla., *American Ass. of Petroleum Geologist,* 14 pp.

Newcomb, K.R. and W.R.McCann, 1987, Seismic history and seismotectonics of the Sunda arc; *Jour. Geophys. Res., 92,* 421-440.

Nishenko, S.P., 1985, Seismic Potential for large and great interplate earthquakes along the Chilean and Southern Peruvian margins of South America: A quantitative reappraisal; *Jour. Geophs. Res., 90.,* 3589-3616.

Nishimura, C., D.S. Wilson and R.N. Hey, 1984, Pole of rotation analysis of present-day Juan de Fuca plate motion; *Jour. Geophys. Res., 89,* 10283-10290.

Oike, K., 1971, On the nature and occurrence of intermediate and deep earthquakes. 1. The world-wide distribution of the earthquake generating stress; *Bull. Disas. Prev. Res. Inst., Kyoto U., 20,* 145-182.

Osada, M. and K. Abe, 1981, Mechanism and tectonic implications of the great Banda Sea earthquake of November 4, 1963; *Phys. Earth and Planet. Int., 25,* 129-139.

Pascal, G., J. Dubouis, M. Barazangi, B.L. Isacks and J. Oliver, 1973, Seismic velocity anomalies beneath the New Hebrides Island arc: evidence for a detached slab in the Upper-mantle; *Jour. Geophys. Res., 78,* 6998-7004.

Pascal, G., B.L. Isacks, M. Barazangi, R. Dubois, 1978, Precise relocations of earthquakes and seismotectonics of the New Hebrides island arc; *Jour. Geophys. Res., 83,* 4957-4973.

Pascal, G., 1979, Seismotectonics of the Papua-New Guinea-Solomon Island region; *Tectonophysics, 57,* 7-34.

Pennington, W.D., 1983, Role of shallow phase changes in the subduction of oceanic crust; *Science, 220,* 1045-1047.

Plafker, G. and J.C. Savage, 1970, Mechanism of the Chilean earthquakes of May 21 and 22, 1960; *Geol. Soc. Am. Bull., 81,* 1001-1030.

Rastogi, B.K. and D.D. Singh, 1978, Source parameters of the Burma-India border earthquake of July 29, 1970 from body waves; *Tectonophysics, 51*, T77-T84.

Reid, I.D., 1976, The Rivera plate: A study in seismology and plate tectonics; *Ph. D. Thesis, Univ. of Calif. San Diego.*

Richter, F.M., 1979, Focal Mechanisms and seismic energy release of deep and intermediate earthquakes in the Tonga-Kermadec region and their bearing on the depth extent of mantle flow; *Jour. Geophys. Res., 84*, 6783-6795.

Ripper, I.D., 1974, Some earthquake mechanisms in the New-Guinea Solomon Island region, 1963-1968; *Bur. Miner. Res. Aust., Report No. 178.*

Ripper, I.D., 1975, Some earthquake focal mechanism in the New Guinea-Solomon Island region, 1969-1971; *Bur. Miner. Res. Aust., Report No. 192.*

Ritsema, A.R., 1964, Some reliable fault plane solutions; *Pure Appl. Geophys., 59*, 58-74.

Ruff, L. and H. Kanamori, 1980, Seismicity and the subduction process; *Phys. Earth Planet. Int., 23*, 240-252.

Ruff, L. and H. Kanamori, 1983; Seismic coupling and uncoupling at subduction zones; *Tectonophysics, 99*, 99-117.

Samowitz, I.R., and D.W. Forsyth, 1981; Double seismic zone beneath the Mariana Island arc; *Jour. Geophys. Res., 86*, 7013-7021.

Sasatani, T., 1976,, Mechanisms of mantle earthquakes near the junction of the Kurile and northern Honshu arcs; *Jour. Phys. Earth, 24*, 341-354.

Schwartz, S. and L.J.Ruff, 1987, Asperity distribution and earthquake occurrence in the Southern Kurile Islands Arc; *submitted to Jour. Geophys. Res.*

Schweller, W.J., L.D. Kulm and R.A. Prince, 1981, Tectonics, structure and sedimentary framework of the Peru-Chile trench; *Geol. Soc. Am. Mem., 154*, 323-349.

Sclatter, J.G. and B. Parsons, 1981, Oceans and Continents: Similarities and differences in the mechanisms of heat loss; *Jour. Geophys. Res., 86*, 11535-11552.

Seismological Notes, 1934, *Bull. Seism. Soc. Am., 24*, 141.

Seismological Notes, 1949, *Bull. Seism. Soc. Am., 39*, 24-225.

Seno, T., 1977, The instantaneous rotation vector of the Philippine Sea plate relative to the Eurasian plate; *Tectonophysics, 42*, 209-226.

Seno, T. and K. Kurita, 1978, Focal mechanism and tectonics in the Taiwan-Philippine region; *J. Phys. Earth, 26 Suppl.,* S249-S263.

Seno, T. and B. Pongswat, 1981, A triple-planed structure of seismicity and earthquake mechanisms at the subduction zone off Miyagi Prefecture, northern Honshu, Japan; *Earth and Planet. Sc. Lett., 55*, 25-36.

Shiono, K., T. Mikumo and Y. Ishikawa, 1980, Tectonics of the Kyushu-Ryukyu arc as evidenced from seismicity and focal mechanisms of shallow to intermediate depth earthquakes; *Jour. Phys. Earth, 28*, 17-43.

Silver, P.G. and T.H. Jordan, 1983, Total moment spectra of fourteen large earthquakes; *Jour. Geophys. Res., 88*, 3273-3293.

Singh, S.K., L. Astiz and J. Havskov, 1981, Seismic gaps and recurrence periods of large

earthquakes along the Mexican subduction zone: A reexamination; *Bull. Seis. Soc. Am., 71,* 827-843.

Singh, S.K., G. Suarez, and T. Dominguez, 1985, The Oaxaca, Mexico, earthquake of 1931: lithospheric normal faulting in the subducted Cocos plate; *Nature, 317,* 56-58.

Sleep, N.H., 1973, Teleseismic P-wave transmission through slabs; *Bull. Seis. Soc. Am., 63,* 1349-1373.

Sleep, N. H., 1979, The double seismic zone in downgoing slabs and the viscocity of the mesosphere; *Jour. Geophys. Res., 84,* 4565-4571.

Soedarmo, P.D., 1973, Focal Mechanisms of earthquake generating stress system in the Indonesia region; *presented at Symposium on Recent Crustal Movements, Bandung.*

Spence, W., 1986, The 1977 Sumba earthquake series: evidence for slab pull force acting at a subduction zone; *Jour. Geophys. Res., 91,* 7693-7701.

Spence, W., 1987, Slab pull and the seismotectonics of subducting lithosphere; *Rev. Geophy., 25,* 55-70.

Stauder, W., 1968, Tensional character of earthquake foci beneath the Aleutian trench with relation to sea-floor spreading; *Jour. Geophys. Res., 73,* 7693-7701.

Stauder, W., 1972, Fault motion and spatially bounded character of earthquakes in Amchitka Pass and the Delarof islands; *Jour. Geophys. Res., 77,* 2072-2080.

Stauder, W. 1973, Mechanisms and spatial distribution of the Chilean earthquakes with relation to subduction of the oceanic plate; *Jour. Geophys. Res., 78,* 5033-5061.

Stauder, W. 1975, Subduction of the Nazca plate under Peru as evidence by focal mechanisms and seismicity; *Jour. Geophys. Res., 80,* 1053-1064.

Stauder, W. and G. A. Bollinger, 1966, The S-wave project for focal mechanism studies: Earthquakes of 1963; *Bull. Seism. Soc. Am. 56,* 1363-1371.

Stauder, W. and L. Maulchin, 1976, Fault motion in the larger earthquakes of the Kurile-Kamchatka arc and the Kurile-Hokkaido corner; *Jour. Geophys. Res., 81,* 2297-308.

Stein, S., J.F. Engeln, D.A. Wiens, R.C. Speed and K. Fujita, 1982, Subduction, seismicity and tectonics in the Lesser Antilles arc; *Jour. Geophys. Res., 87,* 8642-8664.

Stevenson D. and J.S. Turner, 1977, The Angle of Subduction; *Nature, 270,* 334-336.

Suzuki, S. and Y. Motoya, 1978; Microearthquake activity and a two-layered deep seismic zone in the Hokkaido region; *Abst. Progr. Seism. Soc. Jap.,* 1, 32 (in Japanese).

Sykes, L.R., 1966, Seismicity and deep structure of island arcs; *Jour. Geophys. Res., 71,* 2981-3006.

Sykes, L.R., 1971, Aftershock zones of great earthquakes, seismicity, gaps and earthquake prediction for Alaska and the Aleutians; *Jour. Geophys. Res, 76,* 8021-8041.

Sykes, L.R. and R.C. Quitmeyer, 1981, Repeat times of great earthquakes along simple plate boundaries; *In: D.W. Simpson and P.G. Richards (Editors), Earthquake Prediction, an International Review. American Geophysical Union, Washington, D.C.,* pp. 217-247.

Sykes, L.R., W.R. McCann and A.L. Kafka, 1982; Motion of the Caribbean plate during the last 7 m.y. and implications for earlier cenozoic movements; *Jour. Geophys. Res., 87,* 10656-10676.

Tsumara, K., 1973, Microearthquake activity in the Kanto district, in *Special Publication for the 50th Anniversary of the Great Kanto Earthquake, Earthquake Research Institute, Tokyo,* 67-87.

Uyeda, S., 1984, Subduction zones: their diversity, mechanism and human impact; *Geo Journal, 84,* 381-406.

Uyeda, S. and H. Kanamori, 1979, Back-arc opening and the mode of subduction; *Jour. Geophys. Res., 80,* 1053-1064.

Vassiliou, M.S., 1984, The state of stress in subducting slabs as revealed by earthquakes analyzed by moment tensor inversion; *Earth and Planet. Sc. Lett., 69,* 195-202.

Vassiliou, M.S., B.H. Hager and A. Raefsky, 1984, The distribution of earthquakes with depth and stress in subducting slabs; *Jour. Geodynamics, 1,* 11-28.

Veith, K., 1974, The relationship of island and seismicity to plate tectonics, *Ph.D. Thesis, South Methodist Univ., Dallas, Tx.*

Veith, K., 1977, The nature of the dual zone of seismicity in the Kuriles arc; *EOS, 58,* 1232.

Vlaar N.J. and M.J.R. Wortel, 1976. Lithospheric aging, instability, and subduction; *Tectonophysics, 32,* 331-351.

Yamaoka, K., Y. Fukao and M. Kumazawa, 1986, Spherical shell tectonics: effects of sphericity and inextensibility on the geometry of the descending lithosphere; *Reviews of Geophys., 24,* 27-54.

Wesnousky, S.G., L. Astiz and H. Kanamori, 1986, Earthquake multiplets in the Southeastern Solomon Islands; *Phys. Earth and Planet. Int., 44,* 304-318.

Wickens, A.J. and J.H. Hodgon, 1967, Computer re-evaluation of earthquake mechanism solutions 1922-1962; *Publs. Dom. Obs., 33,* 1-560.

Wortel, R., 1982, Seismicity and rheology of subducted slabs; *Nature, 296,* 553-555.

Yoshii, T., 1977, Structure of the Earth's crust and mantle in northeast Japan, *Kagaku, 47,* 170-176.

Yoshii, T., 1979, A detailed cross section of the deep seismic zone beneath Japan; *Tectonophysics, 55,* 349-360.

Appendix 1

The depth and time distribution of large intermediate and deep focus earthquakes that occurred between 1904 and 1984 is shown by a series of figures in this appendix. These events are listed by regions in Table A.1. Earthquake hypocenters were taken from Abe(1981) for all events prior to 1960. The parameters for intermediate-depth events (40 to 200 km deep) are taken from Table 1.3, while data for deeper events are taken from the NOAA catalog. Magnitudes are m_B for events that occurred before 1975. M_w is given for events that occurred thereafter, and m_B values are calculated from the relation $m_B = 0.63M_w + 2.5$ (Kanamori, 1983). In the figures we show the m_B value for all events. The seismic moment, M_o, can be computed from the relation

$$logM_o = 2.4m_B + 10.1$$

given by Kanamori (1983) for intermediate and deep focus events.

The figures on the left hand side show magnitude-depth distribution. Diamonds indicate events that occurred after 1960, presumably with more reliable locations. The arrows indicate the extent of continuous seismicity for each region (Table 1.1). Observations made on the variation of magnitude of this century, large, intraplate earthquakes and depth are strongly dependent not only on the accuracy of m_B to measure earthquake size, but also on the accuracy of the event location. We assume that they are approximately correct. Although some regions in South America (Colombia(1), Ecuador (2), Peru(3) and North Chile (5)) have deep events, it is unclear if a continuous slab is present or if the shallow and deep seismicity is unrelated (Stauder, 1975). The seismic activity stops at about 250 km and reappears at about 550 km depth at

about the same horizontal distance from the trench. Note that the Rivera and the Nankai Trough regions are not included in Table A.1. These regions have young, short subducting slabs (Table 1.1) and no large event deeper than 40 km has occurred there during this century.

The figures on the right-hand side display the time distribution for each region of large a) intermediate and deep focus earthquakes, and b) shallow events with $M_s \geq 7.5$, which are listed in Table A.2. Large, shallow intraplate events (event B in Figure 1.1) are indicated by an open circle in the figures. Note that the occurrence of intraplate large events in some regions such as the Altiplano(4), North Chile(5), Kuriles(17), Northeast Japan(18), Timor(30), New Hebrides(35), Tonga(36), and the Hindu-Kush(39) regions have been relatively constant in the last 80 years. However, some other regions such as the Ryukyu(21) and Sulawesi(23) were especially active in large events in the early part of the century, whereas other regions such as Peru(3) and New Guinea(31) appear more active in recent decades. This text replaces figure captions.

PERU(3)

ALTIPLANO(4)

NORTH CHILE(5)

CENTRAL CHILE(6)

SOUTH CHILE(7)

SCOTIA(8)

MEXICO(9)

CENTRAL AMERICA(10)

GREATER ANTILLES(11)

LESSER ANTILLES(12)

JUAN DE FUCA(13)

ALASKA(14)

ALEUTIANS(15)

KAMCHATKA(16)

KURILES(17)

NORTHEAST JAPAN(18)

LUZON(23)

PHILIPPINES(24)

SULAWESI(25)

BURMA(26)

ANDAMAN(27)

SUNDA(28)

JAVA(29)

TIMOR(30)

NEW GUINEA(31)

NEW BRITAIN(32)

NEW HEBRIDES(35)

TONGA(36)
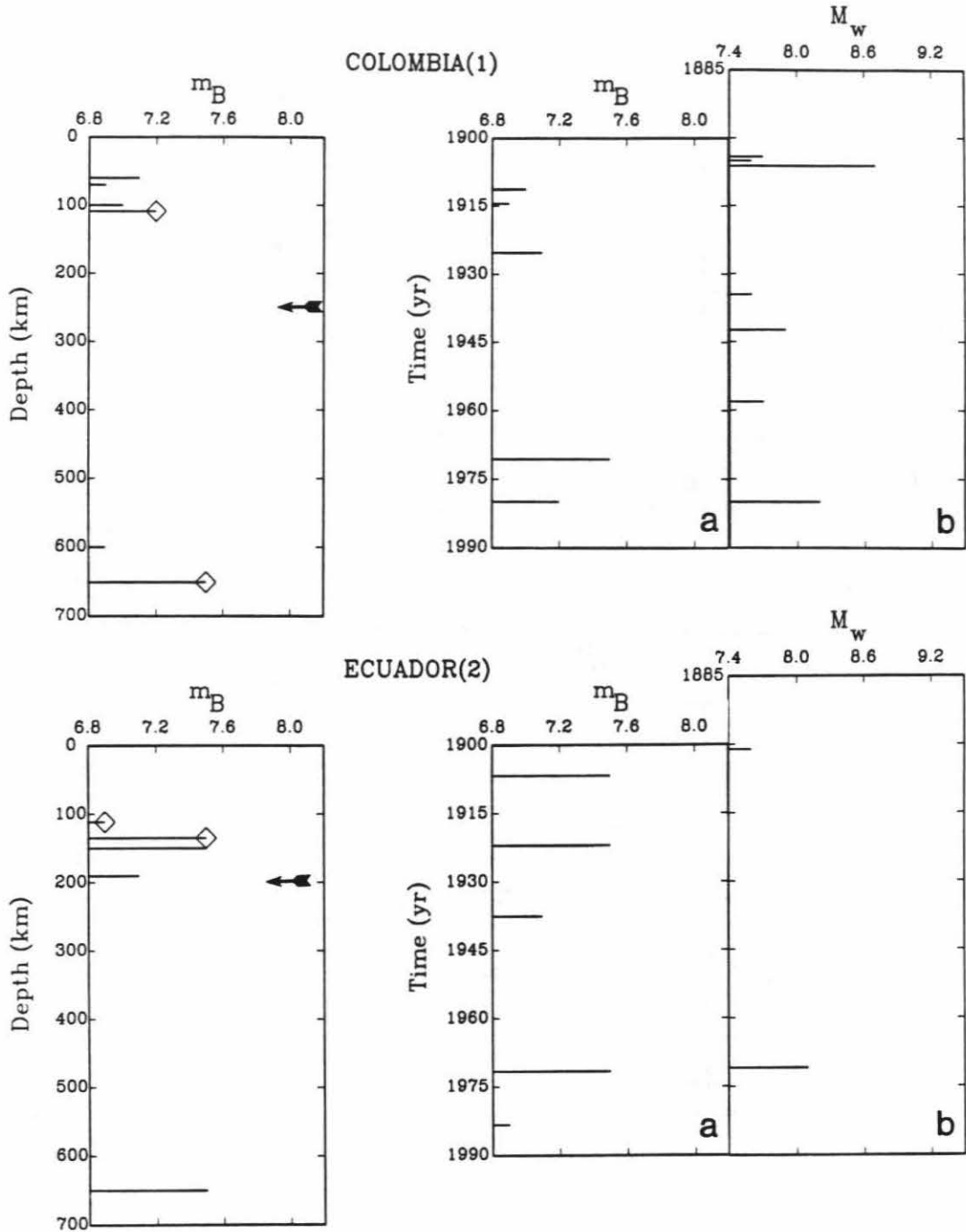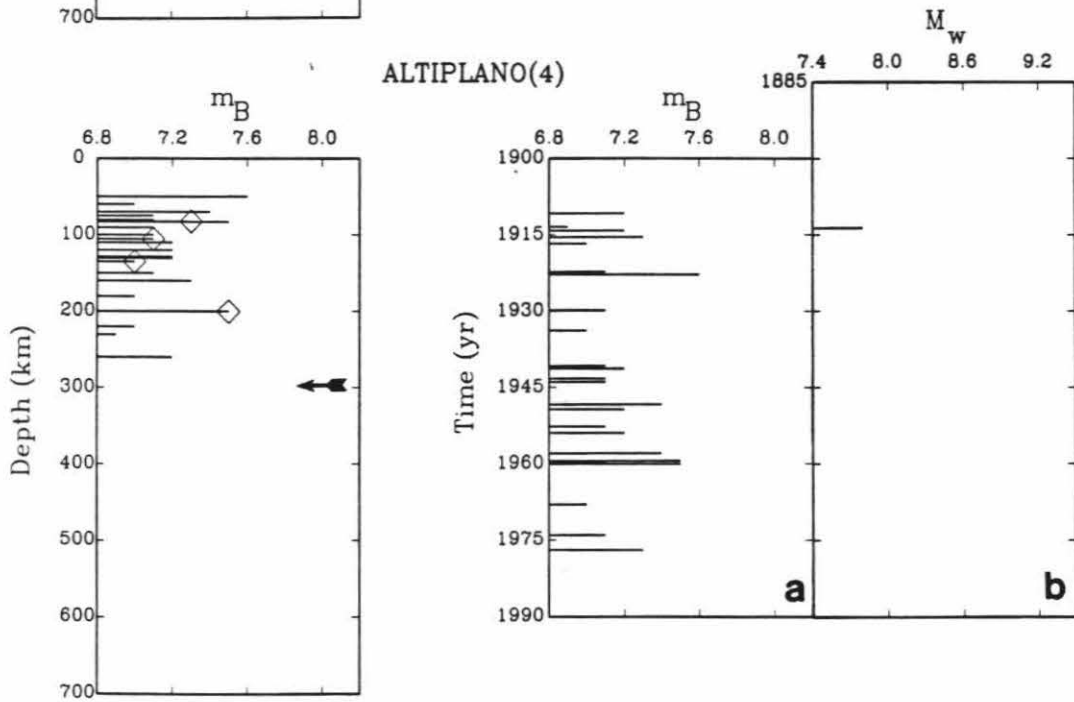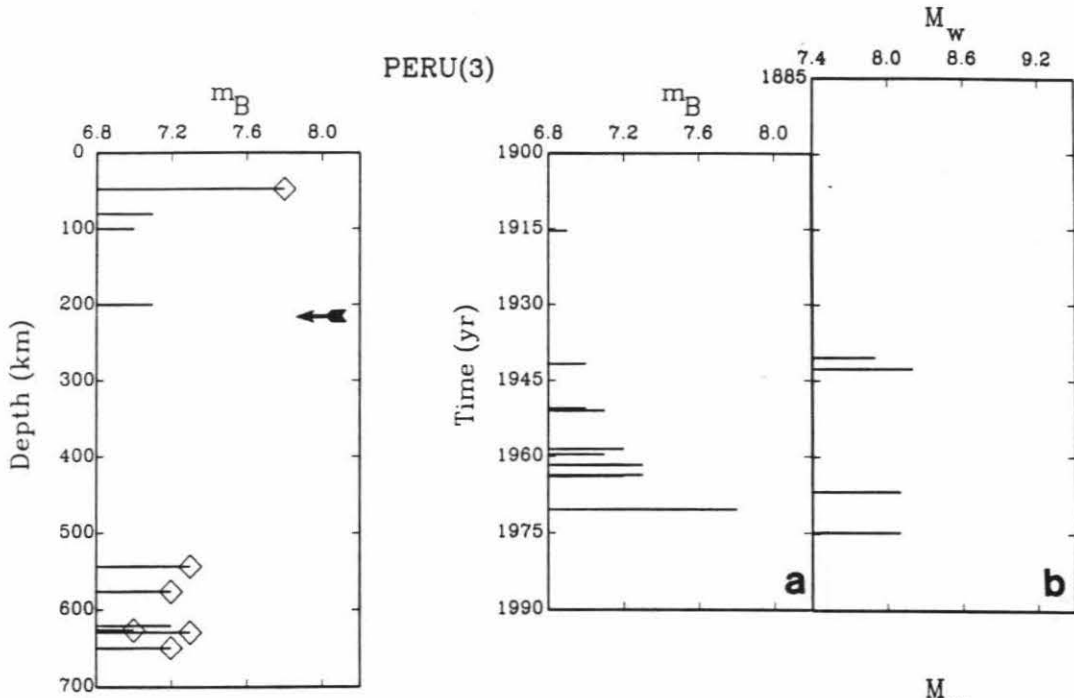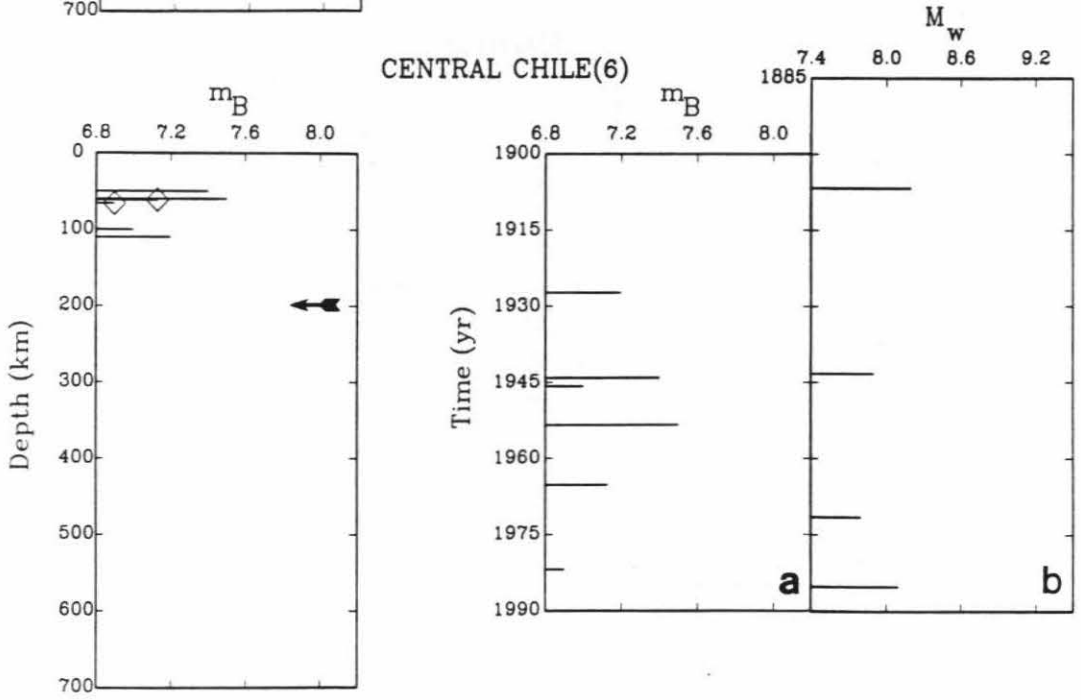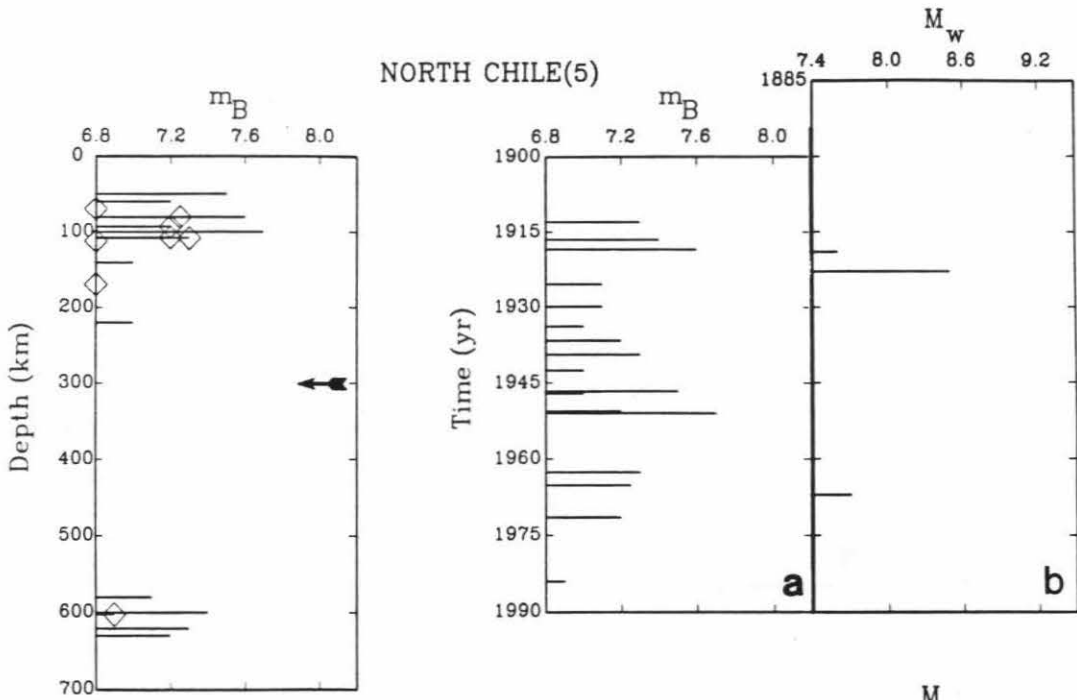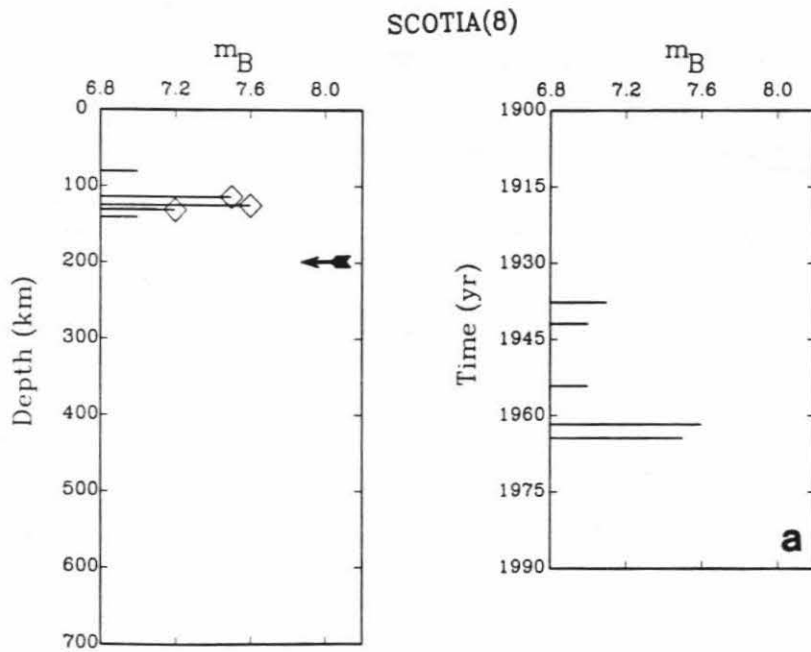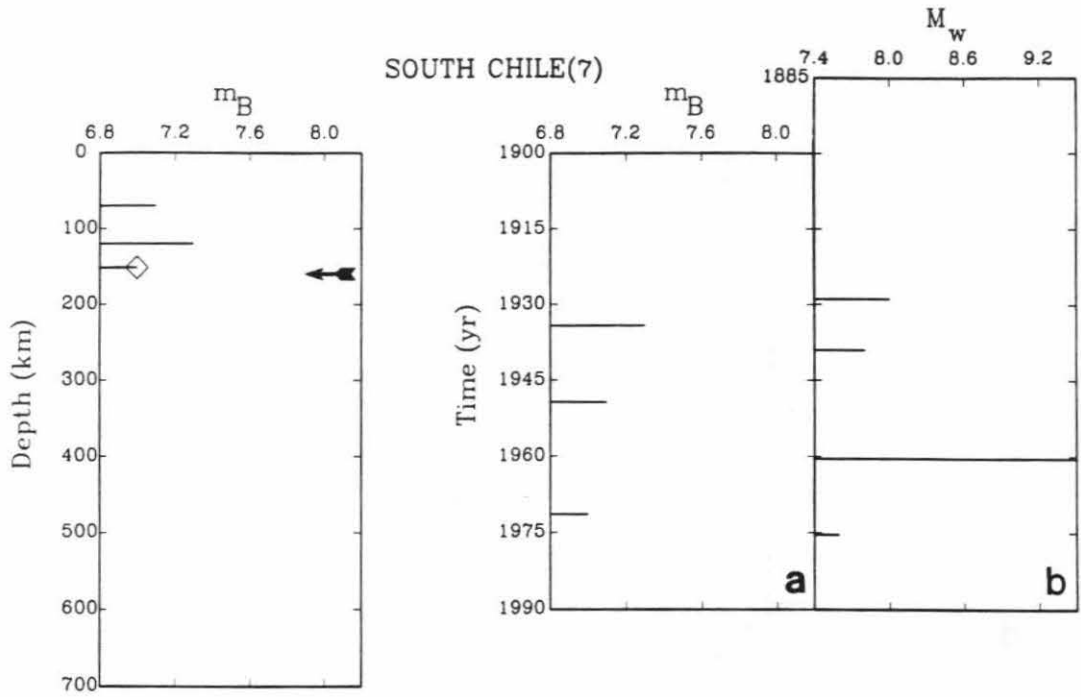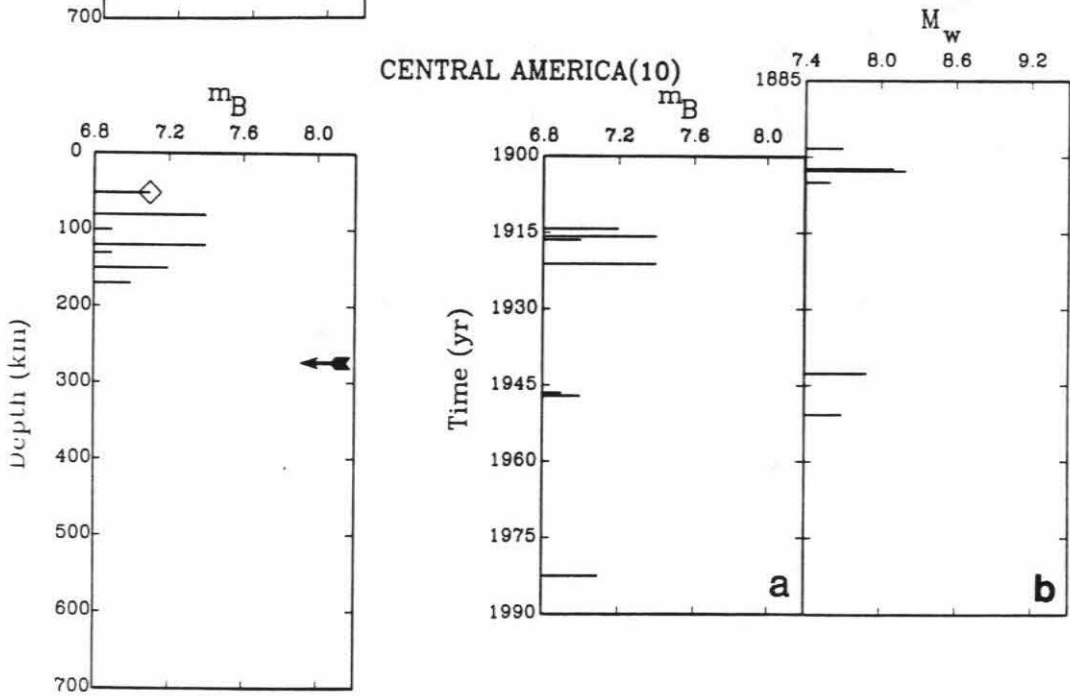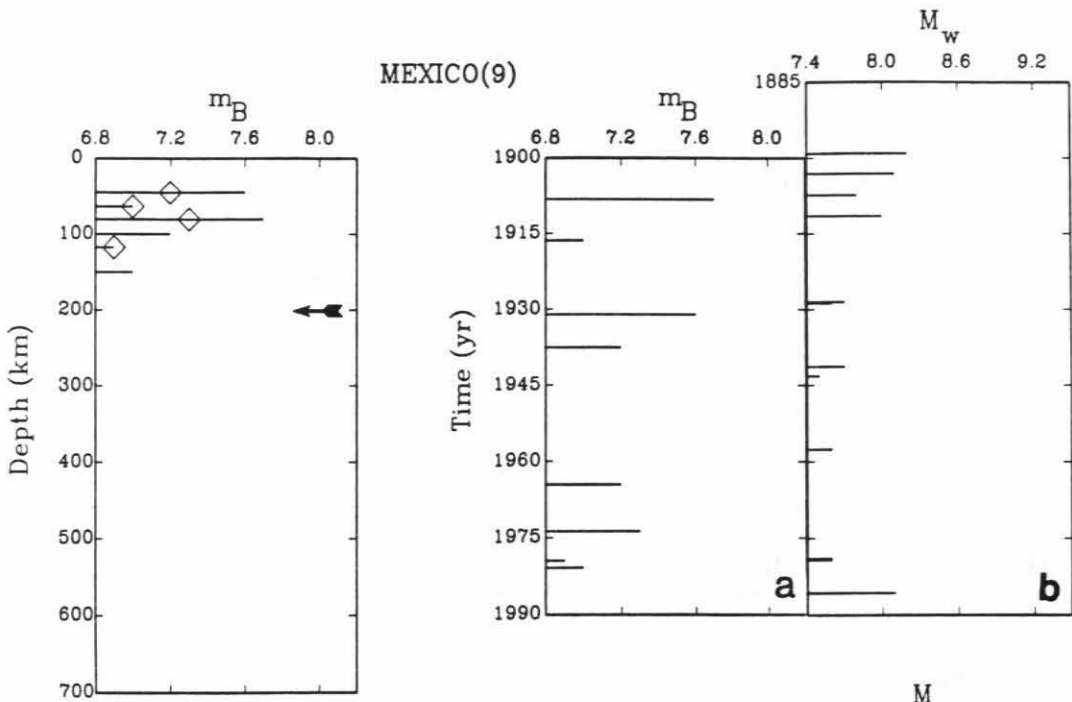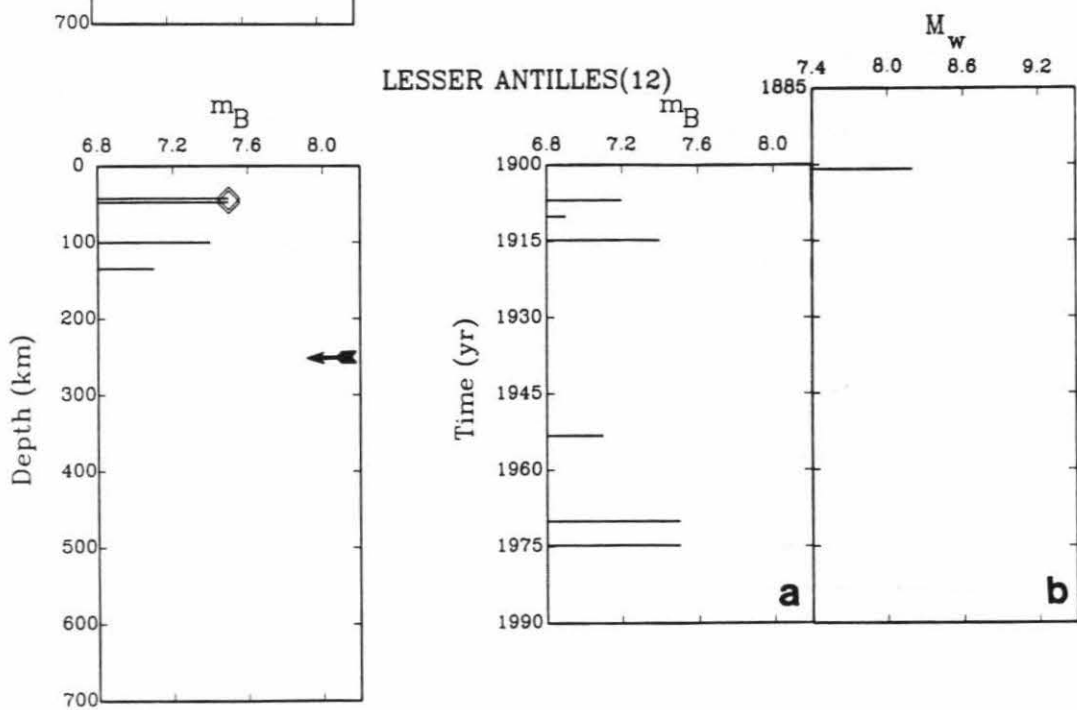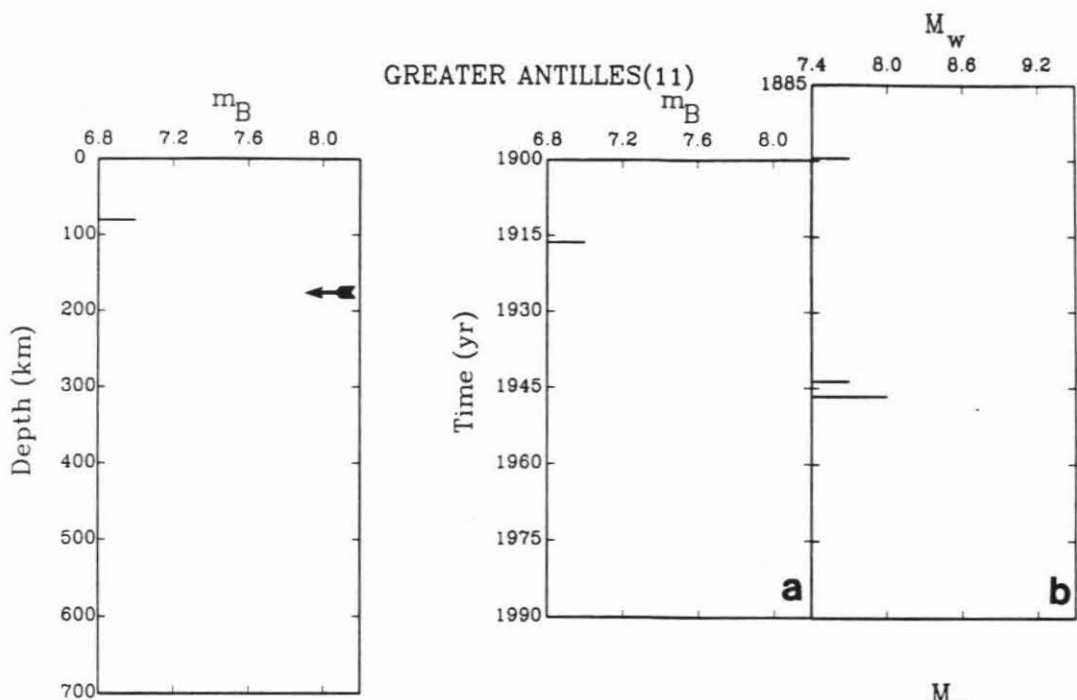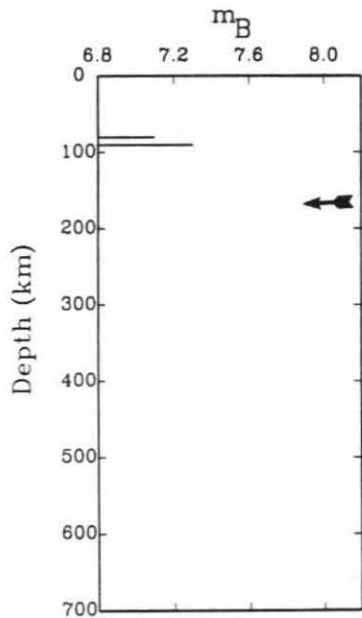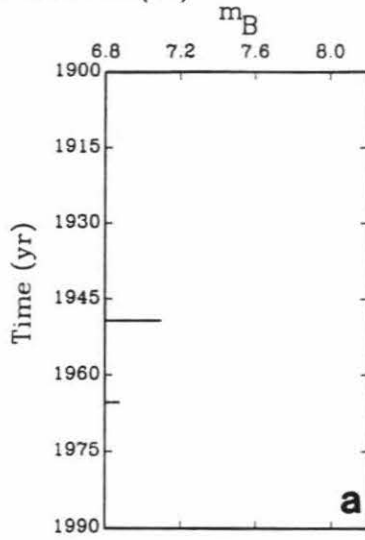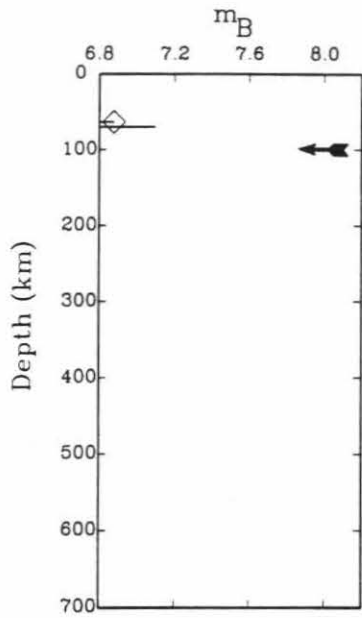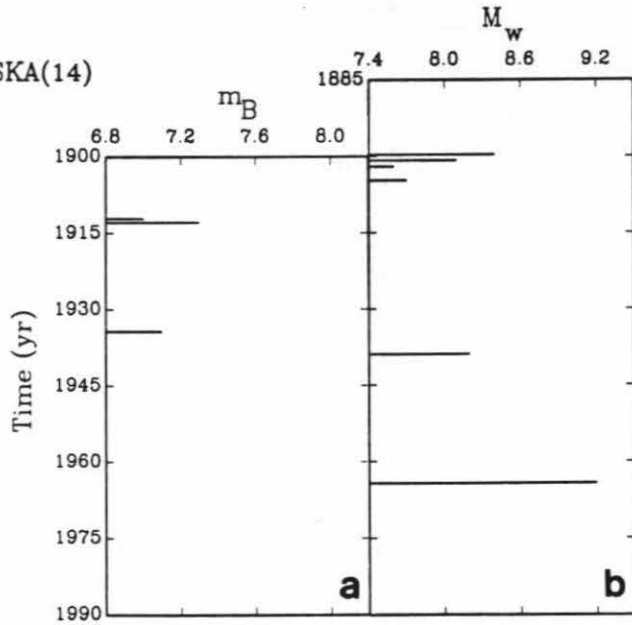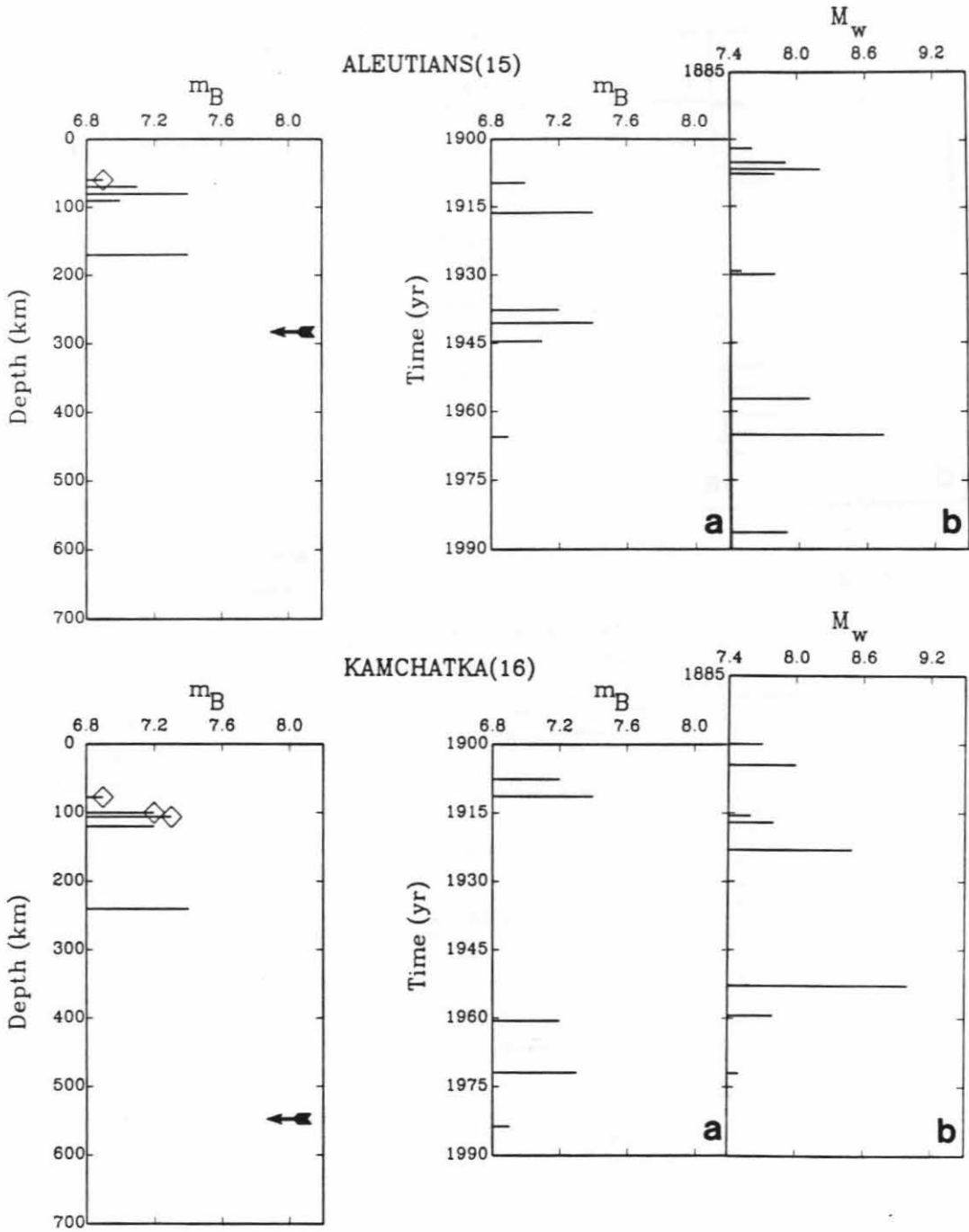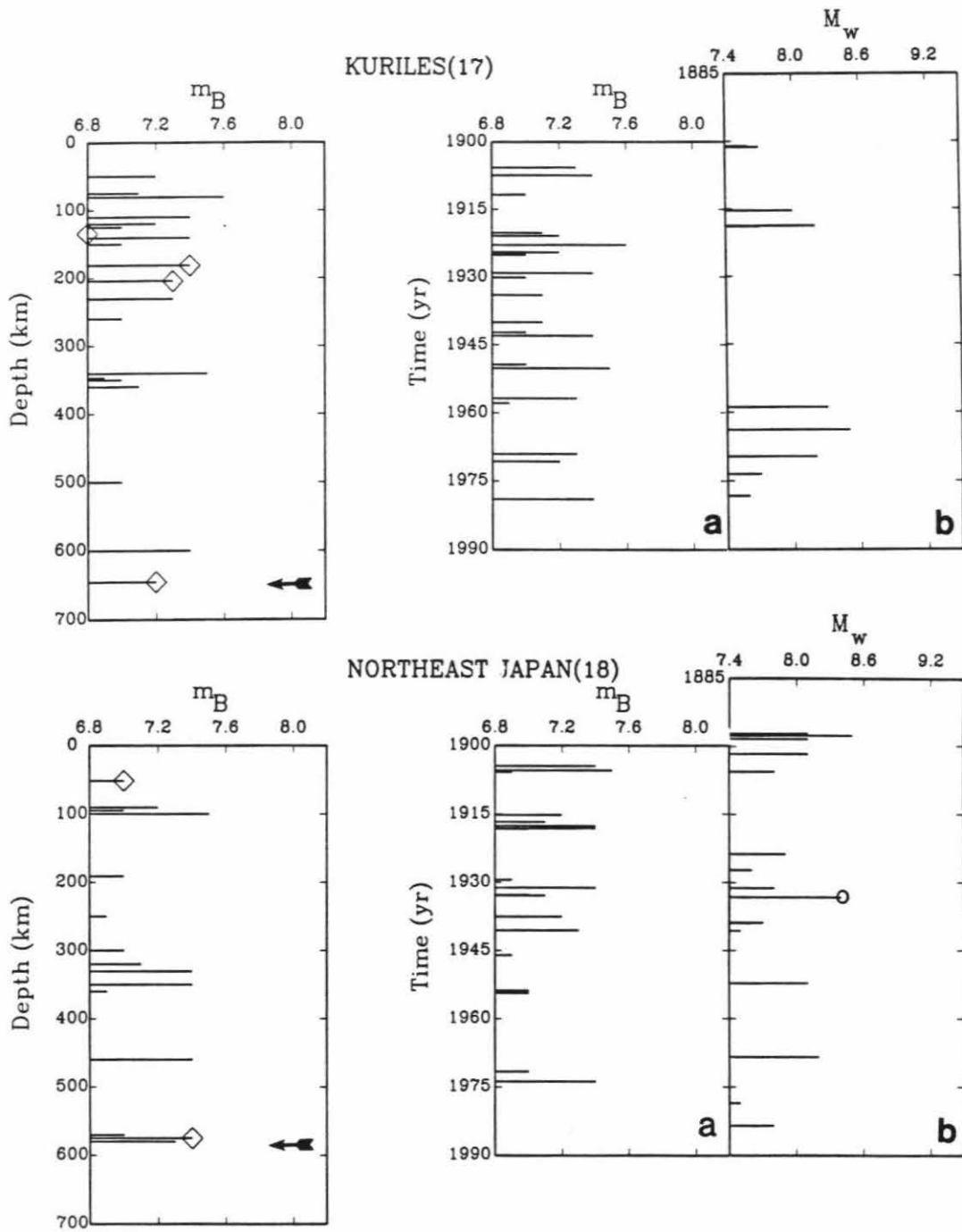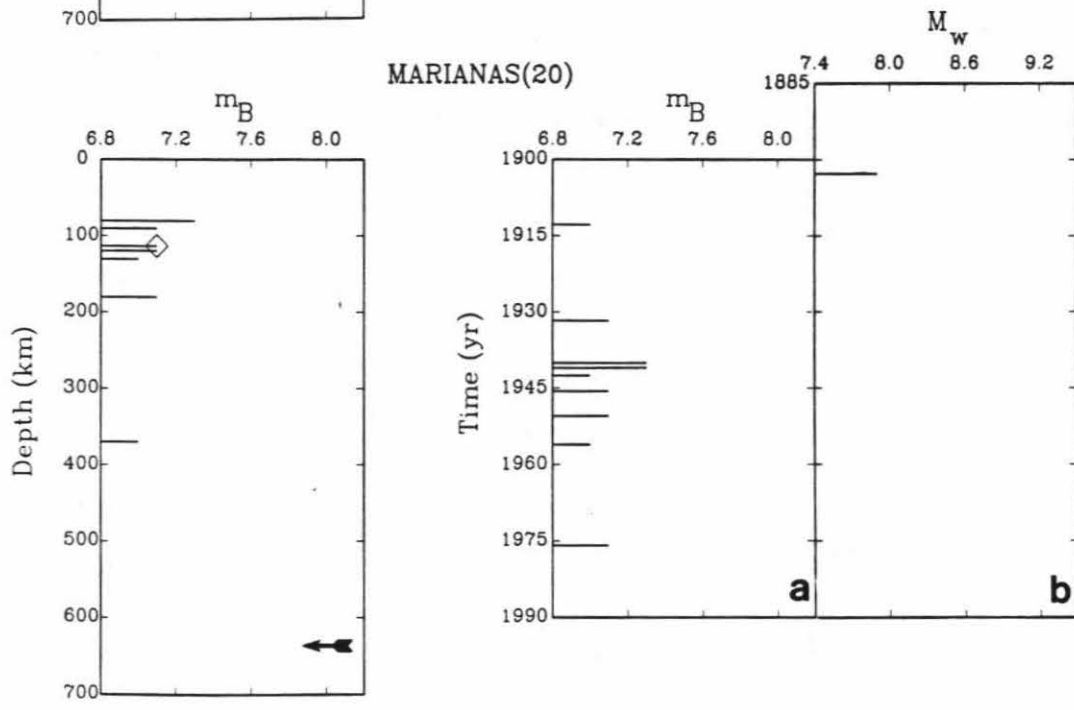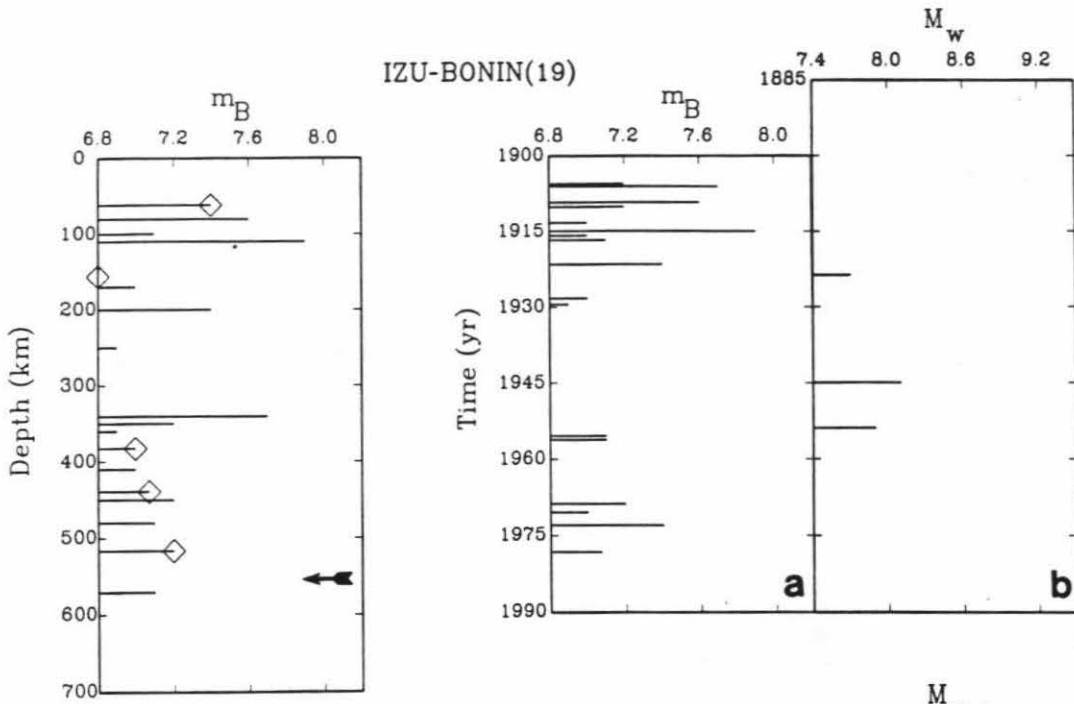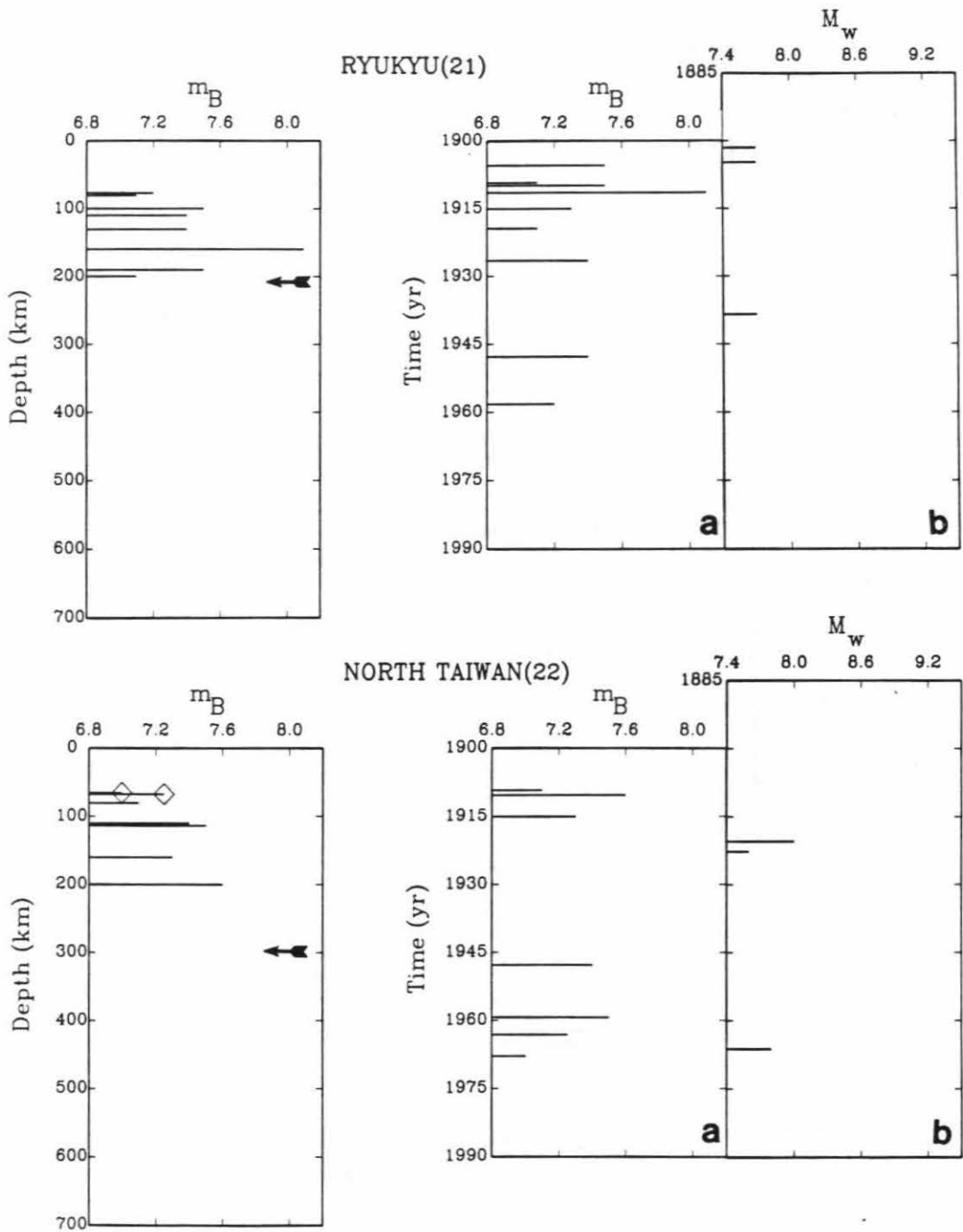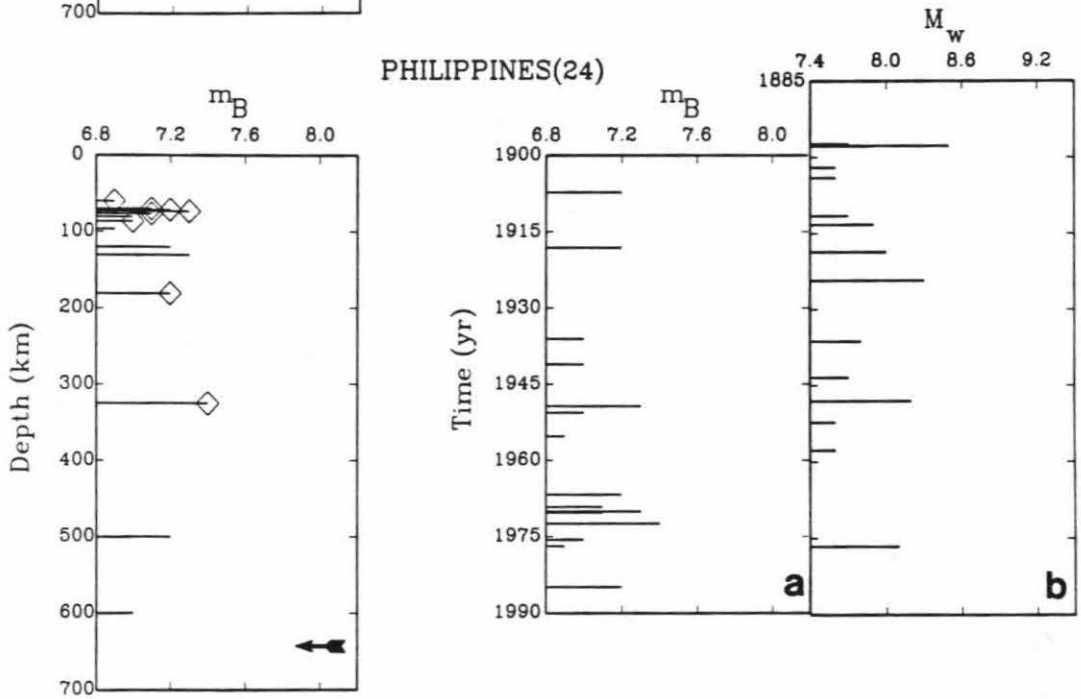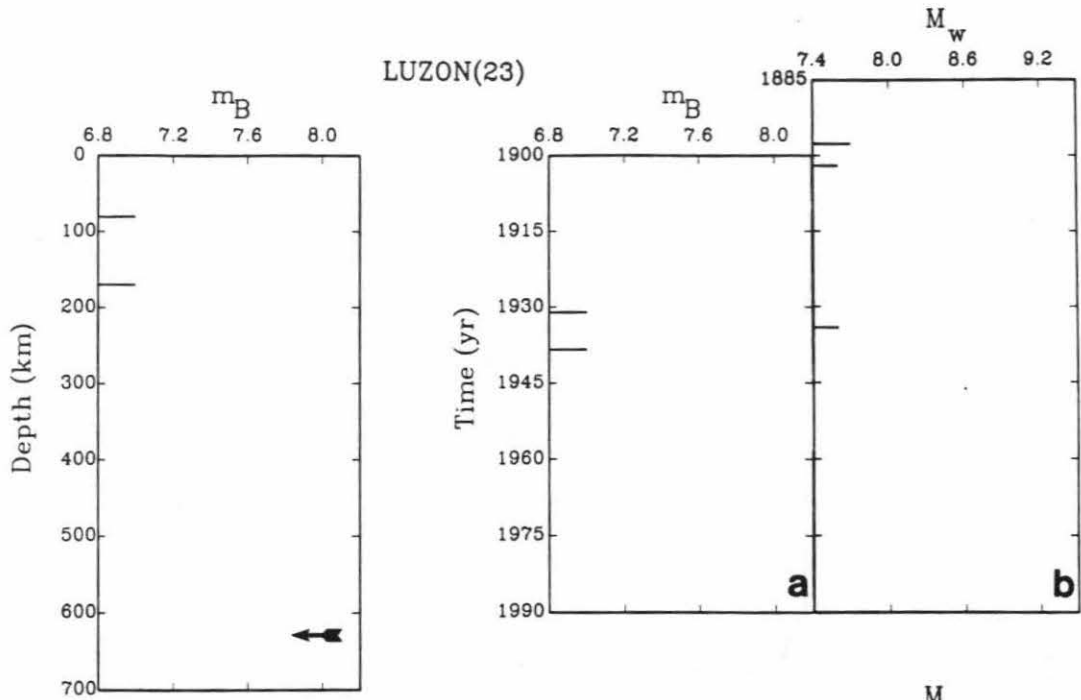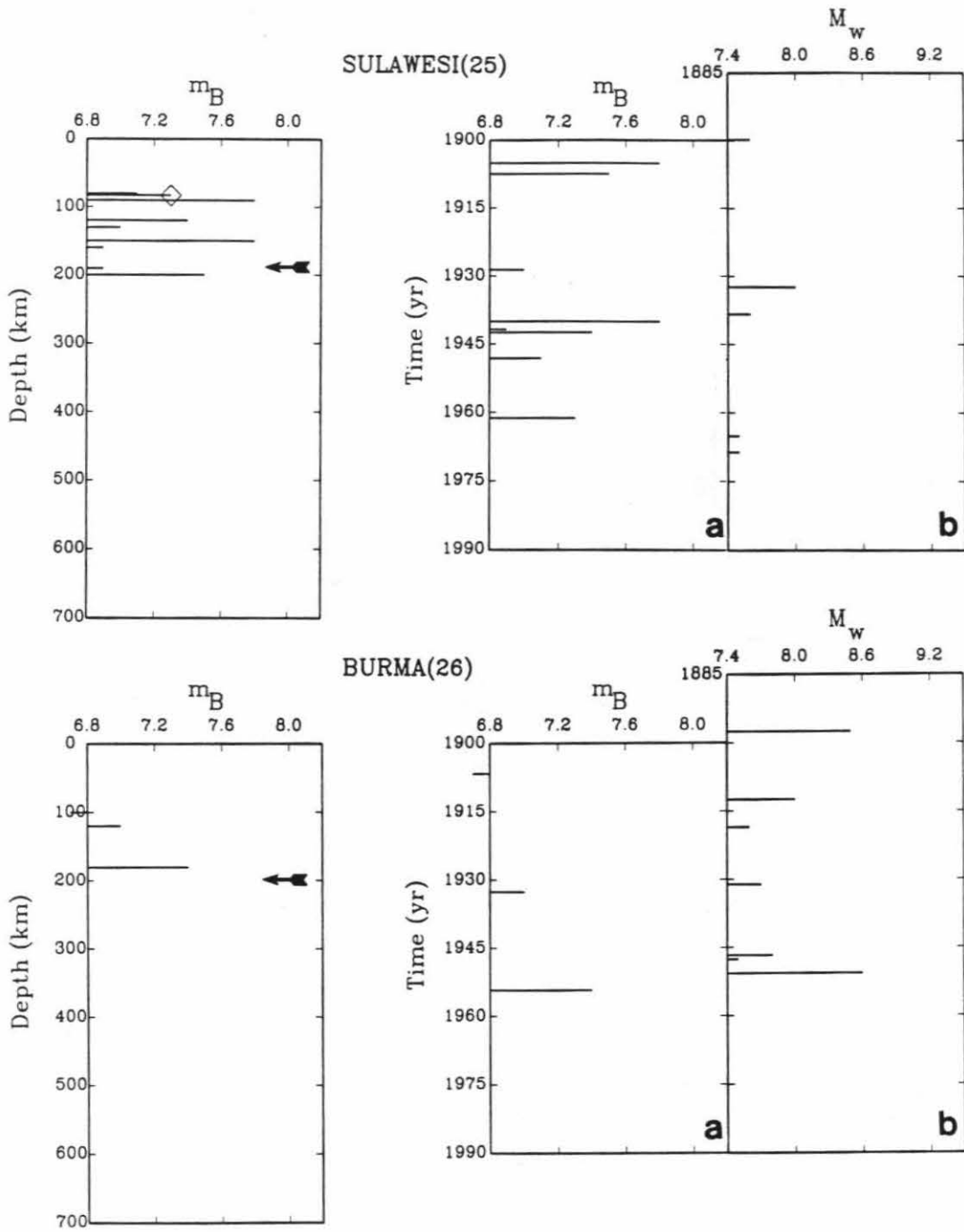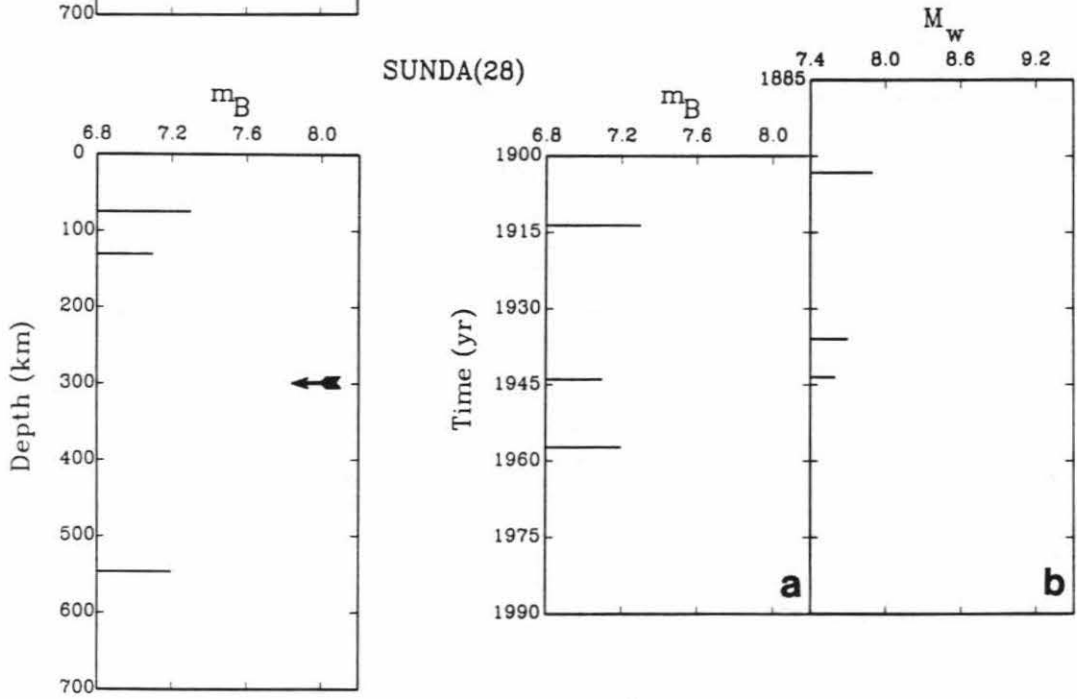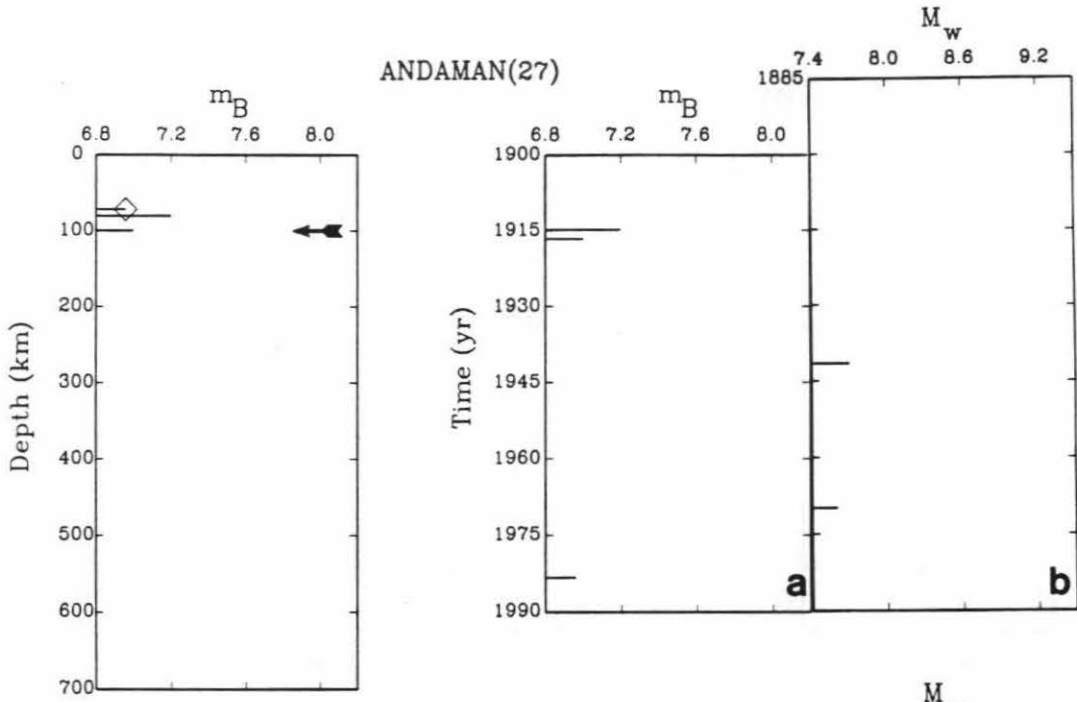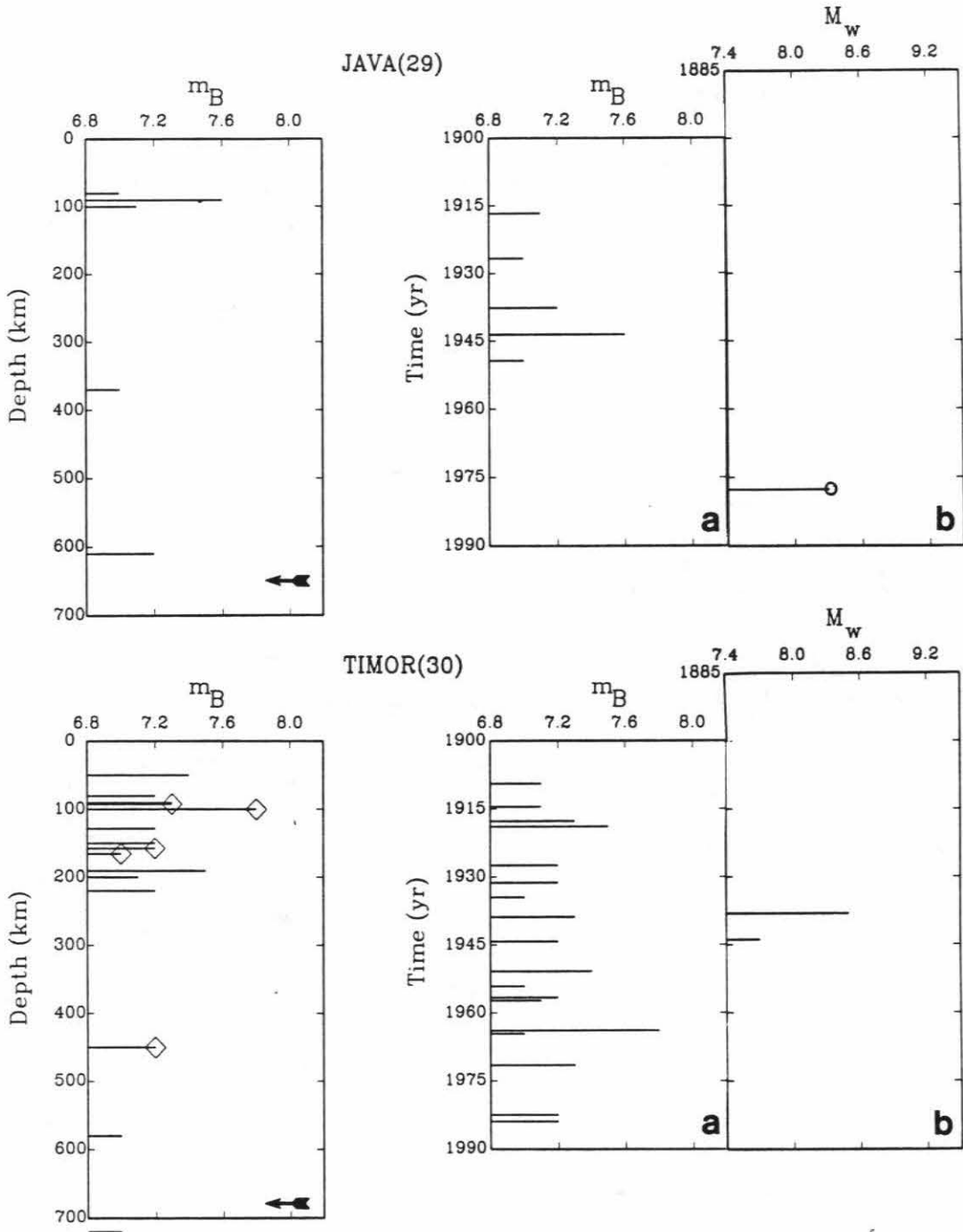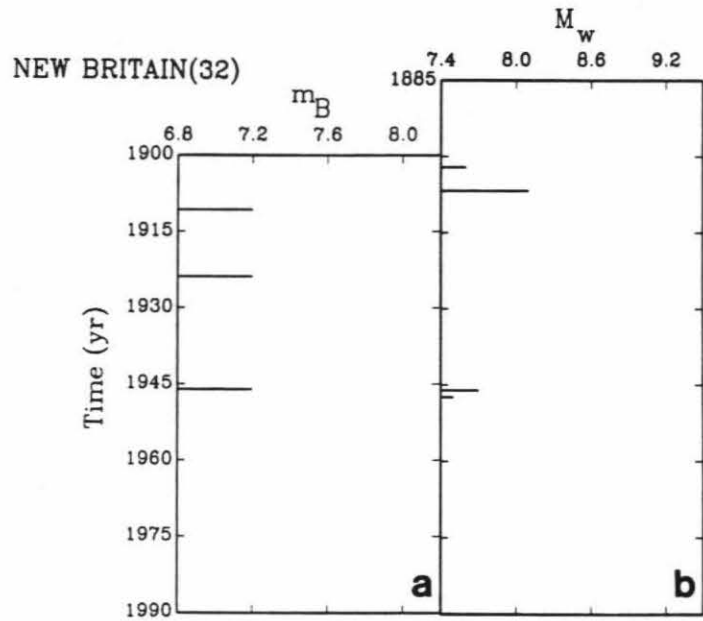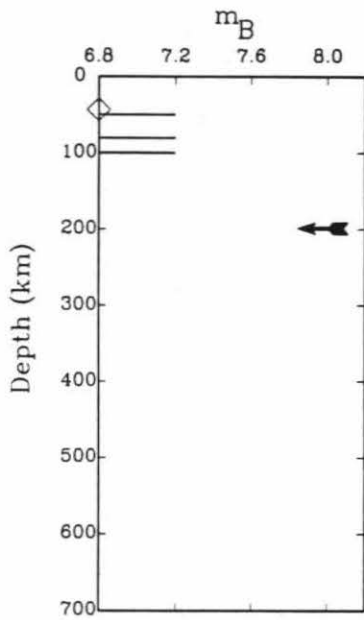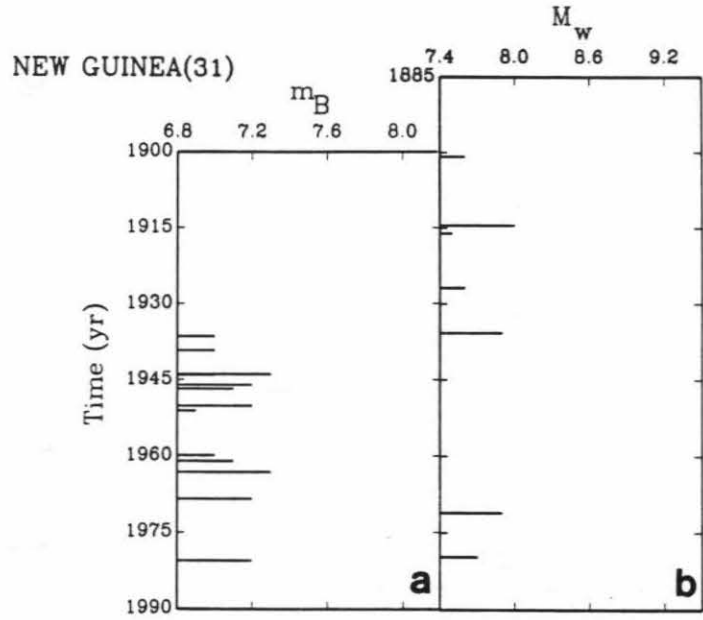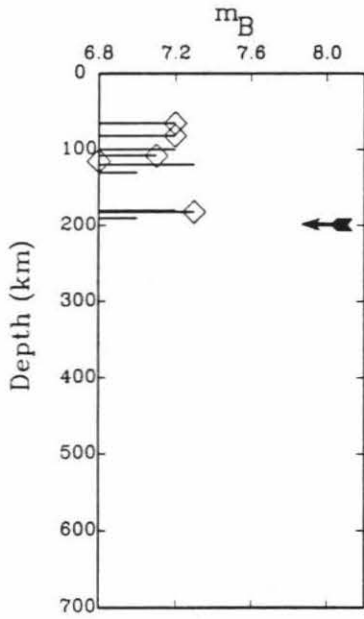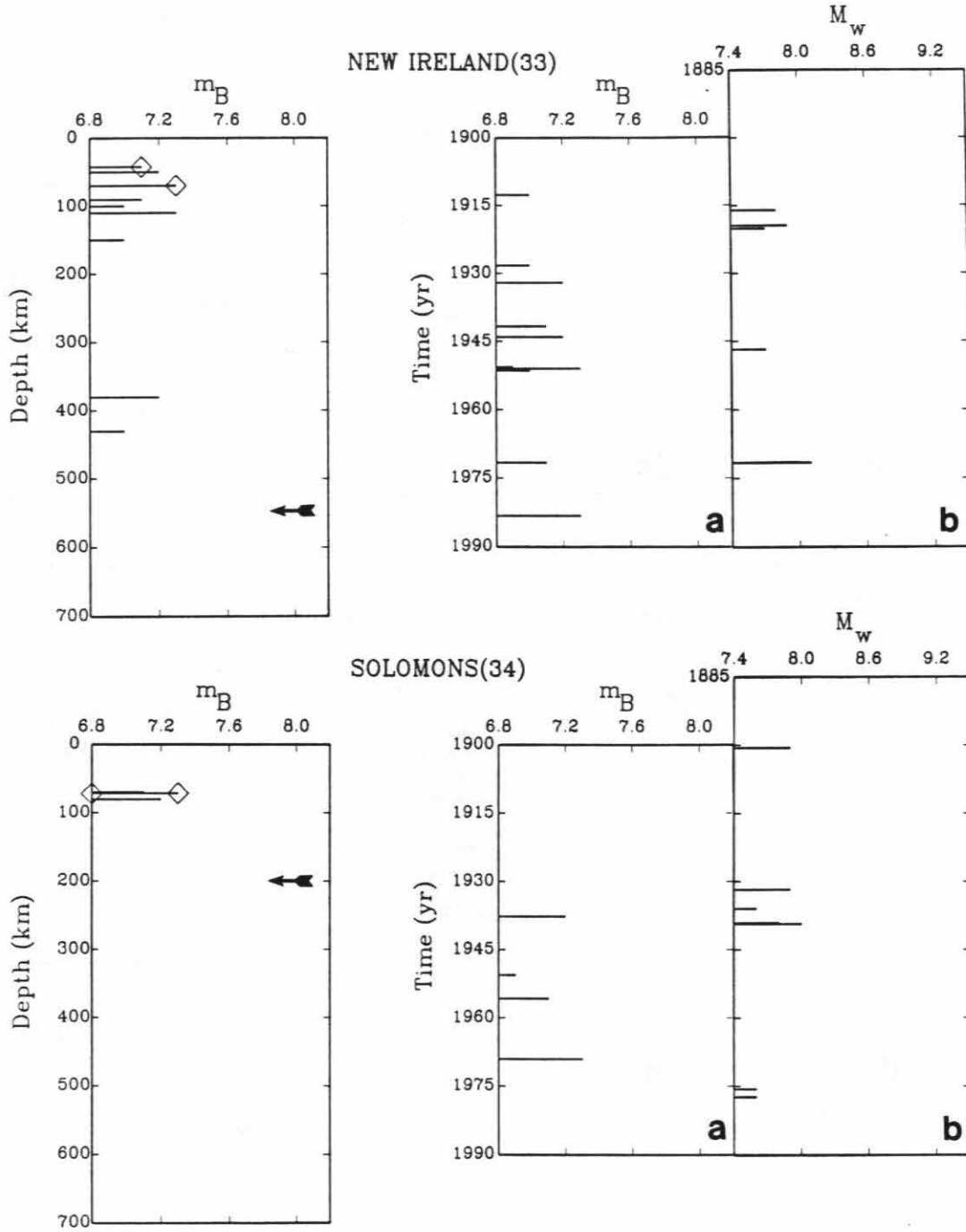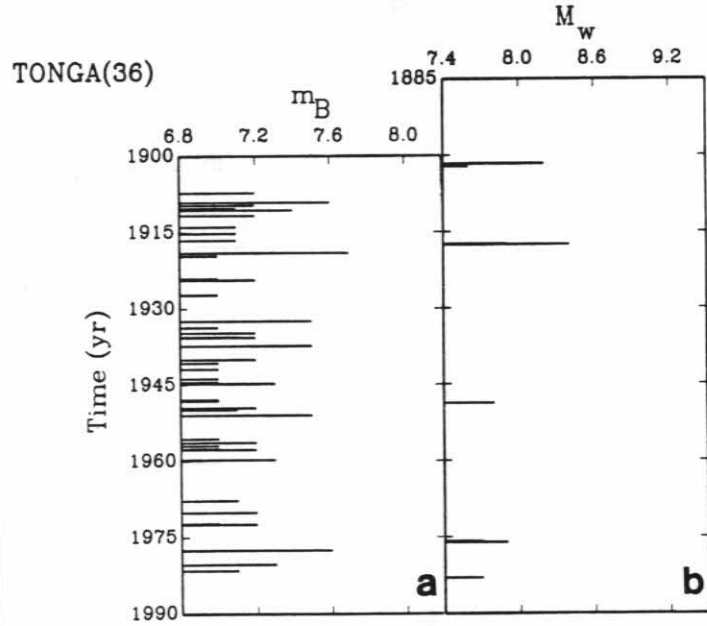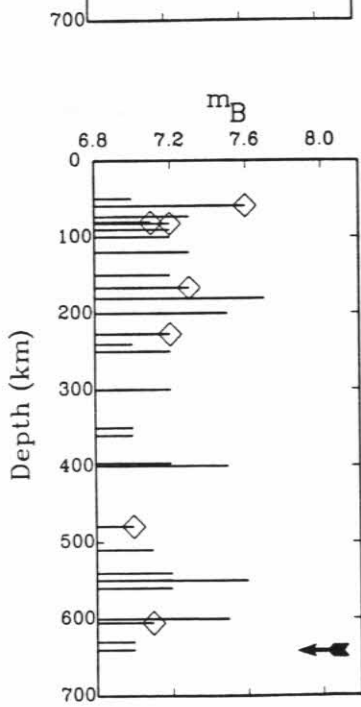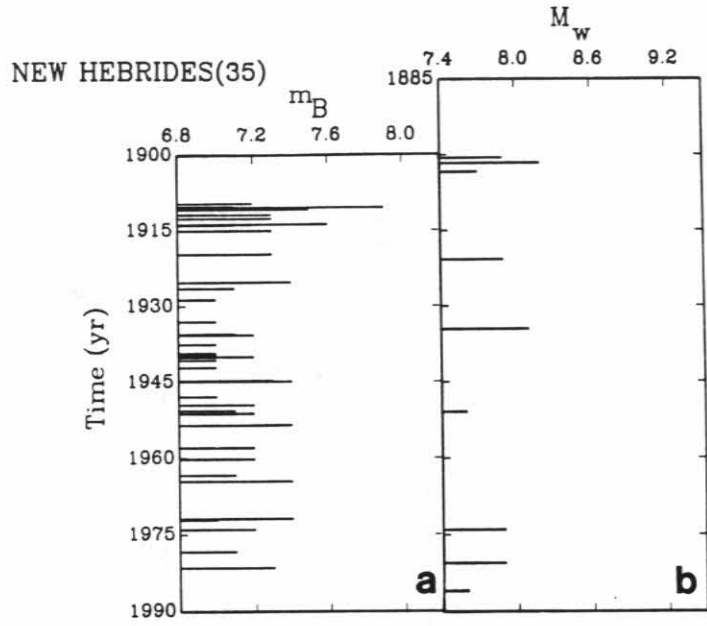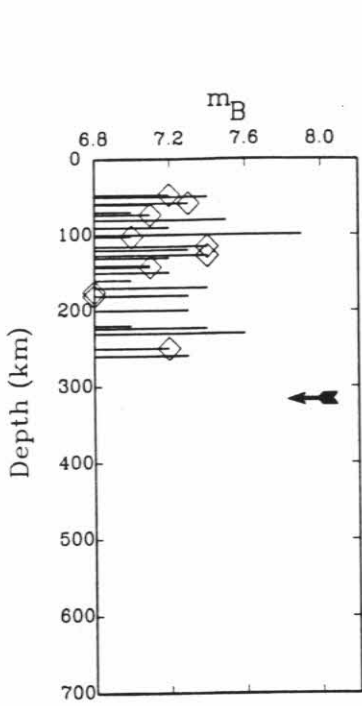
KERMADEC(37)

NEW ZEALAND(38)

HINDU-KUSH(39)

IRAN(40)

GREECE(41)

RUMANIA(42)
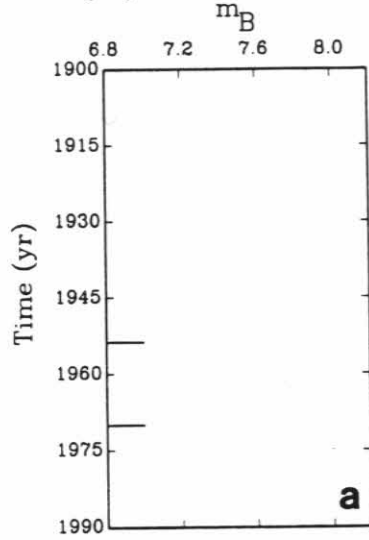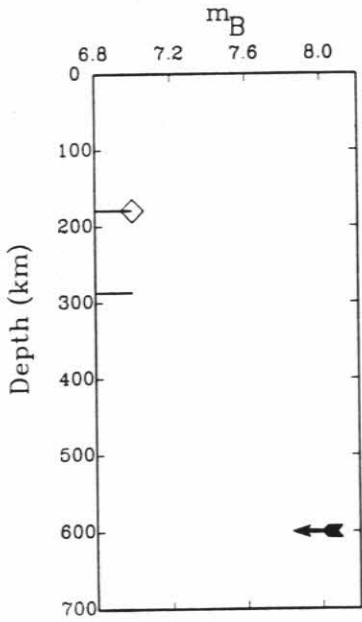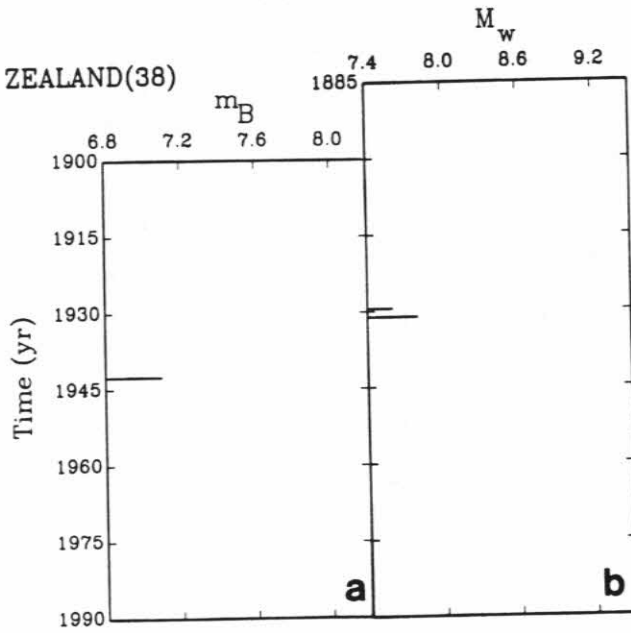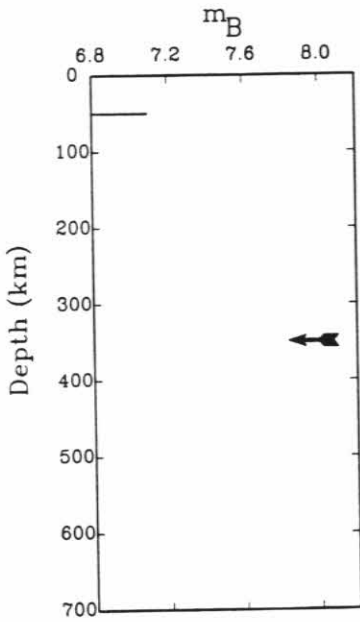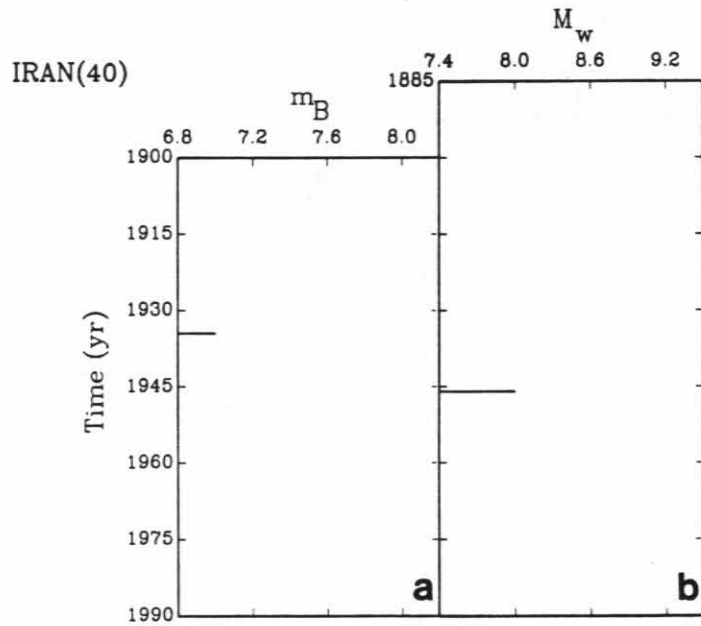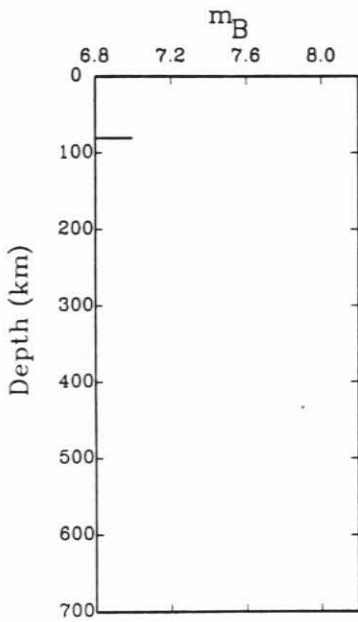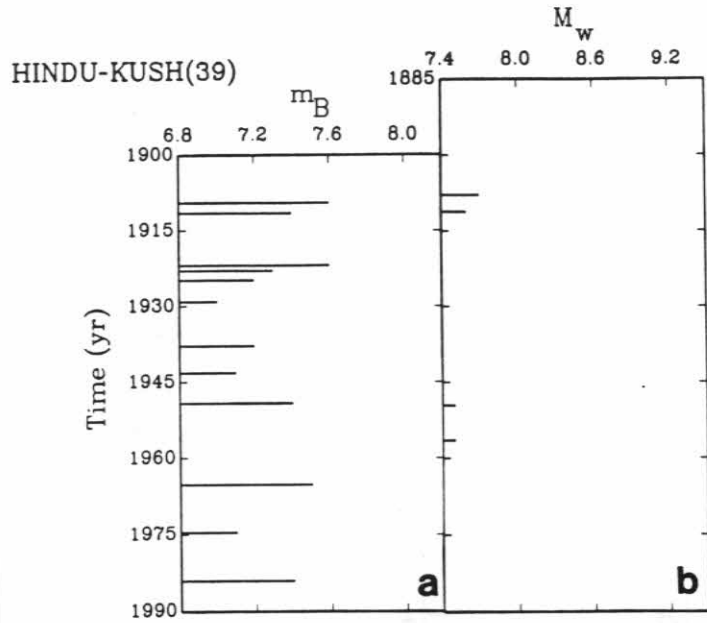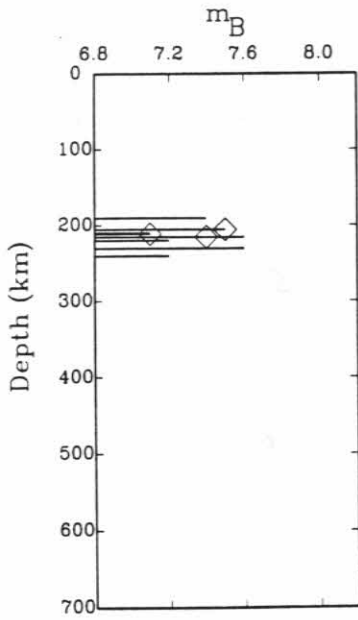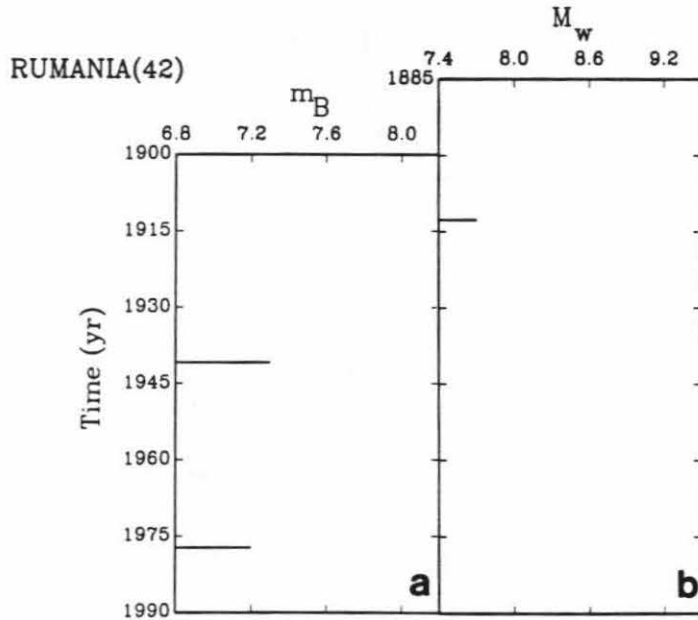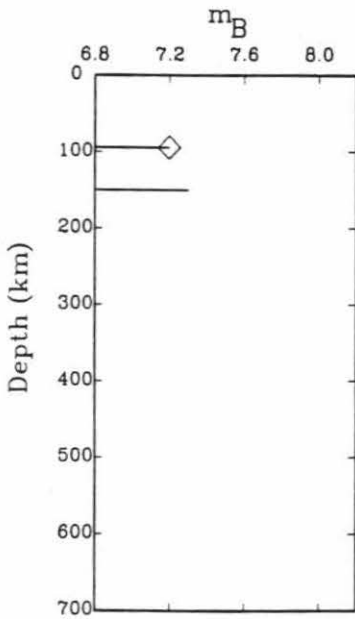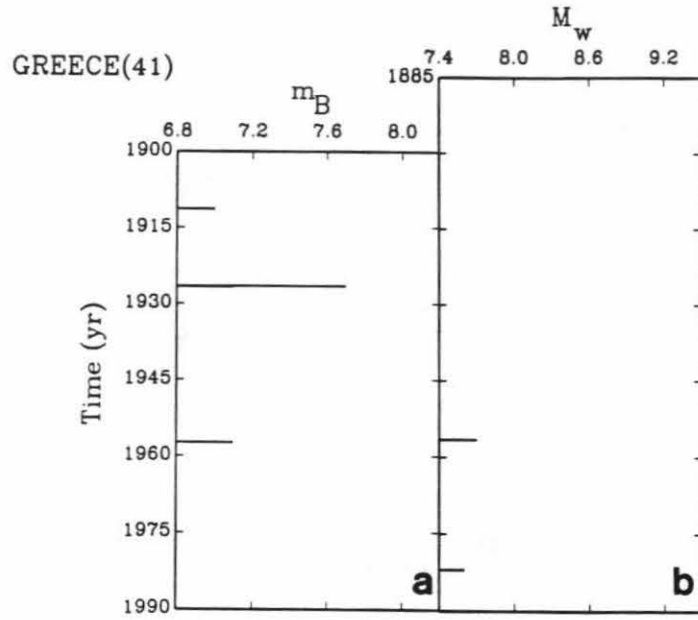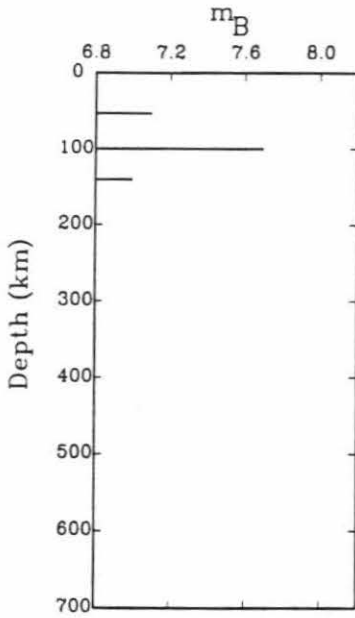
SPAIN(43)
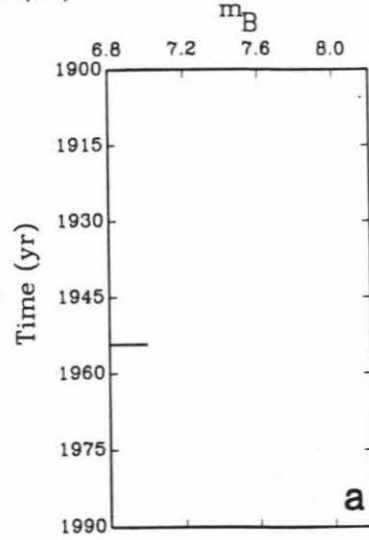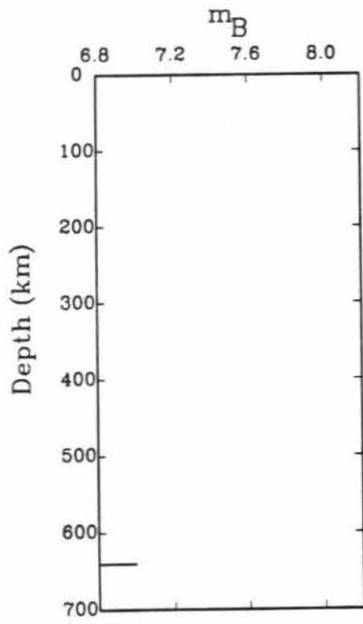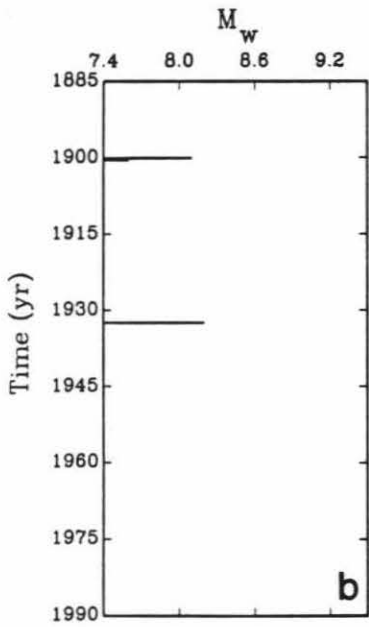
RIVERA(9')   NANKAI(21')
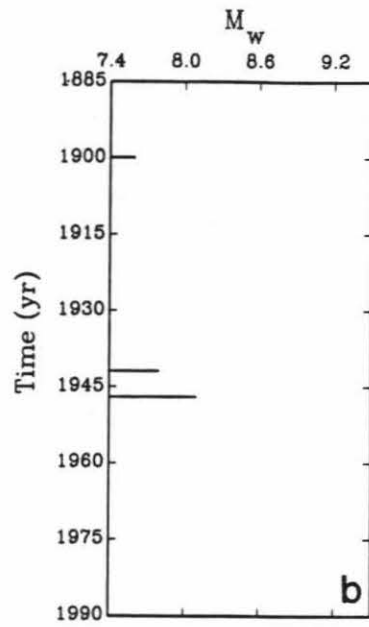
Table A1: Large Intermediate and Deep Focus Events

NEV	REGION										
	DATE			TIME		LATITUDE		LONGITUDE		DEPTH	MAGNITUDE	
Year	Mo	Dy	HrMn	Sec	$(+^\circ N, -^\circ S)$		$(+^\circ E, -^\circ W)$		(km)	m_B	M_w
6	COLOMBIA (1)										
1911	4	10	1842	24.00	9	0.00	-74	0.00	100.0	7.00	
1911	4	28	0952	54.00	0	0.00	-71	0.00	600.0	6.90	
1914	5	28	323	54.00	9	0.00	-78	0.00	70.0	6.90	
1925	3	29	2112	37.00	8	0.00	-78	0.00	60.0	7.10	
1970	7	31	1708	5.40	-1	27.54	-72	33.48	651.0	7.50	
1979	11	23	2340	29.80	4	48.30	-76	13.02	108.6	7.00	7.20
6	ECUADOR (2)										
1906	9	28	1524	54.00	-2	0.00	-79	0.00	150.0	7.50	
1921	12	18	1529	35.00	-2	30.00	-71	0.00	650.0	7.50	
1922	1	17	350	33.00	-2	30.00	-71	0.00	650.0	7.40	
1937	7	19	1935	24.00	-1	30.00	-76	30.00	190.0	7.10	
1971	7	27	202	49.60	-2	44.88	-77	25.74	135.0	7.30	
1983	4	12	1207	54.60	-4	53.40	-78	10.80	111.1	6.90	6.97
13	PERU (3)										
1915	4	23	1529	18.00	-8	0.00	-68	0.00	650.0	6.90	
1941	9	18	1314	9.00	-13	45.00	-72	15.00	100.0	7.00	
1950	7	9	440	4.00	-8	0.00	-70	45.00	650.0	7.00	
1950	7	9	450	5.00	-8	0.00	-70	45.00	650.0	7.00	
1950	12	10	250	42.00	-14	15.00	-75	45.00	80.0	7.10	
1959	7	19	1506	10.00	-15	0.00	-70	30.00	200.0	7.10	
1958	7	26	1737	9.00	-13	30.00	-69	0.00	620.0	7.20	
1961	8	31	148	37.50	-10	42.00	-70	54.00	626.0	7.00	
1961	8	31	157	8.00	-10	30.00	-70	42.00	629.0	7.30	
1961	8	19	509	49.50	-10	48.00	-71	0.00	649.0	7.20	
1963	8	15	1725	6.00	-13	48.00	-69	15.00	543.0	7.30	
1963	11	9	2115	30.00	-8	48.00	-71	42.00	576.0	7.20	
1970	5	31	2023	27.30	-9	10.56	-78	49.38	48.0	7.80	
26	ALTIPLANO (4)										
1910	10	4	2300	6.00	-22	0.00	-69	0.00	120.0	7.20	
1913	5	8	1835	24.00	-17	0.00	-74	30.00	200.0	6.90	
1914	2	26	458	12.00	-18	0.00	-67	0.00	130.0	7.20	
1915	6	6	2129	37.00	-18	30.00	-68	30.00	160.0	7.30	
1916	8	25	944	42.00	-21	0.00	-68	0.00	180.0	7.00	
1922	3	28	357	54.00	-21	0.00	-68	0.00	90.0	7.10	
1922	10	11	1449	50.00	-16	0.00	-72	30.00	50.0	7.60	
1929	10	19	1012	52.00	-23	0.00	-69	0.00	100.0	7.10	
1933	10	25	2328	16.00	-23	0.00	-66	42.00	220.0	7.00	
1940	10	4	754	42.00	-22	0.00	-71	0.00	75.0	7.10	
1940	12	22	1859	46.00	-15	30.00	-68	30.00	230.0	6.90	
1941	4	3	1521	39.00	-22	30.00	-66	0.00	260.0	7.20	
1943	3	14	1837	56.00	-20	0.00	-69	30.00	150.0	7.10	
1943	12	1	1034	46.00	-19	30.00	-69	45.00	80.0	7.10	
1948	5	11	855	41.00	-17	30.00	-70	15.00	70.0	7.40	

NEV   REGION

DATE			TIME		LATITUDE		LONGITUDE		DEPTH	MAGNITUDE	
Year	Mo	Dy	HrMn	Sec	$(+^\circ N, -^\circ S)$		$(+^\circ E, -^\circ W)$		(km)	m_B	M_w
1949	4	25	1354	59.00	-19	45.00	-69	0.00	110.0	7.20	
1952	9	21	230	35.00	-21	45.00	-65	45.00	260.0	7.10	
1953	12	7	205	24.00	-22	6.00	-68	42.00	128.0	7.20	
1959	7	19	1506	10.00	-15	0.00	-70	30.00	200.0	7.10	
1957	11	29	2219	38.00	-21	0.00	-66	0.00	200.0	7.40	
1958	1	15	1914	29.00	-16	30.00	-72	0.00	60.0	7.00	
1959	6	14	12	2.00	-20	25.20	-69	0.00	83.0	7.50	
1960	1	13	1540	34.00	-16	0.00	-72	0.00	200.0	7.50	
1967	12	27	917	55.70	-21	12.00	-68	18.00	135.0	7.00	
1974	1	2	1042	29.90	-22	32.28	-68	23.82	105.0	7.10	
1976	11	30	40	57.80	-20	31.20	-68	55.14	82.0	7.30	

22   NORTH CHILE (5)

Year	Mo	Dy	HrMn	Sec	Lat		Lon		Depth	m_B	M_w
1912	12	7	2246	50.00	-29	0.00	-62	30.00	620.0	7.30	
1916	6	21	2132	30.00	-28	30.00	-63	0.00	600.0	7.40	
1918	5	20	1755	10.00	-28	30.00	-71	30.00	80.0	7.60	
1925	5	15	1156	57.00	-26	0.00	-71	30.00	50.0	7.10	
1929	10	19	1012	52.00	-23	0.00	-69	0.00	100.0	7.10	
1933	10	25	2328	16.00	-23	0.00	-66	42.00	220.0	7.00	
1936	7	13	1112	15.00	-24	30.00	-70	0.00	60.0	7.20	
1939	4	18	622	45.00	-27	0.00	-70	30.00	100.0	7.30	
1942	7	8	655	45.00	-24	0.00	-70	0.00	140.0	7.00	
1946	8	2	1918	48.00	-26	30.00	-70	30.00	50.0	7.50	
1946	8	28	2228	15.00	-26	0.00	-63	0.00	580.0	7.10	
1947	1	29	817	50.00	-26	0.00	-63	0.00	580.0	7.00	
1950	8	14	2251	24.00	-27	15.00	-62	30.00	630.0	7.20	
1950	12	9	2138	48.00	-23	30.00	-67	30.00	100.0	7.70	
1962	8	3	856	17.10	-23	18.00	-68	6.00	107.0	7.20	
1983	12	21	1205	6.30	-28	11.40	-63	10.32	602.0	6.90	
1962	8	3	856	17.10	-23	18.00	-68	6.00	108.0	7.30	
1965	2	23	2211	50.20	-25	42.00	-70	30.00	80.0	7.25	
1970	6	11	602	54.90	-24	31.62	-68	29.94	112.0	6.80	
1971	2	21	1035	20.10	-23	50.70	-67	9.54	169.0	6.80	
1971	6	17	2100	40.90	-25	28.68	-69	9.18	93.0	7.20	
1978	8	3	1811	17.10	-26	30.78	-70	32.64	69.3	6.80	6.83

5   CENTRAL CHILE (6)

Year	Mo	Dy	HrMn	Sec	Lat		Lon		Depth	m_B	M_w
1927	4	14	623	34.00	-32	0.00	-69	30.00	110.0	7.20	
1944	1	15	2349	30.00	-31	15.00	-68	45.00	50.0	7.40	
1945	9	13	1117	11.00	-33	15.00	-70	30.00	100.0	7.00	
1965	3	28	1633	14.60	-32	24.00	-71	12.00	61.0	7.13	
1981	11	7	329	51.10	-32	11.94	-71	20.16	65.6	6.90	6.94

4   SOUTH CHILE (7)

Year	Mo	Dy	HrMn	Sec	Lat		Lon		Depth	m_B	M_w
1934	3	1	2145	25.00	-40	0.00	-72	30.00	120.0	7.30	
1949	4	20	329	7.00	-38	0.00	-73	30.00	70.0	7.10	
1953	5	6	1716	43.00	-36	30.00	-73	0.00	60.0	7.50	
1971	5	8	49	45.60	-42	13.38	-71	41.40	151.0	7.00	7.20

NEV	REGION										

	DATE		TIME		LATITUDE		LONGITUDE		DEPTH	MAGNITUDE	
Year	Mo	Dy	HrMn	Sec	$(+^\circ N, -^\circ S)$		$(+^\circ E, -^\circ W)$		(km)	m_B	M_w
6	SCOTIA (8)										
1937	9	8	40	1.00	-57	0.00	-27	0.00	130.0	7.10	
1941	11	15	419	54.00	-59	0.00	-27	30.00	80.0	7.00	
1954	2	22	1203	36.00	-57	0.00	-26	30.00	140.0	7.00	
1961	9	1	9	34.60	-59	30.00	-27	18.00	131.0	7.20	
1961	9	8	1126	32.90	-56	18.00	-27	6.00	125.0	7.60	
1964	5	26	1059	12.80	-56	27.00	-27	42.00	114.0	7.50	
8	MEXICO (9)										
1908	3	26	2303	30.00	18	0.00	-99	0.00	80.0	7.70	
1916	6	2	1359	24.00	17	30.00	-95	0.00	150.0	7.00	
1931	1	15	150	41.00	16	0.00	-96	45.00	45.0	7.60	
1937	7	26	347	11.00	18	24.00	-95	48.00	100.0	7.20	
1964	7	6	722	11.70	18	18.00	-100	24.00	45.0	7.20	
1973	8	28	950	40.00	18	16.02	-96	35.88	80.0	7.30	
1979	6	22	630	54.30	17	0.00	-94	36.54	117.0	6.90	6.91
1980	10	24	1453	35.10	18	12.66	-98	14.40	63.4	7.00	7.14
8	CENTRAL AMERICA (10)										
1914	3	30	41	18.00	17	0.00	-92	0.00	150.0	7.20	
1915	9	7	120	48.00	14	0.00	-89	0.00	80.0	7.40	
1916	6	2	1359	24.00	17	30.00	-95	0.00	150.0	7.00	
1921	2	4	822	44.00	15	0.00	-91	0.00	120.0	7.40	
1946	6	7	413	20.00	16	30.00	-94	0.00	100.0	6.90	
1946	7	11	446	42.00	17	0.00	-94	30.00	130.0	6.90	
1947	1	26	1006	46.00	12	30.00	-86	15.00	170.0	7.00	
1982	6	19	621	57.40	13	15.00	-89	24.00	51.9	7.10	7.28
1	GREATER ANTILLES (11)										
1916	4	24	426	42.00	18	30.00	-68	0.00	80.0	7.00	
6	LESSER ANTILLES (12)										
1906	12	3	2259	24.00	15	0.00	-61	0.00	100.0	7.20	
1910	1	23	1849	42.00	12	0.00	-60	30.00	100.0	6.90	
1914	10	3	1722	12.00	16	0.00	-61	0.00	100.0	7.40	
1953	3	19	·827	53.00	14	6.00	-61	12.60	134.0	7.10	
1969	12	25	2132	0.00	15	47.40	-59	38.40	42.0	7.50	
1974	10	8	950	58.10	17	18.00	-62	0.00	47.0	7.50	

NEV REGION

DATE			TIME		LATITUDE		LONGITUDE		DEPTH	MAGNITUDE	
Year	Mo	Dy	HrMn	Sec	$(+°N,-°S)$		$(+°E,-°W)$		(km)	m_B	M_w
2	JUAN DE FUCA (13)										
1949	3	13	1955	0.00	47	6.00	-122	0.00	70.0	7.10	
1965	4	29	1528	43.30	47	24.00	-122	24.00	63.0	6.88	
3	ALASKA (14)										
1912	1	31	2011	48.00	61	0.00	-147	30.00	80.0	7.00	
1912	11	7	740	24.00	57	30.00	-155	0.00	90.0	7.30	
1934	5	4	436	7.00	61	15.00	-147	30.00	80.0	7.10	
6	ALEUTIANS (15)										
1909	9	8	1749	48.00	52	30.00	-169	0.00	90.0	7.00	
1916	4	18	401	48.00	53	15.00	-170	0.00	170.0	7.40	
1937	9	3	1848	12.00	52	30.00	-177	30.00	80.0	7.20	
1940	7	14	552	53.00	51	45.00	177	30.00	80.0	7.40	
1944	7	27	4	23.00	54	0.00	-165	30.00	70.0	7.10	
1965	7	2	2058	40.30	53	6.00	-167	36.00	60.0	6.90	
5	KAMCHATKA (16)										
1907	8	17	1727	54.00	52	0.00	157	0.00	120.0	7.20	
1911	5	4	2336	54.00	51	0.00	157	0.00	240.0	7.40	
1960	7	25	1112	0.00	54	0.00	159	36.00	100.0	7.20	
1971	11	24	1935	29.10	52	53.82	159	11.22	106.0	7.30	
1983	8	17	1055	52.80	55	47.40	161	12.60	77.2	6.90	7.01
23	KURILES (17)										
1905	9	1	245	36.00	45	0.00	143	0.00	230.0	7.30	
1907	5	25	1402	8.00	51	30.00	147	0.00	600.0	7.40	
1911	9	6	54	18.00	46	0.00	143	0.00	350.0	7.00	
1920	2	22	1735	50.00	47	30.00	146	0.00	340.0	7.10	
1920	10	18	811	35.00	45	0.00	150	30.00	50.0	7.20	
1922	10	24	2121	6.00	47	0.00	151	30.00	80.0	7.60	
1924	5	28	951	59.00	48	0.00	146	0.00	500.0	7.00	
1924	6	30	1544	25.00	45	0.00	147	30.00	120.0	7.20	
1924	12	27	1122	5.00	45	0.00	146	0.00	150.0	7.00	
1929	1	13	3	12.00	49	45.00	154	45.00	140.0	7.40	
1930	1	5	119	48.00	49	0.00	154	0.00	140.0	7.00	
1933	12	4	1933	55.00	47	0.00	144	0.00	360.0	7.10	
1939	12	16	1046	32.00	43	45.00	147	45.00	75.0	7.10	
1942	3	5	1948	16.00	44	30.00	142	30.00	260.0	7.00	
1942	11	26	1427	28.00	45	30.00	150	0.00	110.0	7.40	
1949	5	3	556	0.00	48	36.00	154	0.00	125.0	7.00	
1950	2	28	1020	57.00	46	0.00	144	0.00	340.0	7.50	
1956	10	11	224	33.00	46	0.00	150	30.00	110.0	7.30	
1957	11	17	557	47.00	48	10.20	148	45.00	347.0	6.90	
1969	1	19	702	4.40	45	0.54	143	10.14	204.0	7.30	
1970	8	30	1746	9.00	52	22.80	151	35.82	645.0	7.20	
1972	3	22	1027	41.90	49	3.66	153	34.44	134.0	6.80	
1978	12	6	1402	1.00	44	35.52	146	34.86	181.0	7.40	7.80

NEV   REGION

DATE			TIME		LATITUDE		LONGITUDE		DEPTH	MAGNITUDE	
Year	Mo	Dy	HrMn	Sec	$(+^\circ N, -^\circ S)$		$(+^\circ E, -^\circ W)$		(km)	m_B	M_w
19	NORTHEAST JAPAN (18)										
1904	6	7	817	54.00	40	0.00	134	0.00	350.0	7.40	
1905	6	2	539	42.00	34	0.00	132	0.00	100.0	7.50	
1905	10	24	346	42.00	34	0.00	139	0.00	250.0	6.90	
1915	3	17	1845	0.00	42	0.00	142	0.00	100.0	7.20	
1916	9	15	701	18.00	34	30.00	141	0.00	100.0	7.10	
1917	7	31	323	10.00	42	30.00	131	0.00	460.0	7.40	
1918	1	30	2118	33.00	45	30.00	135	0.00	330.0	7.40	
1918	4	10	203	54.00	43	30.00	130	30.00	570.0	7.00	
1929	6	2	2138	34.00	34	30.00	137	15.00	360.0	6.90	
1931	2	20	533	24.00	44	18.00	135	30.00	350.0	7.40	
1932	9	23	1422	12.00	44	45.00	138	0.00	300.0	7.00	
1932	11	13	447	0.00	43	45.00	137	0.00	320.0	7.10	
1937	7	26	1956	37.00	38	30.00	141	30.00	90.0	7.20	
1940	7	10	549	55.00	44	0.00	131	0.00	580.0	7.30	
1946	1	11	133	29.00	44	0.00	129	30.00	580.0	6.90	
1953	10	14	1457	23.00	42	48.00	144	36.00	95.0	7.00	
1954	5	14	2239	25.00	36	0.00	137	24.00	191.0	7.00	
1973	9	29	44	0.80	41	53.46	130	52.32	575.0	7.40	
1971	8	2	724	56.80	41	22.86	143	27.78	51.0	7.00	
19	IZU-BONIN (19)										
1905	7	11	1537	30.00	22	0.00	143	0.00	450.0	7.20	
1905	10	24	346	42.00	34	0.00	139	0.00	250.0	6.90	
1906	1	21	1349	35.00	34	0.00	138	0.00	340.0	7.70	
1909	3	13	1429	0.00	31	30.00	142	30.00	80.0	7.60	
1910	2	12	1810	6.00	32	30.00	138	0.00	350.0	7.20	
1913	3	23	2047	18.00	24	0.00	142	0.00	80.0	7.00	
1914	11	24	1153	30.00	22	0.00	143	0.00	110.0	7.90	
1915	10	8	1536	1.80	33	30.00	138	0.00	170.0	7.00	
1916	9	15	701	18.00	34	30.00	141	0.00	100.0	7.10	
1921	7	4	1418	20.00	25	30.00	141	30.00	200.0	7.40	
1928	3	29	506	3.00	31	42.00	138	12.00	410.0	7.00	
1929	6	2	2138	34.00	34	30.00	137	15.00	360.0	6.90	
1955	5	30	1231	41.00	24	30.00	142	30.00	570.0	7.10	
1956	2	18	734	19.00	29	54.00	138	30.00	480.0	7.10	
1968	10	7	1920	20.30	26	17.28	140	35.70	516.0	7.20	
1970	5	27	1205	6.00	27	12.90	140	7.26	382.0	7.00	
1978	3	7	248	47.60	32	0.30	137	36.54	439.0	7.07	
1972	12	4	1016	12.00	33	19.56	140	41.04	62.0	7.40	
1982	9	6	147	1.90	29	18.60	140	16.80	155.6	6.80	6.80
9	MARIANAS (20)										
1912	10	26	900	36.00	14	0.00	146	0.00	130.0	7.00	
1931	9	9	2038	26.00	19	0.00	145	30.00	180.0	7.10	
1940	1	17	115	0.00	17	0.00	148	0.00	80.0	7.30	
1942	6	14	309	45.00	15	0.00	145	0.00	80.0	7.00	
1940	12	28	1637	44.00	18	0.00	147	30.00	80.0	7.30	
1945	7	15	535	13.00	17	30.00	146	30.00	120.0	7.10	
1950	5	25	1835	7.00	13	0.00	143	30.00	90.0	7.10	
1956	2	1	1341	46.00	18	45.00	145	30.00	370.0	7.00	
1975	11	1	117	33.90	13	50.58	144	45.24	113.0	7.10	

NEV   REGION

DATE			TIME		LATITUDE		LONGITUDE		DEPTH	MAGNITUDE	
Year	Mo	Dy	HrMn	Sec	$(+°N,-°S)$		$(+°E,-°W)$		(km)	m_B	M_w

9   RYUKYU (21)

Year	Mo	Dy	HrMn	Sec	Lat°	Lat'	Lon°	Lon'	Depth	m_B	M_w
1905	6	2	539	42.00	34	0.00	132	0.00	100.0	7.50	
1909	4	14	1953	42.00	24	0.00	123	0.00	80.0	7.10	
1909	11	10	613	30.00	32	0.00	131	0.00	190.0	7.50	
1911	6	15	1426	0.00	29	0.00	129	0.00	160.0	8.10	
1915	1	5	2326	42.00	25	0.00	123	0.00	160.0	7.30	
1919	6	1	651	20.00	26	30.00	125	0.00	200.0	7.10	
1926	6	29	1427	6.00	27	0.00	127	0.00	130.0	7.40	
1947	9	26	1601	57.00	24	45.00	123	0.00	110.0	7.40	
1958	3	11	26	1.00	24	37.20	124	17.40	77.0	7.20	

7   NORTH TAIWAN (22)

Year	Mo	Dy	HrMn	Sec	Lat°	Lat'	Lon°	Lon'	Depth	m_B	M_w
1909	4	14	1953	42.00	24	0.00	123	0.00	80.0	7.10	
1910	4	12	22	13.00	25	30.00	122	30.00	200.0	7.60	
1915	1	5	2326	42.00	25	0.00	123	0.00	160.0	7.30	
1947	9	26	1601	57.00	24	45.00	123	0.00	110.0	7.40	
1959	4	26	2040	37.00	24	51.00	122	45.00	113.0	7.50	
1963	2	13	850	4.50	24	30.00	122	6.00	67.0	7.25	
1967	10	25	59	22.60	24	30.00	122	12.00	65.0	7.00	

2   LUZON (23)

Year	Mo	Dy	HrMn	Sec	Lat°	Lat'	Lon°	Lon'	Depth	m_B	M_w
1930	12	21	1451	24.00	20	0.00	122	15.00	170.0	7.00	
1938	5	23	821	53.00	18	0.00	119	30.00	80.0	7.00	

15   PHILIPPINES (24)

Year	Mo	Dy	HrMn	Sec	Lat°	Lat'	Lon°	Lon'	Depth	m_B	M_w
1907	3	29	2046	30.00	3	0.00	122	0.00	500.0	7.20	
1918	2	7	520	30.00	6	30.00	126	30.00	120.0	7.20	
1936	1	20	1656	19.00	6	0.00	127	0.00	80.0	7.00	
1941	2	4	1403	12.00	9	0.00	124	0.00	600.0	7.00	
1950	7	29	1646	2.00	2	30.00	127	0.00	80.0	7.00	
1949	4	30	123	32.00	6	30.00	125	0.00	130.0	7.30	
1955	3	31	1817	19.00	8	6.00	123	12.00	96.0	6.90	
1972	6	11	1641	0.90	3	56.40	124	19.08	325.0	7.40	
1966	9	8	2115	50.50	2	24.00	128	18.00	71.0	7.20	
1969	1	30	1029	40.40	4	48.30	127	26.22	70.0	7.10	
1970	1	10	1207	8.60	6	49.50	126	44.22	73.0	7.30	
1970	3	30	1646	45.60	6	47.82	126	39.06	76.0	7.10	
1975	7	10	1829	16.00	6	30.42	126	38.52	86.0	7.00	
1976	11	7	1709	6.10	8	28.68	126	22.50	60.0	6.90	
1984	11	20	815	16.23	5	10.02	125	7.44	180.7	7.20	7.48

NEV   REGION

DATE			TIME		LATITUDE		LONGITUDE		DEPTH	MAGNITUDE	
Year	Mo	Dy	HrMn	Sec	$(+°N,-°S)$		$(+°E,-°W)$		(km)	m_B	M_w
9	SULAWESI (25)										
1905	1	22	243	54.00	1	0.00	123	0.00	90.0	7.80	
1907	6	25	1754	36.00	1	0.00	127	0.00	200.0	7.50	
1928	8	12	808	50.00	1	0.00	127	0.00	130.0	7.00	
1939	12	21	2100	40.00	0	0.00	123	0.00	150.0	7.80	
1941	9	17	647	57.00	0	-30.00	121	30.00	190.0	6.90	
1942	5	28	101	48.00	0	0.00	124	0.00	120.0	7.40	
1948	1	28	347	21.00	-1	30.00	126	30.00	80.0	7.10	
1948	2	9	1454	22.00	0	0.00	122	30.00	160.0	6.90	
1961	3	28	935	55.00	0	12.00	123	36.00	83.0	7.30	
3	BURMA (26)										
1906	8	31	1457	30.00	27	0.00	97	0.00	100.0	6.70	
1932	8	14	439	32.00	26	0.00	95	30.00	120.0	7.00	
1954	3	21	2342	0.00	24	30.00	95	0.00	180.0	7.40	
3	ANDAMAN (27)										
1914	10	11	1617	6.00	12	0.00	94	0.00	80.0	7.20	
1916	7	27	1152	42.00	4	0.00	96	30.00	100.0	7.00	
1983	4	4	251	34.90	5	43.80	94	48.60	71.6	6.96	
3	SUNDA (28)										
1913	8	13	425	42.00	-5	30.00	105	0.00	75.0	7.30	
1943	11	26	2125	22.00	-2	30.00	100	0.00	130.0	7.10	
1957	4	16	404	3.00	-4	40.80	107	9.60	546.0	7.20	
6	JAVA (29)										
1911	7	5	1840	6.00	-7	30.00	117	30.00	370.0	7.00	
1916	9	11	630	36.00	-9	0.00	113	0.00	100.0	7.10	
1926	9	10	1034	29.00	-9	0.00	111	0.00	80.0	7.00	
1937	8	11	55	54.00	-6	15.00	116	30.00	610.0	7.20	
1943	7	23	1453	9.00	-9	30.00	110	0.00	90.0	7.60	
1949	4	23	1115	39.00	-8	0.00	121	0.00	80.0	7.00	
19	TIMOR (30)										
1909	5	30	2101	18.00	-8	0.00	131	0.00	100.0	7.10	
1914	7	4	2338	54.00	-5	30.00	129	0.00	200.0	7.10	
1917	8	30	407	15.00	-7	30.00	128	0.00	100.0	7.30	
1918	11	18	1841	55.00	-7	0.00	129	0.00	190.0	7.50	
1918	11	23	2257	55.00	-7	0.00	129	0.00	190.0	7.10	
1927	6	3	712	11.00	-7	0.00	131	0.00	150.0	7.20	
1931	3	28	1238	37.00	-7	0.00	129	30.00	80.0	7.20	
1934	6	29	825	17.00	-6	45.00	123	45.00	720.0	7.00	
1938	10	20	219	27.00	-9	0.00	123	0.00	90.0	7.30	
1944	3	22	43	18.00	-8	30.00	123	30.00	220.0	7.20	
1950	11	2	1527	56.00	-6	30.00	129	30.00	50.0	7.40	
1954	2	20	1835	5.00	-6	45.00	124	30.00	580.0	7.00	
1956	7	18	619	34.00	-5	4.20	130	15.60	128.0	7.20	

NEV   REGION

	DATE			TIME		LATITUDE		LONGITUDE		DEPTH	MAGNITUDE	
Year	Mo	Dy	HrMn	Sec	$(+°N,-°S)$		$(+°E,-°W)$		(km)	m_B	M_w
1957	3	23	512	31.00	-5	30.00	131	0.00	100.0	7.10	
1963	11	4	117	11.40	-6	51.60	129	34.80	100.0	7.80	
1964	7	8	1155	39.10	-5	30.00	129	48.00	165.0	7.00	
1971	7	8	1907	7.30	-7	1.86	129	41.76	92.0	7.30	
1982	6	22	418	40.50	-7	20.34	126	2.58	450.0	7.20	7.44
1983	11	24	530	34.90	-7	33.00	128	15.00	157.1	7.20	7.40

14	NEW GUINEA (31)										
1936	6	10	823	21.00	-5	30.00	147	0.00	190.0	7.00	
1939	3	2	700	27.00	-4	0.00	143	0.00	130.0	7.00	
1943	12	1	604	55.00	-4	45.00	144	0.00	120.0	7.30	
1944	1	7	249	20.00	-4	30.00	143	30.00	120.0	7.00	
1946	1	17	939	35.00	-7	30.00	147	30.00	100.0	7.20	
1946	9	23	2330	0.00	-6	0.00	145	0.00	100.0	7.10	
1950	2	17	2107	7.00	-7	0.00	146	0.00	180.0	7.20	
1951	2	17	2107	7.00	-7	0.00	146	0.00	180.0	6.90	
1959	11	19	1108	41.00	-5	30.00	146	0.00	100.0	7.00	
1961	1	5	1553	56.00	-4	6.00	143	0.00	108.0	7.10	
1963	2	26	2014	10.00	-7	36.00	146	12.00	182.0	7.30	
1968	5	28	1327	18.70	-2	54.84	139	19.14	65.0	7.20	
1975	12	25	2322	21.70	-4	5.04	142	2.40	115.0	6.80	
1980	7	16	1956	46.70	-4	27.36	143	31.26	81.9	7.20	7.26

4	NEW BRITAIN (32)										
1910	9	7	711	18.00	-6	0.00	151	0.00	80.0	7.20	
1923	11	2	2108	6.00	-4	30.00	151	30.00	50.0	7.20	
1946	1	17	939	35.00	-7	30.00	147	30.00	100.0	7.20	
1973	1	18	928	14.10	-6	52.08	149	59.58	43.0	6.80	

10	NEW IRELAND (33)										
1912	9	1	410	0.00	-4	30.00	155	0.00	430.0	7.00	
1928	3	13	1831	52.00	-5	30.00	153	0.00	100.0	7.00	
1932	1	9	1021	42.00	-6	12.00	154	30.00	380.0	7.20	
1941	9	4	1021	44.00	-4	45.00	154	0.00	90.0	7.10	
1943	12	23	1900	10.00	-5	30.00	153	30.00	50.0	7.20	
1951	5	21	827	20.00	-6	0.00	154	30.00	150.0	7.00	
1950	7	29	2349	2.00	-6	30.00	155	0.00	70.0	6.90	
1950	12	4	1628	3.00	-5	0.00	153	30.00	110.0	7.30	
1971	7	19	14	45.30	-5	41.28	153	48.00	42.0	7.10	
1983	3	18	905	50.10	-4	51.60	153	30.60	69.9	7.30	7.71

5	SOLOMONS (34)										
1937	9	15	1227	32.00	-10	30.00	161	30.00	80.0	7.20	
1950	7	29	2349	2.00	-6	30.00	155	0.00	70.0	6.90	
1955	10	13	926	49.00	-10	0.00	160	45.00	70.0	7.10	
1969	1	5	1326	39.90	-7	58.50	158	54.54	71.0	7.30	
1970	12	29	226	12.20	-10	32.82	161	24.18	72.0	6.80	

NEV	REGION										
	DATE		TIME		LATITUDE		LONGITUDE		DEPTH	MAGNITUDE	
Year	Mo	Dy	HrMn	Sec	$(+°N,-°S)$		$(+°E,-°W)$		(km)	m_B	M_w
48	NEW HEBRIDES (35)										
1909	8	18	39	30.00	-22	0.00	172	0.00	100.0	7.20	
1910	3	30	1655	48.00	-21	0.00	170	0.00	80.0	7.10	
1910	5	1	1830	36.00	-20	0.00	169	0.00	80.0	7.10	
1910	6	1	555	30.00	-20	0.00	169	0.00	80.0	7.30	
1910	6	1	648	18.00	-20	0.00	169	0.00	80.0	7.10	
1910	6	16	630	42.00	-19	0.00	169	30.00	100.0	7.90	
1910	11	9	602	0.00	-15	0.00	166	0.00	80.0	7.50	
1910	11	10	1219	54.00	-14	0.00	166	30.00	90.0	7.10	
1911	10	20	1744	0.00	-12	30.00	166	0.00	160.0	7.00	
1911	11	22	2305	24.00	-15	0.00	169	0.00	200.0	7.30	
1912	8	6	2111	18.00	-14	0.00	167	0.00	260.0	7.30	
1913	10	14	808	48.00	-19	30.00	169	0.00	230.0	7.60	
1913	11	10	2112	30.00	-18	0.00	169	0.00	80.0	7.20	
1913	11	15	527	6.00	-23	0.00	171	0.00	150.0	7.10	
1915	1	5	1433	15.00	-15	0.00	168	0.00	200.0	7.30	
1919	8	31	1720	46.00	-16	0.00	169	0.00	180.0	7.30	
1925	3	22	841	55.00	-18	30.00	168	30.00	50.0	7.40	
1926	6	3	446	56.00	-15	0.00	168	30.00	60.0	7.10	
1928	8	24	2143	30.00	-15	0.00	168	0.00	220.0	7.00	
1933	1	1	848	39.00	-14	45.00	168	0.00	140.0	7.00	
1935	6	24	2323	14.00	-15	45.00	167	45.00	140.0	7.10	
1935	8	17	144	42.00	-22	30.00	171	0.00	120.0	7.20	
1937	7	2	237	15.00	-14	15.00	167	0.00	80.0	7.00	
1939	4	5	1642	40.00	-19	30.00	168	0.00	70.0	7.00	
1939	8	12	207	27.00	-16	15.00	168	30.00	180.0	7.00	
1940	1	6	1403	24.00	-22	0.00	171	0.00	90.0	7.20	
1940	2	20	218	20.00	-13	30.00	167	0.00	200.0	7.00	
1940	9	19	1819	48.00	-24	0.00	171	0.00	80.0	7.00	
1942	1	29	923	44.00	-19	0.00	169	0.00	130.0	7.00	
1944	10	5	1728	27.00	-22	30.00	172	0.00	120.0	7.30	
1944	11	24	449	3.00	-19	0.00	169	0.00	170.0	7.40	
1947	11	9	457	50.00	-22	30.00	170	0.00	50.0	7.00	
1949	7	23	1026	45.00	-18	30.00	170	0.00	150.0	7.20	
1950	9	10	1516	8.00	-15	30.00	167	0.00	100.0	7.10	
1951	3	10	2157	29.00	-15	0.00	167	30.00	130.0	7.20	
1951	3	24	17	36.00	-10	30.00	166	0.00	150.0	7.10	
1953	7	2	656	59.00	-19	0.00	169	0.00	223.0	7.40	
1957	12	17	1350	20.00	-12	22.20	166	43.80	120.0	7.20	
1960	3	8	1633	38.00	-16	30.00	168	30.00	250.0	7.20	
1963	5	1	1003	20.20	-19	0.00	168	54.00	142.0	7.10	
1964	7	9	1639	49.30	-15	30.00	167	36.00	127.0	7.40	
1971	11	21	557	11.90	-11	49.02	166	31.92	115.0	7.40	
1972	2	14	2329	51.70	-11	21.54	166	20.10	102.0	7.00	
1973	12	29	19	31.10	-15	7.02	166	53.76	47.0	7.20	
1978	5	1	1303	37.10	-21	14.40	169	48.00	73.4	7.10	7.37
1978	5	13	708	46.20	-14	31.26	167	19.14	180.4	6.80	6.80
1981	7	6	308	24.70	-22	15.60	171	43.80	58.3	7.30	7.54
1984	4	6	2308	22.30	-18	54.18	168	51.00	175.0	6.80	6.80
45	TONGA (36)										
1907	3	31	2200	36.00	-18	0.00	-177	0.00	400.0	7.20	

NEV   REGION

DATE			TIME		LATITUDE		LONGITUDE		DEPTH	MAGNITUDE	
Year	Mo	Dy	HrMn	Sec	$(+°N,-°S)$		$(+°E,-°W)$		(km)	m_B	M_w
1909	2	22	921	42.00	-18	0.00	-179	0.00	550.0	7.60	
1909	8	18	39	30.00	-22	0.00	172	0.00	100.0	7.20	
1910	3	30	1655	48.00	-21	0.00	170	0.00	80.0	7.10	
1910	8	21	538	36.00	-17	0.00	-179	0.00	600.0	7.40	
1911	8	21	1628	55.00	-21	0.00	-176	0.00	300.0	7.20	
1913	11	15	527	6.00	-23	0.00	171	0.00	150.0	7.10	
1915	2	25	2036	12.00	-20	0.00	180	0.00	600.0	7.10	
1916	7	8	934	30.00	-18	0.00	180	0.00	600.0	7.10	
1919	1	1	259	57.00	-19	30.00	-176	30.00	180.0	7.70	
1919	8	18	1655	25.00	-20	30.00	-178	30.00	300.0	7.00	
1924	1	16	2138	0.00	-21	0.00	-176	0.00	350.0	7.00	
1924	5	4	1651	43.00	-21	0.00	-178	0.00	560.0	7.20	
1927	4	1	1906	9.00	-20	0.00	-177	30.00	400.0	7.00	
1932	5	26	1609	40.00	-25	30.00	179	15.00	600.0	7.50	
1933	9	6	2208	29.00	-21	30.00	-179	45.00	600.0	7.00	
1934	10	10	1542	6.00	-23	30.00	180	0.00	540.0	7.20	
1935	7	29	738	53.00	-20	45.00	-178	0.00	510.0	7.10	
1935	8	17	144	42.00	-22	30.00	171	0.00	120.0	7.20	
1937	4	16	301	37.00	-21	30.00	-177	0.00	400.0	7.50	
1940	1	6	1403	24.00	-22	0.00	171	0.00	90.0	7.20	
1940	9	19	1819	48.00	-24	0.00	171	0.00	80.0	7.00	
1941	11	24	2146	23.00	-28	0.00	-177	30.00	80.0	7.00	
1943	9	27	2203	44.00	-30	0.00	-178	0.00	90.0	7.00	
1944	5	25	106	37.00	-21	30.00	-179	30.00	640.0	7.00	
1944	10	5	1728	27.00	-22	30.00	172	0.00	120.0	7.30	
1947	11	9	457	50.00	-22	30.00	170	0.00	50.0	7.00	
1948	1	27	1158	28.00	-20	30.00	-178	0.00	630.0	7.00	
1949	7	23	1026	45.00	-18	30.00	170	0.00	150.0	7.20	
1949	11	22	51	49.00	-28	30.00	-178	30.00	180.0	7.10	
1950	12	10	1323	4.00	-28	0.00	-178	30.00	250.0	7.20	
1950	12	14	152	49.00	-19	15.00	-175	45.00	200.0	7.50	
1955	8	6	831	28.00	-21	0.00	-178	0.00	360.0	7.00	
1956	5	23	2048	28.20	-15	24.60	-178	43.80	396.0	7.20	
1956	12	27	14	11.00	-23	30.00	-177	0.00	240.0	7.00	
1957	7	14	623	52.00	-27	0.00	-178	0.00	150.0	7.00	
1957	9	28	1420	0.00	-20	28.80	-178	30.60	549.0	7.20	
1959	9	14	1409	50.00	-28	40.20	-177	42.60	73.0	7.30	
1967	10	9	1721	46.00	-21	6.00	-179	12.00	605.0	7.10	
1970	1	20	719	51.20	-25	48.00	-177	20.94	82.0	7.20	
1972	3	30	534	50.00	-25	42.00	179	36.00	479.0	7.00	
1972	5	22	2045	57.30	-17	41.34	-175	11.34	227.0	7.20	
1977	6	22	1208	33.40	-22	52.68	-175	54.00	59.1	7.60	8.04
1980	4	13	1804	31.90	-23	27.96	-177	17.82	166.2	7.30	7.57
1981	7	6	0308	24.70	-4	27.36	143	31.26	81.0	7.10	7.26
2	KERMADEC (37)										
1953	9	29	136	46.00	-36	54.00	177	6.00	287.0	7.00	
1970	1	8	1712	39.10	-34	44.46	178	34.08	179.0	7.00	
1	NEW ZEALAND (38)										
1942	8	1	1234	3.00	-41	0.00	175	45.00	50.0	7.10	

NEV   REGION

DATE			TIME		LATITUDE		LONGITUDE		DEPTH	MAGNITUDE	
Year	Mo	Dy	HrMn	Sec	$(+°N,-°S)$		$(+°E,-°W)$		(km)	m_B	M_w
12	HINDU-KUSH (39)										
1909	7	7	2137	50.00	36	30.00	70	30.00	230.0	7.60	
1911	7	4	1333	26.00	36	0.00	70	30.00	190.0	7.40	
1921	11	15	2036	38.00	36	30.00	70	30.00	215.0	7.60	
1922	12	6	1355	36.00	36	30.00	70	30.00	230.0	7.30	
1924	10	13	1617	45.00	36	0.00	70	30.00	220.0	7.20	
1929	2	1	1714	26.00	36	30.00	70	30.00	220.0	7.00	
1937	11	14	1058	12.00	36	30.00	70	30.00	240.0	7.20	
1943	2	28	1254	33.00	36	30.00	70	30.00	210.0	7.10	
1949	3	4	1019	25.00	36	0.00	70	30.00	230.0	7.40	
1974	7	30	512	40.60	36	21.18	70	45.78	211.0	7.10	
1983	12	30	2352	39.90	36	22.32	70	44.48	215.0	7.40	
1965	3	14	1553	6.60	36	25.20	70	43.80	205.0	7.50	
1	IRAN (40)										
1934	6	13	2210	28.00	27	30.00	62	30.00	80.0	7.00	
4	GREECE (41)										
1911	4	4	1543	54.00	36	30.00	25	30.00	140.0	7.00	
1926	6	26	1946	34.00	36	30.00	27	30.00	100.0	7.70	
1926	8	30	1138	12.00	36	45.00	23	15.00	100.0	7.10	
1957	4	25	225	42.00	36	28.20	28	33.60	53.0	7.10	
2	RUMANIA (42)										
1940	11	10	139	9.00	45	45.00	26	30.00	150.0	7.30	
1977	3	4	1921	54.10	45	46.32	26	45.66	94.0	7.20	7.40
1	SPAIN (43)										
1954	3	29	617	5.00	37	0.00	-3	36.00	640.0	7.00	

Magnitudes are m_B for events occurred prior to 1975 and M_w thereafter,
where $m_B = 0.63M_w + 2.5$ (Kanamori, 1983)

Table A.2: Large Shallow Focus Events

NEV	REGION									
	DATE			TIME		LATITUDE		LONGITUDE	DEPTH	MAGNITUDE	
Year	Mo	Dy	HrMn	Sec	$(+°N,-°S)$		$(+°E,-°W)$		(km)	M_w	M_s

Year	Mo	Dy	HrMn	Sec	Lat°	Lat'	Lon°	Lon'	Depth	M_w	M_s
7	COLOMBIA(1)										
1904	1	20	1452	6.00	7	0.00	-79	0.00	0.00		7.70
1904	12	20	544	18.00	8	30.00	-83	0.00	25.00		7.60
1906	1	31	1536	0.00	1	0.00	-81	30.00	25.00		8.70
1934	7	18	136	24.00	8	0.00	-82	30.00	0.00		7.60
1942	5	14	213	18.00	0	45.00	-81	30.00	25.00		7.90
1958	1	19	1407	26.00	1	22.20	-79	20.40	0.00	7.70	7.30
1979	12	12	759	3.30	1	35.88	-79	21.48	24.00	8.20	7.60
3	ECUADOR(2)										
1901	1	7	29	0.00	-2	0.00	-82	0.00	25.00		(7.60)
1953	12	12	1731	25.00	-3	24.00	-80	36.00	0.00		7.40
1970	12	10	434	38.80	-3	59.34	-80	43.44	25.00		8.10
3	PERU(3)										
1940	5	24	1633	57.00	-10	30.00	-77	0.00	0.00		7.90
1942	8	24	2250	27.00	-15	0.00	-76	0.00	0.00		8.20
1966	10	17	2141	57.00	-10	42.00	-78	36.00	10.00	8.10	8.00
1974	10	3	1421	29.10	-12	15.90	-77	47.70	13.00	8.10	7.60
2	ALTIPLANO(4)										
1913	8	6	2214	24.00	-17	0.00	-74	0.00	25.00		7.80
1933	2	23	809	12.00	-20	0.00	-71	0.00	40.00		7.30
3	NORTH CHILE(5)										
1918	12	4	1147	48.00	-26	0.00	-71	0.00	0.00		7.60
1922	11	11	432	36.00	-28	30.00	-70	0.00	25.00	8.50	8.30
1966	12	28	0819	0.00	-25	36.00	-70	44.50	23.00	7.70	6.90
4	CENTRAL CHILE(6)										
1906	8	17	40	0.00	-33	0.00	-72	0.00	25.00	8.20	8.40
1943	4	6	1607	15.00	-30	45.00	-72	0.00	0.00		7.90
1971	7	9	0303	0.00	-32	30.00	-71	12.00	42.00	7.80	6.60
1985	3	3	2247	7.20	-33	8.10	-71	52.26	33.00	8.10	7.80
4	SOUTH CHILE(7)										
1928	12	1	406	10.00	-35	0.00	-72	0.00	25.00		8.00
1939	1	25	332	14.00	-36	15.00	-72	15.00	0.00		7.80
1960	5	22	1911	17.00	-39	30.00	-74	30.00	0.00	9.50	8.50
1975	5	10	1427	38.70	-38	10.98	-73	13.92	6.00		7.60

NEV	REGION										

	DATE			TIME		LATITUDE		LONGITUDE		DEPTH	MAGNITUDE	
Year	Mo	Dy	HrMn	Sec	$(+^{\circ}N ,-^{\circ}S)$		$(+^{\circ}E ,-^{\circ}W)$		(km)	M_w	M_s

4	RIVERA(9')										
1900	1	20	633	0.00	20	0.00	-105	0.00	25.00		(8.10)
1900	5	16	2012	0.00	20	0.00	-105	0.00	25.00		(7.60)
1932	6	3	1036	50.00	19	30.00	-104	15.00	0.00	8.20	8.20
1932	6	18	1012	10.00	19	30.00	-103	30.00	25.00	7.80	7.80

14	MEXICO(9)										
1899	1	24	2343	0.00	17	0.00	-98	0.00	0.00		(8.20)
1903	1	14	147	0.00	15	0.00	-98	0.00	25.00		(8.10)
1907	4	15	608	6.00	17	0.00	-100	0.00	25.00	7.80	8.00
1909	7	30	1051	54.00	17	0.00	-100	30.00	0.00	7.40	7.40
1911	6	7	1102	42.00	17	30.00	-102	30.00	25.00	8.00	7.70
1928	6	17	319	27.00	16	15.00	-98	0.00	25.00	7.70	7.80
1928	10	9	301	8.00	16	0.00	-97	0.00	0.00		7.60
1941	4	15	1909	56.00	18	0.00	-103	0.00	0.00		7.70
1943	2	22	0000	0.00	17	40.00	-101	9.50	16.00	7.50	7.30
1957	7	28	840	7.00	17	4.20	-99	9.00	0.00	7.60	7.50
1978	11	29	1952	47.60	16	0.60	-96	35.46	18.00	7.60	7.80
1979	3	14	1107	16.30	17	48.78	-101	16.56	49.00	7.60	7.60
1985	9	19	1317	47.30	18	11.40	-102	31.98	28.00	8.10	8.10
1985	9	21	137	13.40	17	48.12	-101	38.82	31.00	7.50	7.60

6	CENTRAL AMERICA(10)										
1898	4	29	1618	0.00	12	0.00	-86	0.00	0.00		(7.70)
1902	4	19	223	0.00	14	0.00	-91	0.00	25.00		(8.10)
1902	9	23	2018	0.00	16	0.00	-93	0.00	25.00		(8.20)
1904	12	20	544	18.00	8	30.00	-83	0.00	25.00		7.60
1942	8	6	2336	59.00	14	0.00	-91	0.00	0.00		7.90
1950	10	5	1609	31.00	11	0.00	-85	0.00	0.00		7.70

4	GREATER ANTILLES(11)										
1899	6	14	1109	0.00	18	0.00	-77	0.00	0.00		(7.70)
1943	7	29	302	16.00	19	15.00	-67	30.00	25.00		7.70
1946	8	4	1751	5.00	19	15.00	-69	0.00	0.00		8.00
1946	8	8	1328	28.00	19	30.00	-69	30.00	25.00		7.60

1	LESSER ANTILLES(12)										
1900	10	29	911	0.00	11	0.00	-66	0.00	25.00		(8.20)

NEV   REGION

DATE			TIME		LATITUDE		LONGITUDE		DEPTH	MAGNITUDE	
Year	Mo	Dy	HrMn	Sec	$(+°N,-°S)$		$(+°E,-°W)$		(km)	M_w	M_s

8   ALASKA(14)

1899	9	4	22	0.00	60	0.00	-142	0.00	25.00		(8.10)
1899	9	10	1704	0.00	60	0.00	-142	0.00	25.00		(7.60)
1899	9	10	2140	0.00	60	0.00	-140	0.00	0.00		(8.40)
1900	10	9	1228	0.00	60	0.00	-142	0.00	25.00		(8.10)
1902	1	1	520	0.00	55	0.00	-165	0.00	25.00		(7.60)
1904	8	27	2156	6.00	64	0.00	-151	0.00	25.00		7.70
1938	11	10	2018	43.00	55	30.00	-158	0.00	25.00	8.20	8.30
1964	3	28	336	14.00	61	2.40	-147	43.80	33.00	9.20	8.40

11   ALEUTIANS(15)

1901	12	31	902	0.00	52	0.00	-177	0.00	25.00		(7.60)
1902	1	1	520	0.00	55	0.00	-165	0.00	25.00		(7.60)
1905	2	14	846	36.00	53	0.00	-178	0.00	25.00		7.90
1906	8	17	10	42.00	51	0.00	179	0.00	25.00		8.20
1907	9	2	1601	30.00	52	0.00	173	0.00	25.00		7.80
1929	3	7	134	39.00	51	0.00	-170	0.00	50.00		7.50
1929	12	17	1058	30.00	52	30.00	171	30.00	25.00		7.80
1957	3	9	1422	27.50	51	18.00	-175	48.00	0.00		8.10
1965	2	4	501	21.80	51	18.00	178	36.00	40.00	8.70	8.20
1975	2	2	843	39.10	53	6.78	173	29.82	10.00		7.40
1986	5	7	2247	10.80	51	31.20	-174	46.56	33.00	8.00	7.90

10   KAMCHATKA(16)

1899	11	23	949	0.00	53	0.00	159	0.00	0.00		(7.70)
1904	6	25	1445	36.00	52	0.00	159	0.00	25.00		7.90
1904	6	25	2100	30.00	52	0.00	159	0.00	0.00		8.00
1904	6	27	9	0.00	52	0.00	159	0.00	0.00		7.90
1915	7	31	131	24.00	54	0.00	162	0.00	0.00		7.60
1917	1	30	245	36.00	56	30.00	163	0.00	25.00		7.80
1923	2	3	1601	41.00	54	0.00	161	0.00	25.00	8.50	8.30
1952	11	4	1658	26.00	52	45.00	159	30.00	25.00	9.00	8.20
1959	5	4	715	42.00	52	30.00	159	30.00	60.00		7.80
1971	12	15	829	55.30	55	59.76	163	17.70	33.00		7.50

11   KURILES(17)

1900	12	25	504	0.00	43	0.00	146	0.00	25.00		(7.60)
1901	4	5	2330	0.00	45	0.00	148	0.00	25.00		(7.70)
1915	5	1	500	0.00	47	0.00	155	0.00	25.00		8.00
1918	9	7	1716	13.00	45	30.00	151	30.00	25.00		8.20
1918	11	8	438	0.00	44	30.00	151	30.00	25.00		7.70
1935	9	11	1404	2.00	43	0.00	146	30.00	60.00		7.40
1958	11	6	2258	8.00	44	22.80	148	34.80	32.00	8.30	8.10
1963	10	13	0517	51.00	44	54.00	149	36.00	20.00	8.50	8.10
1969	8	11	2127	39.40	43	32.70	147	21.18	28.00	8.20	7.80
1973	6	17	355	2.90	43	13.98	145	47.10	48.00		7.70
1978	3	24	1947	50.70	44	14.64	148	51.72	33.00		7.60

NEV   REGION

DATE			TIME		LATITUDE		LONGITUDE		DEPTH	MAGNITUDE	
Year	Mo	Dy	HrMn	Sec	$(+^{\circ}N,-^{\circ}S)$		$(+^{\circ}E,-^{\circ}W)$		(km)	M_w	M_s

22   NORTHEAST JAPAN(18)

Year	Mo	Dy	HrMn	Sec	Lat°	Lat′	Lon°	Lon′	Depth	M_w	M_s
1897	2	7	736	0.00	40	0.00	140	0.00	0.00		(8.10)
1897	2	19	2048	0.00	38	0.00	142	0.00	0.00		(8.10)
1897	2	19	2348	0.00	38	0.00	142	0.00	0.00		(8.10)
1897	8	5	12	0.00	38	0.00	143	0.00	0.00		(8.50)
1897	8	16	754	0.00	39	0.00	143	0.00	0.00		(7.70)
1898	4	22	2336	0.00	39	0.00	142	0.00	0.00		(8.10)
1901	8	9	923	0.00	40	0.00	144	0.00	25.00		(7.90)
1901	8	9	1833	0.00	40	0.00	144	0.00	25.00		(8.10)
1905	7	6	1621	0.00	39	30.00	142	30.00	25.00		7.80
1923	9	1	258	36.00	35	15.00	139	30.00	25.00	7.90	8.20
1923	9	2	246	40.00	35	0.00	139	30.00	0.00		7.70
1927	3	7	927	36.00	35	45.00	134	45.00	25.00		7.60
1931	3	9	348	50.00	40	30.00	142	30.00	0.00		7.80
1933	3	2	1730	54.00	39	15.00	144	30.00	25.00	8.40	
1938	11	5	843	21.00	36	45.00	141	45.00	60.00		7.70
1938	11	5	1050	15.00	37	15.00	141	45.00	60.00		7.70
1938	11	6	853	53.00	37	15.00	142	15.00	60.00		7.60
1940	8	1	1508	21.00	44	30.00	139	0.00	0.00		7.50
1952	3	4	122	43.00	42	30.00	143	0.00	25.00	8.10	8.30
1968	5	16	48	55.40	40	50.40	143	13.32	7.00	8.20	8.10
1978	6	12	814	26.40	38	11.40	142	1.68	44.00		7.50
1983	5	26	259	59.60	40	27.72	139	6.12	24.00	7.80	7.80

3   IZU-BONIN(19)

Year	Mo	Dy	HrMn	Sec	Lat°	Lat′	Lon°	Lon′	Depth	M_w	M_s
1923	9	2	246	40.00	35	0.00	139	30.00	0.00		7.70
1944	12	7	435	42.00	33	45.00	136	0.00	25.00	8.10	8.00
1953	11	25	1748	54.00	33	54.00	141	30.00	33.00		7.90

1   MARIANAS(20)

Year	Mo	Dy	HrMn	Sec	Lat°	Lat′	Lon°	Lon′	Depth	M_w	M_s
1902	9	22	146	0.00	18	0.00	146	0.00	25.00		(7.90)

4   NANKAI(21')

Year	Mo	Dy	HrMn	Sec	Lat°	Lat′	Lon°	Lon′	Depth	M_w	M_s
1899	11	24	1842	0.00	32	0.00	131	0.00	0.00		(7.60)
1899	11	24	1855	0.00	32	0.00	131	0.00	0.00		(7.60)
1941	11	18	1646	22.00	32	0.00	132	0.00	25.00		7.80
1946	12	20	1919	5.00	32	30.00	134	30.00	25.00	8.10	8.20

3   RYUKYU(21)

Year	Mo	Dy	HrMn	Sec	Lat°	Lat′	Lon°	Lon′	Depth	M_w	M_s
1901	6	24	702	0.00	27	0.00	130	0.00	25.00		(7.70)
1904	8	24	2059	54.00	30	0.00	130	0.00	25.00		7.70
1938	6	10	953	39.00	25	30.00	125	0.00	0.00		7.70

3   NORTH TAIWAN(22)

Year	Mo	Dy	HrMn	Sec	Lat°	Lat′	Lon°	Lon′	Depth	M_w	M_s
1920	6	5	421	28.00	23	30.00	122	0.00	25.00		8.00
1922	9	1	1916	6.00	24	30.00	122	0.00	0.00		7.60
1966	3	12	1631	20.60	24	12.00	122	36.00	48.00		7.80

NEV   REGION

Year	Mo	Dy	HrMn	Sec	\(+°N,-°S\)		\(+°E,-°W\)		(km)	M_w	M_s
	DATE		TIME		LATITUDE		LONGITUDE		DEPTH	MAGNITUDE	

3   LUZON(23)

1897	8	15	1200	0.00	18	0.00	120	0.00	0.00		(7.70)
1901	12	14	2257	0.00	14	0.00	122	0.00	25.00		(7.60)
1934	2	14	359	34.00	17	30.00	119	0.00	25.00		7.60

18   PHILLIPINES(24)

1897	5	13	1230	0.00	12	0.00	124	0.00	0.00		(7.70)
1897	9	20	1906	0.00	6	0.00	122	0.00	0.00		(8.40)
1897	9	21	512	0.00	6	0.00	122	0.00	0.00		(8.50)
1897	10	18	2348	0.00	12	0.00	126	0.00	0.00		(7.90)
1897	10	20	1424	0.00	12	0.00	126	0.00	0.00		(7.70)
1901	12	14	2257	0.00	14	0.00	122	0.00	25.00		(7.60)
1903	12	28	256	0.00	7	0.00	127	0.00	25.00		(7.60)
1911	7	12	407	36.00	9	0.00	126	0.00	0.00		7.70
1913	3	14	845	0.00	4	30.00	126	30.00	25.00		7.90
1918	8	15	1218	12.00	5	30.00	123	0.00	25.00		8.00
1924	4	14	1620	23.00	6	30.00	126	30.00	0.00		8.30
1936	4	1	209	15.00	4	30.00	126	30.00	0.00		7.80
1943	5	25	2307	36.00	7	30.00	128	0.00	0.00		7.70
1948	1	24	1746	40.00	10	30.00	122	0.00	25.00		8.20
1952	3	19	1057	12.00	9	30.00	127	15.00	25.00		7.60
1957	9	24	821	5.00	5	30.00	127	30.00	0.00		7.60
1975	10	31	828	2.60	12	32.40	125	59.58	50.00		7.40
1976	8	16	1611	7.30	6	15.72	124	1.38	33.00	8.10	7.80

7   SULAWESI(25)

1899	9	29	1703	0.00	-3	0.00	128	30.00	0.00		(7.60)
1932	5	14	1311	0.00	0	30.00	126	0.00	25.00		8.00
1938	5	19	1708	21.00	-1	0.00	120	0.00	25.00		7.60
1948	3	1	112	28.00	-3	0.00	127	30.00	50.00		7.10
1950	10	8	323	9.00	-3	45.00	128	15.00	0.00		7.40
1965	1	24	11	12.10	-2	24.00	126	0.00	6.00		7.50
1968	8	10	207	4.30	1	25.38	126	13.32	33.00		7.50

7   BURMA(26)

1897	6	12	1106	0.00	26	0.00	91	0.00	0.00		(8.50)
1912	5	23	224	6.00	21	0.00	97	0.00	25.00		8.00
1918	7	8	1022	7.00	24	30.00	91	0.00	0.00		7.60
1931	1	27	2009	13.00	25	36.00	96	48.00	0.00		7.70
1946	9	12	1520	20.00	23	30.00	96	0.00	0.00		7.80
1947	7	29	1343	22.00	28	30.00	94	0.00	0.00		7.50
1950	8	15	1409	30.00	28	30.00	96	30.00	25.00		8.60

2   ANDAMAN(27)

| 1941 | 6 | 26 | 1152 | 3.00 | 12 | 30.00 | 92 | 30.00 | 0.00 | | 7.70 |
| 1969 | 11 | 21 | 205 | 35.30 | 2 | 3.90 | 94 | 38.40 | 20.00 | | 7.60 |

NEV   REGION

	DATE		TIME		LATITUDE		LONGITUDE		DEPTH	MAGNITUDE	
Year	Mo	Dy	HrMn	Sec	$(+°N,-°S)$		$(+°E,-°W)$		(km)	M_w	M_s
3	SUNDA(28)										
1903	2	27	43	0.00	-8	0.00	106	0.00	25.00		(7.90)
1935	12	28	235	22.00	0	0.00	98	15.00	25.00		7.70
1943	6	9	306	22.00	-1	0.00	101	0.00	50.00		7.60
1	JAVA(29)										
1977	8	19	608	55.20	-11	5.10	118	27.84	33.00	8.30	8.10
2	TIMOR(30)										
1938	2	1	1904	18.00	-5	15.00	130	30.00	25.00	8.50	8.20
1943	11	6	831	37.00	-6	0.00	134	30.00	0.00		7.70
7	NEW GUINEA(31)										
1900	10	7	2104	0.00	-4	0.00	140	0.00	25.00		(7.60)
1914	5	26	1422	42.00	-2	0.00	137	0.00	0.00		8.00
1916	1	13	820	48.00	-3	0.00	135	30.00	25.00		7.50
1926	10	26	344	41.00	-3	15.00	138	30.00	25.00		7.60
1935	9	20	146	33.00	-3	30.00	141	45.00	0.00		7.90
1971	1	10	717	3.70	-3	7.92	139	41.82	33.00		7.90
1979	9	12	517	51.40	-1	40.74	136	2.40	5.00		7.70
4	NEW BRITAIN(32)										
1902	1	24	2327	0.00	-8	0.00	150	0.00	25.00		(7.60)
1906	9	14	1604	18.00	-7	0.00	149	0.00	25.00		8.10
1945	12	28	1748	45.00	-6	0.00	150	0.00	0.00		7.70
1947	5	6	2030	32.00	-6	30.00	148	30.00	0.00		7.50
6	NEW IRELAND(33)										
1916	1	1	1320	36.00	-4	0.00	154	0.00	25.00		7.80
1919	5	6	1941	12.00	-5	0.00	154	0.00	25.00		7.90
1920	2	2	1122	18.00	-4	0.00	152	30.00	0.00		7.70
1946	9	29	301	55.00	-4	30.00	153	30.00	0.00		7.70
1971	7	14	611	29.10	-5	28.44	153	53.10	47.00	8.00	7.80
1971	7	26	123	21.30	-4	56.40	153	10.38	48.00	8.10	7.70

NEV   REGION

DATE			TIME		LATITUDE		LONGITUDE		DEPTH	MAGNITUDE	
Year	Mo	Dy	HrMn	Sec	$(+°N,-°S)$		$(+°E,-°W)$		(km)	M_w	M_s
10	**SOLOMONS(34)**										
1900	7	29	659	0.00	-10	0.00	165	0.00	25.00		(7.90)
1931	10	3	1913	13.00	-10	30.00	161	45.00	25.00		7.90
1931	10	10	19	53.00	-10	0.00	161	0.00	0.00		7.80
1935	12	15	707	48.00	-9	45.00	161	0.00	0.00		7.60
1939	1	30	218	27.00	-6	30.00	155	30.00	25.00		7.80
1939	4	30	255	30.00	-10	30.00	158	30.00	25.00		8.00
1975	7	20	1437	39.90	-6	35.40	155	3.24	49.00	7.30	7.60
1975	7	20	1954	27.70	-7	6.24	155	9.12	44.00	7.40	7.50
1977	4	20	2342	50.50	-9	53.40	160	20.88	19.00		7.60
1977	4	21	424	9.60	-9	57.90	160	43.86	33.00	7.60	7.50
11	**NEW HEBRIDES(35)**										
1900	7	29	659	0.00	-10	0.00	165	0.00	25.00		(7.90)
1901	8	9	1301	0.00	-22	0.00	170	0.00	25.00		(8.20)
1903	5	13	634	0.00	-17	0.00	168	0.00	25.00		(7.70)
1920	9	20	1439	0.00	-20	0.00	168	0.00	25.00		7.90
1934	7	18	1940	15.00	-11	45.00	166	30.00	25.00		8.10
1950	12	2	1951	49.00	-18	15.00	167	30.00	0.00		7.60
1973	12	28	1341	45.80	-14	27.84	166	36.06	26.00		7.90
1980	7	8	2319	19.80	-12	24.60	166	22.86	33.00	7.90	7.70
1980	7	17	1942	23.20	-12	31.50	165	54.96	33.00		7.70
1985	11	28	349	54.10	-13	59.22	166	11.10	33.00		7.60
1985	12	21	113	22.40	-13	57.96	166	30.96	43.00		7.60
8	**TONGA**										
1901	8	9	1301	0.00	-22	0.00	170	0.00	25.00		(8.20)
1902	2	9	735	0.00	-20	0.00	-174	0.00	25.00		(7.60)
1917	5	1	1826	30.00	-29	0.00	-177	0.00	0.00		7.90
1917	6	26	549	42.00	-15	30.00	-173	0.00	25.00		8.40
1948	9	8	1509	11.00	-21	0.00	-174	0.00	25.00		7.80
1975	10	11	1435	15.00	-24	53.64	-175	7.14	9.00		7.70
1976	1	14	1647	33.50	-28	25.62	-177	39.42	33.00		7.90
1982	12	19	1743	54.80	-24	7.98	-175	51.84	33.00		7.70
2	**NEW ZEALAND(38)**										
1929	6	16	2247	32.00	-41	45.00	172	15.00	0.00		7.60
1931	2	2	2246	42.00	-39	30.00	177	0.00	25.00		7.80
4	**HINDU-KUSH(39)**										
1907	10	21	423	36.00	38	0.00	69	0.00	25.00		7.70
1911	2	18	1841	3.00	40	0.00	73	0.00	0.00		7.60
1949	7	10	353	36.00	39	0.00	70	30.00	0.00		7.50
1956	6	9	2313	51.00	35	6.00	67	30.00	0.00		7.50

NEV	REGION									

	DATE			TIME		LATITUDE		LONGITUDE		DEPTH	MAGNITUDE	
Year	Mo	Dy	HrMn	Sec	$(+°N,-°S)$		$(+°E,-°W)$		(km)	M_w	M_s
1	IRAN(40)										
1945	11	27	2156	50.00	24	30.00	63	0.00	25.00		8.00
2	GREECE(41)										
1956	7	9	311	40.00	36	43.80	25	48.00	0.00		7.70
1981	12	19	1410	50.70	39	14.58	25	13.62	10.00		7.60
1	RUMANIA(42)										
1912	8	9	129	0.00	40	30.00	27	0.00	0.00		7.70

M_w is taken from Ruff and Kanamori (1980) for great events, some events are taken from special studies on the events.

M_s is taken from Abe (1981) for events between 1904 and 1980;
magnitude of events before 1904 are Gutenberg and Richter's (1956) magnitude corrected by - 0.2 units as suggested by Abe (1981).

Appendix 2

New focal mechanisms of intermediate-depth earthquakes were determined from first-motion data of long and short-period WWSSN records. The mechanism diagrams in Figures A1 and A2 are shown on an equal angle projection of the lower focal hemisphere. Closed circles are compressions and open circles, dilatations. Numbers correspond to events in Table 1.2. The asterisk next to the event date indicates that one or two of the focal parameters have been constrained by modeling of a few long-period P-waveforms for these events or by timing of (pP-)P and (sp-P) phases in short-period records to constrain the event depth. Figure A1 shows events that occurred from 1964 to 1972 and Figure A2, those events that occurred between 1973 and 1978.

Body-wave modeling of 14 intermediate-depth earthquakes are shown in Figures A3 to A12. In most cases the upper trace shows the P-wave data, unless it is indicated in the figure, and the lower traces are synthetic seismograms that are calculated by Kanamori and Stewart's (1976) method. We assume a half-space model with V_p=7.8km/s , V_s=4.4km/s and ρ=3.3g/cm^3 to determine the synthetic seismograms that include the direct and surface reflected phases. A simple trapezoidal function about 3 to 5 s long was used in all cases. The fault parameters and depths used to calculate the synthetic traces for each event are indicated in the corresponding figure. The asterisk next to the focal parameters in the figures indicate which parameters were varied in trying to fit the body-wave data.
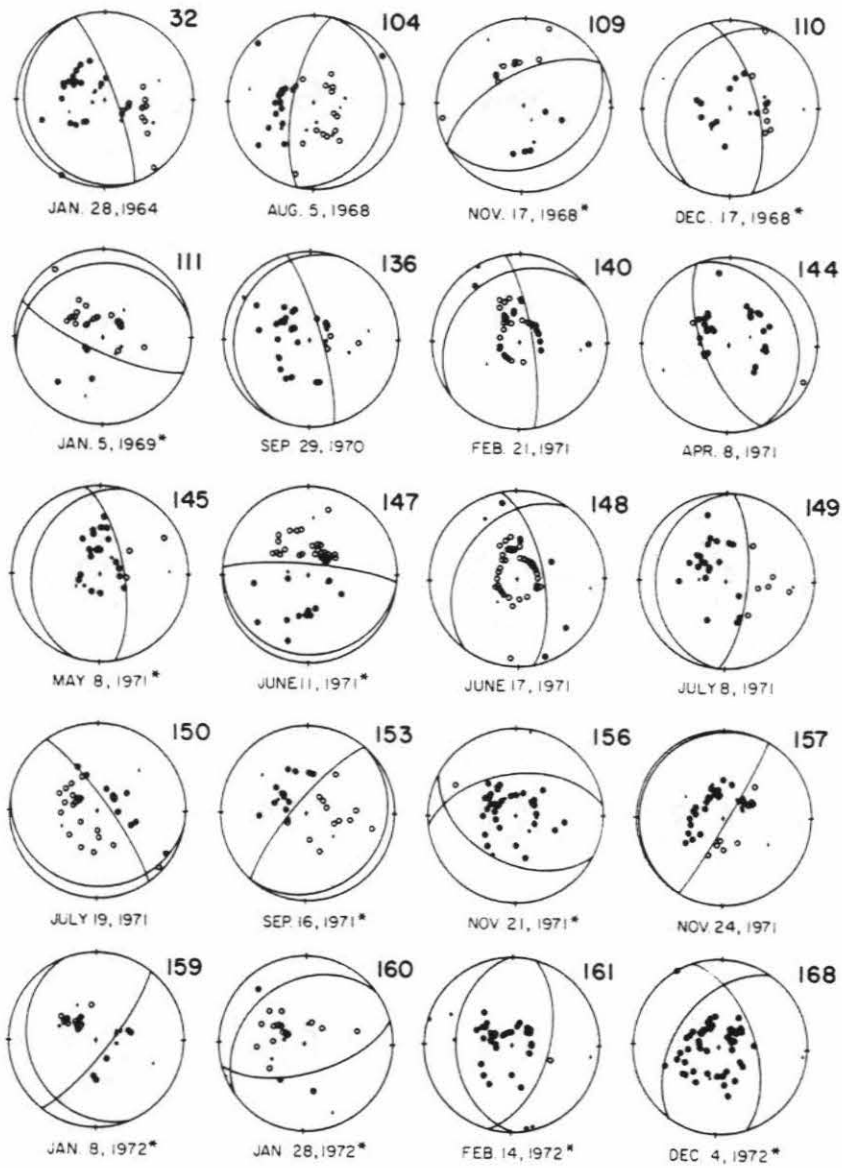
Figure A1: New focal mechanisms for intermediate-depth earthquakes that occurred from 1964 to 1972. See text for symbols
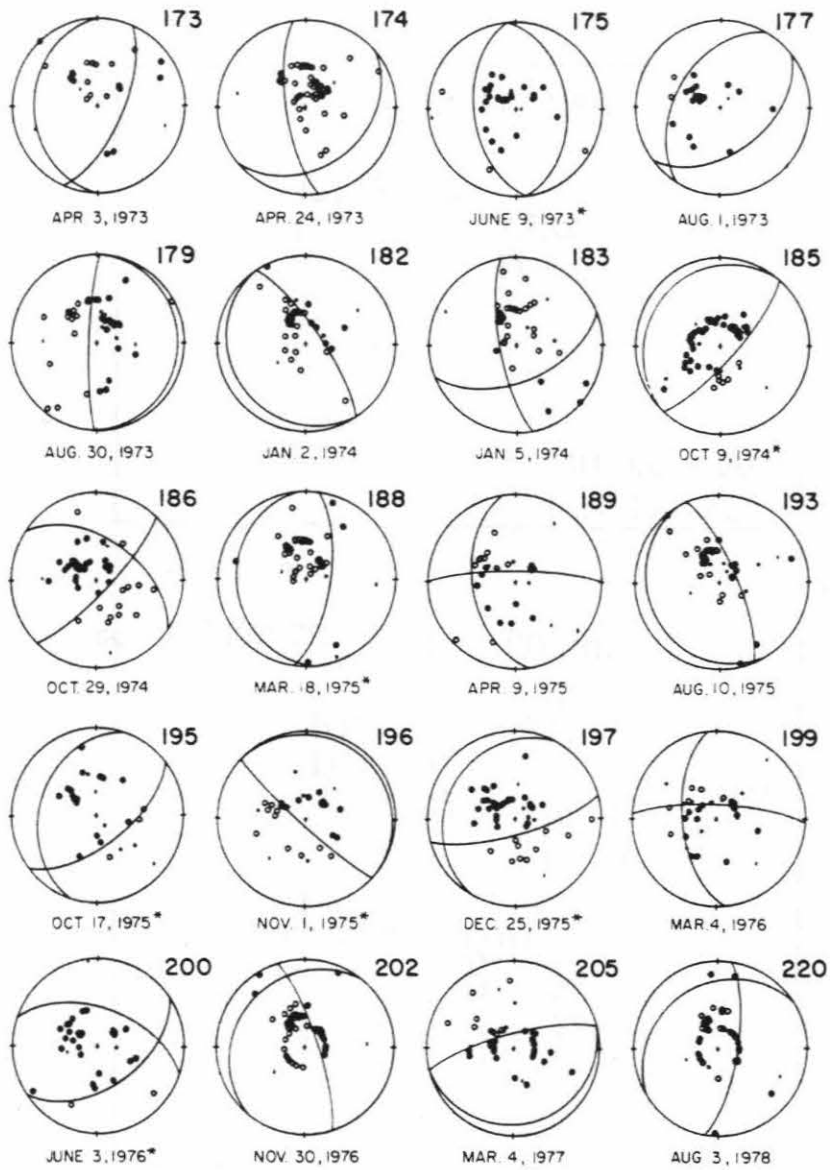
Figure A2: New focal mechanism for intermediate-depth events that occurred between 1973 and 1978. See Figure A1 for symbols.
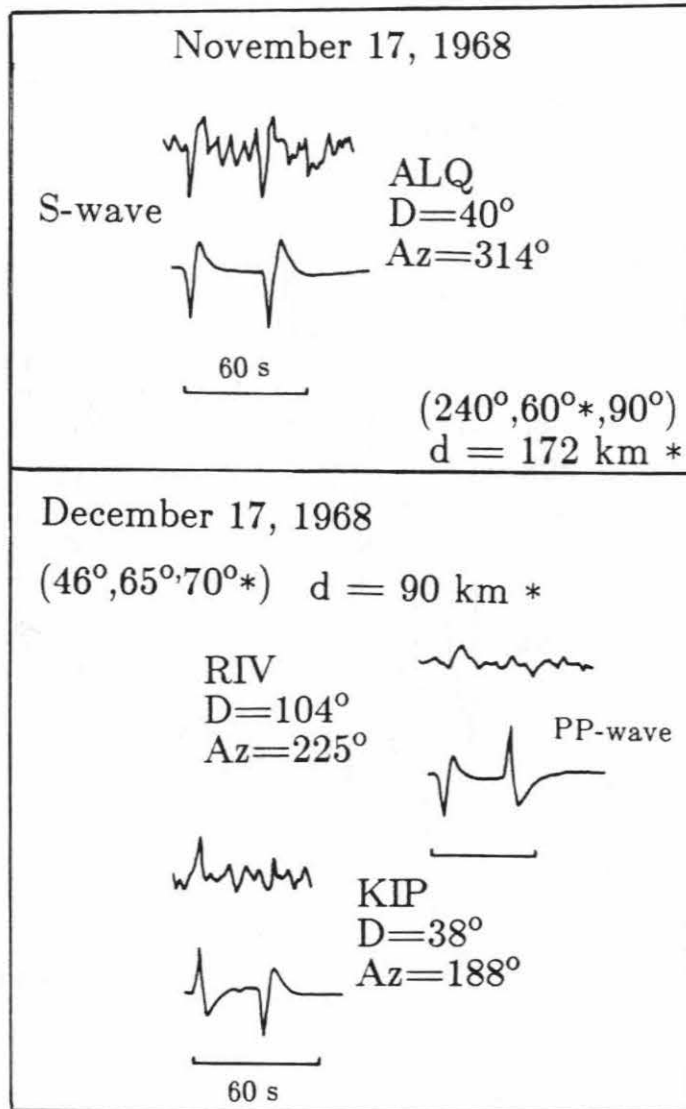
Figure A3: Observed and synthetic seismograms for the November 17, 1968 and the December 17, 1968 earthquakes. The fault parameters, depth and body-wave used to calculate the synthetic seismograms are indicated.
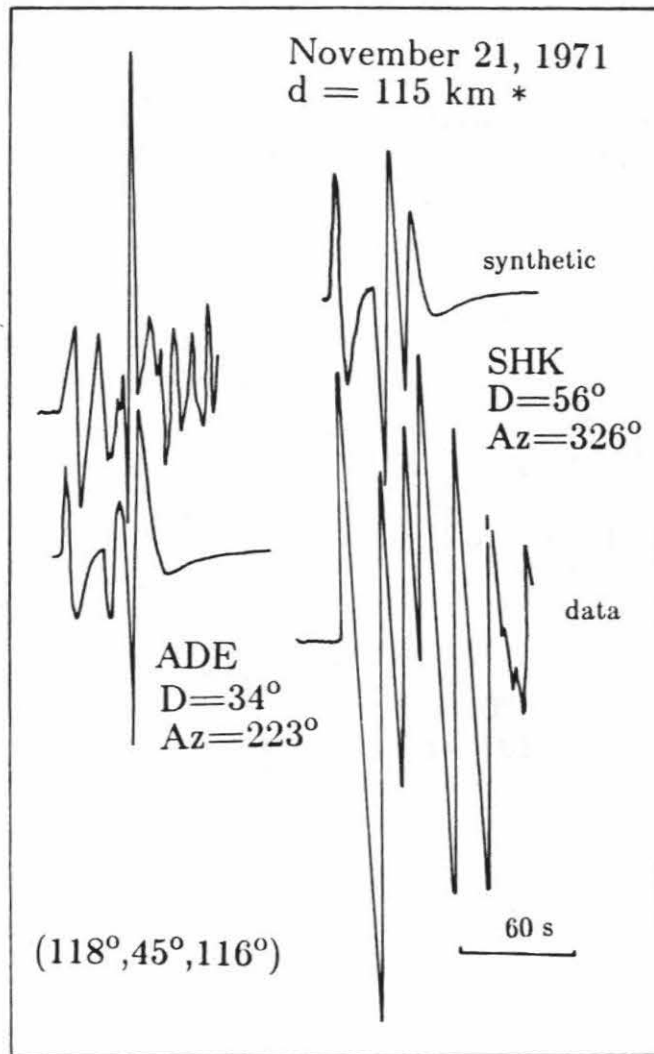
Figure A4: Observed and synthetic seismograms for the November 21, 1971 event. The synthetic traces were calculated for a single source; however note that the observed traces are complex, probably indicating a double source.
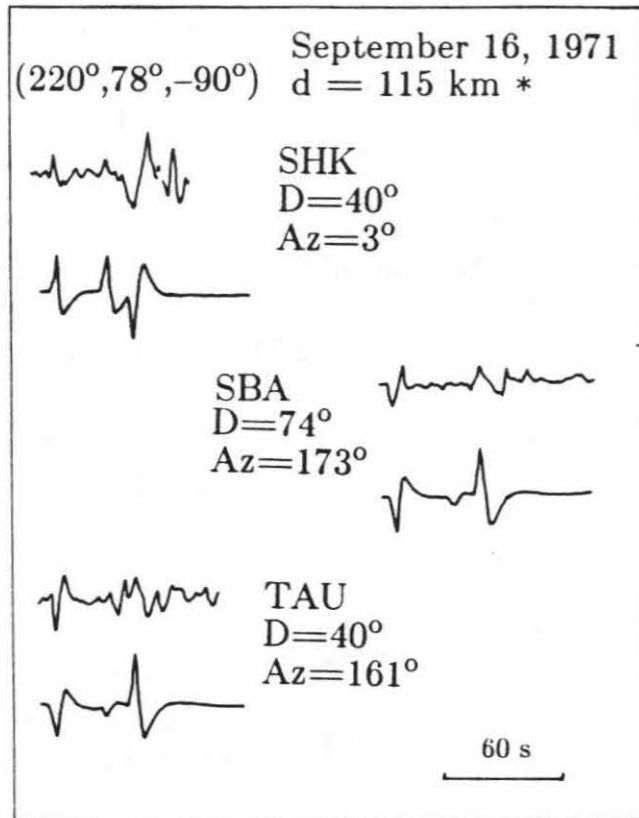
Figure A5: Observed (upper) and calculated seismograms for the September 16, 1971 earthquake.
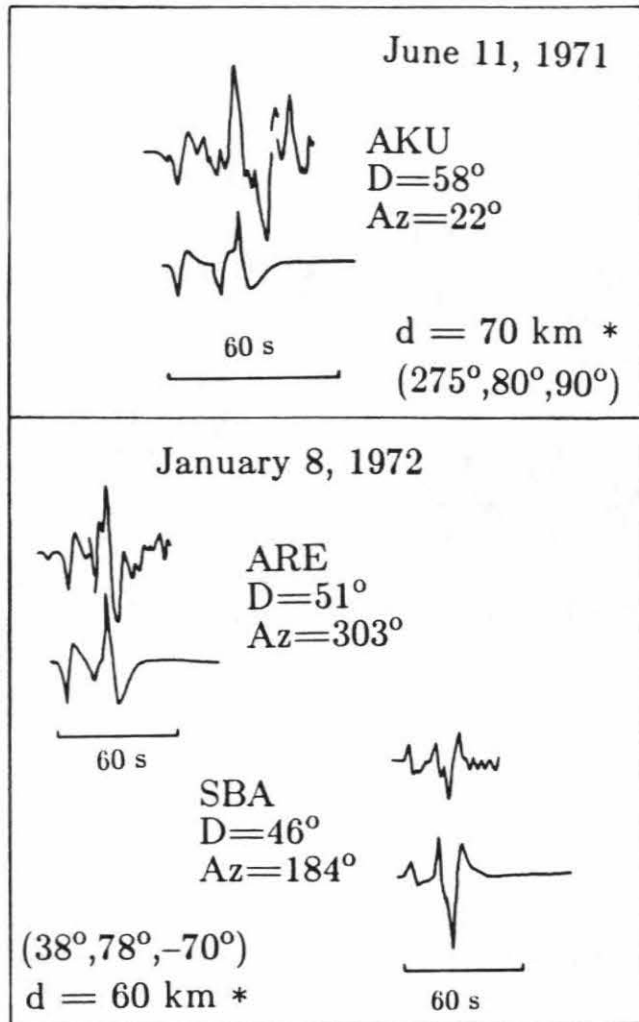
Figure A6: P-waveforms for the events of June 11, 1971 and on January 8, 1972. The focal parameters are indicated on the figure for each event.
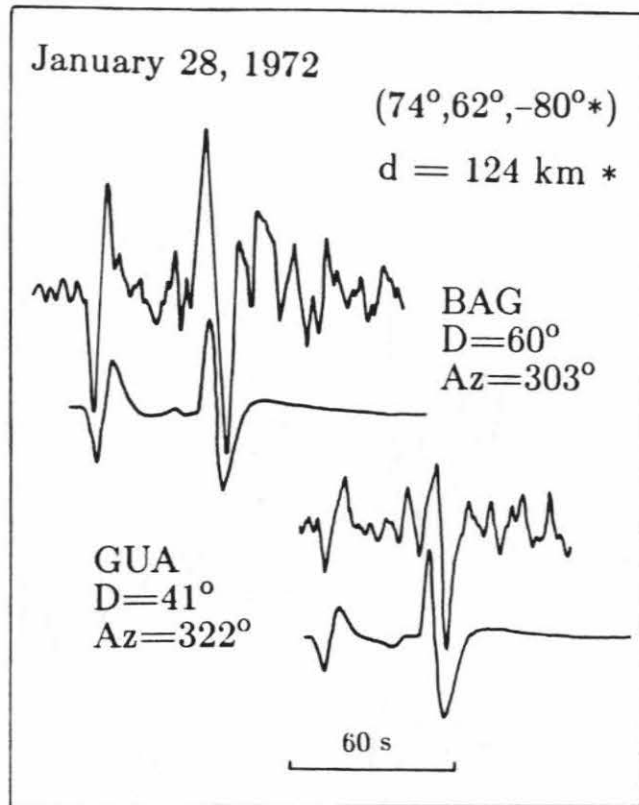
Figure A7: Observed P-wave seismograms (upper trace) and synthetic seismogram for the January 28, 1972 earthquake.
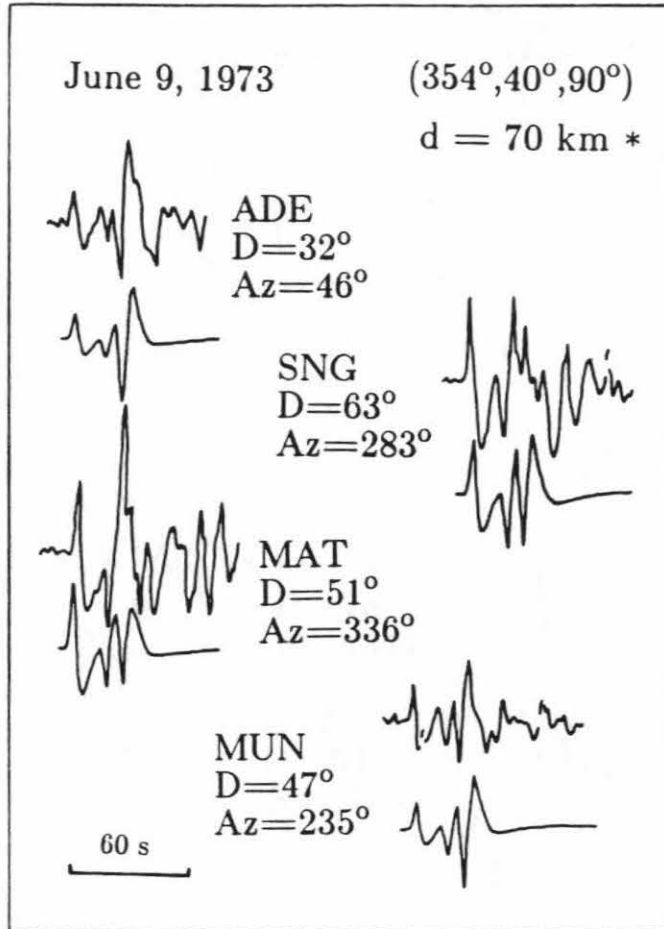
Figure A8: P-waveforms of the June 9, 1973 event. Upper traces are data and lower traces are synthetic waveforms determined with the fault parameters shown.
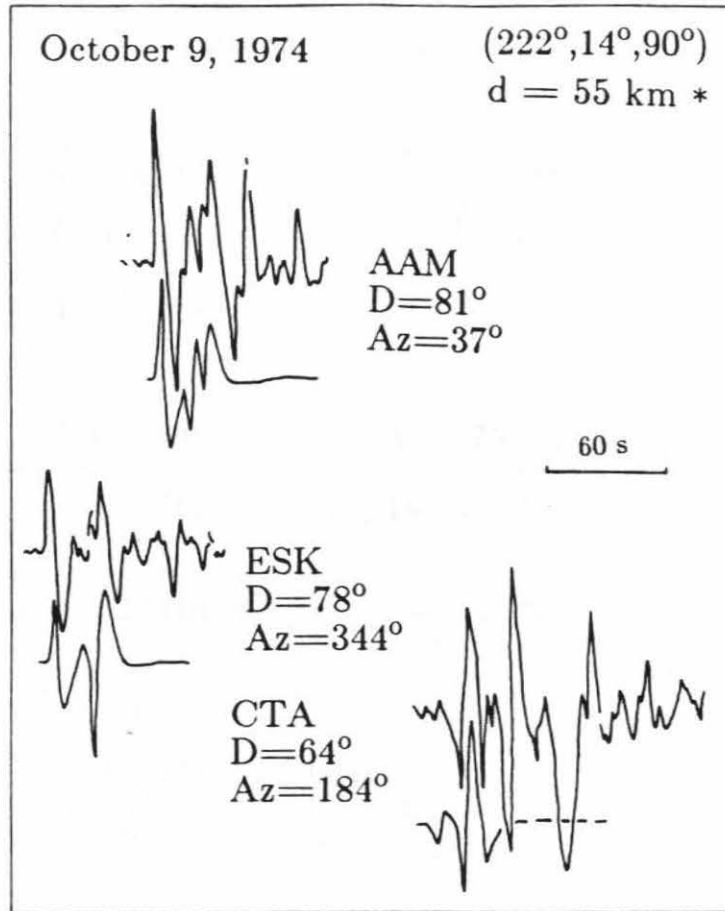
Figure A9: Seismograms of the October 9, 1974 earthquake. The synthetic traces (lower) fit only the first part of the observations. Although this event is complex, it probably has two or more sources with similar focal mechanism, as suggested by inspection of the CTA record.
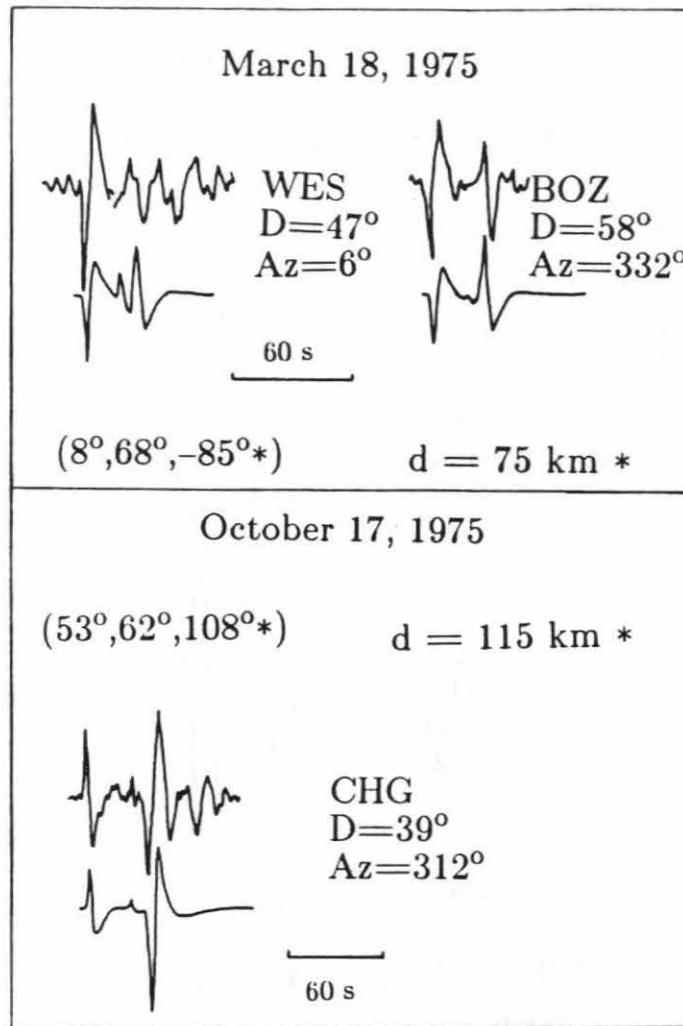
Figure A10: Observed (upper) and synthetic seismograms for the events of March 18, 1975 and October 17, 1975.
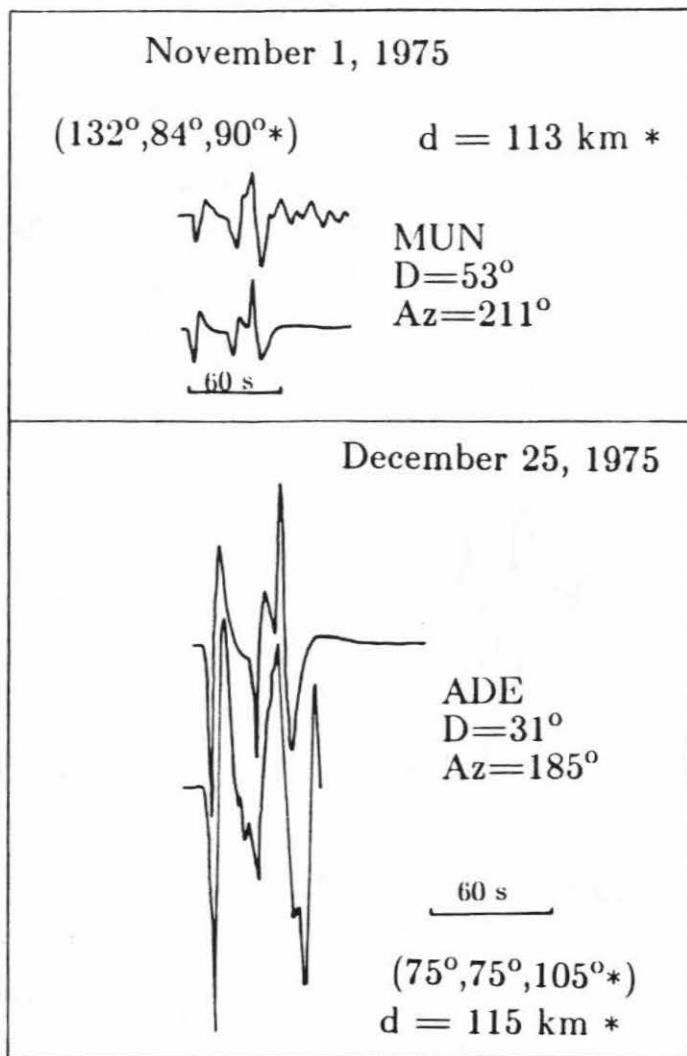
Figure A11: P-wave data (upper traces) and synthetic seismograms for the November 1, 1975 and December 25, 1975 earthquakes.
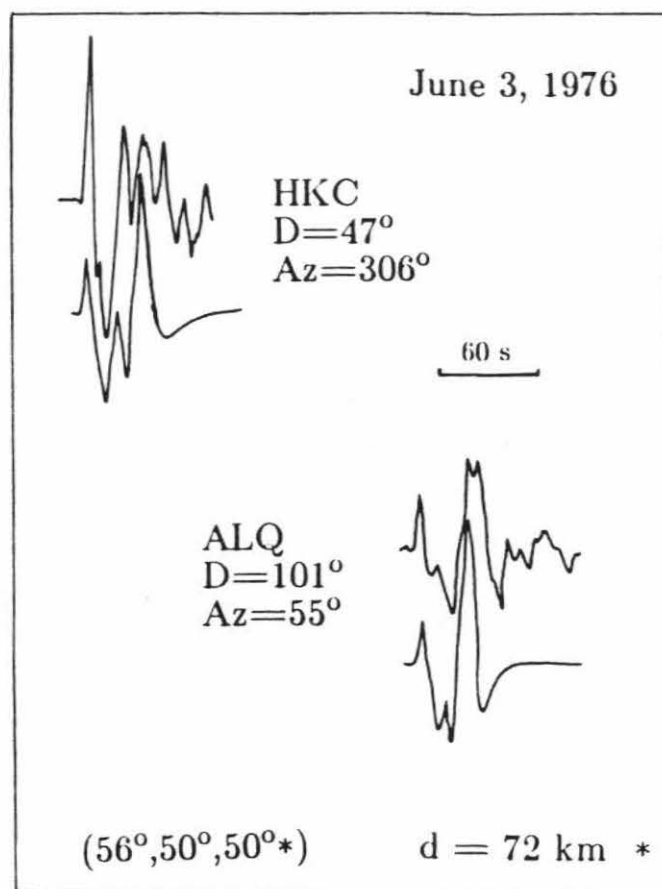
Figure A12: Observed and synthetic (lower) traces for the June 3, 1976 event. The focal parameters used in calculating the synthetics are indicated on the figure.